

# Study of single impurity Anderson model and dynamical mean field theory based on equation-of-motion method

Dissertation  
zur Erlangung des Doktorgrades  
der Naturwissenschaften

vorgelegt beim Fachbereich Physik  
der Goethe-Universität Frankfurt  
in Frankfurt am Main

von  
Qingguo Feng  
aus Shandong (China)

Frankfurt am Main 2009  
(D30)

vom Fachbereich Physik der Goethe-Universität Frankfurt als Dissertation angenommen.

Prüfungskommission:

Prof. Dr. Claudius Gros (Vorsitz)

Dr. Harald O. Jeschke

Prof. Dr. Jens Müller (Protokoll)

Prof. Dr. Jochim Maruhn

Prüfungszeit: 16. November, 2009

Dekan: Prof. Dr. Dirk-Hermann Rischke

Gutachter: Dr. Harald O. Jeschke,

Prof. Dr. Claudius Gros,

Prof. Dr. Fakher Assaad (Universität Würzburg)

to my parents



## Abstract

In this thesis, we studied the single impurity Anderson model and developed a new and fast impurity solver for the dynamical mean field theory (DMFT). Using this new impurity solver, we studied the Hubbard model and periodic Anderson model for various parameters. This work is motivated by the fact that the dynamical mean field theory is widely used for the studies of strongly correlated systems, and the most frequently used methods, *e.g.* the quantum Monte-Carlo method (QMC), and the exact diagonalization method are much CPU time consuming and usually limited by the available computers. Therefore, a fast and reliable impurity solver is needed.

This new impurity solver was explored based on the equation-of-motion method (also called Green's function and decoupling method in some literature). Using the retarded Green's function, we first derived the equations of motion of Green's functions. Then, we employed a decoupling scheme to close the equations. By solving self-consistently the obtained closed set of integral equations, we obtained the single particle Green's function for the single impurity Anderson model. After that, the single impurity Anderson model was solved along with self-consistency conditions within the framework of DMFT. In this work, we studied and compared two decoupling schemes. Moreover, we also derived possible higher order approximations which will be tested in future work.

Besides the theoretical work, we tested the method in numerical calculations. The integral equations are first solved by iterative methods with linear mixing and Broyden mixing, respectively. However, these two methods are not sufficient for finding the self-consistent solutions of the DMFT equations because converged results are difficult to obtain. Moreover, the computing speed of the two methods is also not satisfactory. Especially the iterative method with linear mixing costs always a lot of CPU time due to the required small mixing. Hence, we developed a new method, which is a combination of genetic algorithm and iterative method. This new method converges very fast and removes artifacts appearing in the results from the iterative method with linear and Broyden mixing. It can directly operate on the real axis, where no numerical error from the high frequency tail corrections and the analytical continuation is introduced. In addition, our new technique strongly improves the precision of the numerical results by removing the broadening.

With this newly developed impurity solver and numerical technique, we studied the single impurity Anderson model, the single band Hubbard model and the periodic Anderson model with arbitrary spin and orbital degeneracy  $N$  on the real axis. For the single impurity Anderson model, the spectral functions are calculated for the infinite and finite Coulomb interaction strength. We

also studied the spectral functions in dependence of the parameters of impurity position and hybridization. For the Hubbard model, we studied the bandwidth control and filling control Mott metal-insulator transition for spin and orbital degeneracy  $N = 2$ . It gives qualitatively the critical value of Coulomb interaction strength for the Mott metal-insulator transition, and the spectral functions which are comparable to those obtained in QMC and numerical renormalization group methods. We also studied the quasiparticle weight and the self-energy in metallic states. The latter shows almost Fermi liquid behavior. At last we calculated the densities of states for the Hubbard model with arbitrary spin and orbital degeneracy  $N$ . The periodic Anderson model (PAM) is also studied as another important lattice model. It was solved for various combinations of parameters: the Coulomb interaction strength, the impurity position, the center position of the conduction band, the hybridization, the spin and orbital degeneracy. The PAM results represents the physics of impurities in a metal. In short, our method works for the Hubbard model and the periodic Anderson model in a large range of parameters, and gives good results. Therefore, our impurity solver could be very useful in calculations within LDA+DMFT.

Finally, we also made a preliminary investigation of the multi-band system based on the success in single band case. We first studied the two-band system in a simplified treatment by neglecting the interaction between the two bands through the bath. This has given promising numerical results for the two-band Hubbard model. Moreover, we have studied theoretically the two-band system with mean field approximation and Hubbard-I approximation in dealing with the higher order cross Green's functions which are related to both the two bands. In the mean field approximation, we even generalized the two-band system to arbitrary  $M = N/2$  band system. Potential improvement can be carried out on the basis of this work.

# Contents

<b>1</b>	<b>Introduction</b>	<b>1</b>
1.1	Mott transition . . . . .	2
1.2	Dynamical Mean Field Theory . . . . .	3
1.3	Single impurity Anderson model . . . . .	9
1.4	Hubbard model . . . . .	12
1.5	Periodic Anderson model . . . . .	15
1.6	Summary . . . . .	17
<b>2</b>	<b>Theory and method</b>	<b>19</b>
2.1	Why have we chosen the EOM method? . . . . .	19
2.2	Calculation of equations of motions . . . . .	20
2.2.1	Analytical calculation of equations of motion . . . . .	20
2.2.2	Machine calculation and symbol manipulation . . . . .	27
2.3	Decoupling Scheme and approximations . . . . .	27
2.3.1	Mean field approximation and Hubbard-I approximation . . . . .	28
2.3.2	Lacroix's decoupling scheme . . . . .	30
2.3.3	Wang's decoupling scheme . . . . .	31
2.4	Calculation of integrals on the real axis: analytical method . . . . .	34
2.4.1	$\Delta$ and $\tilde{\Delta}$ . . . . .	34
2.4.2	$\langle d_{\sigma'}^{\dagger} c_{k\sigma'} \rangle$ and $\langle c_{k'\sigma'}^{\dagger} c_{k\sigma'} \rangle$ . . . . .	35
2.4.3	Integrals . . . . .	37
2.5	Calculation on the Matsubara axis . . . . .	41
<b>3</b>	<b>Higher approximations beyond Lacroix's level</b>	<b>45</b>
3.1	Equations of motion for three-particle Green's function . . . . .	45
3.2	EOMs for multi- $c$ operator Green's functions . . . . .	47
3.2.1	Extended Lacroix's decoupling scheme . . . . .	47

3.2.2	Wang's decoupling . . . . .	50
<b>4</b>	<b>Multi-band system</b>	<b>55</b>
4.1	The Hamiltonian and EOMs . . . . .	56
4.2	Approximation without inter-band hybridization . . . . .	58
4.3	Hartree-Fock approximation . . . . .	60
4.4	Hubbard-I approximation . . . . .	64
4.5	Summary . . . . .	66
<b>5</b>	<b>Code realization and optimization</b>	<b>69</b>
5.1	Technique in calculating the integral terms . . . . .	70
5.1.1	Analytical method . . . . .	70
5.1.2	Lorentzian broadening method . . . . .	71
5.2	Iterative method . . . . .	72
5.2.1	Iterative method with linear mixing . . . . .	72
5.2.2	Broyden mixing . . . . .	73
5.3	Genetic algorithm . . . . .	76
5.3.1	Introduction of genetic algorithm . . . . .	76
5.3.2	Implementation . . . . .	77
5.4	Results and discussion . . . . .	80
<b>6</b>	<b>Physical results and Discussion</b>	<b>85</b>
6.1	Single impurity Anderson model . . . . .	85
6.2	Hubbard model . . . . .	89
6.3	Periodic Anderson model . . . . .	103
6.4	Multi-band system . . . . .	110
6.4.1	Two-band Hubbard model . . . . .	111
6.5	Summary . . . . .	114
<b>7</b>	<b>Conclusions</b>	<b>117</b>
	<b>Appendices</b>	<b>120</b>
<b>A</b>	<b>An example of FORM code</b>	<b>121</b>



<i>CONTENTS</i>	iii
<b>B Separating the Green's function into two parts</b>	<b>129</b>
<b>C Calculation of two-particle correlations</b>	<b>133</b>
<b>Bibliography</b>	<b>136</b>



# Chapter 1 Introduction

The discovery of exotic physical properties, such as the heavy Fermion behavior [1, 2], the high  $T_c$  superconductivity and the correlation-driven Mott metal-insulator transition [3], has revived great interest in strongly correlated systems (especially those systems with partially occupied  $d$  or  $f$  electrons, *e.g.* some transition metal oxides, rare-earth and actinide elements). It turns out that the local Coulomb repulsive interaction is essential for a proper understanding of these systems because the strength of the electron-electron Coulomb interaction can be comparable to or even much larger than the kinetic energy of electrons. The density functional theory (DFT) [4, 5, 6, 7] is very successful in describing systems where the electrons are mostly delocalized, but sometimes fails to describe the much more localized electron systems. Though many people have investigated such systems in the past forty years, the quantitative understanding of the properties of the strongly correlated systems remains a hard and challenging fundamental task in modern condensed matter physics. In the past decade, a new theory, the so called dynamical mean field theory (DMFT) [8, 9, 10], has been developed and applied to the study of strongly correlated electron systems. The dynamical mean field theory maps the many-body problem to an impurity problem, which is solved self-consistently so that the many-body problem can be equivalently solved. The dynamical mean field theory includes the quantum fluctuations for the strong Coulomb interactions so that it has led to a considerable improvement in our understanding of strongly correlated systems.

There have been a lot of numerical methods developed to solve the single impurity model, see Sect. 1.2. However, each method has its limitations. One of the most important limitations for those methods is the strong requirement for computer conditions, which has limited their applications on physical systems with large size. This difficulty motivates the work to construct a fast and reliable impurity solver.

In this chapter, we will first introduce the Mott metal-insulator transition, then show the underlying physics described by the dynamical mean field theory. Next, we will introduce the single impurity Anderson model (SIAM) [11], which is the key issue in the dynamical mean field theory and also our main task in this thesis work. Finally, two most frequently used lattice models: the Hubbard model [12] and the periodic Anderson model [11] are introduced. In our work, we

solve these two models in the framework of dynamical mean field theory and obtain the Kondo peak and the Mott metal-insulator transition with our newly constructed impurity solver.

## 1.1 Mott transition

The Mott transition is named after the physicist Nevill Francis Mott [13, 14], who explained theoretically the effect of light on a photographic emulsion and outlined the transition of substances from metallic to insulating states. A lot of work has been done on this topic, and there are many books discussing the Mott metal-insulator transition, e.g. [15]. A recent review can be found in Ref. [16].

In condensed matter physics, the insulators can be divided into four classes according to their different origins of insulation: band insulator, Peierls insulator, Anderson insulator and Mott insulator. The first three classes of insulators are considered to be caused by the electron-ion interaction: the band insulator is due to the interaction between electrons and the periodic potential of ions, the Peierls insulator is caused by the interaction of electrons with lattice deformations, and the Anderson insulator is the result of the presence of impurities. Different to these, the fourth insulator, the Mott-insulator, is considered to be caused by the electron-electron Coulomb interaction.

However, the classification for insulators is not always unambiguous, because in real materials, all the interactions are always simultaneously present and the observed insulators should be a consequence of all the interactions. One dominant interaction may be strongly affected by other interactions so that the classification can not be clearly made. In the following, we make a brief introduction to the Mott metal-insulator transition.

Theoretically one kind of Mott metal-insulator transition can be considered as the phase transition caused by the competition between the kinetic energy and Coulomb interaction energy. The kinetic energy tends to delocalize the electrons and makes the system metallic, while the Coulomb interaction energy tends to localize the electrons in order to minimize the potential energy and brings the system to an insulating state. Another kind of Mott transition is caused by the competition of the internal energy and the entropy. We mention that the strict Mott transition is defined for exactly zero temperature. At finite temperature, it should be a good approximation when the temperature is low enough and much smaller than the electronic energy scale.

For materials with partially filled  $d$  or  $f$  electrons, *e.g.* transition metal oxides, Lanthanide and Actinide elements, the Mott transition becomes dominant because the Coulomb interaction

strength is comparable to the kinetic energy scale and the electrons become much more localized. Due to the wide usage and so many interesting properties of rare-earth elements, the study of strongly correlated system and the Mott transition becomes more and more important and has drawn a lot of attention.

## 1.2 Dynamical Mean Field Theory

The study of strongly correlated systems has drawn more and more interest in the past forty years due to the experiments on transition metal oxides, the discovery of the Kondo problem and itinerant ferromagnetism problem, and so on. It's often possible to write down the effective Hamiltonians for strongly correlated systems. However, it's very difficult to solve such model Hamiltonians theoretically due to the existence of strong correlations, which are non-perturbative in nature. In addition, there are several competing physical mechanisms, which affect the properties of the systems.

Many efforts have been devoted by researchers to circumvent these theoretical difficulties, *e.g.* the method of Bethe Ansatz [17, 18], the decoupling method by Hubbard [12, 19, 20]. However, it was difficult to find an ideal method due to the complexity of the problem. At the end of 1980s, M. Metzner, D. Vollhardt, A. Georges, and G. Kotliar proposed the Dynamical Mean Field Theory (DMFT) [8, 9, 10] to investigate strongly correlated electron systems. This method has been extended from Weiss mean field theory and developed based on some previous works done by other researchers for various lattice models of strongly correlated systems in high dimensions, *e.g.* [21, 22, 23]. Dynamical mean field theory has been applied to the study of strongly correlated electron systems. It has led to a surprising success and to considerable improvement in the understanding of strongly correlated systems.

In the dynamical mean field theory, the essential physics of the many body problem is captured in single impurity models where a single impurity is coupled to a self-consistently determined effective Fermionic host. Considering the Hubbard model [12],

$$\mathcal{H} = - \sum_{ij,\sigma} t_{ij} f_{i\sigma}^\dagger f_{j\sigma} - \mu \sum_{i\sigma} \hat{n}_{i\sigma} + U \sum_i \hat{n}_{i\uparrow} \hat{n}_{i\downarrow} \quad (1.1)$$

where the first term is the hopping term, with one electron destroyed at site  $j$  and created at site  $i$ , the second term relates to the chemical potential, while the last term corresponds to the Coulomb interaction. This simple model, which will be discussed in the following sections, has been widely used and gives a good qualitative description for strongly correlated systems.

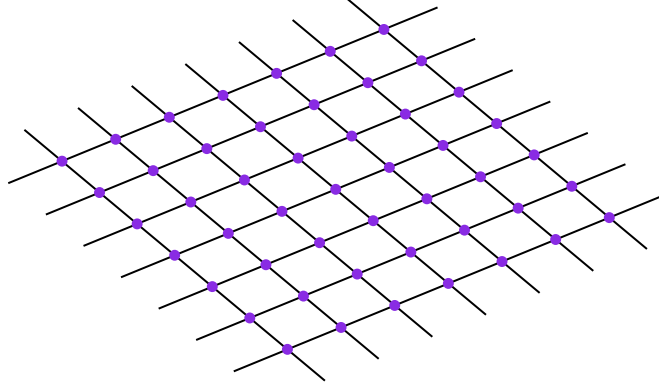


Figure 1.1: illustration for a system with interaction between sites

Let us assume a real system with translational invariance as shown in Fig. 1.1. For a given site, if the number of neighboring sites goes to infinity, the central limit theorem holds so that the fluctuations from site-to-site can be neglected. This means that the influence from other sites can be replaced by an effective medium, *i.e.* all the degrees of freedom on other sites will be integrated out as an external bath to this given site, as shown in Fig. 1.2. Thus the dynamics at this given site (impurity) can be thought of as the interaction (hybridization) of this site with the bath. Moreover, this bath by itself is noninteracting.

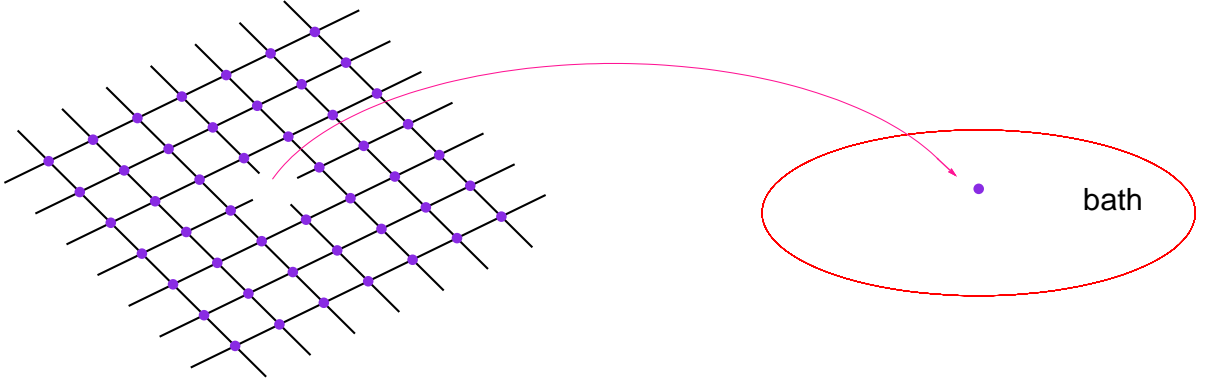


Figure 1.2: illustration of cavity method

Now the effective Hamiltonian derived from Eq. (1.1) can be written in a much clearer way,

$$\mathcal{H} = \sum_{\alpha} \varepsilon_{\alpha} c_{\alpha\sigma}^{\dagger} c_{\alpha\sigma} + U \hat{n}_{\uparrow} \hat{n}_{\downarrow} + \sum_{\sigma} (\varepsilon_f - \mu) \hat{n}_{\sigma} + \sum_{\alpha} \gamma_{\alpha} (c_{\alpha\sigma}^{\dagger} f_{\sigma} + f_{\sigma}^{\dagger} c_{\alpha\sigma}) \quad (1.2)$$

The first term is the energy of the conduction electrons (bath), the second term gives the local

Coulomb interaction for the impurity, the third term denotes the energy of the impurity, the last term is the hybridization term between the impurity and the bath. In the Hamiltonian, the index  $\alpha$  is a degree of freedom of the electronic states of the bath. Thus, the many-body problem has been transferred to a quantum impurity problem. It should be mentioned that the Coulomb interaction only exists on the impurity site.

If the energy of correlated electrons  $\varepsilon_\alpha$  and the hybridization  $\gamma_\alpha$  are known, we can get the Green's function  $\mathcal{G}_\sigma$  for the impurity when the Coulomb interaction strength  $U = 0$ . This Green's function should have all the information of the bath. Therefore, if this Green's function is known, the bath is known. Then we can calculate and get the Green's function  $G_\sigma(i\omega)$  for arbitrary  $U$ . The  $i\omega$  denotes the frequency on the Matsubara axis which will be explained in Chapter 2.

The physical idea of the dynamical mean field theory relies on the observation that the self-energy  $\Sigma(k\sigma, i\omega)$  becomes  $k$  independent in the limit of infinite dimensions, *i.e.*  $\Sigma(k\sigma, i\omega_n) = \Sigma_\sigma(i\omega_n)$ . The calculation of these two quantities are as follows: the self-energy in infinite dimensions can be derived by perturbation theory, which contains only local elements:

$$\Sigma(r_i, r_j, i\omega_n) = \Sigma(i\omega_n)\delta_{i,j} \quad (1.3)$$

where  $i\omega_n$  is the Matsubara frequency.  $r_i$  is the position of  $i$ -th lattice site. The local self-energy only depends on the local Green's function

$$\Sigma(i\omega_n) = \frac{\delta\Psi[G(i\omega_n)]}{\delta G(i\omega_n)} \quad (1.4)$$

where  $\Psi[G(i\omega_n)]$  is the Luttinger-Ward function. The fact that the self-energy is  $k$  independent in infinite dimensions makes the single site treatment exact in the infinite dimension limit if the local fluctuations are treated exactly. When the self-energy is known, we can obtain the lattice Green's function at site  $i$ ,

$$G_{i\sigma}(i\omega) = \frac{1}{N} \sum_k G(k\sigma, i\omega_n) = \frac{1}{N} \sum_k \frac{1}{i\omega_n - \varepsilon_k + \mu - \Sigma_\sigma(i\omega)} \quad (1.5)$$

where  $\mu$  is the chemical potential and  $\varepsilon_k$  is the dispersion. The bare Green's function is the Green's function without interactions

$$G_{i\sigma}^0(i\omega) = \frac{1}{N} \sum_k \frac{1}{i\omega_n - \varepsilon_k + \mu} = \frac{1}{G_\sigma^{-1}(i\omega_n) + \Sigma_\sigma(i\omega_n)} \quad (1.6)$$

From the definition of  $\mathcal{G}_\sigma(i\omega_n)$ , we can get the relation

$$G_{i\sigma}^0(i\omega) = \mathcal{G}_\sigma(i\omega_n) \quad (1.7)$$

and

$$G_{\sigma}^{-1}(i\omega_n) + \Sigma_{\sigma}(i\omega_n) = \mathcal{G}_{\sigma}^{-1}(i\omega_n) \quad (1.8)$$

Thus we have obtained all the information about the bath from the Green's function of the impurity and the self-energy. At the same time, the Green's function and self-energy are also determined by the bath, which is specified by  $\mathcal{G}_{\sigma}$ . Hence, Eq. (1.8) is a **self-consistency** equation. It implies a self-consistent solution of the local quantities for the original lattice problem, which gives the reasoning that the a single impurity coupled to an effective bath is an effective model for the original lattice problem.

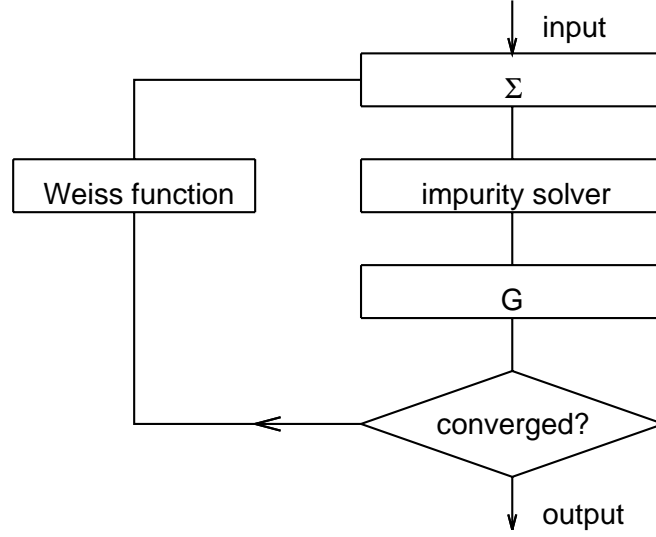


Figure 1.3: Illustration of the DMFT calculation and the relation between DMFT and impurity solver

Although the dynamical mean field theory is derived in the limit  $d \rightarrow \infty$  (or infinite lattice coordination), it has surprising success in providing a good approximation in finite dimensions, even in the low dimension  $d = 3$ , as long as spatial fluctuations are small.

In dynamical mean field theory, all the spatial fluctuations of the self-energy have been neglected, while the local quantum fluctuations are fully taken into account. That's the reason why the theory is called "dynamical". Here the impurity solver describes the local dynamics of the quantum many-body system. Therefore this quantum impurity model remains an interacting many-body problem which needs reliable methods for calculating the local self-energy of the impurity model. Moreover, recently improved dynamical mean field theory has been proposed to include the spatial fluctuations for clusters in momentum space [24] or in real space [25].



By replacing the complicated many-body lattice model with a single impurity model, the degrees of freedom can be greatly reduced and hence the problem is simplified with the dynamical mean field theory. Moreover, the single impurity model has been extensively studied. All the methods that have been developed to solve the Anderson impurity model [11] can be easily used to solve the DMFT equations.

Besides the simplification in calculation, the dynamical mean field theory has its necessity and advantage in physics. Usually the calculation of correlated materials has been done in two different ways. One is the local density approximation (LDA) based on density functional theory (DFT). LDA is a widely used *ab initio* method, which has proven its value in the application to study the electronic structure and properties of simple metals, semiconductors as well as band insulators. However, it fails to predict some strongly correlated materials in agreement with experiments, *e.g.* those materials containing partially filled *d* or *f* bands, because of the strong correlation effect. This is because in LDA the wave like nature is emphasized instead of the atomic feature of the electronic state. So LDA is much more suitable to simulate wide bands contributed by the electrons from outer shells, but poorly to describe the unclosed inner shells. In the LDA+U approach [28], the Coulomb interactions are usually treated in Hartree-Fock approximation, which is not a good approximation to describe the true many-body physics because the self-energy depends on frequency. Though LDA+U has been successful in dealing with the long range ordered insulator state, it fails to describe the paramagnetic state of strongly correlated systems.

Different to LDA schemes, the study of model Hamiltonians provides qualitative understanding of strongly correlated systems because it captures the essence of the frequency dependence of electron-electron interactions. Various approximation schemes have been proposed and applied. However, because of the parameter dependence of the model studies, this kind of method is weak in predictions for new materials. However, the combination of the two approaches mentioned above, *i.e.* LDA+DMFT [26, 27], goes beyond LDA+U and is one of the most promising methods to solve various correlation problems within the framework of DMFT. The combined method has deepened our understanding and demonstrated its success because the DMFT captures the correlation features induced by the on-site Coulomb interaction quite well, while LDA can treat well the periodic potential and the long range part of the Coulomb interaction so that LDA usually gives good parameters which can be used to build the Hamiltonian for real materials. For example, LDA+DMFT nicely describes paramagnetic metals and gives the characteristic three-peak structure: lower and

upper Hubbard bands, and one narrow Kondo peak at the Fermi level.

In the dynamical mean field theory, the most difficult part is the impurity solver where the effective Anderson impurity model has to be solved iteratively. Various impurity solvers have been developed for this purpose. Among them, the most often used impurity solvers are the iterated perturbation theory (IPT) [29, 30, 31], the non-crossing approximation (NCA) [32, 33, 34, 35], the Hubbard I approximation (HIA) [12], the fluctuation exchange (FLEX) approximation [36, 37], the quantum Monte Carlo method (Hirsch-Fye algorithm) (HF-QMC) [10, 38, 39, 40], the continuous time quantum Monte-Carlo method (CTQMC) [41, 42], the exact diagonalization method (ED) [43, 44], the numerical renormalization group method (NRG) [45, 46], the density matrix renormalization group method (DMRG) [47, 48], and the equation-of-motion method (EOM) [49, 50, 51]. However, each impurity solver has its own limitation. The original IPT cannot be applied to the case when the system is away from half-filling. Although the modified IPT can solve this problem, one has to introduce an *ansatz* to interpolate the weak and strong coupling limits. The generalization of IPT to the multi-orbital case requires more assumptions and approximations. NCA cannot yield the Fermi liquid behavior at low energies and in the low temperature limit. The HIA can only be applied to strongly localized electron systems like  $f$  electrons. FLEX works well in the metallic region while it fails in the large  $U$  region. Before the appearance of CTQMC, the HF-QMC was not applicable in the low temperature limit and had serious difficulties in application to multi-orbital systems with spin-flip and pair-hopping terms of the exchange interaction since the Hubbard-Stratonovich transformation [52] cannot be performed in these systems. But even for CTQMC, the requirement to do analytical continuation of the results to the real frequency axis remains, which introduces some uncertainties especially for multi-orbital systems. In the ED method, an additional procedure is required for the discretization of the bath. As a consequence, the method is unable to resolve low-energy features at the Fermi level. Although NRG can give a very precise description of the low-frequency quasiparticle peaks associated with low-energy excitations, it has less precision in the Hubbard bands which are important in calculating the optical conductivity. Furthermore, all the numerically exact impurity solvers QMC, ED, NRG and DMRG are computationally expensive.

However, today, a fast and reliable impurity solver is really urgently needed due to the fact that great achievements have been made in understanding correctly the strongly correlated systems from first principle by combining DMFT and local density approximation (LDA) in density functional theory (DFT), so called LDA+DMFT [27]. The aim of this work is just to construct a fast and

reliable impurity solver based on the EOM method. Equation of motion methods are limited by their decoupling scheme, but EOM has shown its value by working directly on the real frequency axis and at very low temperature. It can be a good candidate for a fast and reliable impurity solver by choosing a suitable decoupling scheme. Our work has already proven this assumption and shown the validity of the EOM method in study of strongly correlated systems with a new impurity solver successfully constructed. To realize this purpose, we have developed a new numerical method based on a genetic algorithm in dealing with the minimization problem and self-consistently solving the integral equations.

### 1.3 Single impurity Anderson model

The impurity solver is the central part of the DMFT so that we should intensively know the physical aspect of the impurity model. Hence, we introduce the single impurity model in this section. The most frequently used impurity model in the dynamical mean theory is the single impurity Anderson model (SIAM), which was proposed by P. W. Anderson over forty years ago [11] and was originally introduced to describe magnetic impurities in weakly correlated non-magnetic metals, *i.e.* the well known Kondo problem. A recent review of the SIAM can be found in the book by A. C. Hewson [53].

In the single impurity Anderson model, a system of an impurity embedded in a metallic host can be described by a Hamiltonian of interacting electrons,

$$\mathcal{H} = \sum_{i=1}^N \left( \frac{\vec{p}_i^2}{2m} + U_{host}(\vec{r}_i) + V_{imp}(\vec{r}_i) \right) + \frac{1}{2} \sum_{i \neq j}^N \frac{e^2}{|\vec{r}_i - \vec{r}_j|} + \sum_{i=1}^N \lambda(\vec{r}_i) \mathbf{l}_i \cdot \sigma_i \quad (1.9)$$

where considering the first sum as three terms, the first term is the kinetic energy of the electrons, the second one is related to the periodic potential  $U_{host}$  in the host metal contributed by the nuclei without the existence of the impurity. The third term  $V_{imp}$  is an additional potential due to the nucleus of the impurity. The Coulomb interactions between the electrons are given by the fourth term, and the spin and orbital interaction is described by the last term. The Coulomb interaction term in the Hamiltonian prohibits perturbational treatments. If the electrons are only weakly correlated, the system can be treated in the framework of density-functional theory (DFT) [54]. For systems with strong local Coulomb interactions, *e.g.* the systems with partially filled  $d$  or  $f$  shells in transition or rare earth elements, DFT based on local density approximation is not sufficient and alternative approaches have to be explored.

One approach is to use simpler model Hamiltonians by considering only the low energy excitations associated with the impurity and neglecting those features not directly related to impurity effects. Such a single impurity model is proposed as

$$\mathcal{H} = \sum_{k\sigma} \varepsilon_k c_{k\sigma}^\dagger c_{k\sigma} + \sum_{\sigma} \varepsilon_f f_{\sigma}^\dagger f_{\sigma} + \frac{U}{2} \sum_{\sigma \neq \sigma'} \hat{n}_{\sigma} \hat{n}_{\sigma'} + \sum_{k\sigma} (V_{k\sigma}^* c_{k\sigma}^\dagger f_{\sigma} + V_{k\sigma} f_{\sigma}^\dagger c_{k\sigma}) \quad (1.10)$$

The first term in this Hamiltonian gives the energy of the conduction electrons, where  $c_{k\sigma}^\dagger$  and  $c_{k\sigma}$  are the corresponding creation and annihilation operators of conduction electrons for Bloch states  $\phi_{k\sigma}(r)$  with the band energy  $\varepsilon_k$ .  $k$  is the wavevector and  $\sigma$  is the spin component. The anticommutation relations are

$$[c_{k\sigma}^\dagger, c_{k'\sigma'}^\dagger]_+ = \delta_{k'k} \delta_{\sigma\sigma'}, \quad [c_{k\sigma}^\dagger, c_{k'\sigma'}]_+ = 0 \quad [c_{k\sigma}, c_{k'\sigma'}]_+ = 0 \quad (1.11)$$

In the model, assumptions have been made that the conduction band is a wide band and the conduction electrons in the system are approximately independent to each other, *i.e.* the Coulomb interaction between the screened conduction electrons is neglected due to the strong delocalization of the wide conduction band.

The second term shows the energy of impurities, where  $\varepsilon_f$  is the energy level of impurity electrons,  $f_{\sigma}^\dagger$  and  $f_{\sigma}$  are the generation and annihilation operators of an electron in  $f - \sigma$  orbital-spin state.

The third term is the Coulomb interaction term, which describes the local Coulomb interactions between  $f$  electrons.  $U$  is the energy that has to be paid for putting a second electron into a singly occupied impurity state, *i.e.* once an energy state with energy  $\varepsilon_f$  has been occupied by one electron, adding one more electron should cost  $\varepsilon_f + U$ . Therefore, one obvious effect of this term is to cause the splitting of the impurity electronic state. Neglecting this term, the Hamiltonian is regarded as the *non-interacting Anderson impurity model*, which has been discussed in detail in A. C. Hewson's book [53].

The last term describes the hybridization between the impurity electronic state and the conduction band with the interaction strength  $V_{k\sigma}$ . The physical picture is that, when the conduction electrons move in the periodic potential, they will be scattered by the impurity. For larger  $V_k$ , the scattering orbital is stronger. Due to the scattering by the impurity, the system shows an additional resistance of conduction electrons at the Fermi level. In experiments, a resistance minimum occurs at a very low temperature when the resistivity contributed by the phonon scattering is suppressed.

This resistance minimum was first observed by W. J. de Haas *et al.* [55]. It was found that the resistance minimum is dependent on the impurity concentration. This phenomenon is caused by the interaction between the local moment and conduction electrons and was first explained by J. Kondo in his work [56]. Such kind of behavior was in honor named as Kondo effect.

The single impurity Anderson model is characterized by the interplay of the delocalization, Coulomb interaction and hybridization, or by the choice of parameters  $U$ ,  $V_{k\sigma}$ ,  $\varepsilon_f$  and  $\varepsilon_k$ . Here we discuss some special and simple systems.

If  $U$  is zero, the Hamiltonian corresponds to the non-interacting system,

$$\mathcal{H} = \sum_{k\sigma} \varepsilon_k c_{k\sigma}^\dagger c_{k\sigma} + \sum_{\sigma} \varepsilon_f f_{\sigma}^\dagger f_{\sigma} + \sum_{k\sigma} (V_{k\sigma}^* c_{k\sigma}^\dagger f_{\sigma} + V_{k\sigma} f_{\sigma}^\dagger c_{k\sigma}) \quad (1.12)$$

Although the localized state and the conduction electronic states are not orthogonal to each other, in a simplified consideration, one can still assume  $\langle f|k \rangle = 0$  because the conduction band is mainly built by the  $s$  or  $p$  orbitals. The equations of motion should be

$$(\omega - \varepsilon_f) \ll f_{\sigma}; f_{\sigma}^\dagger \gg = 1 + \sum_k V_k \ll c_{\sigma}; f_{\sigma}^\dagger \gg \quad (1.13)$$

$$(\omega - \varepsilon_k) \ll c_{\sigma}; f_{\sigma}^\dagger \gg = V_k^* \ll f_{\sigma}; f_{\sigma}^\dagger \gg \quad (1.14)$$

$$(\omega - \varepsilon_k) \ll c_{k\sigma}; c_{k'\sigma}^\dagger \gg = \delta_{kk'} + V_k^* \ll f_{\sigma}; c_{k'\sigma}^\dagger \gg \quad (1.15)$$

$$(\omega - \varepsilon_f) \ll f_{\sigma}; c_{k'\sigma}^\dagger \gg = \sum_{k''} V_{k''} \ll c_{k''\sigma}; c_{k'\sigma}^\dagger \gg \quad (1.16)$$

Then the single electron Green's function for impurity is defined as

$$\ll f_{\sigma}; f_{\sigma}^\dagger \gg = \frac{1}{\omega - \varepsilon_f - \sum_k \frac{V_k^2}{\omega - \varepsilon_k}} \quad (1.17)$$

and the single particle Green's function for conduction electrons is

$$\ll c_{k\sigma}; c_{k'\sigma}^\dagger \gg = \frac{\delta_{kk'}}{\omega - \varepsilon_k} + \frac{V_k^* V_{k'}}{(\omega - \varepsilon_k)(\omega - \varepsilon_{k'})} \ll f_{\sigma}; f_{\sigma}^\dagger \gg \quad (1.18)$$

If the  $V_k$  vanishes (the so called atomic limit), *i.e.* the localized impurity electronic states are decoupled from the conduction electrons, there are three kinds of electronic configurations according to the energy of the system: vacancy ( $E_0 = 0$ ), single electron occupation ( $E_{1,\sigma} = \varepsilon_f$ ) and double electron occupation ( $E_2 = 2\varepsilon_f + U$ ). For the singly occupied state, the impurity energy level  $\varepsilon_f$  should be smaller than the Fermi level while  $\varepsilon_f + U > 0$  so that only one electron occupation is favorable.

If the Coulomb interaction  $U \neq 0$ , a universal three peak structure emerges. The central peak at  $\omega = 0$  is called Kondo peak. The density of states at  $\omega = 0$  is pinned to its non-interacting value  $\rho_0(\omega = 0)$ , which is independent of  $U$  as required by Friedel's sum rule [57]

$$n_{imp} = \int_{-\infty}^{E_F} \Delta\rho(\varepsilon)d\varepsilon = \frac{\eta(\varepsilon_F)}{\pi} \quad (1.19)$$

where  $\eta(\varepsilon)$  is the phase shift. This pinning can be used to check for the reliability of the numerical algorithm.

In the general case, the density of states (DOS) of the impurity is given by

$$\rho(\omega) = -\frac{N}{\pi} \text{Im} \ll f_\sigma; f_\sigma^\dagger \gg \quad (1.20)$$

where  $N$  is the spin and orbital degeneracy. The overall weight should be normalized,

$$\int_{-\infty}^{\infty} \rho(\omega)d\omega = 1 \quad (1.21)$$

For the conduction electrons, the same rule should hold,

$$\int_{-\infty}^{\infty} \rho_0(\varepsilon)d\varepsilon = 1 = \int_{-D}^D \rho_0(\varepsilon)d\varepsilon \quad (1.22)$$

A special case is the so called symmetrical system, when  $2\varepsilon_f + U = 0$ , *i.e.*  $\varepsilon_f = -\frac{U}{2}$ . In this case, the system should possess particle-hole symmetry at zero temperature. The increase of  $U$  from zero leads to the formation of lower and upper Hubbard bands. The position of lower and upper Hubbard bands are shifted from the position of the atomic peaks forward and backward to  $\pm\frac{U}{2}$  due to the level repulsion. If the chemical potential  $\mu$  exists, the two bands are positioned at the energies  $\omega_{up/low} = \pm\frac{U}{2} + \mu$ . At the same time, with increasing  $U$ , the Hubbard bands capture more weight of the density of states and the bands become separated.

## 1.4 Hubbard model

In the Sec. 1.2, we have mentioned the Hubbard model as an example of a lattice model, which is indeed one of the most important models used to study strongly correlated electron systems. The Hubbard model, independently proposed by J. Hubbard, M. C. Gutzwiller, and J. Kanamori almost at the same time in the early sixties [12, 58, 59], is the simplest theoretical lattice model for systems where the electrons are assumed to move by only nearest-neighbor hopping and interact with extremely short range repulsive Coulomb interaction. Some reviews can be found in [60, 61, 62].

In the single band Hubbard model, the Hamiltonian is given by

$$\mathcal{H} = \mathcal{H}_{hop} + \mathcal{H}_{int} \quad (1.23)$$

$$\mathcal{H}_{hop} = - \sum_{ij,\sigma} t_{ij} c_{i\sigma}^\dagger c_{j\sigma} \quad (1.24)$$

$$\mathcal{H}_{int} = U \sum_i n_{i\uparrow} n_{i\downarrow} \quad (1.25)$$

where  $c_{i\sigma}^\dagger$  creates an electron with spin  $\sigma = \uparrow, \downarrow$  at site  $i$ ,  $c_{j\sigma}$  is the corresponding annihilation operator,  $n_i = c_{i\sigma}^\dagger c_{i\sigma}$  is the occupation number operator. These Fermion operators obey the anticommutation relations

$$[c_{i\sigma}^\dagger, c_{j\tau}]_+ = \delta_{ij} \delta_{\sigma\tau} \quad (1.26)$$

and

$$[c_{i\sigma}^\dagger, c_{j\tau}^\dagger]_+ = [c_{i\sigma}, c_{j\tau}]_+ = 0 \quad (1.27)$$

In the Hubbard model, there are two parameters. One parameter  $t_{ij}$ , which is assumed to be real, represents an energy gain of the electrons hopping between different sites. Another parameter  $U$  gives the Coulomb interaction strength which represents the potential energy arising from the charges of electrons. Thus the Hubbard model sets up a quantum mechanical hopping term of electrons and a nonlinear on-site repulsive interaction. In the Hamiltonian given above, the Coulomb interaction term has been given the simplified form with only the strongest part included, for example, the Coulomb interaction between different orbital states has been neglected due to the screening effect.

Neglecting the first term of the Hamiltonian Eq. (1.23), the system becomes a non-hopping system. Neglecting the second term, we obtain the so called "tight binding" band theory. The Hamiltonian containing either the first term or the second term can be diagonalized so that it can be solved analytically. If both of them exist, it is believed that the model will show various non-trivial phenomena, *e.g.* the transition from metal to insulator, ferromagnetism, antiferromagnetism, and superconductivity, due to the competition of two mechanisms. Because of the simplicity of the Hubbard model, and also because the model has captured the essence of strongly correlated systems, the Hubbard model is very widely used. One can find various interesting aspects of strongly correlated electron systems and learn new physical concepts from studying this simplest idealized model.

Usually the band width  $W$  is used as energy scale to compare with the Coulomb interaction parameter  $U$ . For the simple cubic lattice, there is a relation  $W = 2zt$ , where  $z$  is the number of nearest neighbors.

If  $U \gg W$ , the system reaches the atomic limit or strong coupling limit, which corresponds to a strongly correlated system. For  $U$  being infinity, the Hubbard model turns out to be the  $t - J$  model [63, 64], which describes electrons moving on a lattice and forbids the double occupancy on each site. The effective exchange interaction relates to the hopping parameter by

$$J = \frac{4t^2}{U} \quad (1.28)$$

The  $t - J$  model can be solved by a perturbation expansion.

In the weak coupling limit  $U \ll W$ , the Hubbard model describes a Fermi liquid behavior, because the whole system mainly shows the delocalization trends contributed by the hopping term. The most interesting case is the intermediate region between weak and strong coupling, *i.e.*  $U \sim W$ . Many important and interesting properties are shown in this region, *e.g.* the Mott metal-insulator phase transition, due to the competition of two mechanisms. However, in this region the behavior of the system is complex and a full mathematical treatment is difficult.

In history, J. Hubbard showed the splitting of the two Hubbard bands first using the decoupling method, known as Hubbard-I decoupling method. Then, perturbation theory [65, 66] and the Bethe *ansatz* method [17, 67] have been used in later studies. In the limit of dimension  $d = \infty$ , two methods, proposed by Metzner and Vollhardt [9] and Gutzwiller [68], give the exact solution, which has eventually led to the appearance of the dynamical mean field theory. Nowadays, within the framework of DMFT, there are a lot of numerical methods that can be used to solve the Hubbard model through solving Anderson impurity model. This is also the purpose of this thesis.

In the dynamical mean field theory, the local Green's function on a single site is given by the functional equation

$$G(\tau) = -\frac{1}{Z} \int [\mathcal{D}c^\dagger \mathcal{D}c] c_\sigma(\tau) c_\sigma^\dagger(0) e^{-S} \quad (1.29)$$

where  $Z$  is the partition function

$$Z = \int [\mathcal{D}c^\dagger \mathcal{D}c] e^{-S} \quad (1.30)$$

The effective action is given as

$$S = - \int_0^\beta d\tau \int_0^\beta d\tau' \sum_\sigma c_\sigma^\dagger(\tau) \mathcal{G}^{-1}(\tau - \tau') c_\sigma(\tau') + U \int_0^\beta d\tau n_\uparrow(\tau) n_\downarrow(\tau) \quad (1.31)$$



where  $\beta = \frac{1}{kT}$  is the inverse temperature and  $\mathcal{G}^{-1}(\tau - \tau')$  plays a role of Weiss effective field in the mean field theory. It can be shown that

$$\mathcal{G}^{-1}(i\omega_n) = G^{-1}(i\omega_n) + \Sigma(i\omega_n) \quad (1.32)$$

where

$$G(i\omega_n) = \int_0^\beta d\tau e^{i\omega_n\tau} G(\tau) \quad (1.33)$$

$$\mathcal{G}(i\omega_n) = \int_0^\beta d\tau e^{i\omega_n\tau} \mathcal{G}(\tau) \quad (1.34)$$

The local Green's function  $G(i\omega)$  is related to the local self-energy  $\Sigma(i\omega_n)$  by the Dyson equation Eq. (1.5). So it makes a self-consistent set of equations which can be calculated iteratively. One can start with an arbitrary input  $\Sigma_0(i\omega_n)$  and  $\mathcal{G}_0(i\omega_n)$ . If impurity model is solved, one new self-energy can be obtained by the  $\mathcal{G}_0(i\omega_n)$  together with  $G(i\omega_n)$ . Then,  $\mathcal{G}(i\omega_n)$  can be obtained with Dyson equation and Eq.(1.32). The iteration will continue until a self-consistent solution  $(\Sigma, G)$  is reached.

## 1.5 Periodic Anderson model

The periodic Anderson model (also called Anderson lattice model) is another important and frequently used lattice model to study strongly correlated systems, especially heavy Fermion systems. This model was introduced by P. W. Anderson in 1961 [11] to describe the effects of correlations for  $d$  electrons in transition metals. More details of this model can be found in the review paper by C. Noce [69].

As we have mentioned in Sec. 1.3, when localized moments are introduced into a host metal, the system will show unusual behavior in transport properties, especially on a very low energy scale. Usually the rare-earth and actinide elements containing incomplete  $f$  shells will introduce these localized moments. Below a certain temperature, these impurities will act as scattering centers for conduction electrons and enhance the resistivity of the system.

The periodic Anderson model is closely related to the single impurity Anderson model. The difference between them is that the single impurity Anderson model describes an impurity in a metallic host, while the periodic Anderson model has a lattice of impurities. Because the periodic Anderson model captures the essential physics of interactions between the impurities and the conduction electrons of the host metal, it can well describe a large variety of physical phenomena and the main properties of impurity systems.

The original form of the Hamiltonian for periodic Anderson model is as follows:

$$\mathcal{H} = \sum_{ij\sigma} t_{ij} c_{i\sigma}^\dagger c_{j\sigma} + \sum_{j\sigma} \varepsilon_f f_{j\sigma}^\dagger f_{j\sigma} + \frac{U}{2} \sum_{\substack{j,\sigma\sigma' \\ \sigma \neq \sigma'}} \hat{n}_{j\sigma} \hat{n}_{j\sigma'} + \sum_{j,k,\sigma} (V_{k\sigma}^* c_{k\sigma}^\dagger f_{j\sigma} + V_{k\sigma} f_{j\sigma}^\dagger c_{k\sigma}) \quad (1.35)$$

where the first term is the hopping term of conduction electrons, the second term and third term are related to correlated electrons. Here the correlated electrons are localized. When double occupancy exists, the Coulomb repulsive strength is  $U$ . The last term corresponds to the hybridization between the correlated electrons and conduction electrons with hybridization amplitude  $V_k$ . The Fermionic operators in the Hamiltonian are the same as what we have explained in the single impurity Anderson model and fulfill the same anti-commutation relations. The behavior of the impurities will be the consequence of the interplay of the atomic interactions, the exchange interaction and the hybridization term. Moreover, usually only nearest-neighbor hopping is considered.

The Hamiltonian can also be written in the form

$$\mathcal{H} = \sum_{k\sigma} \varepsilon_k c_{k\sigma}^\dagger c_{k\sigma} + \sum_{j\sigma} \varepsilon_f f_{j\sigma}^\dagger f_{j\sigma} + \frac{U}{2} \sum_{\substack{j,\sigma\sigma' \\ \sigma \neq \sigma'}} \hat{n}_{j\sigma} \hat{n}_{j\sigma'} + \sum_{j,k,\sigma} (V_{k\sigma}^* c_{k\sigma}^\dagger f_{j\sigma} + V_{k\sigma} f_{j\sigma}^\dagger c_{k\sigma}) \quad (1.36)$$

with the relation

$$\varepsilon_k = \sum_{ij} t_{ij} e^{-i(\vec{R}_i - \vec{R}_j) \cdot \vec{k}} \quad (1.37)$$

Comparing with the Hamiltonian of the single impurity Anderson model (1.10), the periodic Anderson model requires only one additional summation of  $j$  over the impurities. Actually the two models sometimes also show similar behavior in physical quantities.

Like the Hubbard model, the periodic Anderson model is in the atomic limit when  $t_{ij} = 0$ . In this case, the periodic Anderson model can be exactly solved due to the decoupling of different lattice sites. For the non-interacting case  $U = 0$ , the correlation of electrons for different spin channels vanishes. Then the spin channels are independent to each other so that the model can be simplified. If the hybridization factor  $V_k$  is zero, the conduction band and  $f$  electrons are decoupled. Then the  $f$  electrons gives the trivial case, vacancy, single occupancy and double occupancy, just similar to what we have discussed for the Hubbard model, see Sec. 1.4. For a general case, the periodic Anderson model shows complex behavior and can not be exactly solved.

## 1.6 Summary

In this chapter, we have introduced the motivation of this thesis work and the related scientific background.

The discovery of various exotic properties and interesting phenomena such as heavy Fermions, Mott metal-insulator transition, high  $T_c$  superconductivity, shown in transitional metal oxides and Lanthanides, promotes the study of strongly correlated electron systems. The failure of density functional theory with local density approximation in some insulating systems and the success of studies on model Hamiltonians (parameter dependent) motivates the appearance of the dynamical mean field theory, which has shown the power in LDA+DMFT approaches. Dynamical mean field theory maps the lattice problem to a single impurity problem with self-consistency conditions. Thus the solving of lattice models is transferred to solve the single impurity Anderson model with an additional level of self-consistency. Due to the fact that all existing numerically exact impurity solvers are computationally expensive and usually limited by the available computer powers, a fast and reliable impurity solver is needed, which motivates us to carry out this research.

For the content in order, we have introduced the Mott metal-insulator transition, one of the key phenomena in strongly correlated systems. Then, the objects of our study, the dynamical mean field theory and the single impurity Anderson model, were introduced. In the last part, two important lattice models for the strongly correlated systems, the Hubbard model and the periodic Anderson model, have been introduced briefly.

Moreover, the following Chapters are arranged as follows:

In Chapter 2, starting from the Hamiltonian and Green's function, the equations of motion are derived for the one band single impurity Anderson model with arbitrary spin and orbital degeneracy  $N$ . Then, the decoupling scheme is introduced and employed to close the equations of motion. Finally we derive the single particle Green's function from these closed equations of motion. In this procedure, two different decoupling schemes are applied separately in the calculation of the single particle Green's function. Moreover, besides the calculation on the real frequency axis, we also perform the calculation on the Matsubara axis and use the Pade scheme to transfer the result from imaginary frequencies to real frequencies.

In Chapter 3, based on the equation-of-motion method by taking more equations of motion of higher order Green's function into account, we derive the possible higher order approximations

beyond Lacroix's result. In order to find a suitable decoupling scheme and treatments for dealing with the higher order Green's functions and correlations, future efforts on exploring these formulae in numerical calculations are necessary.

In Chapter 4, a theoretical investigation of multi-band systems is carried out. In most simple cases, we have studied the two band system as a simplest example of multi-band systems. For the sake of simplification, first we neglect the interaction between the two bands through the dispersion. Then we study the system with taking into account the terms generated by the inter-band Coulomb interaction. These terms are treated by the Hartree-Fock as well as Hubbard-I approximation, respectively.

In Chapter 5, we review the detail of the most commonly used numerical techniques and introduce our new numerical method. In our work, we first apply the iterative method with linear mixing, and the iterative method with Broyden mixing. These two methods are difficult to converge in the calculation of dynamical mean field theory. Therefore, a new method based on the genetic algorithm is introduced in our study and proven to be very effective in improving both the convergence speed and the quality of the numerical results.

In Chapter 6, we show the numerical results obtained from the calculations using our new method. We study in detail the single impurity Anderson model, Hubbard model, periodic Anderson model in the single band case with arbitrary spin and orbital degeneracy  $N$  for the two cases when the Coulomb interaction strength  $U$  is infinite or the Coulomb interaction strength  $U$  is finite. It gives numerically comparable result to previous exact results shown in review papers and recent publications. Moreover, we give a first study for the multi-band system and get qualitative results, which will be improved in the future. Finally we summarize all our work in Chapter 7 and make a conclusion.

# Chapter 2 Theory and method

In this chapter, we first explain why the Green's function decoupling method (also called equation-of-motion method) is chosen to construct our impurity solver. Then, the equations of motion are calculated starting from the Hamiltonian of the single impurity Anderson model. Next, the underlying meaning of the decoupling method is explained and the detailed decoupling schemes studied in my work are presented. At last, the analytical results are presented and two different decoupling schemes are compared.

## 2.1 Why have we chosen the EOM method?

The direct purpose of my PhD work is to get a fast and reliable impurity solver for LDA+DMFT, because the impurity solver needs to be repeated again and again even in one-shot LDA+DMFT (this is a LDA+DMFT scheme without self-consistently optimizing the charge density). So a fast and reliable impurity solver is urgently needed. The following are the most frequently used methods: The iterated perturbation theory (IPT) is an analytical method with an expansion of the self-energy up to second order. Moreover, IPT originally can not be applied to the case away from half filling. A modified IPT method can solve this problem, but has to introduce an *ansatz* to interpolate the weak and strong coupling limits, while the generalization of IPT to the multi-band case requires more assumptions and approximations. The Non crossing approximation (NCA) can not yield the Fermi liquid behavior at low energy and in the low temperature limit. The Fluctuation exchange (FLEX) approximation works well in the metallic region while it fails in the large  $U$  region. The Quantum Monte-Carlo method (Hirsch-Fye algorithm) is hard to apply in the low temperature limit and has serious difficulties in application to the multi-orbital system with spin-flip and pair-hopping terms of the exchange interaction. The continuous time quantum Monte-Carlo method, a significantly improved QMC scheme, still requires analytical continuation of the results to real frequency axis, which will introduce some uncertainty especially for multi-orbital systems. In the exact diagonalization (ED) method, an additional procedure is required for the discretization of the bath. It gets also a discrete spectrum (collection of  $\delta$ -peaks). As a consequence, ED is unable to resolve low energy features at the Fermi level. The numerical renormalization group (NRG)

method aims at a very precise description of the low frequency quasiparticle peaks associated with low energy excitations. But NRG has less precision in the Hubbard bands which are important in calculating the optical conductivity. The density matrix renormalization group (DMRG) method is only applicable to the Bethe lattice in the context of DMFT. The equation-of-motion method is an analytical approximation method, whose precision closely depends on the implemented decoupling scheme. Among the numerical methods, NRG, DMRG, QMC, and ED are numerically exact methods, but at the same time all of them are computationally very expensive and strongly limited by available computer resources. Due to the time limitations and the fact that the equation-of-motion method can work on the real axis directly, we have concentrated on the equation-of-motion method to construct our impurity solver. The most important task is to find a suitable decoupling scheme.

## 2.2 Calculation of equations of motions

In this Section, the equations of motion for the Green's function are calculated. Moreover, a machine calculation by computer algebra has been employed as an alternative method in our deriving of the equations of motion, the implementation of the decoupling scheme and the solution of the closed equations. The machine calculation yields results consistent with the calculation by hand and shows its potential applications in the derivation of the Green's function. Some previous works about the derivation of equations of motion can be read in [70, 71, 72, 73, 74].

### 2.2.1 Analytical calculation of equations of motion

For the single impurity Anderson model (SIAM), the Hamiltonian is

$$\mathcal{H} = \sum_{k\sigma} \varepsilon_k c_{k\sigma}^\dagger c_{k\sigma} + \varepsilon_d \sum_{\sigma} d_{\sigma}^\dagger d_{\sigma} + \frac{U}{2} \sum_{\substack{\sigma\sigma' \\ \sigma \neq \sigma'}} \hat{n}_{\sigma} \hat{n}_{\sigma'} + \sum_{k\sigma} (V_{k\sigma}^* c_{k\sigma}^\dagger d_{\sigma} + V_{k\sigma} d_{\sigma}^\dagger c_{k\sigma}) \quad (2.1)$$

where  $\hat{n}_{\sigma} = d_{\sigma}^\dagger d_{\sigma}$ . The first term is the energy of conduction electrons, the second term is the energy of correlated electrons, the third term is the Coulomb interaction on the correlated site and the last term is the hybridization term between conduction electrons and the correlated band. For transition metals or Lanthanides, the Coulomb interaction between  $d$  electrons or  $f$  electrons is strong and comparable to the band energy. So for such systems,  $U$  will be a large energy scale.

In the above Hamiltonian, all the Fermionic operators satisfy the following commutation relations,

$$[c_{k\sigma}^\dagger, c_{k'\sigma'}]_+ = \delta_{kk'} \delta_{\sigma\sigma'} \quad [c_{k\sigma}^\dagger, c_{k'\sigma'}^\dagger]_+ = 0 \quad [c_{k\sigma}, c_{k'\sigma'}]_+ = 0$$

$$[d_{\sigma}^{\dagger}, d_{\sigma'}]_{+} = \delta_{\sigma\sigma'} \quad [d_{\sigma}^{\dagger}, d_{\sigma'}^{\dagger}]_{+} = 0 \quad [d_{\sigma}, d_{\sigma'}]_{+} = 0$$

$$[c_{k\sigma}^{\dagger}, d_{\sigma'}^{\dagger}]_{+} = 0 \quad [c_{k\sigma}^{\dagger}, d_{\sigma'}]_{+} = 0 \quad [c_{k\sigma}, d_{\sigma'}^{\dagger}]_{+} = 0 \quad [c_{k\sigma}, d_{\sigma'}]_{+} = 0$$

In studying the system described by the Hamiltonian of Eq. (2.1), we consider the temperature-dependent retarded Greens function in Zubarev notation [75],

$$G_{AB}(t, t') = \ll A(t); B(t') \gg = -i\Theta(t - t') \langle [A(t), B(t')]_{+} \rangle \quad (2.2)$$

involving the two Heisenberg operators  $A(t)$  and  $B(t')$ .  $\Theta(t - t')$  is the Heavyside function, *i.e.*

$$\Theta(t - t') = \begin{cases} 1 & t > t' \\ 0 & t < t' \end{cases}, \quad (2.3)$$

which determines the defined Green's function as a 'retarded' Green's function.

It is convenient to work with the Fourier transform, which is defined as

$$\ll A; B \gg_{\omega} = \int_{-\infty}^{\infty} dt e^{i\omega(t-t')} \ll A(t); B(t') \gg. \quad (2.4)$$

In the framework of the equation-of-motion method, the Green's function should satisfy the equations of motion

$$\omega \ll A; B \gg = \langle [A, B]_{+} \rangle + \ll [A, \mathcal{H}]; B \gg \quad (2.5)$$

or

$$\omega \ll A; B \gg = \langle [A, B]_{+} \rangle + \ll A; [\mathcal{H}, B] \gg \quad (2.6)$$

where we have neglected the lower indices  $\omega$ . In the following, all the Green's functions depend on frequency  $\omega$ .

For the one particle Green's function  $\ll d_{\sigma}; d_{\sigma}^{\dagger} \gg$ , using the Eq. (2.5), we will determine

$$\omega \ll d_{\sigma}; d_{\sigma}^{\dagger} \gg = \langle [d_{\sigma}, d_{\sigma}^{\dagger}]_{+} \rangle + \ll [d_{\sigma}, \mathcal{H}]; d_{\sigma}^{\dagger} \gg \quad (2.7)$$

Accordingly,

$$[d_\sigma, d_\sigma^\dagger]_+ = 1 \quad (2.8)$$

$$\begin{aligned} [d_\sigma, c_{k\sigma'}^\dagger c_{k\sigma'}] &= d_\sigma c_{k\sigma'}^\dagger c_{k\sigma'} - c_{k\sigma'}^\dagger c_{k\sigma'} d_\sigma \\ &= ([d_\sigma, c_{k\sigma'}^\dagger]_+ - c_{k\sigma'}^\dagger d_\sigma) c_{k\sigma'} - c_{k\sigma'}^\dagger ([c_{k\sigma'}, d_\sigma]_+ - d_\sigma c_{k\sigma'}) \\ &= 0 - c_{k\sigma'}^\dagger d_\sigma c_{k\sigma'} - 0 + c_{k\sigma'}^\dagger d_\sigma c_{k\sigma'} \\ &= 0 \end{aligned} \quad (2.9)$$

$$\begin{aligned} [d_\sigma, d_{\sigma'}^\dagger d_{\sigma'}] &= d_\sigma d_{\sigma'}^\dagger d_{\sigma'} - d_{\sigma'}^\dagger d_{\sigma'} d_\sigma \\ &= ([d_\sigma, d_{\sigma'}^\dagger]_+ - d_{\sigma'}^\dagger d_\sigma) d_{\sigma'} - d_{\sigma'}^\dagger ([d_{\sigma'}, d_\sigma]_+ - d_\sigma d_{\sigma'}) \\ &= [d_\sigma, d_{\sigma'}^\dagger]_+ d_{\sigma'} - d_{\sigma'}^\dagger d_\sigma d_{\sigma'} - 0 + d_{\sigma'}^\dagger d_\sigma d_{\sigma'} \\ &= \delta_{\sigma\sigma'} d_{\sigma'} \end{aligned} \quad (2.10)$$

$$\begin{aligned} [d_\sigma, c_{k\sigma'}^\dagger d_{\sigma'}] &= d_\sigma c_{k\sigma'}^\dagger d_{\sigma'} - c_{k\sigma'}^\dagger d_{\sigma'} d_\sigma \\ &= ([d_\sigma, c_{k\sigma'}^\dagger]_+ - c_{k\sigma'}^\dagger d_\sigma) d_{\sigma'} - c_{k\sigma'}^\dagger ([d_{\sigma'}, d_\sigma]_+ - d_\sigma d_{\sigma'}) \\ &= 0 - c_{k\sigma'}^\dagger d_\sigma d_{\sigma'} - 0 + c_{k\sigma'}^\dagger d_\sigma d_{\sigma'} \\ &= 0 \end{aligned} \quad (2.11)$$

$$\begin{aligned} [d_\sigma, d_{\sigma'}^\dagger c_{k\sigma'}] &= d_\sigma d_{\sigma'}^\dagger c_{k\sigma'} - d_{\sigma'}^\dagger c_{k\sigma'} d_\sigma \\ &= ([d_\sigma, d_{\sigma'}^\dagger]_+ - d_{\sigma'}^\dagger d_\sigma) c_{k\sigma'} - d_{\sigma'}^\dagger ([c_{k\sigma'}, d_\sigma]_+ - d_\sigma c_{k\sigma'}) \\ &= [d_\sigma, d_{\sigma'}^\dagger]_+ c_{k\sigma'} - d_{\sigma'}^\dagger d_\sigma c_{k\sigma'} - 0 + d_{\sigma'}^\dagger d_\sigma c_{k\sigma'} \\ &= \delta_{\sigma\sigma'} c_{k\sigma'} \end{aligned} \quad (2.12)$$

$$\begin{aligned} [d_\sigma, \hat{n}_\zeta \hat{n}_\xi]_{\zeta \neq \xi} &= d_\sigma \hat{n}_\zeta \hat{n}_\xi - \hat{n}_\zeta \hat{n}_\xi d_\sigma \\ &= (\hat{n}_\zeta d_\sigma + [d_\sigma, \hat{n}_\zeta]) \hat{n}_\xi - \hat{n}_\zeta \hat{n}_\xi d_\sigma \\ &= \hat{n}_\zeta d_\sigma \hat{n}_\xi + \delta_{\sigma\zeta} d_\zeta \hat{n}_\xi - \hat{n}_\zeta \hat{n}_\xi d_\sigma \\ &= \hat{n}_\zeta (\hat{n}_\xi d_\sigma + [d_\sigma, \hat{n}_\xi]) + \delta_{\sigma\zeta} (\hat{n}_\xi d_\zeta + [d_\zeta, \hat{n}_\xi]) - \hat{n}_\zeta \hat{n}_\xi d_\sigma \\ &= \hat{n}_\zeta \hat{n}_\xi d_\sigma + \hat{n}_\zeta \delta_{\sigma\xi} d_\xi + \delta_{\sigma\zeta} \hat{n}_\xi d_\zeta + \delta_{\sigma\zeta} \delta_{\zeta\xi} d_\sigma - \hat{n}_\zeta \hat{n}_\xi d_\sigma \\ &= \hat{n}_\zeta \delta_{\sigma\xi} d_\xi + \delta_{\sigma\zeta} \hat{n}_\xi d_\zeta \end{aligned} \quad (2.14)$$

where we obtained the final results in each formula by crossing out the terms with opposite signs and dropping the zero terms (involving  $\delta_{\zeta\xi}$ ) due to  $\zeta \neq \xi$ . Thus we can obtain the equation of



motion of the Green's function  $\ll d_\sigma; d_\sigma^\dagger \gg$

$$\begin{aligned}
(\omega - \varepsilon_d) \ll d_\sigma; d_\sigma^\dagger \gg &= 1 + \frac{U}{2} \sum_{\substack{\zeta\xi \\ \zeta \neq \xi}} \ll \hat{n}_\zeta d_\xi \delta_{\sigma\xi} + \hat{n}_\xi d_\zeta \delta_{\sigma\zeta}; d_\sigma^\dagger \gg + \sum_k V_{k\sigma} \ll c_{k\sigma}; d_\sigma^\dagger \gg \\
&= 1 + U \sum_{\substack{\zeta \\ \zeta \neq \sigma}} \ll \hat{n}_\zeta d_\sigma; d_\sigma^\dagger \gg + \sum_k V_{k\sigma} \ll c_{k\sigma}; d_\sigma^\dagger \gg
\end{aligned} \tag{2.15}$$

For the system with arbitrary degeneracy  $N$ , we consider that the Green's functions with difference only in spin and orbital indices are quantitatively the same (due to degeneracy), *i.e.*

$$\ll \hat{n}_\zeta d_\sigma; d_\sigma^\dagger \gg = \ll \hat{n}_\xi d_\sigma; d_\sigma^\dagger \gg_{\zeta \neq \xi} \tag{2.16}$$

Summing over all spin and orbital indices, we obtain

$$(\omega - \varepsilon_d) \ll d_\sigma; d_\sigma^\dagger \gg = 1 + (N - 1)U \ll \hat{n}_{\sigma'} d_\sigma; d_\sigma^\dagger \gg_{\sigma \neq \sigma'} + \sum_k V_{k\sigma} \ll c_{k\sigma}; d_\sigma^\dagger \gg \tag{2.17}$$

Here, the higher order Green's functions  $\ll \hat{n}_{\sigma'} d_\sigma; d_\sigma^\dagger \gg$  and  $\ll c_{k\sigma}; d_\sigma^\dagger \gg$  appeared on the right hand side of the equation. Similarly, we can calculate the equation of motion of these two higher order Green's functions.

Before calculating the commutators involving operators  $c_{k\sigma}$  and  $c_{k\sigma}^\dagger$  for conduction electrons, we should mention that

$$c_{k\sigma} d_{\sigma'} = [c_{k\sigma}, d_{\sigma'}]_+ - d_{\sigma'} c_{k\sigma} = -d_{\sigma'} c_{k\sigma} \tag{2.18}$$

by using the anti-commutation relation  $[c_{k\sigma}, d_{\sigma'}]_+ = 0$ .

Similarly, we can get the following formulae:

$$c_{k\sigma} d_{\sigma'}^\dagger = [c_{k\sigma}, d_{\sigma'}^\dagger]_+ - d_{\sigma'}^\dagger c_{k\sigma} = -d_{\sigma'}^\dagger c_{k\sigma} \tag{2.19}$$

$$c_{k\sigma}^\dagger d_{\sigma'} = [c_{k\sigma}^\dagger, d_{\sigma'}]_+ - d_{\sigma'} c_{k\sigma}^\dagger = -d_{\sigma'} c_{k\sigma}^\dagger \tag{2.20}$$

$$c_{k\sigma}^\dagger d_{\sigma'}^\dagger = [c_{k\sigma}^\dagger, d_{\sigma'}^\dagger]_+ - d_{\sigma'}^\dagger c_{k\sigma}^\dagger = -d_{\sigma'}^\dagger c_{k\sigma}^\dagger \tag{2.21}$$

As we can see, permuting the  $c$  and  $d$  operators only generates a minus sign. Later, we will simplify

the calculation by just using this conclusion.

$$\begin{aligned}
[c_{k\sigma}, d_{\sigma}^{\dagger}]_+ &= 0 \\
[c_{k\sigma}, c_{k'\sigma'}^{\dagger} c_{k'\sigma'}] &= c_{k\sigma} c_{k'\sigma'}^{\dagger} c_{k'\sigma'} - c_{k'\sigma'}^{\dagger} c_{k'\sigma'} c_{k\sigma} \\
&= ([c_{k\sigma}, c_{k'\sigma'}^{\dagger}]_+ - c_{k'\sigma'}^{\dagger} c_{k\sigma}) c_{k'\sigma'} - c_{k'\sigma'}^{\dagger} ([c_{k'\sigma'}, c_{k\sigma}]_+ - c_{k\sigma} c_{k'\sigma'}) \\
&= [c_{k\sigma}, c_{k'\sigma'}^{\dagger}]_+ c_{k'\sigma'} - c_{k'\sigma'}^{\dagger} c_{k\sigma} c_{k'\sigma'} - 0 + c_{k'\sigma'}^{\dagger} c_{k\sigma} c_{k'\sigma'} \\
&= \delta_{kk'} \delta_{\sigma\sigma'} c_{k'\sigma'}
\end{aligned} \tag{2.22}$$

$$[c_{k\sigma}, d_{\sigma'}^{\dagger} d_{\sigma'}] = 0 \tag{2.23}$$

$$[c_{k\sigma}, \hat{n}_{\zeta} \hat{n}_{\xi}] = 0 \tag{2.24}$$

$$\begin{aligned}
[c_{k\sigma}, c_{k'\sigma'}^{\dagger} d_{\sigma'}] &= c_{k\sigma} c_{k'\sigma'}^{\dagger} d_{\sigma'} - c_{k'\sigma'}^{\dagger} d_{\sigma'} c_{k\sigma} \\
&= c_{k\sigma} c_{k'\sigma'}^{\dagger} d_{\sigma'} + c_{k'\sigma'}^{\dagger} c_{k\sigma} d_{\sigma'} \\
&= [c_{k\sigma}, c_{k'\sigma'}^{\dagger}]_+ d_{\sigma'} \\
&= \delta_{kk'} \delta_{\sigma\sigma'}
\end{aligned} \tag{2.25}$$

$$\begin{aligned}
[c_{k\sigma}, d_{\sigma'}^{\dagger} c_{k'\sigma'}] &= c_{k\sigma} d_{\sigma'}^{\dagger} c_{k'\sigma'} - d_{\sigma'}^{\dagger} c_{k'\sigma'} c_{k\sigma} \\
&= -d_{\sigma'}^{\dagger} c_{k\sigma} c_{k'\sigma'} - d_{\sigma'}^{\dagger} c_{k'\sigma'} c_{k\sigma} \\
&= -d_{\sigma'}^{\dagger} [c_{k\sigma}, c_{k'\sigma'}]_+ \\
&= 0
\end{aligned} \tag{2.26}$$

So the equation of motion of  $\ll c_{k\sigma}; d_{\sigma}^{\dagger} \gg$  is

$$(\omega - \varepsilon_k) \ll c_{k\sigma}; d_{\sigma}^{\dagger} \gg = \sum_{k'} V_{k'\sigma'}^* \delta_{k'k} \delta_{\sigma'\sigma} \ll d_{\sigma'}; d_{\sigma}^{\dagger} \gg = V_{k\sigma} \ll d_{\sigma}; d_{\sigma}^{\dagger} \gg \tag{2.27}$$

yielding,

$$\ll c_{k\sigma}; d_{\sigma}^{\dagger} \gg = \frac{V_{k\sigma} \ll d_{\sigma}; d_{\sigma}^{\dagger} \gg}{\omega - \varepsilon_k} \tag{2.28}$$

Then the EOM of the Green's function  $\ll d_{\sigma}; d_{\sigma}^{\dagger} \gg$  turns out to be

$$(\omega - \varepsilon_d - \sum_k \frac{V_{k\sigma}^2}{\omega - \varepsilon_k}) \ll d_{\sigma}; d_{\sigma}^{\dagger} \gg = 1 + (N-1)U \ll \hat{n}_{\sigma'} d_{\sigma}; d_{\sigma}^{\dagger} \gg_{\sigma \neq \sigma'} \tag{2.29}$$

Similarly, we can obtain the EOMs of other higher order Green's functions

$$\begin{aligned}
& (\omega - \varepsilon_d - U) \ll \hat{n}_{\sigma'} d_{\sigma}; d_{\sigma}^{\dagger} \gg \\
& = \bar{n}_{\sigma'} + (N - 2)U \ll \hat{n}_{\zeta} \hat{n}_{\sigma'} d_{\sigma}; d_{\sigma}^{\dagger} \gg + \sum_k (-V_{k\sigma'}^* \ll c_{k\sigma'}^{\dagger} d_{\sigma'} d_{\sigma}; d_{\sigma}^{\dagger} \gg \\
& + V_{k\sigma} \ll \hat{n}_{\sigma'} c_{k\sigma}; d_{\sigma}^{\dagger} \gg + V_{k\sigma'} \ll d_{\sigma'}^{\dagger} c_{k\sigma'} d_{\sigma}; d_{\sigma}^{\dagger} \gg)
\end{aligned} \tag{2.30}$$

$$\begin{aligned}
& (\omega - \varepsilon_k) \ll \hat{n}_{\sigma'} c_{k\sigma}; d_{\sigma}^{\dagger} \gg \\
& = V_{k\sigma}^* \ll \hat{n}_{\sigma'} d_{\sigma}; d_{\sigma}^{\dagger} \gg + \sum_{k'} (V_{k'\sigma'}^* \ll d_{\sigma'}^{\dagger} c_{k'\sigma'} c_{k\sigma}; d_{\sigma}^{\dagger} \gg - V_{k'\sigma'} \ll c_{k'\sigma'}^{\dagger} d_{\sigma'} c_{k\sigma}; d_{\sigma}^{\dagger} \gg)
\end{aligned} \tag{2.31}$$

$$\begin{aligned}
& (\omega - \varepsilon_k) \ll d_{\sigma'}^{\dagger} c_{k\sigma'} d_{\sigma}; d_{\sigma}^{\dagger} \gg \\
& = \langle d_{\sigma'}^{\dagger} c_{k\sigma'} \rangle + V_{k\sigma'}^* \ll \hat{n}_{\sigma'} d_{\sigma}; d_{\sigma}^{\dagger} \gg + \sum_{k'} (-V_{k'\sigma'}^* \ll c_{\sigma'}^{\dagger} c_{\sigma'} d_{\sigma}; d_{\sigma}^{\dagger} \gg + V_{k'\sigma} \ll d_{\sigma'}^{\dagger} c_{k\sigma'} c_{k'\sigma}; d_{\sigma}^{\dagger} \gg)
\end{aligned} \tag{2.32}$$

$$\begin{aligned}
& (\omega + \varepsilon_k - 2\varepsilon_d) \ll c_{k\sigma'}^{\dagger} d_{\sigma'} d_{\sigma}; d_{\sigma}^{\dagger} \gg \\
& = \langle c_{k\sigma'}^{\dagger} d_{\sigma'} \rangle + U \ll c_{k\sigma'}^{\dagger} d_{\sigma'} d_{\sigma}; d_{\sigma}^{\dagger} \gg + 2(N - 2)U \ll c_{k\sigma'}^{\dagger} \hat{n}_{\zeta} d_{\sigma'} d_{\sigma}; d_{\sigma}^{\dagger} \gg_{\substack{\zeta \neq \sigma \\ \zeta \neq \sigma'}} \\
& - V \ll d_{\sigma'}^{\dagger} d_{\sigma'} d_{\sigma}; d_{\sigma}^{\dagger} \gg + V \sum_{k'} (\ll c_{k\sigma'}^{\dagger} d_{\sigma'} c_{k'\sigma}; d_{\sigma}^{\dagger} \gg + \ll c_{k\sigma'}^{\dagger} c_{k'\sigma'} d_{\sigma}; d_{\sigma}^{\dagger} \gg)
\end{aligned} \tag{2.33}$$

$$\begin{aligned}
& (\omega + \varepsilon_d - \varepsilon_{k'} - \varepsilon_k) \ll d_{\sigma'}^{\dagger} c_{k'\sigma'} c_{k\sigma}; d_{\sigma}^{\dagger} \gg \\
& = -(N - 1)U \ll \hat{n}_{\zeta} d_{\sigma'}^{\dagger} c_{k'\sigma'} c_{k\sigma}; d_{\sigma}^{\dagger} \gg_{\zeta \neq \sigma'} + V (\ll d_{\sigma'}^{\dagger} c_{k'\sigma'} d_{\sigma}; d_{\sigma}^{\dagger} \gg \\
& + \ll \hat{n}_{\sigma'} c_{k\sigma}; d_{\sigma}^{\dagger} \gg - \sum_{k''} \ll c_{k''\sigma'}^{\dagger} c_{k'\sigma'} c_{k\sigma}; d_{\sigma}^{\dagger} \gg)
\end{aligned} \tag{2.34}$$

$$\begin{aligned}
& (\omega + \varepsilon_{k'} - \varepsilon_d - \varepsilon_k) \ll c_{k'\sigma'}^{\dagger} d_{\sigma'} c_{k\sigma}; d_{\sigma}^{\dagger} \gg \\
& = (N - 1)U \ll \hat{n}_{\zeta} c_{k'\sigma'}^{\dagger} d_{\sigma'} c_{k\sigma}; d_{\sigma}^{\dagger} \gg_{\zeta \neq \sigma'} + V (\ll c_{k'\sigma'}^{\dagger} d_{\sigma'} d_{\sigma}; d_{\sigma}^{\dagger} \gg \\
& - \ll \hat{n}_{\sigma'} c_{k\sigma}; d_{\sigma}^{\dagger} \gg + \sum_{k''} \ll c_{k'\sigma'}^{\dagger} c_{k''\sigma'} c_{k\sigma}; d_{\sigma}^{\dagger} \gg)
\end{aligned} \tag{2.35}$$

$$\begin{aligned}
& (\omega + \varepsilon_{k'} - \varepsilon_d - \varepsilon_k) \ll c_{k'\sigma'}^{\dagger} c_{k\sigma'} d_{\sigma}; d_{\sigma}^{\dagger} \gg \\
& = \langle c_{k'\sigma'}^{\dagger} c_{k\sigma'} \rangle + (N - 1)U \ll \hat{n}_{\zeta} c_{k'\sigma'}^{\dagger} c_{k\sigma'} d_{\sigma}; d_{\sigma}^{\dagger} \gg_{\zeta \neq \sigma} + V (\ll c_{k'\sigma'}^{\dagger} d_{\sigma'} d_{\sigma}; d_{\sigma}^{\dagger} \gg \\
& - \ll d_{\sigma'}^{\dagger} c_{k\sigma'} d_{\sigma}; d_{\sigma}^{\dagger} \gg + \sum_{k''} \ll c_{k'\sigma'}^{\dagger} c_{k\sigma'} c_{k''\sigma}; d_{\sigma}^{\dagger} \gg)
\end{aligned} \tag{2.36}$$

Moreover, here we will introduce a small trick in order to simplify the calculation by reducing the number of EOMs for higher order Green's functions. Actually you may notice that six double-c operator Green's functions appear in the first several EOMs, while we only calculated three higher order EOMs. The reason is that here  $k$  and  $k'$  are both momenta running over all  $k$  space. So, if we change the summation order and the symbols in the summation, it does not change the result,

*i. e.*

$$\left\{ \begin{array}{l} \sum_{kk'} \frac{V_{k\sigma'} V_{k'\sigma}}{\omega - \varepsilon_k} \ll d_{\sigma'}^\dagger c_{k\sigma'} c_{k'\sigma}; d_{\sigma'}^\dagger \gg \Rightarrow \sum_{kk'} \frac{V_{k\sigma'} V_{k'\sigma}}{\omega - \varepsilon_{k'}} \ll d_{\sigma'}^\dagger c_{k'\sigma'} c_{k\sigma}; d_{\sigma'}^\dagger \gg \\ \sum_{kk'} \frac{V_{k\sigma'} V_{k'\sigma}}{\omega + \varepsilon_k - 2\varepsilon_d - U} \ll c_{k\sigma'}^\dagger d_{\sigma'} c_{k'\sigma}; d_{\sigma'}^\dagger \gg \Rightarrow \sum_{kk'} \frac{V_{k\sigma'} V_{k'\sigma}}{\omega + \varepsilon_{k'} - 2\varepsilon_d - U} \ll c_{k'\sigma'}^\dagger d_{\sigma'} c_{k\sigma}; d_{\sigma'}^\dagger \gg \\ \sum_{kk'} \frac{V_{k\sigma'} V_{k'\sigma}}{\omega + \varepsilon_k - 2\varepsilon_d - U} \ll c_{k\sigma'}^\dagger c_{k'\sigma'} d_{\sigma}; d_{\sigma'}^\dagger \gg \Rightarrow \sum_{kk'} \frac{V_{k\sigma'} V_{k'\sigma}}{\omega + \varepsilon_{k'} - 2\varepsilon_d - U} \ll c_{k'\sigma'}^\dagger c_{k\sigma'} d_{\sigma}; d_{\sigma'}^\dagger \gg \end{array} \right. \quad (2.37)$$

On the other hand, in order to make the formulae more clearly readable, we will introduce some abbreviations, which will be used later.

$$\begin{aligned} G_d &= \ll d_{\sigma}; d_{\sigma}^\dagger \gg, & G_c &= \ll c_{k\sigma}; d_{\sigma}^\dagger \gg, & G_{nd} &= \ll \hat{n}_{\sigma'} d_{\sigma}; d_{\sigma}^\dagger \gg \\ G_{nc} &= \ll \hat{n}_{\sigma'} c_{k\sigma}; d_{\sigma}^\dagger \gg, & G_{dcd} &= \ll d_{\sigma'}^\dagger c_{k\sigma'} d_{\sigma}; d_{\sigma}^\dagger \gg, & G_{cdd} &= \ll c_{k\sigma'}^\dagger d_{\sigma'} d_{\sigma}; d_{\sigma}^\dagger \gg \\ G_{dc'c} &= \ll d_{\sigma'}^\dagger c_{k'\sigma'} c_{k\sigma}; d_{\sigma}^\dagger \gg, & G_{c'dc} &= \ll c_{k'\sigma'}^\dagger d_{\sigma'} c_{k\sigma}; d_{\sigma}^\dagger \gg, & G_{c'cd} &= \ll c_{k'\sigma'}^\dagger c_{k\sigma'} d_{\sigma}; d_{\sigma}^\dagger \gg \\ G_{nnd} &= \ll \hat{n}_{\zeta} \hat{n}_{\sigma'} d_{\sigma}; d_{\sigma}^\dagger \gg, & G_{nnc} &= \ll \hat{n}_{\zeta} \hat{n}_{\sigma'} c_{k\sigma}; d_{\sigma}^\dagger \gg, & G_{ndcd} &= \ll \hat{n}_{\zeta} d_{\sigma'}^\dagger c_{k\sigma'} d_{\sigma}; d_{\sigma}^\dagger \gg \end{aligned}$$

Here, we used the "d" label for  $d$  operator in all channels, the "c" label for  $c$  operator in all channels, the "c'" label for  $c$  or  $c^+$  operators carrying a  $k'$  index, while "n" labels  $\hat{n}$  in all channels. For those Green's functions we did not mention here, *e.g.*  $G_{dcc'}$ ,  $G_{cdc'}$ ,  $G_{cc'd}$ , we will use the same rule.

Finally, we give the definition of the hybridization function

$$\Delta(\omega) = \sum_k \frac{V_{k\sigma}^2}{\omega - \varepsilon_k} \quad (2.38)$$

and then we list all necessary EOMs as follows:

$$(\omega - \varepsilon_k - \Delta)G_d = 1 + (N - 1)G_{nd} \quad (2.39)$$

$$(\omega - \varepsilon_d - U)G_{nd} = \bar{n}_{\sigma'} + (N - 2)UG_{nnd} + V \sum_k (G_{nc} + G_{dcd} - G_{cdd}) \quad (2.40)$$

$$V \sum_k G_{nc} = \sum_k \frac{V^2}{\omega - \varepsilon_k} G_{nd} + \sum_{kk'} \frac{V^2}{\omega - \varepsilon_k} (G_{dc'c} - G_{c'dc}) \quad (2.41)$$

$$V \sum_k G_{dcd} = \sum_k \frac{V \langle d_{\sigma'}^\dagger c_{k\sigma'} \rangle}{\omega - \varepsilon_k} + \sum_k \frac{V^2}{\omega - \varepsilon_k} G_{nd} - \sum_{kk'} \frac{V^2}{\omega - \varepsilon_k} G_{c'cd} + \sum_{kk'} \frac{V^2}{\omega - \varepsilon_{k'}} G_{dc'c} \quad (2.42)$$

$$V \sum_k G_{cdd} = \sum_k \frac{V \langle d_{\sigma'}^\dagger c_{k\sigma'} \rangle + V(N - 2)UG_{ncdd} - V^2 G_{nd}}{\omega + \varepsilon_k - 2\varepsilon_d - U} + \sum_{kk'} \frac{V^2}{\omega + \varepsilon_{k'} - 2\varepsilon_d - U} (G_{c'dc} + G_{c'cd}) \quad (2.43)$$

$$(\omega + \varepsilon_d - \varepsilon_{k'} - \varepsilon_k)G_{dc'c} = -(N - 1)UG_{ndc'c} + V(G_{dc'd} + G_{nc} - \sum_{k''} G_{c''c'}) \quad (2.44)$$

$$(\omega + \varepsilon_{k'} - \varepsilon_d - \varepsilon_k)G_{c'dc} = (N - 1)UG_{nc'dc} + V(G_{c'dd} - G_{nc} + \sum_{k''} G_{c'c''}) \quad (2.45)$$

$$(\omega + \varepsilon_{k'} - \varepsilon_d - \varepsilon_k)G_{c'cd} = \langle c_{k'\sigma'}^\dagger c_{k\sigma'} \rangle + (N - 1)UG_{nc'cd} + V(G_{c'dd} - G_{dcd} + \sum_{k''} G_{c'c''}) \quad (2.46)$$

### 2.2.2 Machine calculation and symbol manipulation

In our calculation of the equations of motion of Green's functions and implementation of the decoupling scheme, besides the calculation by hand, we have also tried and successfully employed the machine calculation with *FORM* [76], an algebraic programming language that was specifically designed to manipulate large formulae and developed by Jos A.M. Vermaseren at NIKHEF (the Dutch Institute for Nuclear and High-Energy Physics).

With our code written with *FORM*, we have reexamined our calculation and confirmed the result. We have found that *FORM* is a very useful tool in the derivation of large sets of equations. Here we just give a brief introduction to my idea how to calculate the equations of motion and how to do the decoupling. For the *FORM* language, please see the manual which is available on its website.

To calculate the equations of motion, we first defined each kind of operator that appears in a Green's function and the Hamiltonian as symbols. The Green's functions are defined as functions, while the Hamiltonian is stated as a local expression in *FORM*. Then we calculate the relevant (anti)commutators, *e.g.*  $[A, \mathcal{H}]$ . Secondly we input the rule for the order of the arrangement of all the operators, together with the permutation relations for these operators. Then we rearrange the operators in the calculated (anti)commutators and bring them into our predefined order. Finally, we remove the zero terms generated in this rearrangement. Hence, the expanded equations of motion are obtained.

When the equations of motion are obtained, we input the rule of the decoupling scheme about which Green's function should be decoupled and how it is decoupled. Doing this replacement, we get the closed set of equations of motion at the level we designed. Then we solve this closed set of equations of motion by matrix manipulation. Thus, the single particle Green's function is automatically calculated. One example of the *FORM* code has been given in Appendix A.

## 2.3 Decoupling Scheme and approximations

The aim of the decoupling scheme is to decouple the equations of motion in order to close the equation system by expressing higher order Green's functions with lower order Green's functions. It's a necessary step to solve the equations in a manner of certain approximation otherwise more higher order Green's functions and their equations of motion will appear. In the decoupling scheme, the higher order Green's function and those functions whose equation of motion is excluded from

the closed set of equations will be decoupled according to physical considerations or the level of approximation (normally by the order of  $U$  or  $V$ ).

Based on different considerations in theory, people have tried and implemented a lot of different decoupling schemes in their studies. Here we will first introduce two historical lower order approximations, and then mainly study and compare two different decoupling schemes: Lacroix's decoupling [70] and Wang's decoupling scheme [77].

### 2.3.1 Mean field approximation and Hubbard-I approximation

The mean field approximation is the most simple approximation, where the correlation is neglected and electrons are treated as moving in the potential produced by all the other electrons, *i.e.*

$$\ll \hat{n}_{\sigma'} d_{\sigma}; d_{\sigma}^{\dagger} \gg \approx \bar{n}_{\sigma'} \ll d_{\sigma}; d_{\sigma}^{\dagger} \gg \quad (2.47)$$

Then the equation of motion turns out to be

$$(\omega - \varepsilon_d - \Delta)G_d = 1 + (N - 1)U\bar{n}_{\sigma'}G_d \quad (2.48)$$

namely

$$G_d = \frac{1}{\omega - \varepsilon_d - \Delta - (N - 1)U\bar{n}_{\sigma'}} \quad (2.49)$$

This can be compared with the tight-binding result

$$G_d = \frac{1}{\omega - \varepsilon_d - \Delta} \quad (2.50)$$

In Fig 2.1, we can see that the mean field approximation only gives a shift compared to the local Green's function  $G_0$  in the non-interacting case. So it's too simple to describe the correct physics of strongly correlated systems.

The Hubbard-I approximation is a higher order approximation than the mean field approximation. In Hubbard-I approximation,

$$\ll d_{\sigma'}^{\dagger} c_{k\sigma'} d_{\sigma}; d_{\sigma}^{\dagger} \gg \approx \langle d_{\sigma'}^{\dagger} c_{k\sigma'} \rangle \ll d_{\sigma}; d_{\sigma}^{\dagger} \gg \quad (2.51)$$

$$\ll c_{k\sigma'}^{\dagger} d_{\sigma'} d_{\sigma}; d_{\sigma}^{\dagger} \gg \approx \langle c_{k\sigma'}^{\dagger} d_{\sigma'} \rangle \ll d_{\sigma}; d_{\sigma}^{\dagger} \gg \quad (2.52)$$

$$\ll d_{\sigma'}^{\dagger} c_{k'\sigma'} c_{k\sigma}; d_{\sigma}^{\dagger} \gg \approx \langle d_{\sigma'}^{\dagger} c_{k'\sigma'} \rangle \ll c_{k\sigma}; d_{\sigma}^{\dagger} \gg \quad (2.53)$$

$$\ll c_{k'\sigma'}^{\dagger} d_{\sigma'} c_{\sigma}; d_{\sigma}^{\dagger} \gg \approx \langle c_{k'\sigma'}^{\dagger} d_{\sigma'} \rangle \ll c_{k\sigma}; d_{\sigma}^{\dagger} \gg \quad (2.54)$$

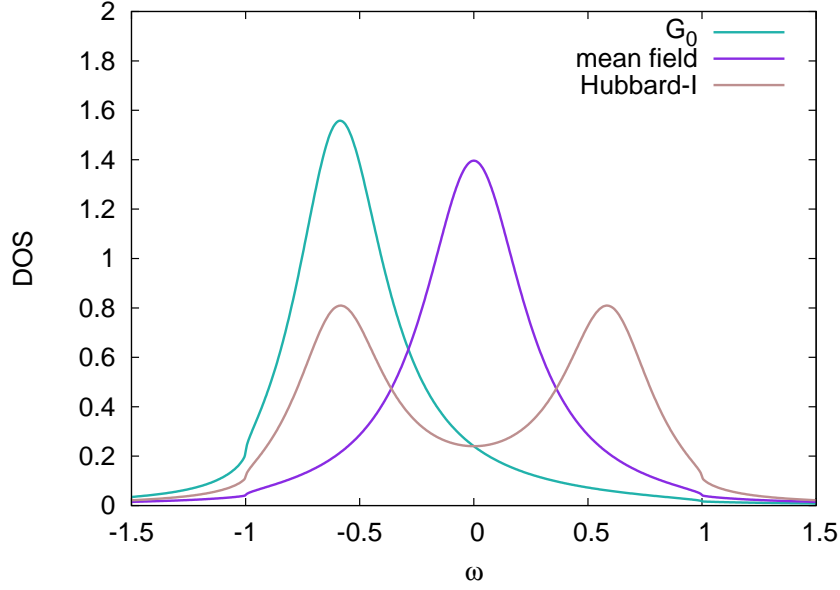


Figure 2.1: Comparison of mean field approximation and Hubbard-I approximation for half-filling case on the Bethe lattice,  $G_0$  is the non-interacting local Green's function

Using the relation  $\langle d_{\sigma'}^\dagger c_{k\sigma'} \rangle = \langle c_{k\sigma'}^\dagger d_{\sigma'} \rangle$  and considering  $V_{k\sigma}^* = V_{k\sigma} = V$ , for the  $N = 2$  case, the Eq. (2.40) turns out to be

$$(\omega - \varepsilon_d - U)G_{nd} = \bar{n}_{\sigma'} + VG_{nc} \quad (2.55)$$

and Eq. (2.41) now is

$$(\omega - \varepsilon_k)G_{nc} = VG_{nd} \quad (2.56)$$

Solving these two equations, we can get

$$G_d = \frac{1 - \frac{\bar{n}_{\sigma'}}{\omega - \varepsilon_d - \Delta - U}}{\omega - \varepsilon_k - \Delta} \quad (2.57)$$

which can be written as

$$G_d = \frac{1 - \bar{n}_{\sigma'}}{\omega - \varepsilon_d - \Delta} + \frac{\bar{n}_{\sigma'}}{\omega - \varepsilon_d - \Delta - U} \quad (2.58)$$

We can see that the equation has two poles, one related to the lower Hubbard band, one related to the upper Hubbard band in Fig 2.1. The Hubbard-I approximation gives the two peak structure of the two Hubbard bands. However, the Hubbard-I approximation has no Kondo peak at the Fermi level. So the Hubbard-I approximation is also a too simple approximation which can not capture the feature of strongly correlated systems. Therefore, we need to pursue a more precise

approximation from now on. Here we will introduce two kinds of decoupling schemes beyond the Hubbard-I approximation: the Lacroix's decoupling scheme and the Wang's decoupling scheme.

### 2.3.2 Lacroix's decoupling scheme

In the Lacroix's decoupling scheme [70], it is assumed that

$$G_{dc'c} = \langle d_{\sigma'}^\dagger c_{k'\sigma'} \rangle G_c \quad (2.59)$$

$$G_{c'dc} = \langle c_{k'\sigma'}^\dagger d_{\sigma'} \rangle G_c \quad (2.60)$$

$$G_{c'cd} = \langle c_{k'\sigma'}^\dagger c_{k\sigma'} \rangle G_d \quad (2.61)$$

$$G_{nnd} \approx \bar{n}_\zeta G_{nd} \quad (2.62)$$

$$G_{ncdd} \approx \bar{n}_\zeta G_{cdd} \quad (2.63)$$

Implementing the decoupling scheme and considering  $\langle d_{\sigma'}^\dagger c_{k\sigma'} \rangle = \langle c_{k\sigma'}^\dagger d_{\sigma'} \rangle$  because they are conjugate terms, we can obtain the EOMs

$$(\omega - \varepsilon_k) G_{nc} = V_k G_{nd} \quad (2.64)$$

$$(\omega - \varepsilon_k) G_{dcd} = \langle d_{\sigma'}^\dagger c_{k\sigma'} \rangle + V_k G_{nd} + \sum_{k'} V_{k'} (\langle d_{\sigma'}^\dagger c_{k\sigma'} \rangle G_{c'} - \langle c_{k'\sigma'}^\dagger c_{k\sigma'} \rangle G_d) \quad (2.65)$$

$$\begin{aligned} (\omega + \varepsilon_k - 2\varepsilon_d - U) G_{cdd} &= \langle c_{k\sigma'}^\dagger d_{\sigma'} \rangle + 2(N-2)U\bar{n}_\zeta G_{cdd} - V_k G_{nd} \\ &+ \sum_{k'} V_{k'} (\langle c_{k\sigma'}^\dagger d_{\sigma'} \rangle G_{c'} + \langle c_{k\sigma'}^\dagger c_{k'\sigma'} \rangle G_d) \end{aligned} \quad (2.66)$$

Solving these equations, we can get

$$(\omega - \varepsilon_d - U - 2\Delta - \tilde{\Delta}) G_{nd} = \bar{n}_\sigma + \sum_k \left( \frac{V_k \langle d_{\sigma'}^\dagger c_{k\sigma'} \rangle}{\omega - \varepsilon_k} - \frac{V_k \langle d_{\sigma'}^\dagger c_{k\sigma'} \rangle}{\omega + \varepsilon_k - 2\varepsilon_d - U - 2(N-2)U\bar{n}_\zeta} \right) \quad (2.67)$$

$$\begin{aligned} &+ \sum_{k'} \frac{V_{k'}^2}{\omega - \varepsilon_{k'}} \sum_k \left( \frac{V_k \langle d_{\sigma'}^\dagger c_{k\sigma'} \rangle}{\omega - \varepsilon_k} - \frac{V_k \langle d_{\sigma'}^\dagger c_{k\sigma'} \rangle}{\omega + \varepsilon_k - 2\varepsilon_d - U - 2(N-2)U\bar{n}_\zeta} \right) \\ &- \sum_{kk'} \left( \frac{V_k V_{k'} \langle c_{k'\sigma'}^\dagger c_{k\sigma'} \rangle}{\omega - \varepsilon_k} + \frac{V_k V_{k'} \langle c_{k'\sigma'}^\dagger c_{k\sigma'} \rangle}{\omega + \varepsilon_k - 2\varepsilon_d - U - 2(N-2)U\bar{n}_\zeta} \right) \end{aligned} \quad (2.68)$$

where we have abbreviated

$$\tilde{\Delta}(\omega) = \sum_k \frac{V_k^2}{\omega + \varepsilon_k - 2\varepsilon_d - U - 2(N-2)U\bar{n}_\zeta} \quad (2.69)$$

Then we can get the Green's function we will mainly study,

$$G_d = \frac{1 + \frac{(N-1)U}{\omega - \varepsilon_d - U - 2\Delta - \tilde{\Delta}} (\bar{n}_\sigma + I_1)}{\omega - \varepsilon_d - \Delta - \frac{(N-1)U}{\omega - \varepsilon_d - U - 2\Delta - \tilde{\Delta}} (\Delta \cdot I_1 + I_2)} \quad (2.70)$$



with

$$I_1 = \sum_k \left( \frac{V_k \langle d_{\sigma'}^\dagger c_{k\sigma'} \rangle}{\omega - \varepsilon_k} - \frac{V_k \langle d_{\sigma'}^\dagger c_{k\sigma'} \rangle}{\omega + \varepsilon_k - 2\varepsilon_d - U - 2(N-2)U\bar{n}_\zeta} \right) \quad (2.71)$$

$$I_2 = - \sum_{kk'} \left( \frac{V_k V_{k'} \langle c_{k'\sigma'}^\dagger c_{k\sigma'} \rangle}{\omega - \varepsilon_k} + \frac{V_k V_{k'} \langle c_{k'\sigma'}^\dagger c_{k\sigma'} \rangle}{\omega + \varepsilon_k - 2\varepsilon_d - U - 2(N-2)U\bar{n}_\zeta} \right) \quad (2.72)$$

This is the general result for arbitrary spin and orbital degeneracy  $N$  and in the finite  $U$  case. One point should be mentioned here: there is a minor difference to the result in Lacroix's paper [71] and Lacroix's original result is not useful for DMFT. For convenience to compare with the Hubbard-I result (2.58), we have separated the result also into two parts,

$$G_d = \frac{1 - A_1}{\omega - \varepsilon_d - \Delta - \frac{UA_2}{\omega - \varepsilon_d - U - (N-2)U\bar{n}_{\sigma'} - 2\Delta - \bar{\Delta}}} + \frac{A_1}{\omega - \varepsilon_d - \Delta - \frac{UA_2 - U(\Delta + \bar{\Delta})}{\omega - \varepsilon_d - U - (N-2)U\bar{n}_{\sigma'} - 2\Delta - \bar{\Delta}}} \quad (2.73)$$

The first term corresponds to the lower Hubbard band, and the second term is corresponding to the upper Hubbard band. For the detailed derivation, please see Appendix B.

When the Coulomb interaction strength  $U \rightarrow \infty$ , the expression for the single particle Green's function is much simpler,

$$G_d = \frac{1 - (N-1) \left( \bar{n}_{\sigma'} + \sum_k \frac{V_{k\sigma'} \langle d_{\sigma'}^\dagger c_{k\sigma'} \rangle}{\omega - \varepsilon_k} \right)}{\omega - \varepsilon_d - \Delta + (N-1) \left( \Delta \cdot \sum_k \frac{V_{k\sigma'} \langle d_{\sigma'}^\dagger c_{k\sigma'} \rangle}{\omega - \varepsilon_k} - \sum_{kk'} \frac{V_k V_{k'} \langle c_{k'\sigma'}^\dagger c_{k\sigma'} \rangle}{\omega - \varepsilon_k} \right)} \quad (2.74)$$

### 2.3.3 Wang's decoupling scheme

In the paper of Wang *et al.* [77], a new idea about connected Green's functions has been introduced. It was considered that the Green's function equals the sum of connected Green's function and correlation terms, i.e.

$$G^{(2)}(1, 2; 1', 2') = G_c^{(2)}(1, 2; 1', 2') + \hat{A}p_{(1', 2')} \hat{S}p_{(2, 2')} G(1; 1') G(2; 2'), \quad (2.75)$$

$$G^{(3)}(1, 2, 3; 1', 2', 3') = G_c^{(3)}(1, 2, 3; 1', 2', 3') + \hat{A}p_{(1', 2', 3')} \hat{S}p_{(2, 3; 2', 3')} \\ \times [G(1; 1') G^{(2)}(2, 3; 2', 3') + G_c^{(2)}(1, 2; 1', 2') G(3; 3')], \quad (2.76)$$

$$G^{(n)}(1, \dots, n; 1', \dots, n') = G_c^{(n)}(1, \dots, n; 1', \dots, n') + \hat{A}p_{(1', \dots, n')} \hat{S}p_{(2, \dots, n; 2', \dots, n')} \\ \times \sum_{k=1}^{n-1} G_c^{(k)}(1, \dots, k; 1', \dots, k') G^{(n-k)}((k+1), \dots, n; (k+1)', \dots, n') \quad (2.77)$$

where  $G_c^{(2)}$  means 2-particle connected Green's function (for the one-particle Green's function, there is no difference between Green's function and connected Green's function),  $\hat{A}p_{(i, j, k)}$  denotes

antisymmetrization for indices  $(i, j, k)$ ,  $\hat{S}p_{(\dots, \dots)}$  denotes symmetrization of pairs  $(i, i')$  and  $(j, j')$ . In combining the operations  $\hat{S}p$  and  $\hat{A}p$ , the repeated terms should be omitted. In this thesis, we refer to this decoupling scheme as "Wang's decoupling scheme".

The connected Green's function means the residual after removing the parts that have been described by the products of lower order Green's functions and correlations. Hence the connected Green's function is not always small. How to treat the connected Green's functions will depend on specific Green's functions and the precision of the approximation that one wants to approach.

Now we make the lowest two order and three order cluster expansions of the Green's functions to show the effect of these permutation and anti-permutation operators and how to get the connected Green's functions. For the two-particle Green's function,

$$\begin{aligned} G^{(2)}(1, 2; 1', 2') &= G_c^{(2)}(1, 2; 1', 2') + \hat{A}p_{(1', 2')} \hat{S}p_{(2, 2')} G(1; 1') G(2; 2') \\ &= G_c^{(2)}(1, 2; 1', 2') + G(1, 1') G(2, 2') - G(1, 2') G(2, 1') \end{aligned} \quad (2.78)$$

For the three-particle Green's function

$$\begin{aligned} G^{(3)}(1, 2, 3; 1', 2', 3') &= G_c^{(3)}(1, 2, 3; 1', 2', 3') + G(1, 1') G(2, 2') G(3, 3') \\ &\quad - G(1, 2') G(2, 1') G(3, 3') - G(1, 3') G(2, 2') G(3, 1') \\ &\quad - G(1, 1') G(2, 3') G(3, 2') + G(1, 2') G(2, 3') G(3, 1') \\ &\quad + G(1, 3') G(2, 1') G(3, 2') + G(1, 1') G_c^{(2)}(2, 3; 2', 3') \\ &\quad - G(1, 2') G_c^{(2)}(2, 3; 1', 3') - G(1, 3') G_c^{(2)}(2, 3; 2', 1') \\ &\quad + G_c^{(2)}(1, 2; 1', 2') G(3, 3') - G_c^{(2)}(1, 2; 3', 2') G(3, 1') \\ &\quad - G_c^{(2)}(1, 2; 1', 3') G(3, 2') + G_c^{(2)}(1, 3; 1', 3') G(2, 2') \\ &\quad - G_c^{(2)}(1, 3; 2', 3') G(2, 1') - G_c^{(2)}(1, 3; 1', 2') G(2, 3') \end{aligned} \quad (2.79)$$

Employing this cluster expansion scheme on Green's functions, we can get

$$\begin{aligned} \ll \hat{n}_{d\sigma'} d_\sigma, d_\sigma^\dagger \gg &= \ll \hat{n}_{d\sigma'} d_\sigma, d_\sigma^\dagger \gg_c + \langle \hat{n}_{d\sigma'} \rangle \ll d_\sigma, d_\sigma^\dagger \gg - \langle d_\sigma d_{\sigma'} \rangle \ll d_{\sigma'}^\dagger, d_\sigma^\dagger \gg \\ &= \ll \hat{n}_{d\sigma'} d_\sigma, d_\sigma^\dagger \gg_c + \langle \hat{n}_{d\sigma'} \rangle \ll d_\sigma, d_\sigma^\dagger \gg \end{aligned} \quad (2.80)$$

where we have considered the correlation terms involving two annihilation operators with different spin indices as zero, *i.e.*

$$\langle d_\sigma d_{\sigma'} \rangle = 0,$$

which is coming from the conservation of particle numbers. Such kinds of terms are non-zero only for superconductor<sup>1</sup>. Similarly, the single particle Green's function and correlation terms involving two creation operators are also treated as zero, *i.e.*

$$\ll d_{\sigma'}^{\dagger}, d_{\sigma}^{\dagger} \gg = -i \langle \hat{T} d_{\sigma'}^{\dagger} d_{\sigma}^{\dagger} \rangle = -i \langle \hat{T} d_{\sigma} d_{\sigma'} \rangle = 0 \quad (2.81)$$

where we have used the condition of Hermiticity  $\langle d_{\sigma'}^{\dagger}, d_{\sigma}^{\dagger} \rangle = \langle d_{\sigma}^{\dagger}, d_{\sigma'}^{\dagger} \rangle^{\dagger} = \langle d_{\sigma} d_{\sigma'} \rangle$ . Using the same rule, we can get the expansion for all other necessary Green's functions. Here we write them as previously using symbols for abbreviations,

$$G_{nd} = G_{nd}^c + \bar{n}_{\sigma'} G_d \quad (2.82)$$

$$G_{nc} = G_{nc}^c + \bar{n}_{\sigma'} G_c \quad (2.83)$$

$$G_{dcd} = G_{dcd}^c + \langle d_{\sigma'}^{\dagger} c_{k\sigma'} \rangle G_d \quad (2.84)$$

$$G_{cdd} = G_{cdd}^c + \langle c_{k\sigma'}^{\dagger} d_{\sigma'} \rangle G_d \quad (2.85)$$

$$G_{dcc} = G_{dcc}^c + \langle d_{\sigma'}^{\dagger} c_{k'\sigma'} \rangle G_c \quad (2.86)$$

$$G_{cdc} = G_{cdc}^c + \langle c_{k'\sigma'}^{\dagger} d_{\sigma'} \rangle G_c \quad (2.87)$$

$$G_{ccd} = G_{ccd}^c + \langle c_{k'\sigma'}^{\dagger} c_{k\sigma'} \rangle G_d \quad (2.88)$$

$$G_{ccc} = G_{ccc}^c + \langle c_{k'\sigma'}^{\dagger} c_{k\sigma'} \rangle G_c \quad (2.89)$$

$$G_{nnd} = G_{nnd}^c + \bar{n}_{\zeta} G_{nd} + \langle \hat{n}_{\zeta} \hat{n}_{\sigma'} \rangle_c G_d + \bar{n}_{\sigma'} G_{n(\zeta)d}^c \quad (2.90)$$

$$G_{ncdd} = G_{ncdd}^c + \bar{n}_{\zeta} G_{cdd} + \langle \hat{n}_{\zeta} c_{\sigma'}^{\dagger} d_{\sigma} \rangle_c G_d + \langle c_{\sigma'}^{\dagger} d_{\sigma} \rangle G_{n(\zeta)d}^c \quad (2.91)$$

Then we can further obtain the needed equations of motion for the connected Green's functions,

$$(\omega - \varepsilon_d - \Delta) G_d = 1 + (N - 1) U G_{nd} \quad (2.92)$$

$$(\omega - \varepsilon_d - U - (N - 2) U \bar{n}_{\zeta}) G_{nd} \quad (2.93)$$

$$= \bar{n}_{\sigma'} + (N - 2) U (G_{nnd}^c + \langle \hat{n}_{\sigma'} \hat{n}_{\zeta} \rangle_c G_d + \bar{n}_{\sigma'} G_{n(\zeta)d}^c) + V \sum_k (-G_{cdd} + G_{nc} + G_{dcd})$$

$$(\omega - \varepsilon_k) G_{nc} = V G_{nd} + V \sum_k (-G_{cdc}^c + G_{dcc}^c) \quad (2.94)$$

$$\begin{aligned} (\omega - \varepsilon_k) G_{dcd} &= \langle d_{\sigma'}^{\dagger} c_{k'\sigma'} \rangle + \left[ \sum_{k'} (-V_{k'\sigma'}^* \langle c_{k'\sigma'}^{\dagger} c_{k\sigma'} \rangle + \frac{V_{k'\sigma} V_{k'\sigma}^*}{\omega - \varepsilon_{k'}} \langle d_{\sigma'}^{\dagger} c_{k\sigma'} \rangle \right] G_d \\ &\quad + V_{k\sigma'}^* G_{nd} + \sum_{k'} (-V_{k'\sigma'}^* G_{c'd}^c + V_{k'\sigma} G_{dcc}^c) \end{aligned} \quad (2.95)$$

---

<sup>1</sup>Note: according to suggestion of Prof. Kotliar

$$\begin{aligned}
& (\omega + \varepsilon_k - 2\varepsilon_d - U - 2(N-2)U\bar{n}_\zeta)G_{cdd} \\
& = \langle c_{k\sigma}^\dagger d_{\sigma'} \rangle + 2(N-2)U(G_{ncdd}^c + \langle \hat{n}_\zeta c_{k\sigma}^\dagger d_{\sigma'} \rangle_c)G_d + \langle c_{\sigma'}^\dagger d_\sigma \rangle G_{n(\zeta)d}^c \\
& + V \sum_{k'} \left( \frac{V}{\omega - \varepsilon_{k'}} \langle c_{k\sigma}^\dagger d_\sigma \rangle + \langle c_{k\sigma}^\dagger c_{k'\sigma} \rangle \right) G_d - VG_{nd} + V \sum_{k'} (G_{cdc}^c + G_{ccd}^c) \quad (2.96)
\end{aligned}$$

Assuming the higher order connected Green's functions are zero, we solve this closed set of equations.

$$\ll d_\sigma; d_\sigma^\dagger \gg = \frac{1 + A \cdot \left\{ \bar{n}_{\sigma'} + \sum_k \left( \frac{V_{k\sigma'} \langle d_{\sigma'}^\dagger c_{k\sigma'} \rangle}{\omega - \varepsilon_k} - \frac{V_{k\sigma'}^* \langle c_{k\sigma'}^\dagger d_{\sigma'} \rangle}{\omega + \varepsilon_k - 2\varepsilon_d - U - 2(N-2)U\bar{n}_\zeta} \right) \right\}}{\omega - \varepsilon_d - \Delta - A \cdot B} \quad (2.97)$$

where

$$A = \frac{(N-1)U}{\omega - \varepsilon_d - U - (N-2)U\bar{n}_\zeta - 2\Delta - \tilde{\Delta}} \quad (2.98)$$

$$\begin{aligned}
B = & \left[ (N-2)U \langle \hat{n}_\zeta \hat{n}_{\sigma'} \rangle_c + \sum_{k,k'} \left( - \frac{V_{k\sigma'} V_{k'\sigma'}^* \langle c_{k'\sigma'}^\dagger c_{k\sigma'} \rangle}{\omega - \varepsilon_k} + \frac{V_{k\sigma'} V_{k'\sigma'}^* V_{k'\sigma}}{(\omega - \varepsilon_k)(\omega - \varepsilon_{k'})} \langle d_{\sigma'}^\dagger c_{k'\sigma'} \rangle \right) \right. \\
& \left. - \sum_k \frac{2(N-2)U \langle \hat{n}_\zeta c_{k\sigma}^\dagger d_{\sigma'} \rangle_c}{\omega + \varepsilon_k - 2\varepsilon_d - U - 2(N-2)U\bar{n}_{\sigma''}} - \sum_k \frac{V_{k\sigma'}^* \sum_{k'} \left( \frac{V_{k'\sigma} V_{k'\sigma}^* \langle c_{k\sigma}^\dagger d_{\sigma'} \rangle + V_{k'\sigma'} \langle c_{k\sigma}^\dagger c_{k'\sigma'} \rangle \right)}{\omega + \varepsilon_k - 2\varepsilon_d - U - 2(N-2)U\bar{n}_{\sigma''}} \right] \quad (2.99)
\end{aligned}$$

## 2.4 Calculation of integrals on the real axis: analytical method

### 2.4.1 $\Delta$ and $\tilde{\Delta}$

In our calculation, we have transferred from the  $k$  summation to the integral over  $\varepsilon$ , which changes the multidimensional problem into a one-dimensional problem and hence simplifies the evolution. For example, in the calculation of the hybridization functions  $\Delta$  and  $\tilde{\Delta}$ ,

$$\Delta(\omega) = \sum_k \frac{V_{k\sigma}^2}{\omega - \varepsilon_k} = \int d\varepsilon \frac{V^2(\varepsilon)\rho(\varepsilon)}{\omega - \varepsilon} = \text{P} \int d\varepsilon \frac{V^2(\varepsilon)\rho(\varepsilon)}{\omega - \varepsilon} - i\pi V^2(\omega)\rho(\omega) \quad (2.100)$$

$$\tilde{\Delta}(\tilde{\omega}) = \sum_k \frac{V_{k\sigma}^2}{\tilde{\omega} + \varepsilon_k} = \int d\varepsilon \frac{V^2(\varepsilon)\rho(\varepsilon)}{\tilde{\omega} + \varepsilon} = \text{P} \int d\varepsilon \frac{V^2(\varepsilon)\rho(\varepsilon)}{\tilde{\omega} + \varepsilon} + i\pi V^2(-\tilde{\omega})\rho(-\tilde{\omega}) \quad (2.101)$$

where  $\tilde{\omega} = \omega - 2\varepsilon_f - U - 2(N-2)U\bar{n}_{\sigma'}$ . However, the calculation of integrals over  $\varepsilon$  needs to know the densities of states of conduction electrons. Hence this technique works only for lattices on which the densities of states of conduction electrons have been given (analytically, computationally or experimentally), *e.g.* Bethe lattice, hypercubic lattice, etc. For arbitrary lattice, we can first calculate the densities of states of conduction electrons in Brillouin zone, then do this calculation.

For the Bethe lattice, the density of states for conduction electrons is of semicircular type,

$$\rho(\varepsilon) = \begin{cases} \frac{2}{\pi W} \sqrt{W^2 - 4\varepsilon^2} & -W/2 < \varepsilon < W/2 \\ 0 & \varepsilon < -W/2 \text{ or } \varepsilon > W/2 \end{cases} \quad (2.102)$$

where  $W$  is the band width.

For the hypercubic lattice, the density of states for the conduction band is of Gaussian type,

$$\rho(\varepsilon) = \sqrt{\frac{8}{\pi W^2}} e^{-8\varepsilon^2/W^2} \quad (2.103)$$

For an arbitrary lattice, we still have to calculate the hybridization function with the original definition or first calculate the noninteracting density of states  $\rho(\varepsilon)$ .

Moreover, we have calculated in the iterative procedure the  $\tilde{\Delta}$  with  $\Delta$  from the relation between them and using an interpolation technique. That's because the numerical approaches can only be done on a mesh which is constructed for  $\omega$ , while for the hybridization function

$$\tilde{\Delta}(\tilde{\omega}) = \int d\varepsilon \frac{V^2(\varepsilon)\rho(\varepsilon)}{\tilde{\omega} + \varepsilon} = \int d\varepsilon \frac{-\text{Im } \Delta/\pi}{\tilde{\omega} + \varepsilon}, \quad (2.104)$$

where the  $\tilde{\omega} = \omega - 2\varepsilon - U - 2(N-2)U\bar{n}_{\sigma'}$  are not on mesh points. Hence we used interpolation to get the  $\tilde{\Delta}(\tilde{\omega})$  from  $\Delta(\omega)$  in order to save time, instead of calculating the  $\tilde{\Delta}(\tilde{\omega})$  with its definition. For the calculation of Hubbard model, we replaced the  $-\pi V^2(\varepsilon)\rho(\varepsilon)$  by the imaginary part of the hybridization function, *i.e.*  $\text{Im } \Delta(\varepsilon)$ . Thus, the hybridization factor  $V(\varepsilon)$  and noninteracting density of states  $\rho(\varepsilon)$  will not appear in the calculations so that they do not need to be calculated in the iterative procedure.

#### 2.4.2 $\langle d_{\sigma'}^\dagger c_{k\sigma'} \rangle$ and $\langle c_{k'\sigma'}^\dagger c_{k\sigma'} \rangle$

Similar to the calculation of occupation number, we calculate these two correlations using the spectral theorem, *i.e.*

$$\begin{aligned} \langle d_{\sigma'}^\dagger c_{k\sigma'} \rangle &= -\frac{1}{\pi} \int d\omega' f(\omega') \text{Im} \frac{V_{k\sigma'} G_d(\omega')}{\omega' - \varepsilon_k} \\ &= -\frac{V_{k\sigma'}}{\pi} \int d\omega' f(\omega') \left\{ \text{P} \frac{\text{Im} G_d(\omega')}{\omega' - \varepsilon_k} + \text{Re} G_d \text{Im} \frac{1}{\omega' - \varepsilon_k} \right\} \\ &= -\frac{V_{k\sigma'}}{\pi} \int d\omega' f(\omega') \left\{ \text{P} \frac{\text{Im} G_d(\omega')}{\omega' - \varepsilon_k} + \text{Re} G_d [-\pi \delta(\omega' - \varepsilon_k)] \right\} \\ &= V_{k\sigma'} f(\varepsilon_k) \text{Re} G_d(\varepsilon_k) - \frac{V_{k\sigma'}}{\pi} \text{P} \int d\omega' f(\omega') \frac{\text{Im} G_d(\omega')}{\omega' - \varepsilon_k} \end{aligned} \quad (2.105)$$

$$\begin{aligned} \langle c_{k'\sigma'}^\dagger c_{k\sigma'} \rangle &= -\frac{1}{\pi} \int d\omega' f(\omega') \text{Im} \left\{ \frac{\delta_{kk'}}{\omega' - \varepsilon_{k'}} + \frac{V_{k\sigma'} V_{k'\sigma'} G_d(\omega')}{(\omega' - \varepsilon_k)(\omega' - \varepsilon_{k'})} \right\} \\ &= -\frac{1}{\pi} \int d\omega' f(\omega') \left\{ \delta_{kk'} [-\pi \delta(\omega' - \varepsilon_{k'})] + \text{Im} \frac{V_{k\sigma'} V_{k'\sigma'} G_d(\omega')}{(\omega' - \varepsilon_k)(\omega' - \varepsilon_{k'})} \right\} \\ &= f(\varepsilon_{k'}) \delta_{kk'} - \frac{V_{k\sigma'} V_{k'\sigma'}}{\pi} \int d\omega' f(\omega') \text{Im} \left\{ \frac{1}{\varepsilon_k - \varepsilon_{k'}} \left( \frac{G_d}{\omega' - \varepsilon_k} - \frac{G_d}{\omega' - \varepsilon_{k'}} \right) + \frac{\delta(\varepsilon_k - \varepsilon_{k'}) G_d}{(\omega' - \varepsilon_k)^2} \right\} \end{aligned} \quad (2.106)$$

where we have used the relation

$$\frac{1}{(\omega' - \varepsilon_k)(\omega' - \varepsilon_{k'})} = \frac{1}{\varepsilon - \varepsilon'} \left( \frac{1}{\omega' - \varepsilon_k} - \frac{1}{\omega' - \varepsilon_{k'}} \right) \quad (2.107)$$

Calculating with another method, we can get

$$\begin{aligned} \frac{1}{(\omega' - \varepsilon_k)(\omega' - \varepsilon_{k'})} &= \left( \text{P} \frac{1}{\omega' - \varepsilon_k} - i\pi\delta(\omega' - \varepsilon_k) \right) \left( \text{P} \frac{1}{\omega' - \varepsilon_{k'}} - i\pi\delta(\omega' - \varepsilon_{k'}) \right) \\ &= \text{P} \frac{1}{\omega' - \varepsilon_k} \text{P} \frac{1}{\omega' - \varepsilon_{k'}} - i\pi \left( \frac{\delta(\omega' - \varepsilon_{k'})}{\omega' - \varepsilon_k} + \frac{\delta(\omega' - \varepsilon_k)}{\omega' - \varepsilon_{k'}} \right) - \pi^2 \delta(\omega' - \varepsilon_k) \delta(\omega' - \varepsilon_{k'}) \end{aligned} \quad (2.108)$$

Comparing the two results (2.107) and (2.108), we can conclude that

$$\frac{\delta(\varepsilon_k - \varepsilon_{k'})}{(\omega' - \varepsilon_k)^2} = -\pi^2 \delta(\omega' - \varepsilon_k) \delta(\omega' - \varepsilon_{k'}) \quad (2.109)$$

which should be real. So the correlation with double  $c$  operators  $\langle c_{k'\sigma'}^\dagger c_{k\sigma'} \rangle$  should be

$$\begin{cases} -\frac{V_{k\sigma'} V_{k'\sigma'}}{\pi} \int d\omega' f(\omega') \frac{1}{\varepsilon_k - \varepsilon_{k'}} \left\{ \text{P} \left( \frac{\text{Im} G_d}{(\omega' - \varepsilon_k)} - \frac{\text{Im} G_d}{(\omega' - \varepsilon_{k'})} \right) + \text{Re} G_d \left( [-\pi\delta(\omega' - \varepsilon_k)] - [-\pi\delta(\omega' - \varepsilon_{k'})] \right) \right\} & \varepsilon_k \neq \varepsilon_{k'} \\ f(\varepsilon_{k'}) \delta_{kk'} - \frac{V_{k'\sigma'}^2 \delta(\varepsilon_k - \varepsilon_{k'})}{\pi} \text{P} \int d\omega' f(\omega') \frac{\text{Im} G_d}{(\omega' - \varepsilon_{k'})^2} & \varepsilon_k = \varepsilon_{k'} \end{cases}$$

namely

$$\langle c_{k'\sigma'}^\dagger c_{k\sigma'} \rangle = \begin{cases} -\frac{1}{\pi} \frac{V_{k\sigma'} V_{k'\sigma'}}{\varepsilon_k - \varepsilon_{k'}} \int d\omega' f(\omega') \text{P} \left( \frac{\text{Im} G_d}{(\omega' - \varepsilon_k)} - \frac{\text{Im} G_d}{(\omega' - \varepsilon_{k'})} \right) + \frac{\text{Re} G_d(\varepsilon_k) f(\varepsilon_k) - \text{Re} G_d(\varepsilon_{k'}) f(\varepsilon_{k'})}{\varepsilon_k - \varepsilon_{k'}} & \varepsilon_k \neq \varepsilon_{k'} \\ f(\varepsilon_{k'}) \delta_{kk'} - \frac{V_{k'\sigma'}^2 \delta(\varepsilon_k - \varepsilon_{k'})}{\pi} \text{P} \int d\omega' f(\omega') \frac{\text{Im} G_d}{(\omega' - \varepsilon_{k'})^2} & \varepsilon_k = \varepsilon_{k'} \end{cases}$$

Comparing with the formula of  $\langle d_{\sigma'}^\dagger c_{k\sigma'} \rangle$ , we can get

$$\langle c_{k'\sigma'}^\dagger c_{k\sigma'} \rangle = \begin{cases} \frac{V_{k'\sigma'} \langle d_{\sigma'}^\dagger c_{k\sigma'} \rangle - V_{k\sigma'} \langle d_{\sigma'}^\dagger c_{k'\sigma'} \rangle}{\varepsilon_k - \varepsilon_{k'}} & \varepsilon_k \neq \varepsilon_{k'} \\ f(\varepsilon_{k'}) \delta_{kk'} - \frac{V_{k'\sigma'}^2 \delta(\varepsilon_k - \varepsilon_{k'})}{\pi} \text{P} \int d\omega' f(\omega') \frac{\text{Im} G_d}{(\omega' - \varepsilon_{k'})^2} & \varepsilon_k = \varepsilon_{k'} \end{cases}$$

Using partial integration, we finally get

$$\langle c_{k'\sigma'}^\dagger c_{k\sigma'} \rangle = \begin{cases} \frac{V_{k'\sigma'} \langle d_{\sigma'}^\dagger c_{k\sigma'} \rangle - V_{k\sigma'} \langle d_{\sigma'}^\dagger c_{k'\sigma'} \rangle}{\varepsilon_k - \varepsilon_{k'}} & \varepsilon_k \neq \varepsilon_{k'} \\ f(\varepsilon_{k'}) \delta_{kk'} - \frac{V_{k'\sigma'}^2 \delta(\varepsilon_k - \varepsilon_{k'})}{\pi} \text{P} \int d\omega' \frac{f(\omega') \text{Im} G_d}{(\omega' - \varepsilon_{k'})} & \varepsilon_k = \varepsilon_{k'} \end{cases}$$

Here we give the formula for calculating correlation terms, which will be used in the calculations of integral terms. However, this is not an inevitable step because there are two kinds of methods to calculate the integral terms. In the method using these correlation terms, we calculate the correlation terms on mesh and then put them numerically into the calculation of integral terms of  $\varepsilon$ , which is an improved and much general method than calculation of integral terms directly from analytical formula. The detailed implementation is shown in the next subsection.

### 2.4.3 Integrals

The integrals are coming from the  $k$ -summation terms involving the correlation functions which are obtained in the decoupling procedure. A general way is to directly sum over  $k$  throughout the Brillouin zone. However, if the density of states of noninteracting electrons is known analytically or numerically, it's convenient to transfer the  $k$  summation to integrals because one dimension integral is much easier to handle.

As mentioned in last subsection, we have developed two different methods to calculate the integral terms. The first method (so called analytical method) is to put the expression of  $\langle d_{\sigma'}^{\dagger} c_{k\sigma'} \rangle$  and  $\langle c_{k'\sigma'}^{\dagger} c_{k\sigma'} \rangle$ , *i.e.*

$$\begin{aligned} \langle d_{\sigma'}^{\dagger} c_{k\sigma'} \rangle &= -\frac{1}{\pi} \int d\omega' f(\omega') \operatorname{Im} \frac{V_{k\sigma'} G_d(\omega')}{\omega' - \varepsilon_k} \\ \langle c_{k'\sigma'}^{\dagger} c_{k\sigma'} \rangle &= -\frac{1}{\pi} \int d\omega' f(\omega') \operatorname{Im} \left\{ \frac{\delta_{kk'}}{\omega' - \varepsilon_{k'}} + \frac{V_{k\sigma'} V_{k'\sigma'} G_d(\omega')}{(\omega' - \varepsilon_k)(\omega' - \varepsilon_{k'})} \right\} \end{aligned} \quad (2.110)$$

into the integral terms, then calculate the double integrals over  $\varepsilon$  and  $\omega'$ , and finally we get an analytical expression for the integral terms. We derive the formula as follows:

Here we give again the integral terms that need to be calculated.

$$\begin{aligned} I_1(\omega) &= V \sum_k \langle d_{\sigma'}^{\dagger} c_{k\sigma'} \rangle \left( \frac{1}{\omega - \varepsilon_k} - \frac{1}{\omega + \varepsilon_k - 2\varepsilon_d - U - 2(N-2)\bar{n}_{\zeta}U} \right) \\ I_2(\omega) &= -V^2 \sum_{kk'} \langle c_{k'\sigma'}^{\dagger} c_{k\sigma'} \rangle \left( \frac{1}{\omega - \varepsilon_k} + \frac{1}{\omega + \varepsilon_k - 2\varepsilon_d - U - 2(N-2)\bar{n}_{\zeta}U} \right) \end{aligned}$$

Then we calculate them term by term. First we calculate the integral terms involving  $\langle d_{\sigma'}^{\dagger} c_{k\sigma'} \rangle$ ,

$$\begin{aligned} I_{1a} &= -\sum_k \frac{V_k \langle d_{\sigma'}^{\dagger} c_{k\sigma'} \rangle}{\omega - \varepsilon_k} \\ &= -\sum_k \frac{V_k}{\omega - \varepsilon_k} \left( -\frac{V_k}{\pi} \right) \int d\omega' f(\omega') \operatorname{Im} \frac{G(\omega')}{\omega' - \varepsilon_k} \\ &= \frac{1}{\pi} \int d\omega' f(\omega') \sum_k \frac{V_k^2}{\omega - \varepsilon_k} \left\{ \operatorname{Re} G(\omega') \operatorname{Im} \frac{1}{\omega' - \varepsilon_k} + \operatorname{Im} G(\omega') \operatorname{Re} \frac{1}{\omega' - \varepsilon_k} \right\} \\ &= \frac{1}{\pi} \int d\omega' f(\omega') \left\{ \operatorname{Re} G(\omega') \int d\varepsilon \frac{V^2(\varepsilon) \rho(\varepsilon) (-\pi \delta(\omega' - \varepsilon))}{\omega - \varepsilon} + \operatorname{Im} G(\omega') \int d\varepsilon \frac{V^2(\varepsilon) \rho(\varepsilon)}{\omega - \varepsilon} \operatorname{Re} \frac{1}{\omega' - \varepsilon} \right\} \\ &= \frac{1}{\pi} \int d\omega' \frac{f(\omega') \operatorname{Re} G(\omega') \Delta''(\omega')}{\omega - \omega'} + \frac{1}{\pi} \int d\omega' \frac{f(\omega') \operatorname{Im} G(\omega') [\Delta(\omega) - \Delta'(\omega')]}{\omega' - \omega} \\ &= \frac{1}{\pi} \int d\omega' \frac{f(\omega') \operatorname{Im} G(\omega') \Delta(\omega)}{\omega' - \omega} - \frac{1}{\pi} \int d\omega' \frac{f(\omega') \operatorname{Im} \{G(\omega') \Delta'(\omega')\}}{\omega' - \omega} \\ &= \frac{1}{\pi} \int d\omega' \frac{f(\omega')}{\omega' - \omega} [\operatorname{Im} G(\omega') \Delta(\omega) - \operatorname{Im} \{G(\omega') \Delta'(\omega')\}] \end{aligned} \quad (2.111)$$

where we have used the identity

$$\frac{1}{\omega - \varepsilon} \frac{1}{\omega - \varepsilon} = \frac{1}{\omega' - \omega} \left\{ \frac{1}{\omega - \varepsilon} - \frac{1}{\omega' - \varepsilon} \right\} \quad (2.112)$$

to separate the integral of a product into two single integrals so that the calculation is simplified. For the case with infinite Coulomb interaction strength, only  $I_{1a}$  is needed. Then,

$$\begin{aligned}
I_{1b} &= \sum_k \frac{V \langle d_{\sigma'}^\dagger c_{k\sigma'} \rangle}{\omega + \varepsilon_k - 2\varepsilon_d - U - 2(N-2)\bar{n}_\zeta U} \\
&= \sum_k \frac{V^2}{\omega + \varepsilon_k - 2\varepsilon_d - U - 2(N-2)\bar{n}_\zeta U} \left(-\frac{1}{\pi}\right) \int d\omega' f(\omega') \operatorname{Im} \frac{G(\omega')}{\omega' - \varepsilon_k} \\
&= \sum_k \frac{V^2}{\omega + \varepsilon_k - 2\varepsilon_d - U - 2(N-2)\bar{n}_\zeta U} \left(-\frac{1}{\pi}\right) \int d\omega' f(\omega') \left\{ \operatorname{Im} G(\omega') \operatorname{P} \frac{1}{\omega' - \varepsilon_k} + \operatorname{Re} G(\omega') \operatorname{Im} \frac{1}{\omega' - \varepsilon_k} \right\} \\
&= \sum_k \frac{V^2}{\omega + \varepsilon_k - 2\varepsilon_d - U - 2(N-2)\bar{n}_\zeta U} \left(-\frac{1}{\pi}\right) \left\{ \operatorname{P} \int d\omega' f(\omega') \frac{\operatorname{Im} G(\omega')}{\omega' - \varepsilon_k} - \pi f(\varepsilon_k) \operatorname{Re} G(\varepsilon) \right\} \\
&= \left(-\frac{1}{\pi}\right) \int d\omega' f(\omega') \operatorname{Im} G(\omega') \sum_k \frac{V^2}{\omega + \varepsilon_k - 2\varepsilon_d - U - 2(N-2)\bar{n}_\zeta U} \operatorname{P} \frac{1}{\omega' - \varepsilon_k} \\
&\quad + \sum_k \frac{V^2}{\omega + \varepsilon_k - 2\varepsilon_d - U - 2(N-2)\bar{n}_\zeta U} f(\varepsilon_k) \operatorname{Re} G(\varepsilon_k) \\
&= \left(-\frac{1}{\pi}\right) \int d\omega' \frac{f(\omega') \operatorname{Im} G(\omega')}{\omega' + \omega - 2\varepsilon_d - U - 2(N-2)\bar{n}_\zeta U} \sum_k V^2 \left\{ \frac{1}{\omega + \varepsilon_k - 2\varepsilon_d - U - 2(N-2)\bar{n}_\zeta U} + \operatorname{P} \frac{1}{\omega' - \varepsilon_k} \right\} \\
&\quad + \sum_k \frac{V^2}{\omega + \varepsilon_k - 2\varepsilon_d - U - 2(N-2)\bar{n}_\zeta U} f(\varepsilon_k) \operatorname{Re} G(\varepsilon_k) \\
&= \left(-\frac{1}{\pi}\right) \int d\omega' \frac{f(\omega') \operatorname{Im} G(\omega')}{\omega' + \omega - 2\varepsilon_d - U - 2(N-2)\bar{n}_\zeta U} \{ \tilde{\Delta}(\omega) + \operatorname{Re} \Delta(\omega') \} \\
&\quad + \int d\varepsilon \frac{V^2(\varepsilon)\rho(\varepsilon)}{\omega + \varepsilon - 2\varepsilon_d - U - 2(N-2)\bar{n}_\zeta U} f(\varepsilon) \operatorname{Re} G(\varepsilon) \\
&= \left(-\frac{1}{\pi}\right) \int d\omega' \frac{f(\omega') \operatorname{Im} G(\omega')}{\omega' + \omega - 2\varepsilon_d - U - 2(N-2)\bar{n}_\zeta U} \{ \tilde{\Delta}(\omega) + \operatorname{Re} \Delta(\omega') \} \\
&\quad + \int d\varepsilon \frac{-\operatorname{Im} \Delta(\varepsilon)/\pi}{\omega + \varepsilon - 2\varepsilon_d - U - 2(N-2)\bar{n}_\zeta U} f(\varepsilon) \operatorname{Re} G(\varepsilon) \\
&= \left(-\frac{1}{\pi}\right) \int d\omega' \frac{f(\omega') \operatorname{Im} G(\omega')}{\omega' + \omega - 2\varepsilon_d - U - 2(N-2)\bar{n}_\zeta U} \{ \tilde{\Delta}(\omega) + \operatorname{Re} \Delta(\omega') \} \\
&\quad - \frac{1}{\pi} \int d\omega' \frac{\operatorname{Im} \Delta(\omega')}{\omega' + \omega - 2\varepsilon_d - U - 2(N-2)\bar{n}_\zeta U} f(\omega') \operatorname{Re} G(\omega') \\
&= -\frac{1}{\pi} \int d\omega' \frac{f(\omega') \operatorname{Im} G(\omega')}{\omega' + \omega - 2\varepsilon_d - U - 2(N-2)\bar{n}_\zeta U} \tilde{\Delta}(\omega) - \frac{1}{\pi} \int d\omega' f(\omega') \frac{\operatorname{Im} \{ \Delta(\omega') G(\omega') \}}{\omega' + \omega - 2\varepsilon_d - U - 2(N-2)\bar{n}_\zeta U}
\end{aligned} \tag{2.113}$$

where we have used

$$\tilde{\Delta}(\omega) = \sum_k \frac{V^2}{\omega + \varepsilon_k - 2\varepsilon_d - U - 2(N-2)\bar{n}_\zeta U}$$

and the identities

$$\frac{1}{\omega + \varepsilon_k - 2\varepsilon_d - U - 2(N-2)\bar{n}_\zeta U} \frac{1}{\omega' - \varepsilon_k} = \frac{1}{\omega' + \omega - 2\varepsilon_d - U - 2(N-2)\bar{n}_\zeta U} \left\{ \frac{1}{\omega + \varepsilon_k - 2\varepsilon_d - U - 2(N-2)\bar{n}_\zeta U} + \frac{1}{\omega' - \varepsilon_k} \right\} \tag{2.114}$$



For the second term  $I_{1b}$ , it's much difficult to calculate in the numerical calculation than  $I_{1a}$  because the mesh is constructed for  $\omega$  and  $\tilde{\omega}$  are not on mesh points. Hence, the interpolation and Lorentzian broadening technique are employed in our implementation of the formular (2.113).

Similarly, we calculate the integral terms involving  $\langle c_{k'\sigma}^\dagger c_{k\sigma} \rangle$  as follows:

$$\begin{aligned}
 I_{2a} &= \sum_{kk'} \frac{V_k V_{k'} \langle c_{k'\sigma}^\dagger c_{k\sigma} \rangle}{\omega - \varepsilon_k} \\
 &= \sum_k \frac{V_k V_{k'}}{\omega - \varepsilon_k} \left( -\frac{1}{\pi} \right) \int d\omega' f(\omega') \operatorname{Im} \left\{ \frac{\delta_{kk'}}{\omega' - \varepsilon_{k'}} + \frac{V_{k\sigma'} V_{k'\sigma'} G_d(\omega')}{(\omega' - \varepsilon_k)(\omega' - \varepsilon_{k'})} \right\} \\
 &= -\frac{1}{\pi} \sum_{kk'} \frac{V_k V_{k'}}{\omega - \varepsilon_k} \int d\omega' f(\omega') \operatorname{Im} \frac{\delta_{kk'}}{\omega' - \varepsilon_{k'}} - \frac{1}{\pi} \sum_{kk'} \frac{V_k^2 V_{k'}^2}{\omega - \varepsilon_k} \int d\omega' f(\omega') \operatorname{Im} \frac{G(\omega')}{(\omega' - \varepsilon_k)(\omega' - \varepsilon_{k'})} \\
 I_{2a1} &= \frac{1}{\pi} \sum_{kk'} \frac{V_k V_{k'}}{\omega - \varepsilon_k} \int d\omega' f(\omega') \operatorname{Im} \frac{\delta_{kk'}}{\omega' - \varepsilon_{k'}} \\
 &= \frac{1}{\pi} \int d\omega' f(\omega') \sum_{kk'} \frac{V_k V_{k'} \delta_{kk'} (-\pi \delta(\omega' - \varepsilon))}{(\omega - \varepsilon_k)} \\
 &= \frac{1}{\pi} \int d\omega' f(\omega') \sum_k \frac{V_k^2 (-\pi \delta(\omega' - \varepsilon))}{(\omega - \varepsilon_k)} \\
 &= \frac{1}{\pi} \int d\omega' f(\omega') \frac{\Delta''(\omega')}{(\omega - \omega')} \\
 &= \frac{1}{\pi} \int d\omega' \frac{f(\omega') \Delta''(\omega')}{(\omega - \omega')} \tag{2.115}
 \end{aligned}$$

$$\begin{aligned}
 I_{2a2} &= \frac{1}{\pi} \sum_{kk'} \frac{V_k^2 V_{k'}^2}{\omega - \varepsilon_k} \int d\omega' f(\omega') \operatorname{Im} \frac{G(\omega')}{(\omega' - \varepsilon_k)(\omega' - \varepsilon_{k'})} \\
 &= \frac{1}{\pi} \int d\omega' f(\omega') \sum_{kk'} \frac{V_k^2 V_{k'}^2}{\omega - \varepsilon_k} \times \\
 &\quad \times \left\{ \operatorname{Im} G(\omega') \operatorname{Re} \frac{1}{\omega' - \varepsilon_k} \operatorname{Re} \frac{1}{\omega' - \varepsilon_{k'}} + \operatorname{Re} G(\omega') \operatorname{Im} \frac{1}{\omega' - \varepsilon_k} \operatorname{Re} \frac{1}{\omega' - \varepsilon_{k'}} + \right. \\
 &\quad \left. + \operatorname{Re} G(\omega') \operatorname{Re} \frac{1}{\omega' - \varepsilon_k} \operatorname{Im} \frac{1}{\omega' - \varepsilon_{k'}} - \operatorname{Im} G(\omega') \operatorname{Im} \frac{1}{\omega' - \varepsilon_k} \operatorname{Im} \frac{1}{\omega' - \varepsilon_{k'}} \right\} \\
 &= \frac{1}{\pi} \int d\omega' f(\omega') \times \\
 &\quad \times \left\{ \operatorname{Im} G(\omega') \Delta'(\omega') \int d\varepsilon \frac{V^2(\varepsilon) \rho(\varepsilon)}{\omega - \varepsilon} \operatorname{Re} \frac{1}{\omega' - \varepsilon_{k'}} + \operatorname{Re} G(\omega') \Delta'(\omega') \int d\varepsilon \frac{V^2(\varepsilon) \rho(\varepsilon) (-\pi \delta(\omega' - \varepsilon))}{\omega - \varepsilon} + \right. \\
 &\quad \left. + \operatorname{Re} G(\omega') \Delta''(\omega') \int d\varepsilon \frac{V^2(\varepsilon) \rho(\varepsilon)}{\omega - \varepsilon} \operatorname{Re} \frac{1}{\omega' - \varepsilon_{k'}} - \operatorname{Im} G(\omega') \Delta''(\omega') \int d\varepsilon \frac{V^2(\varepsilon) \rho(\varepsilon) (-\pi \delta(\omega' - \varepsilon))}{\omega - \varepsilon} \right\} \\
 &= \frac{1}{\pi} \int d\omega' f(\omega') \left\{ \frac{\operatorname{Im} G(\omega') \Delta'(\omega') [\Delta(\omega) - \Delta'(\omega')]}{\omega' - \omega} + \frac{\operatorname{Re} G(\omega') \Delta'(\omega') \Delta''(\omega')}{\omega - \omega'} + \right. \\
 &\quad \left. + \frac{\operatorname{Re} G(\omega') \Delta''(\omega') [\Delta(\omega) - \Delta'(\omega')]}{\omega' - \omega} - \frac{\operatorname{Im} G(\omega') \Delta''(\omega') \Delta''(\omega')}{\omega - \omega'} \right\} \\
 &= \frac{1}{\pi} \int d\omega' \frac{f(\omega')}{\omega' - \omega} \left[ \Delta(\omega) \operatorname{Im} \{G(\omega') \Delta(\omega')\} - \operatorname{Im} \{G(\omega') \Delta^2(\omega')\} \right] \tag{2.116}
 \end{aligned}$$

$$\begin{aligned}
I_{2b} &= \sum_k \frac{V \langle c_{k'\sigma'}^\dagger c_{k\sigma'} \rangle}{\omega + \varepsilon_k - 2\varepsilon_d - U - 2(N-2)\bar{n}_\zeta U} = I_{2b1} + I_{2b2} \\
I_{2b1} &= \sum_{kk'} \frac{V^2}{\omega + \varepsilon_k - 2\varepsilon_d - U - 2(N-2)\bar{n}_\zeta U} \left(-\frac{1}{\pi}\right) \int d\omega' f(\omega') \operatorname{Im} \frac{\delta_{kk'}}{\omega' - \varepsilon_{k'}} \\
&= \sum_k \frac{V^2}{\omega + \varepsilon_k - 2\varepsilon_d - U - 2(N-2)\bar{n}_\zeta U} f(\varepsilon_k) \\
&= \int d\varepsilon f(\varepsilon) \frac{V^2(\varepsilon)\rho(\varepsilon)}{\omega + \varepsilon - 2\varepsilon_d - U} = -\frac{1}{\pi} \int d\varepsilon f(\varepsilon) \frac{\operatorname{Im} \Delta(\varepsilon)}{\omega + \varepsilon - 2\varepsilon_d - U} \\
&= -\frac{1}{\pi} \mathbb{P} \int d\varepsilon f(\varepsilon) \frac{\operatorname{Im} \Delta(\varepsilon)}{\omega + \varepsilon - 2\varepsilon_d - U} + i \cdot f(U + 2\varepsilon_d - \omega) \operatorname{Im} \Delta(U + 2\varepsilon_d - \omega) \tag{2.117} \\
I_{2b2} &= \sum_{kk'} \frac{V^2}{\omega + \varepsilon_k - 2\varepsilon_d - U - 2(N-2)\bar{n}_\zeta U} \left(-\frac{1}{\pi}\right) \int d\omega' f(\omega') \operatorname{Im} \frac{V^2 G(\omega')}{(\omega' - \varepsilon_{k'}) (\omega' - \varepsilon_k)} \\
&= \sum_k \frac{V^2}{\omega + \varepsilon_k - 2\varepsilon_d - U - 2(N-2)\bar{n}_\zeta U} \left(-\frac{1}{\pi}\right) \int d\omega' f(\omega') \operatorname{Im} \frac{G(\omega') \Delta(\omega')}{\omega' - \varepsilon_k} \quad \text{taken sum of } k' \\
&= \sum_k \frac{V^2}{\omega + \varepsilon_k - 2\varepsilon_d - U - 2(N-2)\bar{n}_\zeta U} \left(-\frac{1}{\pi}\right) \int d\omega' f(\omega') [\operatorname{Im} (G(\omega') \Delta(\omega')) \mathbb{P} \frac{1}{\omega' - \varepsilon_k} \\
&\quad + \operatorname{Re} (G(\omega') \Delta(\omega')) \operatorname{Im} \frac{1}{\omega' - \varepsilon_k}] \\
&= \left(-\frac{1}{\pi}\right) \sum_k \frac{V^2}{\omega + \varepsilon_k - 2\varepsilon_d - U - 2(N-2)\bar{n}_\zeta U} \mathbb{P} \int d\omega' f(\omega') \frac{\operatorname{Im} (G(\omega') \Delta(\omega'))}{\omega' - \varepsilon_k} \\
&\quad + \sum_k \frac{V^2}{\omega + \varepsilon_k - 2\varepsilon_d - U - 2(N-2)\bar{n}_\zeta U} \left(-\frac{1}{\pi}\right) (-\pi f(\varepsilon_k) \operatorname{Im} (G(\varepsilon_k) \Delta(\varepsilon_k))) \\
&= \left(-\frac{1}{\pi}\right) \int d\omega' f(\omega') \operatorname{Im} (G(\omega') \Delta(\omega')) \sum_k \frac{V^2}{\omega + \varepsilon_k - 2\varepsilon_d - U - 2(N-2)\bar{n}_\zeta U} \mathbb{P} \frac{1}{\omega' - \varepsilon_k} \\
&\quad + \sum_k \frac{V^2}{\omega + \varepsilon_k - 2\varepsilon_d - U - 2(N-2)\bar{n}_\zeta U} (f(\varepsilon_k) \operatorname{Re} (G(\varepsilon_k) \Delta(\varepsilon_k))) \\
&= \left(-\frac{1}{\pi}\right) \int d\omega' f(\omega') \frac{\operatorname{Im} (G(\omega') \Delta(\omega'))}{\omega' + \omega - 2\varepsilon_d - U - 2(N-2)\bar{n}_\zeta U} \sum_k \left\{ \frac{V^2}{\omega + \varepsilon_k - 2\varepsilon_d - U - 2(N-2)\bar{n}_\zeta U} + \mathbb{P} \frac{V^2}{\omega' - \varepsilon_k} \right\} \\
&\quad - \frac{1}{\pi} \int d\varepsilon \frac{\operatorname{Im} \Delta(\varepsilon)}{\omega + \varepsilon - 2\varepsilon_d - U - 2(N-2)\bar{n}_\zeta U} (f(\varepsilon) \operatorname{Re} (G(\varepsilon) \Delta(\varepsilon))) \\
&= \left(-\frac{1}{\pi}\right) \int d\omega' f(\omega') \frac{\operatorname{Im} (G(\omega') \Delta(\omega'))}{\omega' + \omega - 2\varepsilon_d - U - 2(N-2)\bar{n}_\zeta U} \left\{ \sum_k \frac{V^2}{\omega + \varepsilon_k - 2\varepsilon_d - U - 2(N-2)\bar{n}_\zeta U} + \operatorname{Re} \Delta(\omega') \right\} \\
&\quad - \frac{1}{\pi} \int d\varepsilon f(\varepsilon) \frac{\operatorname{Im} \Delta(\varepsilon) \operatorname{Re} (G(\varepsilon) \Delta(\varepsilon))}{\omega + \varepsilon - 2\varepsilon_d - U - 2(N-2)\bar{n}_\zeta U} \quad \text{changed } \varepsilon \text{ to } \omega' \text{ and added the last two terms} \\
&= \left(-\frac{1}{\pi}\right) \int d\omega' f(\omega') \frac{\operatorname{Im} (G(\omega') \Delta(\omega'))}{\omega' + \omega - 2\varepsilon_d - U - 2(N-2)\bar{n}_\zeta U} \sum_k \frac{V^2}{\omega + \varepsilon_k - 2\varepsilon_d - U - 2(N-2)\bar{n}_\zeta U} \\
&\quad - \frac{1}{\pi} \int d\omega' f(\omega') \frac{\operatorname{Im} \{ \Delta(\omega') G(\omega') \Delta(\omega') \}}{\omega + \omega' - 2\varepsilon_d - U - 2(N-2)\bar{n}_\zeta U} \\
&= -\frac{1}{\pi} \int d\omega' f(\omega') \frac{\operatorname{Im} (G(\omega') \Delta(\omega'))}{\omega' + \omega - 2\varepsilon_d - U - 2(N-2)\bar{n}_\zeta U} \tilde{\Delta}(\omega) - \frac{1}{\pi} \int d\omega' f(\omega') \frac{\operatorname{Im} \{ \Delta(\omega') G(\omega') \Delta(\omega') \}}{\omega + \omega' - 2\varepsilon_d - U - 2(N-2)\bar{n}_\zeta U} \tag{2.118}
\end{aligned}$$

The above formulae give the calculation of integral terms. However, the analytical method can not be easily generalized to higher order approximations due to the presence of more complicated integral terms. Therefore, besides the analytical calculation, we developed another method to

separate this procedure into two steps: first we calculate the two correlations (which are functions of  $\varepsilon$ ) on the mesh as shown in the last subsection, then input these two numerical functions into the integrals and do the integration over  $\varepsilon$  numerically on the mesh, *i.e.*

$$I_1(\omega) = \int d\varepsilon \left\{ \frac{V \langle d_{\sigma'}^\dagger c_{k\sigma'} \rangle(\varepsilon) \rho(\varepsilon)}{\omega - \varepsilon} - \frac{V \langle d_{\sigma'}^\dagger c_{k\sigma'} \rangle(\varepsilon) \rho(\varepsilon)}{\omega + \varepsilon - 2\varepsilon_d - U - 2(N-2)\bar{n}_\zeta U} \right\} \quad (2.119)$$

$$I_2(\omega) = - \int d\varepsilon \left\{ \frac{V^2 \langle c_{k'\sigma'}^\dagger c_{k\sigma'} \rangle(\varepsilon) \rho(\varepsilon)}{\omega - \varepsilon} + \frac{V^2 \langle c_{k'\sigma'}^\dagger c_{k\sigma'} \rangle(\varepsilon) \rho(\varepsilon)}{\omega + \varepsilon - 2\varepsilon_d - U - 2(N-2)\bar{n}_\zeta U} \right\} \quad (2.120)$$

## 2.5 Calculation on the Matsubara axis

The calculation on the Matsubara axis is a mathematical trick that treating time as a complex variable and handling the calculation on Matsubara frequencies. In our study, we want to obtain the Green's function  $G(\omega)$  on the real axis. Let's assume that there exists a function  $G(z)$  which is defined on the whole complex plane and the values of  $G(z)$  on the real axis are same to  $G(\omega)$ . Once we know the  $G(z)$ , the Green's function  $G(\omega)$  will be determined. The calculation on the Matsubara axis is just to calculate the values of  $G(z)$  on some special points (Matsubara frequencies) on the imaginary axis and then obtain the result on the real axis through an analytical continuation. As a consequence, the calculation of  $k$ -summation terms is greatly simplified because there is no singularities any more. In this Section, we only give a brief introduction to the Matsubara axis and show its convenience. For the details, please see [79, 80, 81, 82].

On the Matsubara axis, the Green's function is

$$G(i\omega) = \int_0^\beta d\tau e^{i\omega_n \tau} G(\tau) \quad (2.121)$$

where  $\tau = it$  is real.  $\beta = 1/k_B T$  is here a time scale.  $\omega_n$  is the Matsubara frequency, given as:

$$\omega_n = \begin{cases} \frac{(2n+1)\pi}{\beta} & \text{fermions} \\ \frac{2n\pi}{\beta} & \text{bosons} \end{cases} . \quad (2.122)$$

The relation between the Matsubara axis and the real axis, in practice, is that

$$i\omega \rightleftharpoons \omega + i\delta.$$

Using this relation, we can write  $\Delta(i\omega_n)$  as

$$\Delta(i\omega_n) = \sum_k \frac{V_k^2}{i\omega_n - \varepsilon_k}$$

We can see that the calculation on the poles on the real axis has been avoided by calculating on Matsubara axis.

To solve the equations of motions on the Matsubara axis, we still first calculate the hybridization functions. Now they have the forms

$$\Delta(i\omega) = \sum_k \frac{V_k^2}{i\omega - \varepsilon_k}$$

and

$$\tilde{\Delta}(i\omega) = \sum_k \frac{V_k^2}{i\omega + \varepsilon_k - 2\varepsilon_d - U - 2(N-2)\bar{n}_\zeta U}.$$

With Mathematica, the first hybridization functions are calculated as

$$\Delta(i\omega) = 2V^2(i\omega - i\sqrt{1 + \omega^2}). \quad (2.123)$$

The second hybridization function

$$\begin{aligned} \tilde{\Delta}(i\omega_n) &= \sum_k \frac{V^2}{i\omega + \varepsilon_k - 2\varepsilon_d - U - 2(N-2)\bar{n}_\zeta U} \\ &= -\sum_k \frac{V^2}{(-i\omega + 2\varepsilon_d + U + 2(N-2)\bar{n}_\zeta U) - \varepsilon_k} \end{aligned} \quad (2.124)$$

should be calculated with the analytical continuation. Similarly, the  $k$ -summation terms are calculated as

$$\sum_k \frac{V \langle d_{\sigma'}^\dagger c_{k\sigma'} \rangle}{i\omega - \varepsilon_k} = T \sum_{i\omega'} \frac{\Delta(i\omega') - \Delta(i\omega)}{i\omega' - i\omega} G(i\omega') e^{i\omega' 0^\dagger} \quad (2.125)$$

$$\sum_{k'k} \frac{V \langle c_{k'\sigma'}^\dagger c_{k\sigma'} \rangle}{i\omega - \varepsilon_k} = T \sum_{i\omega'} \frac{\Delta(i\omega') - \Delta(i\omega)}{i\omega' - i\omega} \{1 + \Delta(i\omega') G(i\omega')\} e^{i\omega' 0^\dagger} \quad (2.126)$$

$$n_f = NT \sum_{i\omega'} G(i\omega') e^{i\omega' 0^\dagger}. \quad (2.127)$$

Another two integrals

$$\left\{ \begin{array}{l} \sum_k \frac{V \langle d_{\sigma'}^\dagger c_{k\sigma'} \rangle}{i\omega + \varepsilon_k - 2\varepsilon_d - U - 2(N-2)\bar{n}_\zeta U} \\ \sum_{k'k} \frac{V^2 \langle c_{k'\sigma'}^\dagger c_{k\sigma'} \rangle}{i\omega + \varepsilon_k - 2\varepsilon_d - U - 2(N-2)\bar{n}_\zeta U} \end{array} \right.$$

should also be calculated through analytical continuation.

After the  $k$ -summation terms are obtained, we must do a high frequency correction because we can only sum over a finite size of mesh (Matsubara frequencies) while the tail decays very slow for large  $\omega_n$  values. When this is done, we can obtain the Green's function on the Matsubara axis

$$G(i\omega) = \frac{1 + \frac{(N-1)U}{i\omega - \varepsilon_d - \Delta(i\omega) - U - 2\Delta(i\omega) - \tilde{\Delta}(i\omega)} (\bar{n}_{\sigma'} + I_1(i\omega))}{i\omega - \varepsilon_d - \Delta(i\omega) - \frac{(N-1)U}{i\omega - \varepsilon_d - \Delta(i\omega) - U - 2\Delta(i\omega) - \tilde{\Delta}(i\omega)} (\Delta(i\omega) \cdot I_1(i\omega) + I_2(i\omega))}, \quad (2.128)$$

where  $I_1(i\omega), I_2(i\omega)$  are corresponding to the  $I_1(\omega), I_2(\omega)$  shown in the Green's function on the real axis. This part of work is still under investigation.

Once the Green's function on the Matsubara axis is obtained, the Green's function can be calculated by employing a pade scheme [83, 84]. The theory of pade scheme is as follow:

Given the values  $u_i$  of a complex function at  $N$  complex points

$$G_N(z) = \frac{a_1}{1 + \frac{a_1(z-z_1)}{1 + \dots + a_N(z-z_{N-1})}}, \quad (2.129)$$

the coefficients are chosen so that  $G_N(z) = u_i$  ( $i = 1, \dots, N$ ) by the recursion relation

$$a_i = g_i(z_i), \quad g_1(z_i) = u_i \quad (i = 1, \dots, N) \quad (2.130)$$

$$g_p = \frac{g_{p-1}(z_{p-1}) - g_{p-1}(z)}{(z - z_{p-1})g_{p-1}(z)}, \quad (p \geq 2). \quad (2.131)$$

When the coefficients are obtained, we can construct the formula for  $G_N(z)$ .

$$G_N(z) = \frac{A_N}{B_N} \quad (2.132)$$

with

$$A_{n+1}(z) = A_n(z) + (z - z_n)a_{n+1}A_{n-1}(z) \quad (2.133)$$

$$B_{n+1}(z) = B_n(z) + (z - z_n)a_{n+1}B_{n-1}(z) \quad (2.134)$$

and  $A_0 = 0, A_1 = a_1, B_0 = B_1 = 1$ .

From the Green's function on the Matsubara axis  $G(i\omega_n)$ , we can determine the coefficients in (2.129) and then we can know the formula (2.132), through which we can calculate the value of  $G(z)$  at any points. Hence, the Green's function on the real axis  $G(\omega)$  can be obtained.



# Chapter 3 Higher approximations beyond Lacroix's level

In the last chapter, Wang's decoupling scheme differs from Lacroix's decoupling by taking a more systematic expansion for the Green's functions. However, comparing with Lacroix's decoupling, the included equations of motion and the decoupled Green's functions are completely same. The difference is only in the decoupling. Hence, we say they are in the same level of approximations.

To beyond this level of approximations, in this Chapter we have made some exploratory work for a better decoupling scheme by including more equations of motion of the higher order terms that contributes much in the equations of motion of Green's functions involving one  $c$  operator. Previously these higher order terms are approximated with the decoupling scheme. This study will be helpful to answer the open question: how good the present decoupling scheme is in the approximation to the higher higher order terms.

There are several possibilities to include the higher order equations of motions: expansion with respect to increasing order of  $U$ , expansion with respect to increasing order of  $V$ , and the combination of these two possibilities. The increasing order of  $U$  corresponds to the three-particle and even more particle Green's functions. The increasing order of  $V$  relates to the Green's functions involving more  $c$  operators. In this Chapter we first study the case including the equation of motion of three-particle Green's function, then explore the the case including the equations of motion for double  $c$  operator Green's functions with different decoupling schemes.

## 3.1 Equations of motion for three-particle Green's function

In the last Chapter, we have decoupled all the three-particle Green's functions and replaced them with products of lower order Green's function and lower order Green's function based correlations. One possibility for a higher order approximation is to derive the equations of motion for these three-particle Green's functions so that we can approximate these three-particle Green's functions much better. By studying the three-particle Green's functions, we can know whether one three-particle

Green's function is large or small, which will be in favor of improving the decouple scheme.

The first trial is to involve the equation of motion of  $\ll \hat{n}_\zeta \hat{n}_{\sigma'} d_\sigma; d_\sigma^\dagger \gg$  which is directly related to and also makes apparent contribution to  $\ll \hat{n}_{\sigma'} d_\sigma; d_\sigma^\dagger \gg$ , while the quality of the approximation of  $\ll \hat{n}_{\sigma'} d_\sigma; d_\sigma^\dagger \gg$  determines the precision of the final single-particle Green's function, see Eq. (2.17).

We have calculated the equation of motion as follows:

$$\begin{aligned}
& (\omega - \varepsilon_d - 2U) \ll \hat{n}_\zeta \hat{n}_{\sigma'} d_\sigma; d_\sigma^\dagger \gg \\
& = \langle \hat{n}_\zeta \hat{n}_{\sigma'} \rangle + (N - 3)U \ll \hat{n}_{\sigma''} \hat{n}_\zeta \hat{n}_{\sigma'} d_\sigma; d_\sigma^\dagger \gg + \sum_k (-V_k^* \ll \hat{n}_\zeta c_{k\sigma'}^\dagger d_{\sigma'} d_\sigma; d_\sigma^\dagger \gg \\
& - V_k^* \ll \hat{n}_{\sigma'} c_{k\zeta}^\dagger d_\zeta d_\sigma; d_\sigma^\dagger \gg + V_k \ll \hat{n}_\zeta \hat{n}_{\sigma'} c_{k\sigma}; d_\sigma^\dagger \gg + V_k \ll \hat{n}_\zeta d_{\sigma'}^\dagger c_{k\sigma'} d_\sigma; d_\sigma^\dagger \gg \\
& + V_k \ll \hat{n}_{\sigma'} d_\zeta^\dagger c_{k\zeta} d_\sigma; d_\sigma^\dagger \gg) \tag{3.1}
\end{aligned}$$

We can see that it gives a new constant correlation  $\langle \hat{n}_\zeta \hat{n}_{\sigma'} \rangle$  which will play the same role as  $\bar{n}_{\sigma'}$  in Eq. (2.58). This equation of motion (3.1) should be helpful to explore the decoupling scheme of the three-particle Green's functions. However, taking this equation of motion into account, there is a difficulty that we have to consider how to treat or decouple the four-particle Green's function.

If we decouple the three-particle Green's function as follows:

$$\ll \hat{n}_{\sigma'} d_\zeta^\dagger c_{k\zeta} d_\sigma; d_\sigma^\dagger \gg \approx \langle d_\zeta^\dagger c_{k\zeta} \rangle \ll \hat{n}_{\sigma'} d_\sigma; d_\sigma^\dagger \gg \tag{3.2}$$

$$\ll \hat{n}_{\sigma'} c_{k\zeta}^\dagger d_\zeta d_\sigma; d_\sigma^\dagger \gg \approx \langle c_{k\zeta}^\dagger d_\zeta \rangle \ll \hat{n}_{\sigma'} d_\sigma; d_\sigma^\dagger \gg \tag{3.3}$$

$$\ll \hat{n}_\zeta \hat{n}_{\sigma'} c_{k\sigma}; d_\sigma^\dagger \gg \approx \Delta \ll \hat{n}_\zeta \hat{n}_{\sigma'} d_\sigma; d_\sigma^\dagger \gg \tag{3.4}$$

and decouple the four-particle Green's function as

$$\ll \hat{n}_{\sigma''} \hat{n}_\zeta \hat{n}_{\sigma'} d_\sigma; d_\sigma^\dagger \gg \approx \bar{n}_{\sigma'} \ll \hat{n}_\zeta \hat{n}_{\sigma'} d_\sigma; d_\sigma^\dagger \gg \tag{3.5}$$

we will obtain

$$\ll \hat{n}_\zeta \hat{n}_{\sigma'} d_\sigma; d_\sigma^\dagger \gg \approx \frac{\langle \hat{n}_\zeta \hat{n}_{\sigma'} \rangle}{\omega - \varepsilon_d - 2U - (N - 3)U\bar{n}_{\sigma''} - \Delta} \tag{3.6}$$

Another three-particle Green's function that might be important is  $\ll \hat{n}_\zeta c_{k\sigma'}^\dagger d_{\sigma'} d_\sigma; d_\sigma^\dagger \gg$ . Here we give its equation of motion,

$$\begin{aligned}
& (\omega + \varepsilon_k - 2\varepsilon_f - U) \ll \hat{n}_\zeta c_{k\sigma'}^\dagger d_{\sigma'} d_\sigma; d_\sigma^\dagger \gg \\
& = \langle \hat{n}_\zeta c_{k\sigma'}^\dagger d_{\sigma'} \rangle + 2(N - 3)U \ll \hat{n}_\zeta \hat{n}_\zeta c_{k\sigma'}^\dagger d_{\sigma'} d_\sigma; d_\sigma^\dagger \gg + \sum_k V_k (- \ll \hat{n}_\zeta \hat{n}_{\sigma'} d_\sigma; d_\sigma^\dagger \gg \\
& + \ll \hat{n}_\zeta c_{k\sigma'}^\dagger d_{\sigma'} c_{k'\sigma}; d_\sigma^\dagger \gg + \ll \hat{n}_\zeta c_{k\sigma'}^\dagger c_{k'\sigma'} d_\sigma; d_\sigma^\dagger \gg) \tag{3.7}
\end{aligned}$$



Moreover, for these three particle Green's functions, we can also use a more complicated decoupling scheme, *e.g.* Wang's decoupling scheme, to decouple the multi-particle Green's functions. The study of how to treat these three-particle and four-particle Green's function in advance will be carried out in future works.

## 3.2 EOMs for multi- $c$ operator Green's functions

Another direction is to include and derive the equations of motion for those Green's functions involving double  $c$  operators. Lacroix's level is just to include the equations of motion for the Green's functions involving one  $c$  operator compared to Hubbard-I approximation and proves to be successful in describing the presence of Kondo peak. Therefore, it might give a more exact result by including the equations of motion for higher order Green's function involving double  $c$  operator.

Of course, due to the different treatments to those much higher order Green's functions, *e.g.* three-particle Green's functions involving double  $c$  operators, Green's function involving three  $c$  operators, and so on, we give the discussion in different decoupling schemes: the extended Lacroix's decoupling scheme and Wang's decoupling scheme.

### 3.2.1 Extended Lacroix's decoupling scheme

For a simple consideration, we will decouple the three  $c$  operator Green's functions and three-particle Green's function, *i.e.*

$$\begin{aligned} G_{c'c'c} &\approx \langle c_{k'\sigma'}^\dagger c_{k'\sigma'} \rangle G_c, & G_{nnd} &\approx \bar{n}_\zeta G_{nd}, & G_{ncdd} &\approx \bar{n}_\zeta G_{cdd}, & G_{ndc'c} &\approx \bar{n}_\zeta G_{dc'c}, & G_{nc'dc} &\approx \bar{n}_\zeta G_{c'dc} \\ G_{nc'cd} &\approx \bar{n}_\zeta G_{c'cd}, & G_{n(\sigma)dc'c} &\approx \bar{n}_\sigma G_{dc'c}, & G_{n(\sigma)c'dc} &\approx \bar{n}_\sigma G_{c'dc}, & G_{n(\sigma')c'cd} &\approx \bar{n}_{\sigma'} G_{c'cd} \end{aligned} \quad (3.8)$$

Actually, in a strict sense,  $G_{nnd}, G_{nnc}, G_{ndcd}$  and  $G_{nc'dd}$  should also be treated with the exact form of EOMs because they appeared simultaneously with  $G_{c'cd}, G_{c'dc}$  and  $G_{dc'c}$ . Therefore, they should be of the same order. However, for simplicity, here we just decouple these three-particle Green's functions instead of including their equations of motion.

With the above decoupling, the EOMs are given as

$$(\omega - \varepsilon_k - \Delta)G_d = 1 + (N - 1)G_{nd} \quad (3.9)$$

$$(\omega - \varepsilon_d - U - (N - 2)\bar{n}_\zeta U)G_{nd} = \bar{n}_{\sigma'} + V \sum_k (G_{nc} + G_{dcd} - G_{cdd}) \quad (3.10)$$

$$V \sum_k G_{nc} = \sum_k \frac{V^2}{\omega - \varepsilon_k} G_{nd} + \sum_{kk'} \frac{V^2}{\omega - \varepsilon_k} (G_{dc'c} - G_{c'dc}) \quad (3.11)$$

$$V \sum_k G_{dcd} = \sum_k \frac{V \langle d_{\sigma'}^\dagger c_{k\sigma'} \rangle}{\omega - \varepsilon_k} + \sum_k \frac{V^2}{\omega - \varepsilon_k} G_{nd} - \sum_{kk'} \frac{V^2}{\omega - \varepsilon_k} G_{c'cd} + \sum_{kk'} \frac{V^2}{\omega - \varepsilon_{k'}} G_{dc'c} \quad (3.12)$$

$$V \sum_k G_{cdd} = \sum_k \frac{V \langle d_{\sigma'}^\dagger c_{k\sigma'} \rangle - V^2 G_{nd}}{\omega + \varepsilon_k - 2\varepsilon_d - U - 2(N-2)\bar{n}_\zeta U} + \sum_{kk'} \frac{V^2}{\omega + \varepsilon_{k'} - 2\varepsilon_d - U - 2(N-2)\bar{n}_\zeta U} (G_{c'dc} + G_{c'cd}) \quad (3.13)$$

$$G_{dc'c} = \frac{V \sum_{k''} G_{c'c'c} - V G_{nc} - V G_{dc'd}}{\omega + \varepsilon_d - \varepsilon_{k'} - \varepsilon_k - \bar{n}_\sigma U - (N-2)\bar{n}_\zeta U} \quad (3.14)$$

$$G_{c'dc} = \frac{-V \sum_{k''} G_{c'c'c} + V G_{nc} - V G_{c'dd}}{\omega - \varepsilon_d + \varepsilon_{k'} - \varepsilon_k + \bar{n}_\sigma U + (N-2)\bar{n}_\zeta U} \quad (3.15)$$

$$G_{c'cd} = \frac{\langle c_{k'\sigma'}^\dagger c_{k\sigma'} \rangle - V \sum_{k''} G_{c'c'c} + V G_{dcd} - V G_{c'dd}}{\omega - \varepsilon_d + \varepsilon_{k'} - \varepsilon_k + \bar{n}_{\sigma'} U + (N-2)\bar{n}_\zeta U} \quad (3.16)$$

For infinite  $U$ , all the last three Green's functions are zero. However, for finite  $U$ , they are not zero any more so that we have to take them into account carefully. The simplest treatment is to treat the higher order Green's functions in RHS of Eq. (3.14-3.16) as zero, *i.e.*

$$G_{dc'c} = \frac{-V G_{nc} - V G_{dc'd}}{\omega + \varepsilon_d - \varepsilon_{k'} - \varepsilon_k - \bar{n}_\sigma U - (N-2)\bar{n}_\zeta U} \quad (3.17)$$

$$G_{c'dc} = \frac{V G_{nc} - V G_{c'dd}}{\omega - \varepsilon_d + \varepsilon_{k'} - \varepsilon_k + \bar{n}_\sigma U + (N-2)\bar{n}_\zeta U} \quad (3.18)$$

$$G_{c'cd} = \frac{\langle c_{k'\sigma'}^\dagger c_{k\sigma'} \rangle + V G_{dcd} - V G_{c'dd}}{\omega - \varepsilon_d + \varepsilon_{k'} - \varepsilon_k + \bar{n}_{\sigma'} U + (N-2)\bar{n}_\zeta U} \quad (3.19)$$

However, a more self-consistent approximation is to decouple all these higher order Green's functions. For simplicity, we decoupled all the Green's functions appeared in RHS of Eq. (3.14-3.16),

$$G_{dc'c} \approx \frac{\sum_{k''} \frac{V^2 \langle c_{k''\sigma'}^\dagger c_{k'\sigma'} \rangle}{\omega - \varepsilon_k} G_d - \bar{n}_{\sigma'} \frac{V^2}{\omega - \varepsilon_k} G_d - V \langle d_{\sigma'}^\dagger c_{k'\sigma'} \rangle G_d}{\omega + \varepsilon_d - \varepsilon_{k'} - \varepsilon_k - \bar{n}_\sigma U - (N-2)\bar{n}_\zeta U} \quad (3.20)$$

$$G_{c'dc} \approx \frac{-\sum_{k''} \frac{V^2 \langle c_{k''\sigma'}^\dagger c_{k'\sigma'} \rangle}{\omega - \varepsilon_k} G_d + \bar{n}_{\sigma'} \frac{V^2}{\omega - \varepsilon_k} G_d - V \langle c_{k'\sigma'}^\dagger d_{\sigma'} \rangle G_d}{\omega - \varepsilon_d + \varepsilon_{k'} - \varepsilon_k + \bar{n}_\sigma U + (N-2)\bar{n}_\zeta U} \quad (3.21)$$

$$G_{c'cd} \approx \frac{\langle c_{k'\sigma'}^\dagger c_{k\sigma'} \rangle - \sum_{k''} \frac{V^2}{\omega - \varepsilon_{k''}} \langle c_{k'\sigma'}^\dagger c_{k\sigma'} \rangle G_d + V \langle d_{\sigma'}^\dagger c_{k\sigma'} \rangle G_d - V \langle c_{k'\sigma'}^\dagger d_{\sigma'} \rangle G_d}{\omega - \varepsilon_d + \varepsilon_{k'} - \varepsilon_k + \bar{n}_{\sigma'} U + (N-2)\bar{n}_\zeta U} \quad (3.22)$$

To write the above formula in a more compact and clear way, we define a reduced correlation

$$C_c^{red}(\varepsilon_k) = \sum_{k''} \langle c_{k''\sigma'}^\dagger c_{k'\sigma'} \rangle = f(\varepsilon_{k'}) - \frac{1}{\pi} \int d\omega' \mathcal{P} \frac{f(\omega') \text{Im} [\Delta(\omega') G_d(\omega')]}{\omega' - \varepsilon_{k'}} + f(\varepsilon_{k'}) \text{Re} [\Delta(\varepsilon_{k'}) G_d(\varepsilon_{k'})].$$

"reduced" means that the internal degree of freedom  $k''$  has been summed out. At the same time we mention that

$$\sum_{k''} \frac{V^2}{\omega - \varepsilon_{k''}} = \Delta(\omega).$$

Thus, we can write the formulae (3.20-3.22) as

$$G_{dc'c} \approx \frac{C_c^{red}(\varepsilon_{k'}) \frac{V^2}{\omega - \varepsilon_k} G_d - \bar{n}_{\sigma'} \frac{V^2}{\omega - \varepsilon_k} G_d - V \langle d_{\sigma'}^\dagger, c_{k'\sigma'} \rangle G_d}{\omega + \varepsilon_d - \varepsilon_{k'} - \varepsilon_k - \bar{n}_{\sigma'} U - (N-2) \bar{n}_\zeta U} \quad (3.23)$$

$$G_{c'dc} \approx \frac{-C_c^{red}(\varepsilon_{k'}) \frac{V^2}{\omega - \varepsilon_k} G_d + \bar{n}_{\sigma'} \frac{V^2}{\omega - \varepsilon_k} G_d - V \langle c_{k'\sigma'}^\dagger, d_{\sigma'} \rangle G_d}{\omega - \varepsilon_d + \varepsilon_{k'} - \varepsilon_k + \bar{n}_{\sigma'} U + (N-2) \bar{n}_\zeta U} \quad (3.24)$$

$$G_{c'cd} \approx \frac{\langle c_{k'\sigma'}^\dagger, c_{k\sigma'} \rangle - \Delta(\omega) \langle c_{k'\sigma'}^\dagger, c_{k\sigma'} \rangle G_d + V \langle d_{\sigma'}^\dagger, c_{k\sigma'} \rangle G_d - V \langle c_{k'\sigma'}^\dagger, d_{\sigma'} \rangle G_d}{\omega - \varepsilon_d + \varepsilon_{k'} - \varepsilon_k + \bar{n}_{\sigma'} U + (N-2) \bar{n}_\zeta U} \quad (3.25)$$

After lengthy calculation, we finally obtain

$$\begin{aligned} & (\omega - \varepsilon_d - 2\Delta - \tilde{\Delta} - U - (N-2) \bar{n}_\zeta U) G_{nd} \\ = & \bar{n}_{\sigma'} + \sum_k \frac{V \langle d_{\sigma'}^\dagger, c_{k\sigma'} \rangle}{\omega - \varepsilon_k} - \sum_k \frac{V \langle d_{\sigma'}^\dagger, c_{k\sigma'} \rangle}{\omega + \varepsilon_k - 2\varepsilon_d - U - 2(N-2) \bar{n}_\zeta U} \\ + & \sum_{kk'} \left( -\frac{V^2}{\omega - \varepsilon_k} - \frac{V^2}{\omega + \varepsilon_{k'} - 2\varepsilon_d - U - 2(N-2) \bar{n}_\zeta U} \right) \frac{\langle c_{k'\sigma'}^\dagger, c_{k\sigma'} \rangle}{\omega - \varepsilon_d + \varepsilon_{k'} - \varepsilon_k + \bar{n}_{\sigma'} U + (N-2) \bar{n}_\zeta U} \\ + & \sum_{kk'} \frac{V^2}{\omega - \varepsilon_k} \left( \frac{C_c^{red}(\varepsilon_{k'}) \frac{V^2}{\omega - \varepsilon_k} G_d - \bar{n}_{\sigma'} \frac{V^2}{\omega - \varepsilon_k} G_d - V \langle d_{\sigma'}^\dagger, c_{k'\sigma'} \rangle G_d}{\omega + \varepsilon_d - \varepsilon_{k'} - \varepsilon_k - \bar{n}_{\sigma'} U - (N-2) \bar{n}_\zeta U} \right. \\ & \left. - \frac{-C_c^{red}(\varepsilon_{k'}) \frac{V^2}{\omega - \varepsilon_k} G_d + \bar{n}_{\sigma'} \frac{V^2}{\omega - \varepsilon_k} G_d - V \langle c_{k'\sigma'}^\dagger, d_{\sigma'} \rangle G_d}{\omega - \varepsilon_d + \varepsilon_{k'} - \varepsilon_k + \bar{n}_{\sigma'} U + (N-2) \bar{n}_\zeta U} - \frac{-\Delta(\omega) \langle c_{k'\sigma'}^\dagger, c_{k\sigma'} \rangle G_d + V \langle d_{\sigma'}^\dagger, c_{k\sigma'} \rangle G_d - V \langle c_{k'\sigma'}^\dagger, d_{\sigma'} \rangle G_d}{\omega - \varepsilon_d + \varepsilon_{k'} - \varepsilon_k + \bar{n}_{\sigma'} U + (N-2) \bar{n}_\zeta U} \right) \\ + & \sum_{kk'} \frac{V^2}{\omega - \varepsilon_{k'}} \frac{C_c^{red}(\varepsilon_{k'}) \frac{V^2}{\omega - \varepsilon_k} G_d - \bar{n}_{\sigma'} \frac{V^2}{\omega - \varepsilon_k} G_d - V \langle d_{\sigma'}^\dagger, c_{k'\sigma'} \rangle G_d}{\omega + \varepsilon_d - \varepsilon_{k'} - \varepsilon_k - \bar{n}_{\sigma'} U - (N-2) \bar{n}_\zeta U} \\ - & \sum_{kk'} \frac{V^2}{\omega + \varepsilon_{k'} - 2\varepsilon_d - U - 2(N-2) \bar{n}_\zeta U} \left( \frac{-C_c^{red}(\varepsilon_{k'}) \frac{V^2}{\omega - \varepsilon_k} G_d + \bar{n}_{\sigma'} \frac{V^2}{\omega - \varepsilon_k} G_d - V \langle c_{k'\sigma'}^\dagger, d_{\sigma'} \rangle G_d}{\omega - \varepsilon_d + \varepsilon_{k'} - \varepsilon_k + \bar{n}_{\sigma'} U + (N-2) \bar{n}_\zeta U} \right. \\ & \left. + \frac{-\Delta(\omega) \langle c_{k'\sigma'}^\dagger, c_{k\sigma'} \rangle G_d + V \langle d_{\sigma'}^\dagger, c_{k\sigma'} \rangle G_d - V \langle c_{k'\sigma'}^\dagger, d_{\sigma'} \rangle G_d}{\omega - \varepsilon_d + \varepsilon_{k'} - \varepsilon_k + \bar{n}_{\sigma'} U + (N-2) \bar{n}_\zeta U} \right) \\ = & \bar{n}_{\sigma'} + \sum_k \frac{V \langle d_{\sigma'}^\dagger, c_{k\sigma'} \rangle}{\omega - \varepsilon_k} - \sum_k \frac{V \langle d_{\sigma'}^\dagger, c_{k\sigma'} \rangle}{\omega + \varepsilon_k - 2\varepsilon_d - U - 2(N-2) \bar{n}_\zeta U} \\ + & \sum_{kk'} \left( -\frac{V^2}{\omega - \varepsilon_k} - \frac{V^2}{\omega + \varepsilon_{k'} - 2\varepsilon_d - U - 2(N-2) \bar{n}_\zeta U} \right) \frac{\langle c_{k'\sigma'}^\dagger, c_{k\sigma'} \rangle}{\omega - \varepsilon_d + \varepsilon_{k'} - \varepsilon_k + \bar{n}_{\sigma'} U + (N-2) \bar{n}_\zeta U} \\ + & \sum_{kk'} \frac{V^2}{\omega - \varepsilon_k} \left( \frac{C_c^{red}(\varepsilon_{k'}) \frac{V^2}{\omega - \varepsilon_k} G_d - \bar{n}_{\sigma'} \frac{V^2}{\omega - \varepsilon_k} G_d - V \langle d_{\sigma'}^\dagger, c_{k'\sigma'} \rangle G_d}{\omega + \varepsilon_d - \varepsilon_{k'} - \varepsilon_k - \bar{n}_{\sigma'} U - (N-2) \bar{n}_\zeta U} \right. \\ & \left. + \frac{C_c^{red}(\varepsilon_{k'}) \frac{V^2}{\omega - \varepsilon_k} G_d - \bar{n}_{\sigma'} \frac{V^2}{\omega - \varepsilon_k} G_d + 2V \langle d_{\sigma'}^\dagger, c_{k'\sigma'} \rangle G_d + \Delta(\omega) \langle c_{k'\sigma'}^\dagger, c_{k\sigma'} \rangle G_d - V \langle d_{\sigma'}^\dagger, c_{k\sigma'} \rangle G_d}{\omega - \varepsilon_d + \varepsilon_{k'} - \varepsilon_k + \bar{n}_{\sigma'} U + (N-2) \bar{n}_\zeta U} \right) \\ + & \sum_{kk'} \frac{V^2}{\omega - \varepsilon_{k'}} \frac{C_c^{red}(\varepsilon_{k'}) \frac{V^2}{\omega - \varepsilon_k} G_d - \bar{n}_{\sigma'} \frac{V^2}{\omega - \varepsilon_k} G_d - V \langle d_{\sigma'}^\dagger, c_{k'\sigma'} \rangle G_d}{\omega + \varepsilon_d - \varepsilon_{k'} - \varepsilon_k - \bar{n}_{\sigma'} U - (N-2) \bar{n}_\zeta U} \\ - & \sum_{kk'} \frac{V^2}{\omega + \varepsilon_{k'} - 2\varepsilon_d - U - 2(N-2) \bar{n}_\zeta U} \\ & \cdot \frac{-C_c^{red}(\varepsilon_{k'}) \frac{V^2}{\omega - \varepsilon_k} G_d + \bar{n}_{\sigma'} \frac{V^2}{\omega - \varepsilon_k} G_d - 2V \langle c_{k'\sigma'}^\dagger, d_{\sigma'} \rangle G_d + V \langle d_{\sigma'}^\dagger, c_{k\sigma'} \rangle G_d - \Delta(\omega) \langle c_{k'\sigma'}^\dagger, c_{k\sigma'} \rangle G_d}{\omega - \varepsilon_d + \varepsilon_{k'} - \varepsilon_k + \bar{n}_{\sigma'} U + (N-2) \bar{n}_\zeta U} \end{aligned} \quad (3.26)$$

This is a crucial form because we have made several approximations to simplify the derivation, *e.g.* here the two particle correlations are simply treated within the decoupling scheme. The lower

order Green's functions in RHS of Eq. (3.14-3.16) are all decoupled for simplicity. For more exact approximation, these two particle correlations and lower order Green's functions must be calculated with the corresponding Green's functions and equations of motion self-consistently.

### 3.2.2 Wang's decoupling

Using Wang's decoupling scheme, the three-particle Green's functions should be decoupled as follows:

$$G_{nnd} = G_{nnd}^c + \bar{n}_\zeta G_{nd} + \langle \hat{n}_\zeta \hat{n}_{\sigma'} \rangle_c G_d + \bar{n}_{\sigma'} G_{n(\zeta)d}^c \quad (3.27)$$

$$G_{ncdd} = G_{ncdd}^c + \bar{n}_\zeta G_{cdd} + \langle \hat{n}_\zeta c_{\sigma'}^\dagger d_\sigma \rangle_c G_d + \langle c_{\sigma'}^\dagger d_\sigma \rangle G_{n(\zeta)d}^c \quad (3.28)$$

$$G_{ndc'c} = G_{ndc'c}^c + \bar{n}_\zeta G_{dc'c} + \langle \hat{n}_\zeta d_{\sigma'}^\dagger c_{k'\sigma'} \rangle_c G_c + \langle d_{\sigma'}^\dagger c_{k'\sigma'} \rangle G_{n(\zeta)c}^c \quad (3.29)$$

$$G_{nc'dc} = G_{nc'dc}^c + \bar{n}_\zeta G_{c'dc} + \langle \hat{n}_\zeta c_{k'\sigma'}^\dagger d_{\sigma'} \rangle_c G_c + \langle c_{k'\sigma'}^\dagger d_{\sigma'} \rangle G_{n(\zeta)c}^c \quad (3.30)$$

$$G_{nc'cd} = G_{nc'cd}^c + \bar{n}_\zeta G_{c'cd} + \langle \hat{n}_\zeta c_{k'\sigma'}^\dagger c_{k\sigma'} \rangle_c G_d + \langle c_{k'\sigma'}^\dagger c_{k\sigma'} \rangle G_{n(\zeta)d}^c \quad (3.31)$$

$$\begin{aligned} G_{n(\sigma)dc'c} &= G_{n(\sigma)dc'c}^c + \bar{n}_\sigma G_{dc'c} + \langle \hat{n}_\sigma d_{\sigma'}^\dagger c_{k'\sigma'} \rangle_c G_c + \langle d_{\sigma'}^\dagger c_{k'\sigma'} \rangle G_{n(\sigma)c}^c \\ &\quad - \langle d_{\sigma'}^\dagger c_\sigma \rangle G_{dc'd} - \langle d_{\sigma'}^\dagger c_{k\sigma} d_{\sigma'}^\dagger c_{k'\sigma'} \rangle_c G_d \end{aligned} \quad (3.32)$$

$$\begin{aligned} G_{n(\sigma)c'dc} &= G_{n(\sigma)c'dc}^c + \bar{n}_\sigma G_{c'dc} + \langle \hat{n}_\sigma c_{k'\sigma'}^\dagger d_{\sigma'} \rangle_c G_c + \langle c_{k'\sigma'}^\dagger d_{\sigma'} \rangle G_{n(\sigma)c}^c \\ &\quad - \langle d_{\sigma'}^\dagger c_\sigma \rangle G_{c'dd} - \langle d_{\sigma'}^\dagger c_{k\sigma} c_{k'\sigma'}^\dagger d_{\sigma'} \rangle_c G_d \end{aligned} \quad (3.33)$$

$$G_{n(\sigma')c'cd} = G_{n(\sigma')c'cd}^c + \bar{n}_{\sigma'} G_{c'cd} + \langle \hat{n}_{\sigma'} c_{k'\sigma'}^\dagger c_{k\sigma'} \rangle_c G_d + \langle c_{k'\sigma'}^\dagger c_{k\sigma'} \rangle G_{nd}^c - \langle d_{\sigma'}^\dagger c_{\sigma'} \rangle G_{c'dd} \quad (3.34)$$

If all the three-particle connected Green's function and newly generated two-particle connected Green's function are set to zero, *e.g.*

$$\begin{aligned} G_{nnd}^c = 0, \quad G_{ncdd}^c = 0, \quad G_{ndc'c}^c = 0, \quad G_{nc'dc}^c = 0, \\ G_{nc'cd}^c = 0, \quad G_{n(\sigma)dc'c}^c = 0, \quad G_{n(\sigma)c'dc}^c = 0, \quad G_{n(\sigma')c'cd}^c = 0 \end{aligned} \quad (3.35)$$

Then the equations of motion turn out to be

$$(\omega - \varepsilon_k - \Delta)G_d = 1 + (N - 1)G_{nd} \quad (3.36)$$

$$(\omega - \varepsilon_d - U - (N - 2)\bar{n}_\zeta U)G_{nd} = \bar{n}_{\sigma'} + V \sum_k (G_{nc} + G_{dcd} - G_{cdd}) \quad (3.37)$$

$$V \sum_k G_{nc} = \sum_k \frac{V^2}{\omega - \varepsilon_k} G_{nd} + \sum_{kk'} \frac{V^2}{\omega - \varepsilon_k} (G_{dc'c} - G_{c'dc}) \quad (3.38)$$

$$V \sum_k G_{dcd} = \sum_k \frac{V \langle d_{\sigma'}^\dagger c_{k\sigma'} \rangle}{\omega - \varepsilon_k} + \sum_k \frac{V^2}{\omega - \varepsilon_k} G_{nd} - \sum_{kk'} \frac{V^2}{\omega - \varepsilon_k} G_{c'cd} + \sum_{kk'} \frac{V^2}{\omega - \varepsilon_{k'}} G_{dc'c} \quad (3.39)$$

$$\begin{aligned} V \sum_k G_{cdd} &= \sum_k \frac{V \langle d_{\sigma'}^\dagger c_{k\sigma'} \rangle + V(N - 2)U \langle \hat{n}_\zeta c_{k\sigma'}^\dagger d_{\sigma'} \rangle_c G_d - V^2 G_{nd}}{\omega + \varepsilon_k - 2\varepsilon_d - U - 2(N - 2)\bar{n}_\zeta U} \\ &\quad + \sum_{kk'} \frac{V^2}{\omega + \varepsilon_{k'} - 2\varepsilon_d - U - 2(N - 2)\bar{n}_\zeta U} (G_{c'dc} + G_{c'cd}) \end{aligned} \quad (3.40)$$

$$G_{dc'c} \approx \frac{U(\langle \hat{n}_\sigma d_{\sigma'}^\dagger c_{k'\sigma'} \rangle_c G_c - \langle d_{\sigma'}^\dagger c_{k\sigma} d_{\sigma'}^\dagger c_{k'\sigma'} \rangle G_d + (N-2)\langle \hat{n}_\zeta d_{\sigma'}^\dagger c_{k'\sigma'} \rangle_c G_c)}{\omega + \varepsilon_d - \varepsilon_{k'} - \varepsilon_k - \bar{n}_\sigma U - (N-2)\bar{n}_\zeta U} + \frac{V \sum_{k''} G_{c''c'c} - V G_{nc} - V G_{dc'd}}{\omega + \varepsilon_d - \varepsilon_{k'} - \varepsilon_k - \bar{n}_\sigma U - (N-2)\bar{n}_\zeta U} + \frac{V \sum_{k''} G_{c''c'c} - V G_{nc} - V G_{dc'd}}{\omega + \varepsilon_d - \varepsilon_{k'} - \varepsilon_k - \bar{n}_\sigma U - (N-2)\bar{n}_\zeta U} \quad (3.41)$$

$$G_{c'dc} \approx \frac{U(-\langle \hat{n}_\sigma c_{k'\sigma'}^\dagger d_{\sigma'} \rangle_c G_c + \langle d_{\sigma'}^\dagger c_{k\sigma} c_{k'\sigma'}^\dagger d_{\sigma'} \rangle G_d - (N-2)\langle \hat{n}_\zeta c_{k'\sigma'}^\dagger d_{\sigma'} \rangle_c G_c)}{\omega - \varepsilon_d + \varepsilon_{k'} - \varepsilon_k + \bar{n}_\sigma U + (N-2)\bar{n}_\zeta U} + \frac{-V \sum_{k''} G_{c'c''c} + V G_{nc} - V G_{c'dd}}{\omega - \varepsilon_d + \varepsilon_{k'} - \varepsilon_k + \bar{n}_\sigma U + (N-2)\bar{n}_\zeta U} + \frac{-V \sum_{k''} G_{c'c''c} + V G_{nc} - V G_{c'dd}}{\omega - \varepsilon_d + \varepsilon_{k'} - \varepsilon_k + \bar{n}_\sigma U + (N-2)\bar{n}_\zeta U} \quad (3.42)$$

$$G_{c'cd} \approx \frac{U(-\langle \hat{n}_\sigma c_{k'\sigma'}^\dagger c_{k\sigma'} \rangle_c G_d + \langle d_{\sigma'}^\dagger c_{\sigma'} \rangle \langle c_{k'\sigma'}^\dagger d_{\sigma'} \rangle G_d - (N-2)\langle \hat{n}_\zeta c_{k'\sigma'}^\dagger c_{k\sigma'} \rangle_c G_d)}{\omega - \varepsilon_d + \varepsilon_{k'} - \varepsilon_k + \bar{n}_\sigma U + (N-2)\bar{n}_\zeta U} + \frac{\langle c_{k'\sigma'}^\dagger c_{k\sigma'} \rangle - V \sum_{k''} G_{c'cc''} + V G_{dcd} - V G_{c'dd}}{\omega - \varepsilon_d + \varepsilon_{k'} - \varepsilon_k + \bar{n}_\sigma U + (N-2)\bar{n}_\zeta U} \quad (3.43)$$

For the simplest treatment, here we apply Hartree-Fock approximations for the two-particle Green's functions appearing on the right hand side in Eq. (3.41)-Eq. (3.43). Now the last three equations are

$$G_{dc'c} \approx \frac{U(\langle \hat{n}_\sigma d_{\sigma'}^\dagger c_{k'\sigma'} \rangle_c G_c - \langle d_{\sigma'}^\dagger c_{k\sigma} d_{\sigma'}^\dagger c_{k'\sigma'} \rangle G_d + (N-2)\langle \hat{n}_\zeta d_{\sigma'}^\dagger c_{k'\sigma'} \rangle_c G_c)}{\omega + \varepsilon_d - \varepsilon_{k'} - \varepsilon_k - \bar{n}_\sigma U - (N-2)\bar{n}_\zeta U} + \frac{\sum_{k''} \frac{V^2 \langle c_{k''\sigma'}^\dagger c_{k'\sigma'} \rangle}{\omega - \varepsilon_k} G_d - \bar{n}_{\sigma'} \frac{V^2}{\omega - \varepsilon_k} G_d - V \langle d_{\sigma'}^\dagger c_{k'\sigma'} \rangle G_d}{\omega + \varepsilon_d - \varepsilon_{k'} - \varepsilon_k - \bar{n}_\sigma U - (N-2)\bar{n}_\zeta U} \quad (3.44)$$

$$G_{c'dc} \approx \frac{U(-\langle \hat{n}_\sigma c_{k'\sigma'}^\dagger d_{\sigma'} \rangle_c G_c + \langle d_{\sigma'}^\dagger c_{k\sigma} c_{k'\sigma'}^\dagger d_{\sigma'} \rangle G_d - (N-2)\langle \hat{n}_\zeta c_{k'\sigma'}^\dagger d_{\sigma'} \rangle_c G_c)}{\omega - \varepsilon_d + \varepsilon_{k'} - \varepsilon_k + \bar{n}_\sigma U + (N-2)\bar{n}_\zeta U} + \frac{-\sum_{k''} \frac{V^2 \langle c_{k''\sigma'}^\dagger c_{k'\sigma'} \rangle}{\omega - \varepsilon_k} G_d + \bar{n}_{\sigma'} \frac{V^2}{\omega - \varepsilon_k} G_d - V \langle c_{k'\sigma'}^\dagger d_{\sigma'} \rangle G_d}{\omega - \varepsilon_d + \varepsilon_{k'} - \varepsilon_k + \bar{n}_\sigma U + (N-2)\bar{n}_\zeta U} \quad (3.45)$$

$$G_{c'cd} \approx \frac{U(-\langle \hat{n}_\sigma c_{k'\sigma'}^\dagger c_{k\sigma'} \rangle_c G_d + \langle d_{\sigma'}^\dagger c_{\sigma'} \rangle \langle c_{k'\sigma'}^\dagger d_{\sigma'} \rangle G_d - (N-2)\langle \hat{n}_\zeta c_{k'\sigma'}^\dagger c_{k\sigma'} \rangle_c G_d)}{\omega - \varepsilon_d + \varepsilon_{k'} - \varepsilon_k + \bar{n}_\sigma U + (N-2)\bar{n}_\zeta U} + \frac{\langle c_{k'\sigma'}^\dagger c_{k\sigma'} \rangle - \sum_{k''} \frac{V^2}{\omega - \varepsilon_{k''}} \langle c_{k'\sigma'}^\dagger c_{k\sigma'} \rangle G_d + V \langle d_{\sigma'}^\dagger c_{k\sigma'} \rangle G_d - V \langle c_{k'\sigma'}^\dagger d_{\sigma'} \rangle G_d}{\omega - \varepsilon_d + \varepsilon_{k'} - \varepsilon_k + \bar{n}_\sigma U + (N-2)\bar{n}_\zeta U} \quad (3.46)$$

Then we can calculate the equations of motion of  $G_{nd}$ ,

$$\begin{aligned} & (\omega - \varepsilon_d - U - 2\Delta - \bar{\Delta} - (N-2)\bar{n}_\zeta U) G_{nd} \\ = & \bar{n}_{\sigma'} + \sum_k \frac{V \langle d_{\sigma'}^\dagger c_{k\sigma'} \rangle}{\omega - \varepsilon_k} - \sum_k \frac{V \langle c_{k\sigma'}^\dagger d_{\sigma'} \rangle}{\omega + \varepsilon_k - 2\varepsilon_d - U - 2(N-2)U\bar{n}_\zeta} \\ & + \sum_{kk'} \left( -\frac{V^2}{\omega - \varepsilon_k} - \frac{V^2}{\omega + \varepsilon_k - 2\varepsilon_d - U - 2(N-2)U\bar{n}_\zeta} \right) \frac{\langle c_{k'\sigma'}^\dagger c_{k\sigma'} \rangle}{\omega - \varepsilon_d + \varepsilon_{k'} - \varepsilon_k + \bar{n}_\sigma U + (N-2)\bar{n}_\zeta U} \\ & + (N-2)U \left( \sum_k \frac{V \langle \hat{n}_\zeta c_{k\sigma'}^\dagger d_{\sigma'} \rangle_c G_d}{\omega + \varepsilon_k - 2\varepsilon_d - U - 2(N-2)\bar{n}_\zeta U} + \sum_{kk'} \frac{V^2}{\omega - \varepsilon_k} \frac{\langle \hat{n}_\zeta d_{\sigma'}^\dagger c_{k'\sigma'} \rangle_c \frac{V}{\omega - \varepsilon_k} G_d}{\omega + \varepsilon_d - \varepsilon_{k'} - \varepsilon_k - \bar{n}_\sigma U - (N-2)\bar{n}_\zeta U} \right. \\ & + \sum_{kk'} \frac{V^2}{\omega - \varepsilon_k} \frac{\langle \hat{n}_\zeta c_{k'\sigma'}^\dagger d_{\sigma'} \rangle_c \frac{V}{\omega - \varepsilon_k} G_d + \langle \hat{n}_\zeta c_{k'\sigma'}^\dagger c_{k\sigma'} \rangle_c G_d}{\omega - \varepsilon_d + \varepsilon_{k'} - \varepsilon_k + \bar{n}_\sigma U + (N-2)\bar{n}_\zeta U} + \sum_{kk'} \frac{V^2}{\omega - \varepsilon_{k'}} \frac{\langle \hat{n}_\zeta d_{\sigma'}^\dagger c_{k'\sigma'} \rangle_c \frac{V}{\omega - \varepsilon_k} G_d}{\omega + \varepsilon_d - \varepsilon_{k'} - \varepsilon_k - \bar{n}_\sigma U - (N-2)\bar{n}_\zeta U} \\ & \left. - \sum_{kk'} \frac{V^2}{\omega + \varepsilon_k - 2\varepsilon_d - U - 2(N-2)\bar{n}_\zeta U} \frac{-\langle \hat{n}_\zeta c_{k'\sigma'}^\dagger d_{\sigma'} \rangle_c \frac{V}{\omega - \varepsilon_k} G_d - \langle \hat{n}_\zeta c_{k'\sigma'}^\dagger c_{k\sigma'} \rangle_c G_d}{\omega - \varepsilon_d + \varepsilon_{k'} - \varepsilon_k + \bar{n}_\sigma U + (N-2)\bar{n}_\zeta U} \right) + \end{aligned}$$

$$\begin{aligned}
& + G_d \sum_{kk'} \frac{V^2}{\omega - \varepsilon_k} \left( \frac{U(\langle \hat{n}_\sigma d_{\sigma'}^\dagger c_{k'\sigma'} \rangle_c \frac{V}{\omega - \varepsilon_k} - \langle d_{\sigma'}^\dagger c_{k\sigma} d_{\sigma'}^\dagger c_{k'\sigma'} \rangle) + \sum_{k''} \frac{V^2 \langle c_{k''\sigma'}^\dagger c_{k'\sigma'} \rangle}{\omega - \varepsilon_k} - \bar{n}_{\sigma'} \frac{V^2}{\omega - \varepsilon_k} - V \langle d_{\sigma'}^\dagger c_{k'\sigma'} \rangle}{\omega + \varepsilon_d - \varepsilon_{k'} - \varepsilon_k - \bar{n}_\sigma U - (N-2)\bar{n}_\zeta U} \right. \\
& \quad - \frac{U(-\langle \hat{n}_\sigma c_{k'\sigma'}^\dagger d_{\sigma'} \rangle_c \frac{v}{\omega - \varepsilon_k} + \langle d_{\sigma'}^\dagger c_{k\sigma} c_{k'\sigma'}^\dagger d_{\sigma'} \rangle) - \sum_{k''} \frac{V^2 \langle c_{k''\sigma'}^\dagger c_{k'\sigma'} \rangle}{\omega - \varepsilon_k} + \bar{n}_{\sigma'} \frac{V^2}{\omega - \varepsilon_k} - V \langle c_{k'\sigma'}^\dagger d_{\sigma'} \rangle}{\omega - \varepsilon_d + \varepsilon_{k'} - \varepsilon_k + \bar{n}_\sigma U + (N-2)\bar{n}_\zeta U} \\
& \quad \left. - \frac{U(-\langle \hat{n}_{\sigma'} c_{k'\sigma'}^\dagger c_{k\sigma'} \rangle_c + \langle d_{\sigma'}^\dagger c_{\sigma'} \rangle \langle c_{k'\sigma'}^\dagger d_{\sigma'} \rangle) - \sum_{k''} \frac{V^2}{\omega - \varepsilon_{k''}} \langle c_{k'\sigma'}^\dagger c_{k\sigma'} \rangle + V \langle d_{\sigma'}^\dagger c_{k\sigma'} \rangle - V \langle c_{k'\sigma'}^\dagger d_{\sigma'} \rangle}{\omega - \varepsilon_d + \varepsilon_{k'} - \varepsilon_k + \bar{n}_{\sigma'} U + (N-2)\bar{n}_\zeta U} \right) \\
& + G_d \sum_{kk'} \frac{V^2}{\omega - \varepsilon_{k'}} \frac{U(\langle \hat{n}_\sigma d_{\sigma'}^\dagger c_{k'\sigma'} \rangle_c \frac{V}{\omega - \varepsilon_k} - \langle d_{\sigma'}^\dagger c_{k\sigma} d_{\sigma'}^\dagger c_{k'\sigma'} \rangle) + \sum_{k''} \frac{V^2 \langle c_{k''\sigma'}^\dagger c_{k'\sigma'} \rangle}{\omega - \varepsilon_k} - \bar{n}_{\sigma'} \frac{V^2}{\omega - \varepsilon_k} - V \langle d_{\sigma'}^\dagger c_{k'\sigma'} \rangle}{\omega + \varepsilon_d - \varepsilon_{k'} - \varepsilon_k - \bar{n}_\sigma U - (N-2)\bar{n}_\zeta U} \\
& - G_d \sum_{kk'} \frac{V^2}{\omega + \varepsilon_{k'} - 2\varepsilon_d - U - 2(N-2)\bar{n}_\zeta U} \cdot \\
& \quad \cdot \left( \frac{U(-\langle \hat{n}_\sigma c_{k'\sigma'}^\dagger d_{\sigma'} \rangle_c \frac{V}{\omega - \varepsilon_k} + \langle d_{\sigma'}^\dagger c_{k\sigma} c_{k'\sigma'}^\dagger d_{\sigma'} \rangle) - \sum_{k''} \frac{V^2 \langle c_{k''\sigma'}^\dagger c_{k'\sigma'} \rangle}{\omega - \varepsilon_k} + \bar{n}_{\sigma'} \frac{V^2}{\omega - \varepsilon_k} - V \langle c_{k'\sigma'}^\dagger d_{\sigma'} \rangle}{\omega - \varepsilon_d + \varepsilon_{k'} - \varepsilon_k + \bar{n}_\sigma U + (N-2)\bar{n}_\zeta U} \right. \\
& \quad \left. + \frac{U(-\langle \hat{n}_{\sigma'} c_{k'\sigma'}^\dagger c_{k\sigma'} \rangle_c + \langle d_{\sigma'}^\dagger c_{\sigma'} \rangle \langle c_{k'\sigma'}^\dagger d_{\sigma'} \rangle) - \sum_{k''} \frac{V^2}{\omega - \varepsilon_{k''}} \langle c_{k'\sigma'}^\dagger c_{k\sigma'} \rangle + V \langle d_{\sigma'}^\dagger c_{k\sigma'} \rangle - V \langle c_{k'\sigma'}^\dagger d_{\sigma'} \rangle}{\omega - \varepsilon_d + \varepsilon_{k'} - \varepsilon_k + \bar{n}_{\sigma'} U + (N-2)\bar{n}_\zeta U} \right) \quad (3.47)
\end{aligned}$$

For the infinite  $U$  case,

$$\begin{aligned}
& (\omega - \varepsilon_d - U - 2\Delta - \tilde{\Delta} - (N-2)\bar{n}_\zeta U) G_{nd} \\
& = \bar{n}_{\sigma'} + \sum_k \frac{V \langle d_{\sigma'}^\dagger c_{k\sigma'} \rangle}{\omega - \varepsilon_k} + G_d \sum_k \frac{(N-2)V \langle \hat{n}_\zeta c_{k\sigma'}^\dagger d_{\sigma'} \rangle_c}{-1 - 2(N-2)\bar{n}_\zeta} \\
& + \sum_{kk'} \left( \frac{1}{-\bar{n}_\sigma - (N-2)\bar{n}_\zeta} \langle \hat{n}_\zeta d_{\sigma'}^\dagger c_{k'\sigma'} \rangle_c \frac{V}{\omega - \varepsilon_k} G_d + \frac{1}{\bar{n}_\sigma + (N-2)\bar{n}_\zeta} (\langle \hat{n}_\zeta c_{k'\sigma'}^\dagger d_{\sigma'} \rangle_c \frac{V}{\omega - \varepsilon_k} G_d + \langle \hat{n}_\zeta c_{k'\sigma'}^\dagger c_{k\sigma'} \rangle_c G_d) \right) \\
& + \sum_{kk'} \frac{V^2}{\omega - \varepsilon_{k'}} \left( \frac{1}{-\bar{n}_\sigma - (N-2)\bar{n}_\zeta} \langle \hat{n}_\zeta d_{\sigma'}^\dagger c_{k'\sigma'} \rangle_c \frac{V}{\omega - \varepsilon_k} G_d \right. \\
& + G_d \sum_{kk'} \frac{V^2}{\omega - \varepsilon_k} \left( \frac{(\langle \hat{n}_\sigma d_{\sigma'}^\dagger c_{k'\sigma'} \rangle_c \frac{V}{\omega - \varepsilon_k} - \langle d_{\sigma'}^\dagger c_{k\sigma} d_{\sigma'}^\dagger c_{k'\sigma'} \rangle)}{-\bar{n}_\sigma - (N-2)\bar{n}_\zeta} - \frac{(-\langle \hat{n}_\sigma c_{k'\sigma'}^\dagger d_{\sigma'} \rangle_c \frac{v}{\omega - \varepsilon_k} + \langle d_{\sigma'}^\dagger c_{k\sigma} c_{k'\sigma'}^\dagger d_{\sigma'} \rangle)}{\bar{n}_\sigma + (N-2)\bar{n}_\zeta} \right. \\
& \quad \left. - \frac{(-\langle \hat{n}_{\sigma'} c_{k'\sigma'}^\dagger c_{k\sigma'} \rangle_c + \langle d_{\sigma'}^\dagger c_{\sigma'} \rangle \langle c_{k'\sigma'}^\dagger d_{\sigma'} \rangle)}{\bar{n}_{\sigma'} + (N-2)\bar{n}_\zeta} \right) \\
& + G_d \sum_{kk'} \frac{V^2}{\omega - \varepsilon_{k'}} \frac{\langle \hat{n}_\sigma d_{\sigma'}^\dagger c_{k'\sigma'} \rangle_c \frac{V}{\omega - \varepsilon_k} - \langle d_{\sigma'}^\dagger c_{k\sigma} d_{\sigma'}^\dagger c_{k'\sigma'} \rangle}{-\bar{n}_\sigma - (N-2)\bar{n}_\zeta} \quad (3.48)
\end{aligned}$$

For the  $(N=2)$  case,

$$\begin{aligned}
& (\omega - \varepsilon_d - U - 2\Delta - \tilde{\Delta}) G_{nd} \\
& = \bar{n}_{\sigma'} + \sum_k \frac{V \langle d_{\sigma'}^\dagger c_{k\sigma'} \rangle}{\omega - \varepsilon_k} - \sum_k \frac{V \langle c_{k\sigma'}^\dagger d_{\sigma'} \rangle}{\omega + \varepsilon_k - 2\varepsilon_d - U} \\
& + \sum_{kk'} \left( -\frac{V^2}{\omega - \varepsilon_k} - \frac{V^2}{\omega + \varepsilon_k - 2\varepsilon_d - U} \right) \frac{\langle c_{k'\sigma'}^\dagger c_{k\sigma'} \rangle}{\omega - \varepsilon_d + \varepsilon_{k'} - \varepsilon_k + \bar{n}_{\sigma'} U} \\
& + G_d \sum_{kk'} \frac{V^2}{\omega - \varepsilon_k} \left( \frac{U(\langle \hat{n}_\sigma d_{\sigma'}^\dagger c_{k'\sigma'} \rangle_c \frac{V}{\omega - \varepsilon_k} - \langle d_{\sigma'}^\dagger c_{k\sigma} d_{\sigma'}^\dagger c_{k'\sigma'} \rangle) + \sum_{k''} \frac{V^2 \langle c_{k''\sigma'}^\dagger c_{k'\sigma'} \rangle}{\omega - \varepsilon_k} - \bar{n}_{\sigma'} \frac{V^2}{\omega - \varepsilon_k} - V \langle d_{\sigma'}^\dagger c_{k'\sigma'} \rangle}{\omega + \varepsilon_d - \varepsilon_{k'} - \varepsilon_k - \bar{n}_\sigma U} \right. \\
& \quad - \frac{U(-\langle \hat{n}_\sigma c_{k'\sigma'}^\dagger d_{\sigma'} \rangle_c \frac{v}{\omega - \varepsilon_k} + \langle d_{\sigma'}^\dagger c_{k\sigma} c_{k'\sigma'}^\dagger d_{\sigma'} \rangle) - \sum_{k''} \frac{V^2 \langle c_{k''\sigma'}^\dagger c_{k'\sigma'} \rangle}{\omega - \varepsilon_k} + \bar{n}_{\sigma'} \frac{V^2}{\omega - \varepsilon_k} - V \langle c_{k'\sigma'}^\dagger d_{\sigma'} \rangle}{\omega - \varepsilon_d + \varepsilon_{k'} - \varepsilon_k + \bar{n}_\sigma U} \left. \right)
\end{aligned}$$

$$\begin{aligned}
& - \frac{U(-\langle \hat{n}_{\sigma'} c_{k'\sigma'}^\dagger, c_{k\sigma'} \rangle_c + \langle d_{\sigma'}^\dagger, c_{\sigma'} \rangle \langle c_{k'\sigma'}^\dagger, d_{\sigma'} \rangle) + \langle c_{k'\sigma'}^\dagger, c_{k\sigma'} \rangle - \sum_{k''} \frac{V^2}{\omega - \varepsilon_{k''}} \langle c_{k'\sigma'}^\dagger, c_{k\sigma'} \rangle + V \langle d_{\sigma'}^\dagger, c_{k\sigma'} \rangle - V \langle c_{k'\sigma'}^\dagger, d_{\sigma'} \rangle)}{\omega - \varepsilon_d + \varepsilon_{k'} - \varepsilon_k + \bar{n}_{\sigma'} U} \\
& + G_d \sum_{kk'} \frac{V^2}{\omega - \varepsilon_{k'}} \frac{U(\langle \hat{n}_{\sigma'} d_{\sigma'}^\dagger, c_{k'\sigma'} \rangle_c \frac{V}{\omega - \varepsilon_k} - \langle d_{\sigma'}^\dagger c_{k\sigma} d_{\sigma'}^\dagger, c_{k'\sigma'} \rangle) + \sum_{k''} \frac{V^2 \langle c_{k''\sigma'}^\dagger, c_{k'\sigma'} \rangle}{\omega - \varepsilon_k} - \bar{n}_{\sigma'} \frac{V^2}{\omega - \varepsilon_k} - V \langle d_{\sigma'}^\dagger, c_{k'\sigma'} \rangle}{\omega + \varepsilon_d - \varepsilon_{k'} - \varepsilon_k - \bar{n}_{\sigma'} U} \\
& - G_d \sum_{kk'} \frac{V^2}{\omega + \varepsilon_{k'} - 2\varepsilon_d - U} \cdot \\
& \cdot \left( \frac{U(-\langle \hat{n}_{\sigma'} c_{k'\sigma'}^\dagger, d_{\sigma'} \rangle_c \frac{v}{\omega - \varepsilon_k} + \langle d_{\sigma'}^\dagger c_{k\sigma} c_{k'\sigma'}^\dagger, d_{\sigma'} \rangle) - \sum_{k''} \frac{V^2 \langle c_{k''\sigma'}^\dagger, c_{k'\sigma'} \rangle}{\omega - \varepsilon_k} + \bar{n}_{\sigma'} \frac{V^2}{\omega - \varepsilon_k} - V \langle c_{k'\sigma'}^\dagger, d_{\sigma'} \rangle}{\omega - \varepsilon_d + \varepsilon_{k'} - \varepsilon_k + \bar{n}_{\sigma'} U} \right. \\
& \left. + \frac{U(-\langle \hat{n}_{\sigma'} c_{k'\sigma'}^\dagger, c_{k\sigma'} \rangle_c + \langle d_{\sigma'}^\dagger, c_{\sigma'} \rangle \langle c_{k'\sigma'}^\dagger, d_{\sigma'} \rangle) - \sum_{k''} \frac{V^2}{\omega - \varepsilon_{k''}} \langle c_{k'\sigma'}^\dagger, c_{k\sigma'} \rangle + V \langle d_{\sigma'}^\dagger, c_{k\sigma'} \rangle - V \langle c_{k'\sigma'}^\dagger, d_{\sigma'} \rangle)}{\omega - \varepsilon_d + \varepsilon_{k'} - \varepsilon_k + \bar{n}_{\sigma'} U} \right) \quad (3.49)
\end{aligned}$$

For the infinite  $U$  case, when  $N = 2$ , we find

$$\begin{aligned}
& (\omega - \varepsilon_d - U - 2\Delta - \tilde{\Delta}) G_{nd} \\
& = \bar{n}_{\sigma'} + \sum_k \frac{V \langle d_{\sigma'}^\dagger, c_{k\sigma'} \rangle}{\omega - \varepsilon_k} \\
& + \sum_{kk'} \left( \frac{1}{-\bar{n}_{\sigma'}} \langle \hat{n}_{\zeta} d_{\sigma'}^\dagger, c_{k'\sigma'} \rangle_c \frac{V}{\omega - \varepsilon_k} G_d + \frac{1}{\bar{n}_{\sigma'}} (\langle \hat{n}_{\zeta} c_{k'\sigma'}^\dagger, d_{\sigma'} \rangle_c \frac{V}{\omega - \varepsilon_k} G_d + \langle \hat{n}_{\zeta} c_{k'\sigma'}^\dagger, c_{k\sigma'} \rangle_c G_d) \right) \\
& + \sum_{kk'} \frac{V^2}{\omega - \varepsilon_{k'}} \left( \frac{1}{-\bar{n}_{\sigma'}} \langle \hat{n}_{\zeta} d_{\sigma'}^\dagger, c_{k'\sigma'} \rangle_c \frac{V}{\omega - \varepsilon_k} G_d \right. \\
& + G_d \sum_{kk'} \frac{V^2}{\omega - \varepsilon_k} \left( \frac{(\langle \hat{n}_{\sigma} d_{\sigma'}^\dagger, c_{k'\sigma'} \rangle_c \frac{V}{\omega - \varepsilon_k} - \langle d_{\sigma'}^\dagger c_{k\sigma} d_{\sigma'}^\dagger, c_{k'\sigma'} \rangle)}{-\bar{n}_{\sigma'}} - \frac{(-\langle \hat{n}_{\sigma} c_{k'\sigma'}^\dagger, d_{\sigma'} \rangle_c \frac{v}{\omega - \varepsilon_k} + \langle d_{\sigma'}^\dagger c_{k\sigma} c_{k'\sigma'}^\dagger, d_{\sigma'} \rangle)}{\bar{n}_{\sigma'}} \right. \\
& \left. \left. - \frac{(-\langle \hat{n}_{\sigma'} c_{k'\sigma'}^\dagger, c_{k\sigma'} \rangle_c + \langle d_{\sigma'}^\dagger, c_{\sigma'} \rangle \langle c_{k'\sigma'}^\dagger, d_{\sigma'} \rangle)}{\bar{n}_{\sigma'}} \right) \right) \\
& + G_d \sum_{kk'} \frac{V^2}{\omega - \varepsilon_{k'}} \frac{\langle \hat{n}_{\sigma} d_{\sigma'}^\dagger, c_{k'\sigma'} \rangle_c \frac{V}{\omega - \varepsilon_k} - \langle d_{\sigma'}^\dagger c_{k\sigma} d_{\sigma'}^\dagger, c_{k'\sigma'} \rangle}{-\bar{n}_{\sigma'}} \quad (3.50)
\end{aligned}$$

This can be matched with the result of Luo *et al.* [78] with some assumptions and simplifications.





# Chapter 4 Multi-band system

Due to the success of the impurity solver for the single band Hubbard model and the periodic Anderson model, it's easy to extend the method to multi-band systems. Actually it's also an interesting and valuable work because most of the real systems showing Mott metal-insulator transition usually have orbital degrees of freedom though most theoretical works have been carried out on the orbitally non-degenerate model for the aim of simplicity. For example, in some materials, near the Fermi surface there are more than one band with similar energies and all of these bands have to be considered localized, *e.g.* the  $e_g$  and  $t_{2g}$  orbitals of  $d$  electrons. Therefore, such kind of multi-band systems have been studied based on the multi-band Hubbard model [89, 90, 91]. Then multi-band models and systems with degenerate orbitals have been extensively studied [92, 93]. Recently, an interesting phenomenon called orbital selective Mott transition has been investigated intensively by DMFT with some numerically exact impurity solvers such as QMC and ED [94, 95]. Moreover, we have mentioned before that both methods have their limitations. Hence, a fast and reliable multi-band impurity solver will be useful to corroborate such phenomena.

For the multi-band system, the main difference to the single band system is that all the interactions of the localized electrons with orbital degrees of freedom take into account the orbital degrees of freedom. The multi-band system is different from the system with large degeneracy  $N$ . With more parameters, it can describe more systems and get more interesting information.

Here we have explored the multi-band single impurity Anderson model with the equation of motion and decoupling method. With this multi-band impurity solver, it is possible to study the multi-band Hubbard model and periodic Anderson model in the framework of the dynamical mean field theory. In this Chapter, we study the multi-band system with various approximations. For example, one assumption is to consider the interaction between two bands through the bath is negligible; another one is to treat the inter-band interaction with Hartree and Hubbard-I approximations, while our well developed decoupling method is used for the local on-site single electron Green's function. In this Chapter we only show the methods. The results will be shown in Chapter 6.

## 4.1 The Hamiltonian and EOMs

For the multi-band system, the Hamiltonian should be written as

$$\begin{aligned} \mathcal{H} = & \sum_{k\sigma} \varepsilon_k c_{k\sigma}^\dagger c_{k\sigma} + \sum_{\tau\sigma} \varepsilon_\tau d_{\tau\sigma}^\dagger d_{\tau\sigma} + \frac{1}{2} \sum_{\tau\sigma\sigma'} U_\tau \hat{n}_{\tau\sigma} \hat{n}_{\tau\sigma'} + \sum_{\substack{\tau \neq \tau' \\ \sigma}} U'_{\tau\tau'} \hat{n}_{\tau\sigma} \hat{n}_{\tau'\sigma} + \sum_{\substack{\tau \neq \tau' \\ \sigma \neq \sigma'}} U''_{\tau\tau'} \hat{n}_{\tau\sigma} \hat{n}_{\tau'\sigma'} \\ & + \sum_{\tau\sigma} (V_{\tau k}^* c_{k\sigma}^\dagger d_{\tau\sigma} + V_{\tau k} d_{\tau\sigma}^\dagger c_{k\sigma}) \end{aligned} \quad (4.1)$$

where the first term is the energy of conduction electrons. Comparing with the single band Hamiltonian (2.1), the electrons in different bands are labeled with band index  $\tau$ . The second term is the energy of electrons in different bands. The third term containing  $U$  is describing the intra-band Coulomb interaction between electrons in the same band. The fourth and fifth term are inter-band Coulomb interactions for electrons in different bands with the same spin and different spin respectively. The last term is the hybridization term for all the bands.

Because of the existence of inter-band cross interactions, the multi-band system is much more complicated than the single band system. Here our first effort has concentrated on the simplest case: the two band system. Now we first use the same techniques as in the previous two Chapters to calculate the single electron Green's function's equations of motion. Please note, there will be two single electron Green's functions simultaneously corresponding to the two different bands. Here, we use  $d$  and  $f$  to label the two bands, which are only symbols and not related to real  $d$  and  $f$  bands because the two bands can also be two  $d$  bands or two  $f$  bands.

If we define the (anti-)commutation relations for the newly appearing inter-band operators as follows,

$$[d_\sigma, f_\zeta]_+ = 0, \quad [d_\sigma^\dagger, f_\zeta^\dagger]_+ = 0, \quad [d_\sigma^\dagger, f_\zeta]_+ = 0, \quad [d_\sigma, f_\zeta^\dagger]_+ = 0 \quad (4.2)$$

where the  $\sigma, \zeta$  are any spin indices, the equations of motion should be

$$(\omega - \varepsilon_d) \ll d_\sigma; d_\sigma^\dagger \gg = 1 + U \ll \hat{n}_{d\sigma'} d_\sigma; d_\sigma^\dagger \gg + U' \ll \hat{n}_{f\sigma} d_\sigma; d_\sigma^\dagger \gg + U'' \ll \hat{n}_{d\sigma'} d_\sigma; d_\sigma^\dagger \gg + V_{dk} \ll c_{k\sigma}; d_\sigma^\dagger \gg \quad (4.3)$$

$$(\omega - \varepsilon_f) \ll f_\sigma; f_\sigma^\dagger \gg = 1 + U \ll \hat{n}_{f\sigma'} f_\sigma; f_\sigma^\dagger \gg + U' \ll \hat{n}_{d\sigma} f_\sigma; f_\sigma^\dagger \gg + U'' \ll \hat{n}_{d\sigma'} f_\sigma; f_\sigma^\dagger \gg + V_{fk} \ll c_{k\sigma}; f_\sigma^\dagger \gg \quad (4.4)$$

$$(\omega - \varepsilon_k) \ll c_{k\sigma}; d_\sigma^\dagger \gg = V_{dk}^* \ll d_\sigma; d_\sigma^\dagger \gg + V_{fk}^* \ll f_\sigma; d_\sigma^\dagger \gg \quad (4.5)$$

$$(\omega - \varepsilon_k) \ll c_{k\sigma}; f_\sigma^\dagger \gg = V_{dk}^* \ll d_\sigma; f_\sigma^\dagger \gg + V_{fk}^* \ll f_\sigma; f_\sigma^\dagger \gg \quad (4.6)$$

$$(\omega - \varepsilon_f) \ll f_\sigma; d_\sigma^\dagger \gg = U \ll \hat{n}_{f\sigma'} f_\sigma; d_\sigma^\dagger \gg + U' \ll \hat{n}_{d\sigma} f_\sigma; d_\sigma^\dagger \gg + U'' \ll \hat{n}_{d\sigma'} f_\sigma; d_\sigma^\dagger \gg + V_{fk} \ll c_{k\sigma}; d_\sigma^\dagger \gg \quad (4.7)$$

$$(\omega - \varepsilon_d) \ll d_\sigma; f_\sigma^\dagger \gg = U \ll \hat{n}_{d\sigma'} d_\sigma; f_\sigma^\dagger \gg + U' \ll \hat{n}_{f\sigma} d_\sigma; f_\sigma^\dagger \gg + U'' \ll \hat{n}_{f\sigma'} d_\sigma; f_\sigma^\dagger \gg + V_{dk} \ll c_{k\sigma}; f_\sigma^\dagger \gg \quad (4.8)$$

Here, for convenience, we have assumed that  $V_{\tau k}$  is identical for the two bands for the single impurity Anderson model or the periodic Anderson model. For the Hubbard model, we don't have

to pay attention to it because it will be automatically updated by the self-consistency condition. From the above equations, we can see that some new type of Green's functions such as  $\ll f_\sigma; d_\sigma^\dagger \gg$ ,  $\ll \hat{n}_{d\sigma'} f_\sigma; f_\sigma^\dagger \gg$  etc. appear in the equations of motion and there are inter-band terms that do not appear in the previous single band equations.

The next higher order equations are calculated as follows ( $\sigma = \zeta$ ,  $\sigma' = \xi$ ):

$$(\omega - \varepsilon_d - U) \ll \hat{n}_{d\sigma'} d_\sigma; d_\sigma^\dagger \gg = \bar{n}_{d\sigma'} + U' \ll \hat{n}_{f\zeta} \hat{n}_{d\sigma'} d_\sigma; d_\sigma^\dagger \gg + U'' \ll \hat{n}_{f\xi} \hat{n}_{d\sigma'} d_\sigma; d_\sigma^\dagger \gg \quad (4.9)$$

$$+ \sum_k (-V_{dk}^* \ll c_{k\sigma'}^\dagger d_\sigma; d_\sigma^\dagger \gg + V_{dk} \ll \hat{n}_{d\sigma'} c_{k\sigma}; d_\sigma^\dagger \gg + V_{dk} \ll d_\sigma^\dagger c_{k\sigma'}; d_\sigma^\dagger \gg)$$

$$(\omega - \varepsilon_d - U') \ll \hat{n}_{f\zeta} d_\sigma; d_\sigma^\dagger \gg = \bar{n}_{f\zeta} + U \ll \hat{n}_{f\zeta} \hat{n}_{d\sigma'} d_\sigma; d_\sigma^\dagger \gg + U'' \ll \hat{n}_{f\zeta} \hat{n}_{f\xi} d_\sigma; d_\sigma^\dagger \gg \quad (4.10)$$

$$+ \sum_k (V_{dk} \ll \hat{n}_{f\zeta} c_{k\sigma}; d_\sigma^\dagger \gg - V_{fk}^* \ll c_{k\zeta}^\dagger f_\zeta d_\sigma; d_\sigma^\dagger \gg + V_{fk} \ll f_\zeta^\dagger c_{k\zeta} d_\sigma; d_\sigma^\dagger \gg)$$

$$(\omega - \varepsilon_d - U'') \ll \hat{n}_{f\xi} d_\sigma; d_\sigma^\dagger \gg = \bar{n}_{f\xi} + U \ll \hat{n}_{f\xi} \hat{n}_{d\sigma'} d_\sigma; d_\sigma^\dagger \gg + U' \ll \hat{n}_{f\xi} \hat{n}_{f\zeta} d_\sigma; d_\sigma^\dagger \gg \quad (4.11)$$

$$+ \sum_k (V_{dk} \ll \hat{n}_{f\xi} c_{k\sigma}; d_\sigma^\dagger \gg - V_{fk}^* \ll c_{k\xi}^\dagger f_\xi d_\sigma; d_\sigma^\dagger \gg + V_{fk} \ll f_\xi^\dagger c_{k\xi} d_\sigma; d_\sigma^\dagger \gg)$$

$$(\omega - \varepsilon_f - U) \ll \hat{n}_{f\xi} f_\zeta; f_\zeta^\dagger \gg = \bar{n}_{f\xi} + U' \ll \hat{n}_{d\sigma'} \hat{n}_{f\xi} f_\zeta; f_\zeta^\dagger \gg + U'' \ll \hat{n}_{d\sigma'} \hat{n}_{f\xi} f_\zeta; f_\zeta^\dagger \gg \quad (4.12)$$

$$+ \sum_k (-V_{fk}^* \ll c_{k\xi} f_\xi f_\zeta; f_\zeta^\dagger \gg + V_{fk} \ll \hat{n}_{f\xi} f_\zeta; f_\zeta^\dagger \gg + V_{fk} \ll f_\xi c_{k\xi} f_\zeta; f_\zeta^\dagger \gg)$$

$$(\omega - \varepsilon_f - U') \ll \hat{n}_{d\sigma} f_\zeta; f_\zeta^\dagger \gg = \bar{n}_{d\sigma} + U \ll \hat{n}_{d\sigma} \hat{n}_{f\xi} f_\zeta; f_\zeta^\dagger \gg + U'' \ll \hat{n}_{d\sigma} \hat{n}_{d\sigma'} f_\zeta; f_\zeta^\dagger \gg \quad (4.13)$$

$$+ \sum_k (V_{fk} \ll \hat{n}_{d\sigma} c_{k\zeta}; f_\zeta^\dagger \gg - V_{dk}^* \ll c_{k\sigma}^\dagger d_\sigma d_\zeta; f_\zeta^\dagger \gg + V_{dk} \ll d_\sigma^\dagger c_{k\sigma} f_\zeta; f_\zeta^\dagger \gg)$$

$$(\omega - \varepsilon_f - U'') \ll \hat{n}_{d\sigma'} f_\zeta; f_\zeta^\dagger \gg = \bar{n}_{d\sigma'} + U \ll \hat{n}_{d\sigma'} \hat{n}_{f\xi} f_\zeta; f_\zeta^\dagger \gg + U' \ll \hat{n}_{d\sigma'} \hat{n}_{d\sigma} f_\zeta; f_\zeta^\dagger \gg \quad (4.14)$$

$$+ \sum_k (V_{fk} \ll \hat{n}_{d\sigma'} c_{k\zeta}; f_\zeta^\dagger \gg - V_{dk}^* \ll c_{k\sigma'}^\dagger d_{\sigma'} f_\zeta; f_\zeta^\dagger \gg + V_{dk} \ll d_{\sigma'}^\dagger c_{k\sigma'} f_\zeta; f_\zeta^\dagger \gg)$$

For the further equations of motion, we here only give the equations originating from the  $d$  band single particle Green's function. For the  $f$  band, it can be easily obtained by permuting the symbols.

$$(\omega - \varepsilon_k) \ll \hat{n}_{d\sigma'} c_{k\sigma}; d_\sigma^\dagger \gg = V_{dk}^* \ll \hat{n}_{d\sigma'} d_\sigma; d_\sigma^\dagger \gg + \sum_{dk'} (-V_{k'}^* \ll c_{k'\sigma'}^\dagger d_{\sigma'} c_{k\sigma}; d_\sigma^\dagger \gg \quad (4.15)$$

$$+ V_{dk'} \ll d_{\sigma'}^\dagger c_{k'\sigma'} c_{k\sigma}; d_\sigma^\dagger \gg) + V_{fk}^* \ll \hat{n}_{d\sigma'} f_\sigma; d_\sigma^\dagger \gg$$

$$(\omega - \varepsilon_k) \ll d_{\sigma'}^\dagger c_{k\sigma'} d_\sigma; d_\sigma^\dagger \gg = \langle d_{\sigma'}^\dagger c_{k\sigma'} \rangle + V_{dk}^* \ll \hat{n}_{d\sigma'} d_\sigma; d_\sigma^\dagger \gg + \sum_{k'} (-V_{dk'}^* \ll c_{k'\sigma'}^\dagger c_{k\sigma'} d_\sigma; d_\sigma^\dagger \gg \quad (4.16)$$

$$+ V_{dk'} \ll d_{\sigma'}^\dagger c_{k\sigma'} c_{k'\sigma}; d_\sigma^\dagger \gg) + V_{fk'}^* \ll d_{\sigma'}^\dagger f_{\sigma'} d_\sigma; d_\sigma^\dagger \gg$$

$$(\omega + \varepsilon_k - 2\varepsilon_d - U) \ll c_{k\sigma'}^\dagger d_{\sigma'} d_\sigma; d_\sigma^\dagger \gg = \langle c_{k\sigma'}^\dagger d_{\sigma'} \rangle + (U' + U'') \ll \hat{n}_{f\zeta} c_{k\sigma'}^\dagger d_{\sigma'} d_\sigma; d_\sigma^\dagger \gg + (U' + U'') \ll \hat{n}_{f\xi} c_{k\sigma'}^\dagger d_{\sigma'} d_\sigma; d_\sigma^\dagger \gg \quad (4.17)$$

$$- V_{dk} \ll \hat{n}_{d\sigma'} d_\sigma; d_\sigma^\dagger \gg + \sum_{k'} V_{dk'} (\ll c_{k'\sigma'}^\dagger d_{\sigma'} c_{k'\sigma}; d_\sigma^\dagger \gg + \ll c_{k'\sigma'}^\dagger c_{k'\sigma'} d_\sigma; d_\sigma^\dagger \gg)$$

$$- V_{fk} \ll f_\xi^\dagger d_{\sigma'} d_\sigma; d_\sigma^\dagger \gg$$

$$(\omega - \varepsilon_k) \ll \hat{n}_{f\zeta} c_{k\sigma}; d_\sigma^\dagger \gg = V_{dk}^* \ll \hat{n}_{f\zeta} d_\sigma; d_\sigma^\dagger \gg + \sum_{k'} (-V_{fk'}^* \ll c_{k'\zeta}^\dagger f_\zeta c_{k\sigma}; d_\sigma^\dagger \gg \quad (4.18)$$

$$+ V_{fk'} \ll f_\zeta^\dagger c_{k'\zeta} c_{k\sigma}; d_\sigma^\dagger \gg) + V_{fk}^* \ll \hat{n}_{f\zeta} f_\sigma; d_\sigma^\dagger \gg$$

$$\begin{aligned}
(\omega + \varepsilon_f - \varepsilon_k - \varepsilon_d) \ll f_\zeta^\dagger c_{k\zeta} d_\sigma; d_\sigma^\dagger \gg &= \langle f_\zeta^\dagger c_{k\zeta} \rangle + (U - U'') \ll \hat{n}_{d\sigma'} f_\zeta^\dagger c_{k\zeta} d_\sigma; d_\sigma^\dagger \gg + (-U + U'') \ll \hat{n}_{f\zeta} f_\zeta^\dagger c_{k\zeta} d_\sigma; d_\sigma^\dagger \gg \\
&+ V_{dk}^* \ll f_\zeta^\dagger d_\zeta d_\sigma; d_\sigma^\dagger \gg + \sum_{k'} (V_{dk'} \ll f_\zeta^\dagger c_{k\zeta} c_{k'\sigma}; d_\sigma^\dagger \gg - V_{fk'}^* \ll c_{k'\zeta}^\dagger c_{k\zeta} d_\sigma; d_\sigma^\dagger \gg) \\
&+ V_{fk}^* \ll \hat{n}_{f\zeta} d_\sigma; d_\sigma^\dagger \gg \tag{4.19}
\end{aligned}$$

$$\begin{aligned}
(\omega + \varepsilon_k - \varepsilon_f - \varepsilon_d - U') \ll c_{k\zeta}^\dagger f_\zeta d_\sigma; d_\sigma^\dagger \gg &= \langle c_{k\zeta}^\dagger f_\zeta \rangle + (U + U'') \ll \hat{n}_{d\sigma'} c_{k\zeta}^\dagger f_\zeta d_\sigma; d_\sigma^\dagger \gg + (U + U'') \ll \hat{n}_{f\zeta} c_{k\zeta}^\dagger f_\zeta d_\sigma; d_\sigma^\dagger \gg \\
&- V_{dk} \ll d_\sigma^\dagger f_\zeta d_\sigma; d_\sigma^\dagger \gg + \sum_{k'} (V_{dk'} \ll c_{k\zeta}^\dagger f_\zeta c_{k'\sigma}; d_\sigma^\dagger \gg + V_{fk'} \ll c_{k\zeta}^\dagger c_{k'\zeta} d_\sigma; d_\sigma^\dagger \gg) \\
&- V_{fk} \ll f_\zeta^\dagger f_\zeta d_\sigma; d_\sigma^\dagger \gg \tag{4.20}
\end{aligned}$$

Here will discuss some simplifications due to the complexity of the inter-band interactions and the difficulty of solving the equations of motion fully self-consistently.

## 4.2 Approximation without inter-band hybridization

From the equations we derived in the last section, we mentioned that  $\ll f_\sigma; d_\sigma^\dagger \gg$  appears in the second order equation of motion

$$(\omega - \varepsilon_k) \ll c_{k\sigma}; d_\sigma^\dagger \gg = V_{dk}^* \ll d_\sigma; d_\sigma^\dagger \gg + V_{fk}^* \ll f_\sigma; d_\sigma^\dagger \gg$$

and in the EOM of the single particle Green's function.  $\ll c_{k\sigma}; d_\sigma^\dagger \gg$  arises from the hybridization term in the Hamiltonian. Hence,  $\ll f_\sigma; d_\sigma^\dagger \gg$  describes the inter-band interaction through the bath. On the other hand, it means that one electron is created in the  $d$  band and one electron is destroyed in the  $f$  band. Hence, it is a higher order quantum effect than  $\ll d_\sigma; d_\sigma^\dagger \gg$ . Therefore, naturally one can consider that it has a much smaller amplitude, which is reasonable for those systems where the interaction matrix element  $V_{dk} \cdot V_{fk}$  is suppressed.

For simplicity, in this Section we take the limit

$$\ll f_\sigma; d_\sigma^\dagger \gg \approx 0 \tag{4.21}$$

Under the same consideration, some other Green's function (involving odd number of  $d$  or  $f$  operators) can be neglected and are listed as follows:

$$\begin{aligned}
\ll \hat{n}_{d\sigma'} f_\sigma; d_\sigma^\dagger \gg &\approx 0, & \ll d_{\sigma'}^\dagger f_{\sigma'} d_\sigma; d_\sigma^\dagger \gg &\approx 0, \\
\ll f_{\sigma'}^\dagger d_{\sigma'} d_\sigma; d_\sigma^\dagger \gg &\approx 0, & \ll \hat{n}_{f\sigma'} f_\sigma; d_\sigma^\dagger \gg &\approx 0,
\end{aligned}$$

Then with this approximation, the equations of motion can be simplified as (we only list changed

equations):

$$(\omega - \varepsilon_k)G_c = V_{dk}^*G_d \quad (4.22)$$

$$\begin{aligned} (\omega - \varepsilon_k) \ll \hat{n}_{d\sigma'} c_{k\sigma}; d_\sigma^\dagger \gg &= V_{dk}^* \ll \hat{n}_{d\sigma'} d_\sigma; d_\sigma^\dagger \gg + \sum_{dk'} (-V_{k'}^* \ll c_{k'\sigma'}^\dagger d_\sigma c_{k\sigma}; d_\sigma^\dagger \gg \\ &+ V_{dk'} \ll d_\sigma^\dagger c_{k'\sigma'} c_{k\sigma}; d_\sigma^\dagger \gg) \end{aligned} \quad (4.23)$$

$$\begin{aligned} (\omega - \varepsilon_k) \ll d_\sigma^\dagger c_{k\sigma'} d_\sigma; d_\sigma^\dagger \gg &= \langle d_\sigma^\dagger c_{k\sigma'} \rangle + V_{dk}^* \ll \hat{n}_{d\sigma'} d_\sigma; d_\sigma^\dagger \gg + \sum_{k'} (-V_{dk'}^* \ll c_{k'\sigma'}^\dagger c_{k\sigma} d_\sigma; d_\sigma^\dagger \gg \\ &+ V_{dk'} \ll d_\sigma^\dagger c_{k\sigma'} c_{k'\sigma}; d_\sigma^\dagger \gg) \end{aligned} \quad (4.24)$$

$$\begin{aligned} (\omega + \varepsilon_k - 2\varepsilon_d - U) \ll c_{k\sigma'}^\dagger d_\sigma d_\sigma; d_\sigma^\dagger \gg &= \langle c_{k\sigma'}^\dagger d_\sigma \rangle + (U' + U'') \ll \hat{n}_{f\zeta} c_{k\sigma'}^\dagger d_\sigma d_\sigma; d_\sigma^\dagger \gg \\ &+ (U' + U'') \ll \hat{n}_{f\xi} c_{k\sigma'}^\dagger d_\sigma d_\sigma; d_\sigma^\dagger \gg - V_{dk} \ll \hat{n}_{d\sigma'} d_\sigma; d_\sigma^\dagger \gg \\ &+ \sum_{k'} V_{dk'} (\ll c_{k\sigma'}^\dagger d_\sigma c_{k'\sigma}; d_\sigma^\dagger \gg + \ll c_{k\sigma'}^\dagger c_{k'\sigma} d_\sigma; d_\sigma^\dagger \gg) \end{aligned} \quad (4.25)$$

$$\begin{aligned} (\omega - \varepsilon_k) \ll \hat{n}_{f\zeta} c_{k\sigma}; d_\sigma^\dagger \gg &= V_{dk}^* \ll \hat{n}_{f\zeta} d_\sigma; d_\sigma^\dagger \gg + \sum_{k'} (-V_{fk'}^* \ll c_{k'\zeta}^\dagger f_\zeta c_{k\sigma}; d_\sigma^\dagger \gg \\ &+ V_{fk'} \ll f_\zeta^\dagger c_{k'\zeta} c_{k\sigma}; d_\sigma^\dagger \gg) \end{aligned} \quad (4.26)$$

$$\begin{aligned} (\omega + \varepsilon_f - \varepsilon_k - \varepsilon_d) \ll f_\zeta^\dagger c_{k\zeta} d_\sigma; d_\sigma^\dagger \gg &= \langle f_\zeta^\dagger c_{k\zeta} \rangle + (U - U'') \ll \hat{n}_{d\sigma'} f_\zeta^\dagger c_{k\zeta} d_\sigma; d_\sigma^\dagger \gg \\ &+ (-U + U'') \ll \hat{n}_{f\xi} f_\zeta^\dagger c_{k\zeta} d_\sigma; d_\sigma^\dagger \gg + V_{fk}^* \ll \hat{n}_{f\zeta} d_\sigma; d_\sigma^\dagger \gg \\ &+ \sum_{k'} (V_{dk'} \ll f_\zeta^\dagger c_{k\zeta} c_{k'\sigma}; d_\sigma^\dagger \gg - V_{fk'}^* \ll c_{k'\zeta}^\dagger c_{k\zeta} d_\sigma; d_\sigma^\dagger \gg) \end{aligned} \quad (4.27)$$

$$\begin{aligned} (\omega + \varepsilon_k - \varepsilon_f - \varepsilon_d - U') \ll c_{k\zeta}^\dagger f_\zeta d_\sigma; d_\sigma^\dagger \gg &= \langle c_{k\zeta}^\dagger f_\zeta \rangle + (U + U'') \ll \hat{n}_{d\sigma'} c_{k\zeta}^\dagger f_\zeta d_\sigma; d_\sigma^\dagger \gg \\ &+ (U + U'') \ll \hat{n}_{f\xi} c_{k\zeta}^\dagger f_\zeta d_\sigma; d_\sigma^\dagger \gg - V_{fk} \ll f_\zeta^\dagger f_\zeta d_\sigma; d_\sigma^\dagger \gg \\ &+ \sum_{k'} (V_{dk'} \ll c_{k\zeta}^\dagger f_\zeta c_{k'\sigma}; d_\sigma^\dagger \gg + V_{fk'} \ll c_{k\zeta}^\dagger c_{k'\zeta} d_\sigma; d_\sigma^\dagger \gg) \end{aligned} \quad (4.28)$$

Thus, the single particle Green's function is calculated as

$$G_d = \frac{1 + A_1 + A_2 + A_3}{\omega - \varepsilon_d - \Delta_{dd} - B_1 - B_2 - B_3} \quad (4.29)$$

$$P_1 = \frac{U}{\omega - \varepsilon_d - U - 2\Delta_{dd} - \tilde{\Delta}_{dd} - U' \bar{n}_{f\sigma} - U'' \bar{n}_{f\sigma'}} \quad (4.30)$$

$$P_2 = \frac{U'}{\omega - \varepsilon_d - U' - \Delta_{dd} - \Delta_{ff}^a - \tilde{\Delta}_{ff}^a - U \bar{n}_{d\sigma'} - U'' \bar{n}_{f\sigma'}} \quad (4.31)$$

$$P_3 = \frac{U''}{\omega - \varepsilon_d - U'' - \Delta_{dd} - \Delta_{ff}^b - \tilde{\Delta}_{ff}^b - U \bar{n}_{d\sigma'} - U' \bar{n}_{f\sigma}} \quad (4.32)$$

$$A_1 = P_1 \left( \bar{n}_{d\sigma'} + \sum_k \left( \frac{V_{dk} \langle d_\sigma^\dagger c_{k\sigma'} \rangle}{\omega - \varepsilon_k} - \frac{V_{dk} \langle d_\sigma^\dagger c_{k\sigma'} \rangle}{\omega + \varepsilon_k - 2\varepsilon_d - U - (U' + U'')(\bar{n}_{f\sigma} + \bar{n}_{f\sigma'})} \right) \right) \quad (4.33)$$

$$A_2 = P_2 \left( \bar{n}_{f\sigma} + \sum_k \left( \frac{V_{fk} \langle f_\sigma^\dagger c_{k\sigma} \rangle}{\omega - \varepsilon_k + \varepsilon_f - \varepsilon_d - (U - U'')(\bar{n}_{d\sigma'} - \bar{n}_{f\sigma})} - \frac{V_{fk} \langle f_\sigma^\dagger c_{k\sigma} \rangle}{\omega + \varepsilon_k - \varepsilon_f - \varepsilon_d - U' - (U + U'')(\bar{n}_{d\sigma'} + \bar{n}_{f\sigma'})} \right) \right) \quad (4.34)$$

$$A_3 = P_3 \left( \bar{n}_{f\sigma'} + \sum_k \left( \frac{V_{fk} \langle f_\sigma^\dagger c_{k\sigma'} \rangle}{\omega - \varepsilon_k + \varepsilon_f - \varepsilon_d - (U - U')(\bar{n}_{d\sigma'} - \bar{n}_{f\sigma})} - \frac{V_{fk} \langle f_\sigma^\dagger c_{k\sigma'} \rangle}{\omega + \varepsilon_k - \varepsilon_f - \varepsilon_d - U'' - (U + U')(\bar{n}_{d\sigma'} + \bar{n}_{f\sigma'})} \right) \right) \quad (4.35)$$

$$\begin{aligned}
B_1 = & P_1 \left( \Delta_{dd} \cdot \sum_k \left( \frac{V_{dk} \langle d_{\sigma'}^\dagger c_{k\sigma'} \rangle}{\omega - \varepsilon_k} - \frac{V_{dk} \langle d_{\sigma'}^\dagger c_{k\sigma'} \rangle}{\omega + \varepsilon_k - 2\varepsilon_d - U - (U' + U'')(\bar{n}_{f\sigma} + \bar{n}_{f\sigma'})} \right) \right. \\
& \left. + \sum_{kk'} \left( -\frac{V_{dk}^2 \langle c_{k'\sigma'}^\dagger c_{k\sigma'} \rangle}{\omega - \varepsilon_k} - \frac{V_{dk}^2 \langle c_{k'\sigma'}^\dagger c_{k\sigma'} \rangle}{\omega + \varepsilon_k - 2\varepsilon_d - U - (U' + U'')(\bar{n}_{f\sigma} + \bar{n}_{f\sigma'})} \right) \right) \quad (4.36)
\end{aligned}$$

$$\begin{aligned}
B_2 = & P_2 \left( \Delta_{dd} \cdot \sum_k \left( \frac{V_{fk} \langle f_{\sigma'}^\dagger c_{k\sigma} \rangle}{\omega - \varepsilon_k + \varepsilon_f - \varepsilon_d - (U - U'')(\bar{n}_{d\sigma'} - \bar{n}_{f\sigma'})} - \frac{V_{fk} \langle f_{\sigma'}^\dagger c_{k\sigma} \rangle}{\omega + \varepsilon_k - \varepsilon_f - \varepsilon_d - U' - (U + U'')(\bar{n}_{d\sigma'} + \bar{n}_{f\sigma'})} \right) \right. \\
& \left. + \sum_{kk'} \left( -\frac{V_{fk}^2 \langle c_{k'\sigma}^\dagger c_{k\sigma} \rangle}{\omega - \varepsilon_k + \varepsilon_f - \varepsilon_d - (U - U'')(\bar{n}_{d\sigma'} - \bar{n}_{f\sigma'})} - \frac{V_{fk}^2 \langle c_{k'\sigma}^\dagger c_{k\sigma} \rangle}{\omega + \varepsilon_k - \varepsilon_f - \varepsilon_d - U' - (U + U'')(\bar{n}_{d\sigma'} + \bar{n}_{f\sigma'})} \right) \right) \quad (4.37)
\end{aligned}$$

$$\begin{aligned}
B_3 = & P_3 \left( \Delta_{dd} \cdot \sum_k \left( \frac{V_{fk} \langle f_{\sigma'}^\dagger c_{k\sigma'} \rangle}{\omega - \varepsilon_k + \varepsilon_f - \varepsilon_d - (U - U'')(\bar{n}_{d\sigma'} - \bar{n}_{f\sigma'})} - \frac{V_{fk} \langle f_{\sigma'}^\dagger c_{k\sigma'} \rangle}{\omega + \varepsilon_k - \varepsilon_f - \varepsilon_d - U'' - (U + U')(\bar{n}_{d\sigma'} + \bar{n}_{f\sigma'})} \right) \right. \\
& \left. + \sum_{kk'} \left( -\frac{V_{fk}^2 \langle c_{k'\sigma'}^\dagger c_{k\sigma'} \rangle}{\omega - \varepsilon_k + \varepsilon_f - \varepsilon_d - (U - U'')(\bar{n}_{d\sigma'} - \bar{n}_{f\sigma'})} - \frac{V_{fk}^2 \langle c_{k'\sigma'}^\dagger c_{k\sigma'} \rangle}{\omega + \varepsilon_k - \varepsilon_f - \varepsilon_d - U'' - (U + U')(\bar{n}_{d\sigma'} + \bar{n}_{f\sigma'})} \right) \right) \quad (4.38)
\end{aligned}$$

where the hybridization functions are defined as

$$\Delta_{dd} = \sum_k \frac{V_{dk}^2}{\omega - \varepsilon_k} \quad (4.39)$$

$$\Delta_{ff}^a = \sum_k \frac{V_{fk}^2}{\omega - \varepsilon_k + \varepsilon_f - \varepsilon_d - (U - U'')(\bar{n}_{d\sigma'} - \bar{n}_{f\sigma'})} \quad (4.40)$$

$$\Delta_{ff}^b = \sum_k \frac{V_{fk}^2}{\omega - \varepsilon_k + \varepsilon_f - \varepsilon_d - (U - U')(\bar{n}_{d\sigma'} - \bar{n}_{f\sigma'})} \quad (4.41)$$

$$\tilde{\Delta}_{dd} = \sum_k \frac{V_{dk}^2}{\omega + \varepsilon_k - 2\varepsilon_d - U - (U' + U'')(\bar{n}_{f\sigma} + \bar{n}_{f\sigma'})} \quad (4.42)$$

$$\tilde{\Delta}_{ff}^a = \sum_k \frac{V_{fk}^2}{\omega + \varepsilon_k - \varepsilon_f - \varepsilon_d - U' - (U + U'')(\bar{n}_{d\sigma'} + \bar{n}_{f\sigma'})} \quad (4.43)$$

$$\tilde{\Delta}_{ff}^b = \sum_k \frac{V_{fk}^2}{\omega + \varepsilon_k - \varepsilon_f - \varepsilon_d - U'' - (U + U')(\bar{n}_{d\sigma'} + \bar{n}_{f\sigma'})} \quad (4.44)$$

When we take the parameter  $U = U' = U''$ , the system should be very similar (not identical due to the difference on the degeneracy of the bath) to the large  $N(=4)$  degenerate case in the single band system. This should be a good comparison for these two different considerations. Moreover, it can also be used as an evaluation of how good the decoupling of the three-particle Green's functions is.

### 4.3 Hartree-Fock approximation

In this Section, we discuss another approximation for the simplification of the equations of motion. If we apply the Hartree approximation for the two-particle inter-band terms, i.e.

$$(\omega - \varepsilon_d) \ll d_{\sigma}; d_{\sigma}^{\dagger} \gg = 1 + U \ll \hat{n}_{d\sigma'} d_{\sigma}; d_{\sigma}^{\dagger} \gg + U' \bar{n}_{f\sigma} \ll d_{\sigma}; d_{\sigma}^{\dagger} \gg + U'' \hat{n}_{f\sigma'} \ll d_{\sigma}; d_{\sigma}^{\dagger} \gg + V \ll c_{k\sigma}; d_{\sigma}^{\dagger} \gg \quad (4.45)$$

$$(\omega - \varepsilon_f) \ll f_{\sigma}; f_{\sigma}^{\dagger} \gg = 1 + U \ll \hat{n}_{f\sigma'} f_{\sigma}; f_{\sigma}^{\dagger} \gg + U' \bar{n}_{d\sigma} \ll f_{\sigma}; f_{\sigma}^{\dagger} \gg + U'' \bar{n}_{d\sigma'} \ll f_{\sigma}; f_{\sigma}^{\dagger} \gg + V \ll c_{k\sigma}; f_{\sigma}^{\dagger} \gg \quad (4.46)$$

$$(\omega - \varepsilon_f) \ll f_\sigma; d_\sigma^\dagger \gg = U \bar{n}_{f\sigma'} \ll f_\sigma; d_\sigma^\dagger \gg + U' \bar{n}_{d\sigma} \ll f_\sigma; d_\sigma^\dagger \gg + U'' \bar{n}_{d\sigma'} \ll f_\sigma; d_\sigma^\dagger \gg + V \ll c_{k\sigma}; d_\sigma^\dagger \gg \quad (4.47)$$

$$(\omega - \varepsilon_d) \ll d_\sigma; f_\sigma^\dagger \gg = U \bar{n}_{d\sigma'} \ll d_\sigma; f_\sigma^\dagger \gg + U' \bar{n}_{f\sigma} \ll d_\sigma; f_\sigma^\dagger \gg + U'' \hat{n}_{f\sigma'} \ll d_\sigma; f_\sigma^\dagger \gg + V \ll c_{k\sigma}; f_\sigma^\dagger \gg \quad (4.48)$$

Then we will get

$$\ll f_\sigma; d_\sigma^\dagger \gg = \frac{\Delta_{df} \ll d_\sigma; d_\sigma^\dagger \gg}{\omega - \varepsilon_f - \Delta_{ff} - U \bar{n}_{f\sigma'} - U' \bar{n}_{d\sigma} - U'' \bar{n}_{d\sigma'}} \quad (4.49)$$

$$\ll d_\sigma; f_\sigma^\dagger \gg = \frac{\Delta_{df} \ll f_\sigma; f_\sigma^\dagger \gg}{\omega - \varepsilon_d - \Delta_{dd} - U \bar{n}_{d\sigma'} - U' \bar{n}_{f\sigma} - U'' \bar{n}_{f\sigma'}} \quad (4.50)$$

$$\begin{aligned} \sum_k V_{dk} \ll c_{k\sigma}; d_\sigma^\dagger \gg &= \sum_k \left( \frac{V_{dk}^2}{\omega - \varepsilon_k} \ll d_\sigma; d_\sigma^\dagger \gg + \frac{V_{dk} V_{fk}}{\omega - \varepsilon_k} \ll f_\sigma; d_\sigma^\dagger \gg \right) \\ &= \left( \Delta_{dd} + \frac{\Delta_{df}^2}{\omega - \varepsilon_f - \Delta_{ff} - U \bar{n}_{f\sigma'} - U' \bar{n}_{d\sigma} - U'' \bar{n}_{d\sigma'}} \right) \ll d_\sigma; d_\sigma^\dagger \gg \end{aligned} \quad (4.51)$$

$$\begin{aligned} \sum_k V_{fk} \ll c_{k\sigma}; f_\sigma^\dagger \gg &= \sum_k \left( \frac{V_{fk} V_{dk}}{\omega - \varepsilon_k} \ll d_\sigma; f_\sigma^\dagger \gg + \frac{V_{fk}^2}{\omega - \varepsilon_k} \ll f_\sigma; f_\sigma^\dagger \gg \right) \\ &= \left( \frac{\Delta_{df}^2}{\omega - \varepsilon_d - \Delta_{dd} - U \bar{n}_{d\sigma'} - U' \bar{n}_{f\sigma} - U'' \bar{n}_{f\sigma'}} + \Delta_{ff} \right) \ll f_\sigma; f_\sigma^\dagger \gg \end{aligned} \quad (4.52)$$

Now the single electron EOMs are obtained as,

$$(\omega - \varepsilon_d - (\Delta_{dd} + \frac{\Delta_{df}^2}{\omega - \varepsilon_f - \Delta_{ff} - U \bar{n}_{f\sigma'} - U' \bar{n}_{d\sigma} - U'' \bar{n}_{d\sigma'}})) - U' \bar{n}_{f\sigma} - U'' \bar{n}_{f\sigma'} \ll d_\sigma; d_\sigma^\dagger \gg = 1 + U \ll \hat{n}_{d\sigma'} d_\sigma; d_\sigma^\dagger \gg \quad (4.53)$$

$$(\omega - \varepsilon_f - (\Delta_{ff} + \frac{\Delta_{df}^2}{\omega - \varepsilon_d - \Delta_{dd} - U \bar{n}_{d\sigma'} - U' \bar{n}_{f\sigma} - U'' \bar{n}_{f\sigma'}})) - U' \bar{n}_{d\sigma} - U'' \bar{n}_{d\sigma'} \ll f_\sigma; f_\sigma^\dagger \gg = 1 + U \ll \hat{n}_{f\sigma'} f_\sigma; f_\sigma^\dagger \gg \quad (4.54)$$

Comparing with the single band model, we can see that the inter-band interaction introduces obvious changes to the single electron equations of motion. Moreover, in order to inherit the success of the single band results, we treat  $\ll \hat{n}_{d\sigma'} d_\sigma; d_\sigma^\dagger \gg$  in the same order of approximation as done in the single band model, *i.e.* we replace the previous Hamiltonian with the new multi-band Hamiltonian and just decouple the inter-band terms and treat them in Hartree approximation. Now we should only take into account

$$\begin{aligned} &(\omega - \varepsilon_d - U) \ll \hat{n}_{d\sigma'} d_\sigma; d_\sigma^\dagger \gg \\ &= \bar{n}_{d\sigma'} + U' \ll \hat{n}_{f\sigma} \hat{n}_{d\sigma'} d_\sigma; d_\sigma^\dagger \gg + U'' \ll \hat{n}_{f\sigma'} \hat{n}_{d\sigma'} d_\sigma; d_\sigma^\dagger \gg - V_{dk}^* \ll c_{k\sigma'}^\dagger d_\sigma; d_\sigma^\dagger \gg + V_{dk} \ll \hat{n}_{d\sigma'} c_{k\sigma}; d_\sigma^\dagger \gg \\ &+ V_{dk} \ll d_\sigma^\dagger c_{k\sigma'} d_\sigma; d_\sigma^\dagger \gg \\ &(\omega - \varepsilon_k) \ll \hat{n}_{d\sigma'} c_{k\sigma}; d_\sigma^\dagger \gg \\ &= V_{dk}^* \ll \hat{n}_{d\sigma'} d_\sigma; d_\sigma^\dagger \gg + \sum_{k'} (V_{dk'}^* \ll d_\sigma^\dagger c_{k'\sigma'} c_{k\sigma}; d_\sigma^\dagger \gg - V_{dk'} \ll c_{k'\sigma'}^\dagger d_\sigma; c_{k\sigma}; d_\sigma^\dagger \gg) + V_{fk}^* \ll \hat{n}_{d\sigma'} f_\sigma; d_\sigma^\dagger \gg \\ &(\omega - \varepsilon_k) \ll d_\sigma^\dagger c_{k\sigma'} d_\sigma; d_\sigma^\dagger \gg \\ &= \langle d_\sigma^\dagger c_{k\sigma'} \rangle + U' \ll \hat{n}_{f\sigma} d_\sigma^\dagger c_{k\sigma'} d_\sigma \gg - U' \ll \hat{n}_{f\sigma'} d_\sigma^\dagger c_{k\sigma'} d_\sigma \gg + U'' \ll \hat{n}_{f\sigma} d_\sigma^\dagger c_{k\sigma'} d_\sigma \gg - U'' \ll \hat{n}_{f\sigma'} d_\sigma^\dagger c_{k\sigma'} d_\sigma \gg \\ &+ V_{dk}^* \ll \hat{n}_{d\sigma'} d_\sigma; d_\sigma^\dagger \gg + \sum_{k'} (-V_{dk'}^* \ll c_{k'\sigma'}^\dagger d_\sigma; d_\sigma^\dagger \gg + V_{dk'} \ll d_\sigma^\dagger c_{k\sigma'} c_{k'\sigma}; d_\sigma^\dagger \gg) + V_{fk}^* \ll d_\sigma^\dagger f_\sigma; d_\sigma; d_\sigma^\dagger \gg \end{aligned}$$

$$\begin{aligned}
& (\omega + \varepsilon_k - 2\varepsilon_d - U) \ll c_{k\sigma'}^\dagger d_{\sigma'} d_\sigma; d_\sigma^\dagger \gg \\
& = \langle c_{k\sigma'}^\dagger d_{\sigma'} \rangle + U' \ll \hat{n}_{f\sigma} c_{k\sigma'}^\dagger d_{\sigma'} d_\sigma; d_\sigma^\dagger \gg + U' \ll \hat{n}_{f\sigma'} c_{k\sigma'}^\dagger d_{\sigma'} d_\sigma; d_\sigma^\dagger \gg + U'' \ll \hat{n}_{f\sigma} c_{k\sigma'}^\dagger d_{\sigma'} d_\sigma; d_\sigma^\dagger \gg \\
& + U'' \ll \hat{n}_{f\sigma'} c_{k\sigma'}^\dagger d_{\sigma'} d_\sigma; d_\sigma^\dagger \gg - V_{dk} \ll \hat{n}_{d\sigma'} d_\sigma; d_\sigma^\dagger \gg + \sum_{k'} (V_{dk'} \ll c_{k\sigma'}^\dagger d_{\sigma'} c_{k'\sigma}; d_\sigma^\dagger \gg + V_{dk'} \ll c_{k\sigma'}^\dagger c_{k'\sigma'} d_\sigma; d_\sigma^\dagger \gg) \\
& - V_{fk} \ll f_{\sigma'}^\dagger d_{\sigma'} d_\sigma; d_\sigma^\dagger \gg
\end{aligned}$$

When the decoupling is applied, the equations should be written as

$$(\omega - \varepsilon_d - U - U' \bar{n}_{f\sigma} - U'' \bar{n}_{f\sigma'}) \ll \hat{n}_{d\sigma'} d_\sigma; d_\sigma^\dagger \gg \quad (4.55)$$

$$\begin{aligned}
& = \bar{n}_{d\sigma'} - V_{dk}^* \ll c_{k\sigma'}^\dagger d_{\sigma'} d_\sigma; d_\sigma^\dagger \gg + V_{dk} \ll \hat{n}_{d\sigma'} c_{k\sigma}; d_\sigma^\dagger \gg + V_{dk} \ll d_{\sigma'}^\dagger c_{k\sigma'} d_\sigma; d_\sigma^\dagger \gg \\
& (\omega - \varepsilon_k) \ll \hat{n}_{d\sigma'} c_{k\sigma}; d_\sigma^\dagger \gg \quad (4.56)
\end{aligned}$$

$$\begin{aligned}
& = V_{dk}^* \ll \hat{n}_{d\sigma'} d_\sigma; d_\sigma^\dagger \gg + V_{fk}^* \bar{n}_{d\sigma'} \ll f_\sigma; d_\sigma^\dagger \gg \\
& (\omega - \varepsilon_k) \ll d_{\sigma'}^\dagger c_{k\sigma'} d_\sigma; d_\sigma^\dagger \gg \quad (4.57)
\end{aligned}$$

$$\begin{aligned}
& = \langle d_{\sigma'}^\dagger c_{k\sigma'} \rangle + V_{dk}^* \ll \hat{n}_{d\sigma'} d_\sigma; d_\sigma^\dagger \gg + \sum_{k'} (-V_{dk'}^* \langle c_{\sigma'}^\dagger c_{\sigma'} \rangle \ll d_\sigma; d_\sigma^\dagger \gg + V_{dk'} \langle d_{\sigma'}^\dagger c_{k\sigma'} \rangle \ll c_{k'\sigma}; d_\sigma^\dagger \gg) \\
& + V_{fk}^* \langle d_{\sigma'}^\dagger f_{\sigma'} \rangle \ll d_\sigma; d_\sigma^\dagger \gg \\
& (\omega + \varepsilon_k - 2\varepsilon_d - U - U' \bar{n}_{f\sigma'} - U' \bar{n}_{f\sigma} - U'' \bar{n}_{f\sigma'} - U'' \bar{n}_{f\sigma}) \ll c_{k\sigma'}^\dagger d_{\sigma'} d_\sigma; d_\sigma^\dagger \gg \quad (4.58) \\
& = \langle c_{k\sigma'}^\dagger d_{\sigma'} \rangle - V_{dk} \ll \hat{n}_{d\sigma'} d_\sigma; d_\sigma^\dagger \gg + \sum_{k'} (V_{dk'} \langle c_{k\sigma'}^\dagger d_{\sigma'} \rangle \ll c_{k'\sigma}; d_\sigma^\dagger \gg + V_{dk'} \langle c_{k\sigma'}^\dagger c_{k'\sigma'} \rangle \ll d_\sigma; d_\sigma^\dagger \gg) \\
& - V_{fk} \langle f_{\sigma'}^\dagger d_{\sigma'} \rangle \ll d_\sigma; d_\sigma^\dagger \gg
\end{aligned}$$

Finally, we get the expression of the single electron Green's functions with Hartree-Fock approximation for the inter-band Green's functions,

$$\ll d_\sigma; d_\sigma^\dagger \gg = \frac{1 + A(\bar{n}_{d\sigma'} + I_{d1})}{\omega - \varepsilon_d - (\Delta_{dd} + B) - U' \bar{n}_{f\sigma} - U'' \bar{n}_{f\sigma'} - A[(\Delta_{dd} + B)I_{d1} + I_{d2} + (\Delta_{df} + \tilde{\Delta}_{df}^d) \langle f_{\sigma'}^\dagger d_{\sigma'} \rangle + \bar{n}_{d\sigma'} B]} \quad (4.59)$$

$$\ll f_\sigma; f_\sigma^\dagger \gg = \frac{1 + C(\bar{n}_{f\sigma'} + I_{f1})}{\omega - \varepsilon_f - (\Delta_{ff} + D) - U' \bar{n}_{d\sigma} - U'' \bar{n}_{d\sigma'} - C[(\Delta_{ff} + D)I_{f1} + I_{f2} + (\Delta_{df} + \tilde{\Delta}_{df}^f) \langle f_{\sigma'}^\dagger d_{\sigma'} \rangle + \bar{n}_{f\sigma'} D]} \quad (4.60)$$

where  $I_{d1}, I_{d2}, I_{f1}, I_{f2}$  are just like  $I_1, I_2$  in the case of the single band, and

$$A = \frac{U}{\omega - \varepsilon_d - U - 2\Delta_{dd} - \tilde{\Delta}_{dd} - U' \bar{n}_{f\sigma'} - U'' \bar{n}_{f\sigma}} \quad (4.61)$$

$$C = \frac{U}{\omega - \varepsilon_f - U - 2\Delta_{ff} - \tilde{\Delta}_{ff} - U' \bar{n}_{d\sigma'} - U'' \bar{n}_{d\sigma}} \quad (4.62)$$

$$B = \frac{\Delta_{df}^2}{\omega - \varepsilon_f - \Delta_{ff} - U' \bar{n}_{f\sigma'} - U'' \bar{n}_{d\sigma} - U'' \bar{n}_{d\sigma'}} \quad (4.63)$$

$$D = \frac{\Delta_{df}^2}{\omega - \varepsilon_d - \Delta_{dd} - U' \bar{n}_{d\sigma'} - U' \bar{n}_{f\sigma} - U'' \bar{n}_{f\sigma'}} \quad (4.64)$$

For three band systems, with similar calculation to two band systems, we can get

$$\ll d_\sigma; d_\sigma^\dagger \gg = \frac{1 + A(\bar{n}_{d\sigma'} + I_{d1})}{A_0 - (\Delta_{dd} + B) - A[(\Delta_{dd} + B)I_{d1} + I_{d2} + (\Delta_{df} + \tilde{\Delta}_{df}^d) \langle f_{\sigma'}^\dagger d_{\sigma'} \rangle + (\Delta_{dg} + \tilde{\Delta}_{dg}^d) \langle g_{\sigma'}^\dagger d_{\sigma'} \rangle + \bar{n}_{d\sigma'} B]} \quad (4.65)$$

$$\ll f_\sigma; f_\sigma^\dagger \gg = \frac{1 + C(\bar{n}_{f\sigma'} + I_{f1})}{B_0 - (\Delta_{ff} + D) - C[(\Delta_{ff} + D)I_{f1} + I_{f2} + (\Delta_{df} + \tilde{\Delta}_{df}^f) \langle d_{\sigma'}^\dagger f_{\sigma'} \rangle + (\Delta_{fg} + \tilde{\Delta}_{fg}^f) \langle g_{\sigma'}^\dagger f_{\sigma'} \rangle + \bar{n}_{f\sigma'} D]} \quad (4.66)$$



$$\ll g_{\sigma}; g_{\sigma}^{\dagger} \gg = \frac{1 + E(\bar{n}_{g\sigma'} + I_{g1})}{C_0 - (\Delta_{gg} + F) - E[(\Delta_{gg} + F)I_{g1} + I_{g2} + (\Delta_{dg} + \tilde{\Delta}_{dg}^g)\langle d_{\sigma'}^{\dagger}, g_{\sigma'} \rangle + (\Delta_{fg} + \tilde{\Delta}_{fg}^g)\langle f_{\sigma'}^{\dagger}, g_{\sigma'} \rangle + \bar{n}_{g\sigma'} F]} \quad (4.67)$$

where

$$A = \frac{U}{\omega - \varepsilon_d - U - 2\Delta_{dd} - \tilde{\Delta}_{dd} - U'\bar{n}_{f\sigma'} - U''\bar{n}_{f\sigma} - U'\bar{n}_{g\sigma'} - U''\bar{n}_{g\sigma}} \quad (4.68)$$

$$C = \frac{U}{\omega - \varepsilon_f - U - 2\Delta_{ff} - \tilde{\Delta}_{ff} - U'\bar{n}_{d\sigma'} - U''\bar{n}_{d\sigma} - U'\bar{n}_{g\sigma'} - U''\bar{n}_{g\sigma}} \quad (4.69)$$

$$E = \frac{U}{\omega - \varepsilon_g - U - 2\Delta_{gg} - \tilde{\Delta}_{gg} - U'\bar{n}_{d\sigma'} - U''\bar{n}_{d\sigma} - U'\bar{n}_{f\sigma'} - U''\bar{n}_{f\sigma}} \quad (4.70)$$

$$B = \frac{\Delta_{df}^2}{A_1 - \Delta_{ff}(1 + \frac{A_1}{A_2})} + \frac{\Delta_{dg}^2}{A_2 - \Delta_{gg}(1 + \frac{A_2}{A_1})} \quad (4.71)$$

$$D = \frac{\Delta_{df}^2}{B_1 - \Delta_{dd}(1 + \frac{B_1}{B_2})} + \frac{\Delta_{fg}^2}{B_2 - \Delta_{gg}(1 + \frac{B_2}{B_1})} \quad (4.72)$$

$$F = \frac{\Delta_{dg}^2}{C_1 - \Delta_{dd}(1 + \frac{C_1}{C_2})} + \frac{\Delta_{fg}^2}{C_2 - \Delta_{ff}(1 + \frac{C_2}{C_1})} \quad (4.73)$$

$$A_0 = \omega - \varepsilon_d - U'\bar{n}_{f\sigma} - U''\bar{n}_{f\sigma'} - U'\bar{n}_{g\sigma} - U''\bar{n}_{g\sigma'}$$

$$B_0 = \omega - \varepsilon_f - U'\bar{n}_{d\sigma} - U''\bar{n}_{d\sigma'} - U'\bar{n}_{g\sigma} - U''\bar{n}_{g\sigma'}$$

$$C_0 = \omega - \varepsilon_g - U'\bar{n}_{d\sigma} - U''\bar{n}_{d\sigma'} - U'\bar{n}_{f\sigma} - U''\bar{n}_{f\sigma'}$$

$$A_1 = \omega - \varepsilon_f - U'\bar{n}_{f\sigma'} - U'\bar{n}_{d\sigma} - U''\bar{n}_{d\sigma'} - U'\bar{n}_{g\sigma} - U''\bar{n}_{g\sigma'}$$

$$A_2 = \omega - \varepsilon_g - U'\bar{n}_{g\sigma'} - U'\bar{n}_{d\sigma} - U''\bar{n}_{d\sigma'} - U'\bar{n}_{f\sigma} - U''\bar{n}_{f\sigma'}$$

$$B_1 = \omega - \varepsilon_d - U'\bar{n}_{d\sigma'} - U'\bar{n}_{f\sigma} - U''\bar{n}_{f\sigma'} - U'\bar{n}_{g\sigma} - U''\bar{n}_{g\sigma'}$$

$$B_2 = \omega - \varepsilon_g - U'\bar{n}_{g\sigma'} - U'\bar{n}_{d\sigma} - U''\bar{n}_{d\sigma'} - U'\bar{n}_{f\sigma} - U''\bar{n}_{f\sigma'}$$

$$C_1 = \omega - \varepsilon_d - U'\bar{n}_{d\sigma'} - U'\bar{n}_{f\sigma} - U''\bar{n}_{f\sigma'} - U'\bar{n}_{g\sigma} - U''\bar{n}_{g\sigma'}$$

$$C_2 = \omega - \varepsilon_f - U'\bar{n}_{f\sigma'} - U'\bar{n}_{d\sigma} - U''\bar{n}_{d\sigma'} - U'\bar{n}_{g\sigma} - U''\bar{n}_{g\sigma'}$$

Then it can be generalized to the case of arbitrary number of bands. With the Hartree-Fock approximation for the inter-band interactions and Lacroix's level of approximation for the intra-band interactions, the single particle Green's function in the  $\tau$  band  $\ll d_{\tau\sigma}; d_{\tau\sigma}^{\dagger} \gg$  should be

$$\frac{1 + Y(\bar{n}_{\tau\sigma'} + I_{\tau 1})}{\omega - \varepsilon_{\tau} - (\Delta_{\tau\tau} + X) - U' \sum_{\tau'} \bar{n}_{\tau'\sigma} - U'' \sum_{\tau'} \bar{n}_{\tau'\sigma'} - Y[(\Delta_{\tau\tau} + X)I_{d1} + I_{\tau 2} + \sum_{\tau'} (\Delta_{\tau\tau'} + \tilde{\Delta}_{\tau\tau'})\langle d_{\tau'\sigma'}^{\dagger}, d_{\tau\sigma'} \rangle + \bar{n}_{\tau\sigma'} X]} \quad (4.74)$$

where

$$Y = \frac{U}{\omega - \varepsilon_{\tau} - U - 2\Delta_{\tau\tau} - \tilde{\Delta}_{\tau\tau} - U' \sum_{\tau'} \bar{n}_{\tau'\sigma'} - U'' \sum_{\tau'} \bar{n}_{\tau'\sigma}} \quad (4.75)$$

$$X = \sum_{\tau'} \frac{\Delta_{\tau\tau'}^2}{\omega - \varepsilon_{\tau'} - U\bar{n}_{\tau'\sigma'} - U' \sum_{\zeta} \bar{n}_{\zeta\sigma} - U'' \sum_{\zeta} \bar{n}_{\zeta\sigma'} - \Delta_{\tau'\tau'}(1 + \sum_{\tau''} \frac{\omega - \varepsilon_{\tau'} - U\bar{n}_{\tau'\sigma'} - U' \sum_{\zeta} \bar{n}_{\zeta\sigma} - U'' \sum_{\zeta} \bar{n}_{\zeta\sigma'}}{\omega - \varepsilon_{\tau''} - U\bar{n}_{\tau''\sigma'} - U' \sum_{\xi} \bar{n}_{\xi\sigma} - U'' \sum_{\xi} \bar{n}_{\xi\sigma'}})} \quad (4.76)$$

$$I_{\tau 1} = \sum_k \left\{ \frac{V_{\tau k} \langle d_{\tau\sigma'}^{\dagger}, c_{k\sigma'} \rangle}{\omega - \varepsilon_k} - \frac{V_{\tau k} \langle d_{\tau\sigma'}^{\dagger}, c_{k\sigma'} \rangle}{\omega + \varepsilon_k - 2\varepsilon_{\tau} - U - U' \sum_{\tau'} (\bar{n}_{\tau'\sigma} + \bar{n}_{\tau'\sigma'}) - U'' \sum_{\tau'} (\bar{n}_{\tau'\sigma} + \bar{n}_{\tau'\sigma'})} \right\} \quad (4.77)$$

$$I_{\tau 2} = \sum_{kk'} \left\{ - \frac{V_{\tau k} V_{\tau k'} \langle c_{k'\sigma'}^{\dagger}, c_{k\sigma'} \rangle}{\omega - \varepsilon_k} - \frac{V_{\tau k} V_{\tau k'} \langle c_{k'\sigma'}^{\dagger}, c_{k\sigma'} \rangle}{\omega + \varepsilon_k - 2\varepsilon_{\tau} - U - U' \sum_{\tau'} (\bar{n}_{\tau'\sigma} + \bar{n}_{\tau'\sigma'}) - U'' \sum_{\tau'} (\bar{n}_{\tau'\sigma} + \bar{n}_{\tau'\sigma'})} \right\} \quad (4.78)$$

with  $\tau' \neq \tau \neq \tau''$  and  $\tau' \neq \zeta$ ,  $\tau'' \neq \xi$

## 4.4 Hubbard-I approximation

This approximation is an improvement over the Hartree-Fock approximation. The difference is that we used the Hubbard-I approximation to the two-particle inter-band terms. If the Hartree-Fock approximation should turn out not to be exact enough, we can try the Hubbard-I approximation. Moreover, by the comparison of Hubbard-I approximation and Hartree-Fock approximation, we can also see the difference by the inclusion of higher order EOMs in order to check the validity of methods and know where we should stop the truncation.

$$(\omega - \varepsilon_d - U) \ll \hat{n}_{d\sigma'} d_\sigma; d_\sigma^\dagger \gg = \bar{n}_{d\sigma'} + U' \ll \hat{n}_{f\sigma} \hat{n}_{d\sigma'} d_\sigma; d_\sigma^\dagger \gg + U'' \ll \hat{n}_{f\sigma'} \hat{n}_{d\sigma'} d_\sigma; d_\sigma^\dagger \gg \quad (4.79)$$

$$+ (-V_{dk}^* \ll c_{k\sigma'}^\dagger d_{\sigma'} d_\sigma; d_\sigma^\dagger \gg + V_{dk} \ll \hat{n}_{d\sigma'} c_{k\sigma}; d_\sigma^\dagger \gg + V_{dk} \ll d_{\sigma'}^\dagger c_{k\sigma'} d_\sigma; d_\sigma^\dagger \gg)$$

$$(\omega - \varepsilon_f - U) \ll \hat{n}_{f\sigma'} f_\sigma; f_\sigma^\dagger \gg = \bar{n}_{f\sigma'} + U' \ll \hat{n}_{d\sigma} \hat{n}_{f\sigma'} f_\sigma; f_\sigma^\dagger \gg + U'' \ll \hat{n}_{d\sigma'} \hat{n}_{f\sigma'} f_\sigma; f_\sigma^\dagger \gg \quad (4.80)$$

$$+ (-V_{fk}^{ast} \ll c_{k\sigma'}^\dagger f_{\sigma'} f_\sigma; f_\sigma^\dagger \gg + V_{fk} \ll \hat{n}_{f\sigma'} c_{k\sigma}; f_\sigma^\dagger \gg + V_{fk} \ll f_{\sigma'}^\dagger c_{k\sigma'} f_\sigma; f_\sigma^\dagger \gg)$$

$$(\omega - \varepsilon_d - U') \ll \hat{n}_{f\sigma} d_\sigma; d_\sigma^\dagger \gg = \bar{n}_{f\sigma} + U \ll \hat{n}_{f\sigma} \hat{n}_{d\sigma'} d_\sigma; d_\sigma^\dagger \gg + U'' \ll \hat{n}_{f\sigma} \hat{n}_{f\sigma'} d_\sigma; d_\sigma^\dagger \gg \quad (4.81)$$

$$+ V_{dk} \ll \hat{n}_{f\sigma} c_{k\sigma}; d_\sigma^\dagger \gg - V_{fk}^* \ll c_{k\sigma'}^\dagger f_{\sigma'} d_\sigma; d_\sigma^\dagger \gg + V_{fk} \ll f_{\sigma'}^\dagger c_{k\sigma'} d_\sigma; d_\sigma^\dagger \gg$$

$$(\omega - \varepsilon_f - U') \ll \hat{n}_{d\sigma} f_\sigma; f_\sigma^\dagger \gg = \bar{n}_{d\sigma} + U \ll \hat{n}_{d\sigma} \hat{n}_{f\sigma'} f_\sigma; f_\sigma^\dagger \gg + U'' \ll \hat{n}_{d\sigma} \hat{n}_{f\sigma'} f_\sigma; f_\sigma^\dagger \gg \quad (4.82)$$

$$+ V_{fk} \ll \hat{n}_{d\sigma} c_{k\sigma}; f_\sigma^\dagger \gg - V_{dk}^* \ll c_{k\sigma'}^\dagger d_{\sigma'} f_\sigma; f_\sigma^\dagger \gg + V_{dk} \ll d_{\sigma'}^\dagger c_{k\sigma'} f_\sigma; f_\sigma^\dagger \gg$$

$$(\omega - \varepsilon_d - U'') \ll \hat{n}_{f\sigma'} d_\sigma; d_\sigma^\dagger \gg = \bar{n}_{f\sigma'} + U \ll \hat{n}_{f\sigma'} \hat{n}_{d\sigma'} d_\sigma; d_\sigma^\dagger \gg + U' \ll \hat{n}_{f\sigma'} \hat{n}_{f\sigma} d_\sigma; d_\sigma^\dagger \gg \quad (4.83)$$

$$+ V_{dk} \ll \hat{n}_{f\sigma'} c_{k\sigma}; d_\sigma^\dagger \gg - V_{fk}^* \ll c_{k\sigma'}^\dagger f_{\sigma'} d_\sigma; d_\sigma^\dagger \gg + V_{fk} \ll f_{\sigma'}^\dagger c_{k\sigma'} d_\sigma; d_\sigma^\dagger \gg$$

$$(\omega - \varepsilon_f - U'') \ll \hat{n}_{d\sigma'} f_\sigma; f_\sigma^\dagger \gg = \bar{n}_{d\sigma'} + U \ll \hat{n}_{d\sigma'} \hat{n}_{f\sigma'} f_\sigma; f_\sigma^\dagger \gg + U' \ll \hat{n}_{d\sigma'} \hat{n}_{d\sigma} f_\sigma; f_\sigma^\dagger \gg \quad (4.84)$$

$$+ V_{fk} \ll \hat{n}_{d\sigma'} c_{k\sigma}; f_\sigma^\dagger \gg - V_{dk}^* \ll c_{k\sigma'}^\dagger d_{\sigma'} f_\sigma; f_\sigma^\dagger \gg + V_{dk} \ll d_{\sigma'}^\dagger c_{k\sigma'} f_\sigma; f_\sigma^\dagger \gg$$

Moreover, the six two-particle Green's functions that appeared in  $\ll f_\sigma; d_\sigma^\dagger \gg$  (4.7) and  $\ll d_\sigma; f_\sigma^\dagger \gg$  (4.8) should also be taken into account.

$$(\omega - \varepsilon_f - U) \ll \hat{n}_{f\sigma'} f_\sigma; d_\sigma^\dagger \gg = U' \ll \hat{n}_{d\sigma} \hat{n}_{f\sigma'} f_\sigma; d_\sigma^\dagger \gg + U'' \ll \hat{n}_{d\sigma'} \hat{n}_{f\sigma'} f_\sigma; d_\sigma^\dagger \gg \quad (4.85)$$

$$+ (-V_{fk}^* \ll c_{k\sigma'}^\dagger f_{\sigma'} f_\sigma; d_\sigma^\dagger \gg + V_{fk} \ll \hat{n}_{f\sigma'} c_{k\sigma}; d_\sigma^\dagger \gg + V_{fk} \ll f_{\sigma'}^\dagger c_{k\sigma'} f_\sigma; d_\sigma^\dagger \gg)$$

$$(\omega - \varepsilon_d - U) \ll \hat{n}_{d\sigma'} d_\sigma; f_\sigma^\dagger \gg = U' \ll \hat{n}_{f\sigma} \hat{n}_{d\sigma'} d_\sigma; f_\sigma^\dagger \gg + U'' \ll \hat{n}_{f\sigma'} \hat{n}_{d\sigma'} d_\sigma; f_\sigma^\dagger \gg \quad (4.86)$$

$$+ (-V_{dk}^* \ll c_{k\sigma'}^\dagger d_{\sigma'} d_\sigma; f_\sigma^\dagger \gg + V_{dk} \ll \hat{n}_{d\sigma'} c_{k\sigma}; f_\sigma^\dagger \gg + V_{dk} \ll d_{\sigma'}^\dagger c_{k\sigma'} d_\sigma; f_\sigma^\dagger \gg)$$

$$(\omega - \varepsilon_f - U') \ll \hat{n}_{d\sigma} f_\sigma; d_\sigma^\dagger \gg = -\langle d_\sigma^\dagger f_\sigma \rangle + U \ll \hat{n}_{d\sigma} \hat{n}_{f\sigma'} f_\sigma; d_\sigma^\dagger \gg + U'' \ll \hat{n}_{d\sigma'} \hat{n}_{d\sigma} f_\sigma; d_\sigma^\dagger \gg \quad (4.87)$$

$$+ V_{dk}^* \ll c_{k\sigma}^\dagger f_\sigma d_\sigma; d_\sigma^\dagger \gg + V_{dk} \ll d_{\sigma'}^\dagger c_{k\sigma} f_\sigma; d_\sigma^\dagger \gg + V_{fk} \ll \hat{n}_{d\sigma} c_{k\sigma}; d_\sigma^\dagger \gg$$

$$(\omega - \varepsilon_f - U'') \ll \hat{n}_{d\sigma'} f_\sigma; d_\sigma^\dagger \gg = U \ll \hat{n}_{d\sigma'} \hat{n}_{f\sigma'} f_\sigma; d_\sigma^\dagger \gg + U' \ll \hat{n}_{d\sigma'} \hat{n}_{d\sigma} f_\sigma; d_\sigma^\dagger \gg \quad (4.88)$$

$$- V_{dk}^* \ll c_{k\sigma'}^\dagger d_{\sigma'} f_\sigma; d_\sigma^\dagger \gg + V_{dk} \ll d_{\sigma'}^\dagger c_{k\sigma'} f_\sigma; d_\sigma^\dagger \gg + V_{fk} \ll \hat{n}_{d\sigma'} c_{k\sigma}; d_\sigma^\dagger \gg$$

$$(\omega - \varepsilon_d - U') \ll \hat{n}_{f\sigma} d_\sigma; f_\sigma^\dagger \gg = -\langle f_\sigma^\dagger d_\sigma \rangle + U \ll \hat{n}_{f\sigma} \hat{n}_{d\sigma'} d_\sigma; f_\sigma^\dagger \gg + U'' \ll \hat{n}_{f\sigma'} \hat{n}_{f\sigma} d_\sigma; f_\sigma^\dagger \gg \quad (4.89)$$

$$+ V_{fk}^* \ll c_{k\sigma}^\dagger d_\sigma f_\sigma; f_\sigma^\dagger \gg + V_{fk} \ll f_{\sigma'}^\dagger c_{k\sigma} d_\sigma; f_\sigma^\dagger \gg + V_{dk} \ll \hat{n}_{f\sigma} c_{k\sigma}; f_\sigma^\dagger \gg$$

$$(\omega - \varepsilon_d - U'') \ll \hat{n}_{f\sigma'} d_\sigma; f_\sigma^\dagger \gg = U \ll \hat{n}_{f\sigma'} \hat{n}_{d\sigma'} d_\sigma; f_\sigma^\dagger \gg + U' \ll \hat{n}_{f\sigma'} \hat{n}_{f\sigma} d_\sigma; f_\sigma^\dagger \gg \quad (4.90)$$

$$- V_{fk}^* \ll c_{k\sigma'}^\dagger f_{\sigma'} d_\sigma; f_\sigma^\dagger \gg + V_{fk} \ll f_{\sigma'}^\dagger c_{k\sigma'} d_\sigma; f_\sigma^\dagger \gg + V_{dk} \ll \hat{n}_{f\sigma'} c_{k\sigma}; f_\sigma^\dagger \gg$$

Applying Implementing the decoupling scheme, these equations turn out to be

$$(\omega - \varepsilon_d - U - U' \bar{n}_{f\sigma} - U'' \bar{n}_{f\sigma'}) \ll \hat{n}_{d\sigma'} d_\sigma; d_\sigma^\dagger \gg = \bar{n}_{d\sigma'} + V_{dk} \bar{n}_{d\sigma'} \ll c_{k\sigma}; d_\sigma^\dagger \gg \quad (4.91)$$

$$(\omega - \varepsilon_f - U - U' \bar{n}_{d\sigma} - U'' \bar{n}_{d\sigma'}) \ll \hat{n}_{f\sigma'} f_\sigma; f_\sigma^\dagger \gg = \bar{n}_{f\sigma'} + V_{fk} \bar{n}_{f\sigma'} \ll c_{k\sigma}; f_\sigma^\dagger \gg \quad (4.92)$$

$$\begin{aligned} (\omega - \varepsilon_d - U' - U \bar{n}_{d\sigma'} - U'' \bar{n}_{f\sigma}) \ll \hat{n}_{f\sigma} d_\sigma; d_\sigma^\dagger \gg &= \bar{n}_{f\sigma} + V_{dk} \bar{n}_{f\sigma} \ll c_{k\sigma}; d_\sigma^\dagger \gg - V_{fk}^* \langle c_{k\sigma'}^\dagger f_{\sigma'} \rangle \ll d_\sigma; d_\sigma^\dagger \gg \\ &+ V_{fk} \langle c_{k\sigma}^\dagger f_\sigma \rangle \ll d_\sigma; d_\sigma^\dagger \gg \end{aligned} \quad (4.93)$$

$$\begin{aligned} (\omega - \varepsilon_f - U' - U \bar{n}_{f\sigma'} - U'' \bar{n}_{d\sigma}) \ll \hat{n}_{d\sigma} f_\sigma; f_\sigma^\dagger \gg &= \bar{n}_{d\sigma} + V_{fk} \bar{n}_{d\sigma} \ll c_{k\sigma}; f_\sigma^\dagger \gg - V_{dk}^* \langle c_{k\sigma'}^\dagger d_{\sigma'} \rangle \ll f_\sigma; f_\sigma^\dagger \gg \\ &+ V_{dk} \langle c_{k\sigma}^\dagger d_\sigma \rangle \ll f_\sigma; f_\sigma^\dagger \gg \end{aligned} \quad (4.94)$$

$$(\omega - \varepsilon_d - U'' - U \bar{n}_{d\sigma'} - U' \bar{n}_{f\sigma}) \ll \hat{n}_{f\sigma'} d_\sigma; d_\sigma^\dagger \gg = \bar{n}_{f\sigma} + V_{dk} \bar{n}_{f\sigma'} \ll c_{k\sigma}; d_\sigma^\dagger \gg \quad (4.95)$$

$$(\omega - \varepsilon_f - U'' - U \bar{n}_{f\sigma'} - U' \bar{n}_{d\sigma}) \ll \hat{n}_{d\sigma'} f_\sigma; f_\sigma^\dagger \gg = \bar{n}_{d\sigma} + V_{fk} \bar{n}_{d\sigma'} \ll c_{k\sigma}; f_\sigma^\dagger \gg \quad (4.96)$$

$$(\omega - \varepsilon_f - U - U' \bar{n}_{d\sigma} - U'' \bar{n}_{d\sigma'}) \ll \hat{n}_{f\sigma'} f_\sigma; d_\sigma^\dagger \gg = V_{fk} \bar{n}_{f\sigma'} \ll c_{k\sigma}; d_\sigma^\dagger \gg \quad (4.97)$$

$$(\omega - \varepsilon_d - U - U' \bar{n}_{f\sigma} - U'' \bar{n}_{f\sigma'}) \ll \hat{n}_{d\sigma'} d_\sigma; f_\sigma^\dagger \gg = V_{dk} \bar{n}_{d\sigma'} \ll c_{k\sigma}; f_\sigma^\dagger \gg \quad (4.98)$$

$$(\omega - \varepsilon_f - U' - U \bar{n}_{f\sigma'} - U'' \bar{n}_{d\sigma'}) \ll \hat{n}_{d\sigma} f_\sigma; d_\sigma^\dagger \gg = -\langle d_\sigma^\dagger f_\sigma \rangle + V_{fk} \bar{n}_{d\sigma} \ll c_{k\sigma}; d_\sigma^\dagger \gg \quad (4.99)$$

$$(\omega - \varepsilon_d - U' - U \bar{n}_{d\sigma'} - U'' \bar{n}_{f\sigma'}) \ll \hat{n}_{f\sigma} d_\sigma; f_\sigma^\dagger \gg = -\langle f_\sigma^\dagger d_\sigma \rangle + V_{dk} \bar{n}_{f\sigma} \ll c_{k\sigma}; f_\sigma^\dagger \gg \quad (4.100)$$

$$(\omega - \varepsilon_f - U'' - U \bar{n}_{f\sigma'} - U' \bar{n}_{d\sigma}) \ll \hat{n}_{d\sigma'} f_\sigma; d_\sigma^\dagger \gg = V_{fk} \bar{n}_{d\sigma'} \ll c_{k\sigma}; d_\sigma^\dagger \gg \quad (4.101)$$

$$(\omega - \varepsilon_d - U'' - U \bar{n}_{d\sigma'} - U' \bar{n}_{f\sigma}) \ll \hat{n}_{f\sigma'} d_\sigma; f_\sigma^\dagger \gg = V_{dk} \bar{n}_{f\sigma'} \ll c_{k\sigma}; f_\sigma^\dagger \gg \quad (4.102)$$

Then we can solve this closed set of equations and get

$$\ll f_\sigma; d_\sigma^\dagger \gg = \frac{(A_1 \bar{n}_{f\sigma'} + B_1 \bar{n}_{d\sigma} + C_1 \bar{n}_{d\sigma'} + 1) \Delta_{df} \ll d_\sigma; d_\sigma^\dagger \gg - B_1 \langle d_\sigma^\dagger f_\sigma \rangle}{\omega - \varepsilon_f - \Delta_{ff} (A_1 \bar{n}_{f\sigma'} + B_1 \bar{n}_{d\sigma} + C_1 \bar{n}_{d\sigma'} + 1)} \quad (4.103)$$

$$\ll d_\sigma; f_\sigma^\dagger \gg = \frac{(A_2 \bar{n}_{d\sigma'} + B_2 \bar{n}_{f\sigma} + C_2 \bar{n}_{f\sigma'} + 1) \Delta_{df} \ll f_\sigma; f_\sigma^\dagger \gg - B_2 \langle f_\sigma^\dagger d_\sigma \rangle}{\omega - \varepsilon_d - \Delta_{dd} (A_2 \bar{n}_{d\sigma'} + B_2 \bar{n}_{f\sigma} + C_2 \bar{n}_{f\sigma'} + 1)} \quad (4.104)$$

where the abbreviations are correspondingly

$$A_1 = U / (\omega - \varepsilon_f - U - U' \bar{n}_{d\sigma} - U'' \bar{n}_{d\sigma'})$$

$$A_2 = U / (\omega - \varepsilon_d - U - U' \bar{n}_{f\sigma} - U'' \bar{n}_{f\sigma'})$$

$$B_1 = U' / (\omega - \varepsilon_f - U' - U \bar{n}_{f\sigma'} - U'' \bar{n}_{d\sigma'})$$

$$B_2 = U' / (\omega - \varepsilon_d - U' - U \bar{n}_{d\sigma'} - U'' \bar{n}_{f\sigma'})$$

$$C_1 = U'' / (\omega - \varepsilon_f - U'' - U \bar{n}_{f\sigma'} - U' \bar{n}_{d\sigma})$$

$$C_2 = U'' / (\omega - \varepsilon_d - U'' - U \bar{n}_{d\sigma'} - U' \bar{n}_{f\sigma})$$

Here the two-particle inter-band terms are one order higher than in the Hartree-Fock approximation. We can take the same method to calculate the intra-band terms at the Lacroix level of approximation and decouple the inter-band terms.

Another approximation is that both the inter-band and intra-band two-particle Green's function are approximated with the Hubbard-I approximation. Here we only gives the result:

$$\langle\langle d_\sigma; d_\sigma^\dagger \rangle\rangle = \frac{(1 + \alpha_1 \bar{n}_{d\sigma'} + \beta_1 \bar{n}_{f\sigma} + \gamma_1 \bar{n}_{f\sigma'}) \left(1 - \frac{\Delta_{df} B_1 \langle d_\sigma^\dagger f_\sigma \rangle}{\omega - \varepsilon_f - \Delta_{ff} (A_1 \bar{n}_{f\sigma'} + B_1 \bar{n}_{d\sigma} + C_1 \bar{n}_{d\sigma'} + 1)}\right)}{\omega - \varepsilon_d - (1 + \alpha_1 \bar{n}_{d\sigma'} + \beta_1 \bar{n}_{f\sigma} + \gamma_1 \bar{n}_{f\sigma'}) \left(\Delta_{dd} + \frac{(A_1 \bar{n}_{f\sigma'} + B_1 \bar{n}_{d\sigma} + C_1 \bar{n}_{d\sigma'} + 1) \Delta_{df}^2}{\omega - \varepsilon_f - \Delta_{ff} (A_1 \bar{n}_{f\sigma'} + B_1 \bar{n}_{d\sigma} + C_1 \bar{n}_{d\sigma'} + 1)}\right)} \quad (4.105)$$

$$\langle\langle f_\sigma; f_\sigma^\dagger \rangle\rangle = \frac{(1 + \alpha_2 \bar{n}_{f\sigma'} + \beta_2 \bar{n}_{d\sigma} + \gamma_2 \bar{n}_{d\sigma'}) \left(1 - \frac{\Delta_{df} B_2 \langle f_\sigma^\dagger d_\sigma \rangle}{\omega - \varepsilon_d - \Delta_{dd} (A_2 \bar{n}_{d\sigma'} + B_2 \bar{n}_{f\sigma} + C_2 \bar{n}_{f\sigma'} + 1)}\right)}{\omega - \varepsilon_f - (1 + \alpha_2 \bar{n}_{f\sigma'} + \beta_2 \bar{n}_{d\sigma} + \gamma_2 \bar{n}_{d\sigma'}) \left(\Delta_{ff} + \frac{(A_2 \bar{n}_{d\sigma'} + B_2 \bar{n}_{f\sigma} + C_2 \bar{n}_{f\sigma'} + 1) \Delta_{df}^2}{\omega - \varepsilon_d - \Delta_{dd} (A_2 \bar{n}_{d\sigma'} + B_2 \bar{n}_{f\sigma} + C_2 \bar{n}_{f\sigma'} + 1)}\right)} \quad (4.106)$$

where

$$\begin{aligned} \alpha_1 &= U / (\omega - \varepsilon_d - U - U' \bar{n}_{f\sigma} - U'' \bar{n}_{f\sigma'}) \\ \alpha_2 &= U / (\omega - \varepsilon_f - U - U' \bar{n}_{d\sigma} - U'' \bar{n}_{d\sigma'}) \\ \beta_1 &= U' / (\omega - \varepsilon_d - U' - U \bar{n}_{d\sigma'} - U'' \bar{n}_{f\sigma}) \\ \beta_2 &= U' / (\omega - \varepsilon_f - U' - U \bar{n}_{f\sigma'} - U'' \bar{n}_{d\sigma}) \\ \gamma_1 &= U'' / (\omega - \varepsilon_d - U'' - U \bar{n}_{d\sigma'} - U' \bar{n}_{f\sigma}) \\ \gamma_2 &= U'' / (\omega - \varepsilon_f - U'' - U \bar{n}_{f\sigma'} - U' \bar{n}_{d\sigma}) \end{aligned}$$

## 4.5 Summary

For multi-band systems, we have realized that the approximation without inter-band hybridization in the code has given valuable and interesting information. The latter two approximations are work in progress. Moreover, the approximation, higher than the approximation without inter-band hybridization but lower than the Hartree-Fock approximation, *i.e.* making one step further by taking into account  $\langle\langle f_\sigma; d_\sigma^\dagger \rangle\rangle$  and  $\langle\langle d_\sigma; f_\sigma^\dagger \rangle\rangle$  but neglecting the two-particle inter-band Green's function can also be tried, which may hopefully give an improvement to the approximation without inter-band hybridization.

Moreover, one small trick about the coding technique should be mentioned here. For the case that two bands have different hybridization amplitude, *i.e.*  $V_{dk} \neq V_{fk}$ , there will be cross terms such as  $\sum_k \frac{V_{dk} V_{fk}}{\omega - \varepsilon_k}$  that appear in the EOMs. In the DMFT calculation, the hybridization amplitudes will be changed for each DMFT iteration instead of being the given fixed value. Therefore, we have to calculate them from the new hybridization function obtained from the self-consistency condition.

In the approximation without inter-band hybridization, we need to calculate  $\Delta_{dd}$  and  $\Delta_{ff}$ , where

$$\Delta_{dd}(\omega) = \sum_k \frac{V_{dk}^2}{\omega - \varepsilon_k} = \text{P} \int d\varepsilon \frac{V_d^2(\varepsilon)\rho(\varepsilon)}{\omega - \varepsilon} - i\pi V_d^2(\omega)\rho(\omega) \quad (4.107)$$

$$\Delta_{ff}(\omega) = \sum_k \frac{V_{fk}^2}{\omega - \varepsilon_k} = \text{P} \int d\varepsilon \frac{V_f^2(\varepsilon)\rho(\varepsilon)}{\omega - \varepsilon} - i\pi V_f^2(\omega)\rho(\omega) \quad (4.108)$$

Thus

$$V_d^2(\varepsilon)\rho(\varepsilon) = -\frac{1}{\pi} \text{Im} \Delta_{dd}(\varepsilon), \quad V_f^2(\varepsilon)\rho(\varepsilon) = -\frac{1}{\pi} \text{Im} \Delta_{ff}(\varepsilon)$$

So we can make the calculation

$$V_d(\varepsilon)V_f(\varepsilon)\rho(\varepsilon) = \sqrt{V_d^2(\varepsilon)V_f^2(\varepsilon)\rho^2(\varepsilon)} = \frac{1}{\pi} \sqrt{\text{Im} \Delta_{dd}(\varepsilon) \text{Im} \Delta_{ff}(\varepsilon)} \quad (4.109)$$

Thus, we can calculate the cross hybridization functions

$$\Delta_{df}(\omega) = \Delta_{fd}(\omega) = \sum_k \frac{V_{dk}V_{fk}}{\omega - \varepsilon_k} = \int d\varepsilon \frac{V_d(\varepsilon)V_f(\varepsilon)\rho(\varepsilon)}{\omega - \varepsilon} \quad (4.110)$$

Meanwhile, if  $\ll d_\sigma; f_\sigma^\dagger \gg$  or  $\ll f_\sigma; d_\sigma^\dagger \gg$  have been calculated, we can also calculate  $\Delta_{df}$  or  $\Delta_{fd}$  from the self-consistency condition, *e.g.* for the Hubbard model on the Bethe lattice and in a simple approximation, we may use

$$\Delta_{fd} = t^2 \ll d_\sigma; f_\sigma^\dagger \gg$$



# Chapter 5 Code realization and optimization

In this Chapter, we will describe the numerical realization of the EOM method described in Chap. 2 and 4. The technical problems we have met and the corresponding technical solutions will be discussed.

Concerning the code, we want to realize the following two aims: it should solve the single impurity Anderson model and get physical results; it should work as an impurity solver to solve the DMFT self-consistently and efficiently. The main problem we have to resolve is how to make the code converge. The other problem is how to make the code fast. In this Chapter we will introduce two classes of techniques we have implemented in our code. The first one is the method to solve integral equations. The second is the calculation of hybridization functions and integral terms.

The solving of integral equations is initially performed by an iterative method with linear mixing. It is found that it is difficult to converge and also very slow. Therefore, we have tried the iterative method with Broyden mixing. Although the iterative method with Broyden mixing has shown its effectiveness of reducing CPU time, it is less useful for solving the problem of convergence. In a further step, we have developed a combined method of iterative method and genetic algorithms (GA method). This new numerical method has proven very effective for overcoming the technical problems we have met in the previous two methods. This combined method not only speeds the DMFT calculations up, especially in the Mott transition region, but it also improves the quality of the results. We found that the GA method is a very powerful tool and has wide potential in solving minimization problems.

The integral terms have been calculated in two different ways. In a first implementation, we calculated the imaginary part of  $\Delta$  and the integral terms by an analytical method. So the imaginary part of the calculated terms are exact for the given integrals. Then, the Kramers-Kronig relations are used to calculate the real part from the existing imaginary part, which is the most natural way to calculate the complex quantities. As an improvement on techniques of the iterative

method with linear mixing, we have tried a method to calculate the hybridization functions and integral terms fully numerically. We call this Lorentzian broadening method. In the Lorentzian broaden method, the  $\omega + i0^\dagger$  is replaced by  $\omega + i\eta$  where  $\eta$  is a small finite number. Thus the real and imaginary parts can be calculated simultaneously, automatically and fully numerically.

In this Chapter, we first introduce the technique to calculate hybridization functions and integral terms, then we describe the iterative method with linear mixing and the iterative method with Broyden mixing. Finally, we present the details of our GA method. In the discussion we will provide a comparison of iterative method and GA method.

## 5.1 Technique in calculating the integral terms

In our programming, we have calculated the hybridization functions and integral terms with two different methods. One is an analytical method, which can give the exact imaginary part. Another is the Lorentzian broadening method, which is a fully numerical method. The integral terms are coming from those  $k$  summation terms, which has been explained in previous chapters.

### 5.1.1 Analytical method

Initially, we calculated the imaginary part of  $\Delta$  and the integral terms by an analytical method. Here we take the hybridization function as an example. In calculating the hybridization function, for a given noninteracting DOS, we can obtain the imaginary part exactly. Then we use the Kramers-Kronig relation to calculate the real part, *i.e.*

$$\Delta = \sum_k \frac{V_k^2}{\omega - \varepsilon_k} = \int d\varepsilon \frac{V^2(\varepsilon)\rho(\varepsilon)}{\omega - \varepsilon} \quad (5.1)$$

The theoretically exact imaginary part is given as

$$\text{Im } \Delta(\omega) = -\pi V^2(\omega)\rho(\omega) \quad (5.2)$$

Afterwards, the real part is calculated as

$$\text{Re } \Delta(\omega) = \frac{1}{\pi} \int d\omega' \frac{\text{Im } \Delta(\omega')}{\omega' - \omega} \quad (5.3)$$

In this method, the imaginary parts of the results are exact. However, the real parts are limited to the precision of the Principal integral on a discrete mesh. However, for the impurity solver with iterative method and linear mixing, we found that it is very difficult to make the code converge by calculating the integral terms with the analytical method. Hence, we have tried a method adding



a continuous tail on noninteracting DOS, which proves to be effective and improves convergency greatly. However, a new problem appears. For the DMFT iteration, DOS will be zero outside the Hubbard bands. Through the self-consistency condition, this will enter the hybridization function and make the DMFT self-consistency difficult to achieve. So adding a tail is not an effective method. In order to overcome the difficulties explained above, we have tested the Lorentzian broadening method.

### 5.1.2 Lorentzian broadening method

Besides the analytical method, we have also used the Lorentzian broadening method in calculating the hybridization functions and integral terms. That's because the iterative method with linear mixing has got serious unsolvable numerical problems. Hence, we explored the Lorentzian broadening method, which originates from the fact that

$$\delta(x) = \lim_{a \rightarrow 0} \delta_a(x) = \lim_{a \rightarrow 0} \frac{1}{\pi} \frac{a}{a^2 + x^2} \quad (5.4)$$

so that  $\delta_a(x)$  can be used as an approximation to Dirac  $\delta$  function when for small  $x$ . We use this to approximate the imaginary part of integral terms. We can show it is a good approximation. Still using the hybridization function as an example, we calculate it as

$$\Delta = \sum_k \frac{V_k^2}{\omega - \varepsilon_k} = \lim_{\eta \rightarrow 0^+} \int d\varepsilon \frac{V^2(\varepsilon)\rho(\varepsilon)}{\omega + i\eta - \varepsilon} = \lim_{\eta \rightarrow 0^+} \int d\varepsilon \frac{V^2(\varepsilon)\rho(\varepsilon)(\omega - i\eta - \varepsilon)}{(\omega - \varepsilon)^2 + \eta^2} \quad (5.5)$$

Here the small imaginary part  $\eta$  means a broadening. We can see that, if  $\eta$  is small,

$$\text{Im } \Delta(\omega) = \lim_{\eta \rightarrow 0^+} \int d\varepsilon V^2(\varepsilon)\rho(\varepsilon) \frac{-\eta}{(\omega - \varepsilon)^2 + \eta^2} = -\pi V^2(\omega)\rho(\omega) \quad (5.6)$$

Thus, we get the exact result. Moreover, when  $\eta$  is small, it will contribute very little to the real part except in a small region near  $\omega$ . At the same time, in the calculation of the real part,  $\varepsilon = \omega$  is not singularity any more. So we can calculate it as a regular integral on discrete mesh. From Fig. 5.1, we can see the influence of taking various  $\eta$  to the final result by comparing with the exact result.

This method has been tested to be effective in reducing the CPU time and in enabling convergence of the code for a large range of parameters. However, there is still a problem. For the DOS of the insulating state, there is a continuous and nonzero plateau between the two Hubbard bands. Moreover, near the Fermi level, there exists a nonphysical semicircular peak, which makes it difficult to distinguish the metal-insulator transition clearly. We will discuss this problem in Section 5.4.

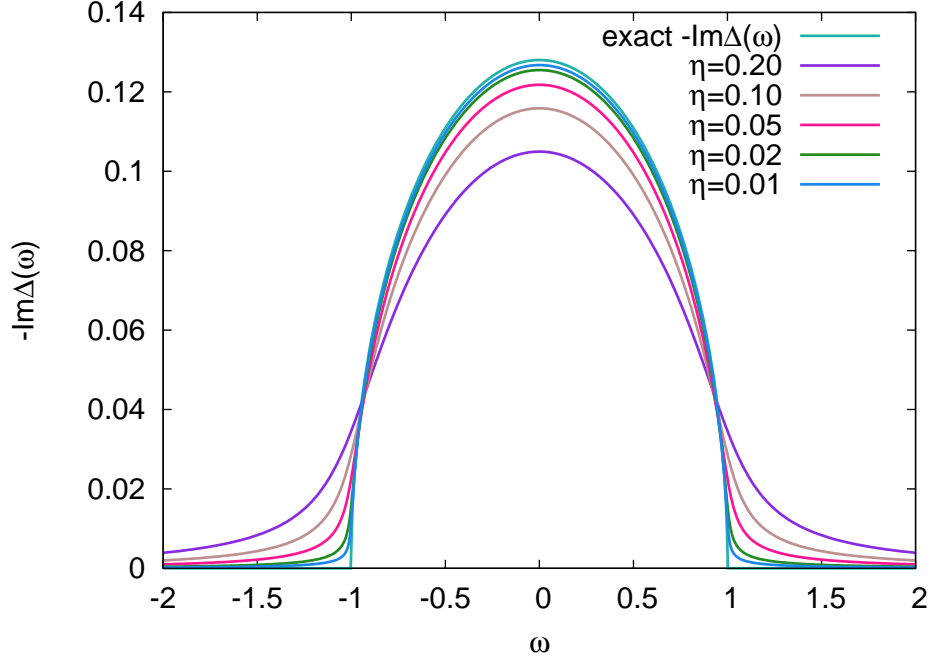


Figure 5.1: Comparison of results obtained with Lorentzian broadening method and exact theoretical result of imaginary part of  $\Delta(\omega)$

## 5.2 Iterative method

From this section to the end of the chapter, we will discuss the solution of the integral equation and search a scheme for obtaining a converged result. As is well known, the iterative method is an important method in the solution of integral equations. In our calculation, we have used this technique to solve the integral equations. We use the newly generated Green's function from the EOMs as input of the next iteration, and repeat until we get the norm of the difference between Green's functions from two consecutive iteration steps below a threshold of error. We say we get a converged result at that order of accuracy. However, if the DOS oscillates drastically between two iterations, it will be difficult to approach a converged result, or even does not work at all. In past studies, different methods have been developed to overcome these difficulties, in which the iterative method with linear mixture and the Newton-Raphson method are two commonly used methods.

### 5.2.1 Iterative method with linear mixing

For the iterative method, linear mixing is the simplest and commonly used technique, where a linear mixture of initial input and output is used to be the input of the new iteration instead of

using the full output directly, *i.e.*

$$y_{in}^{new}(x) = (1 - \alpha)y_{in}(x) + \alpha y_{out}(x) \quad (5.7)$$

where  $\alpha$  ( $0 < \alpha < 1$ ) is the parameter that can be chosen to determine the degree of mixing; this decides how large the change of input between subsequent iterations is. A small change between inputs can make sure that the new output also changes only slightly. Thus possible drastic changes between the subsequent iterations can be avoided.

The iterative method with linear mixing does improve the properties of convergency when iterations approach convergence. However, it is still not enough for some systems. A smaller mixing parameter also means that it takes much longer time to obtain convergence. In our calculations, if we want to get a converged result at very high accuracy, it takes a very long time to achieve this with linear mixing. The closer the Green's function approaches the desired accuracy, the slower the convergence speed becomes. Especially for DMFT calculations, this becomes more serious because we have to use even smaller mixing parameters to make the calculation converge.

Besides the problem of slow convergence of the linear mixing approach we have discussed above, the iterative method with linear mixing has more difficulties. Some of them have been mentioned in the last section when we describe the shortcomings of the two methods in calculating integral terms. Moreover, iterative method tends to generate artificial peaks on the edge of the Hubbard bands. This is considered a difficulty that prevents the code from converging smoothly.

In a word, the EOM method using the iterative approach with linear mixing is not satisfactory in convergence and speed. So we have tried to improve the code in two directions. One aim is to speed up the program. For this purpose, we have tried Broyden mixing. Another one is to improve the result by reducing the influence of the numerical treatment as much as possible. As a final solution to both the aims, we have developed the combined method of EOM and a genetic algorithm.

### 5.2.2 Broyden mixing

To approach the solution quickly, we have implemented the Broyden mixing searching scheme. The iterative method with Broyden mixing is a quasi Newton-Raphson method. The basic idea of the method is: for a function  $y(x)$ , if we only keep the first order term in the Taylor expansion, it has the form

$$y(x) = y(x_0) + y'(x_0)(x - x_0) \quad (5.8)$$

which can be used to construct an iteration relation.

Then a new function  $F$  is constructed,

$$F(y_{in}) = y_{out}(y_{in}) - y_{in} \quad (5.9)$$

where all the functions are functions of  $x$ . Now the problem is to find the  $y_{in}$  so that  $F(y_{in}) = 0$ . If we get  $F(y_{in})$  to take this value, we have the converged result that we are looking for.

When an initial  $y^{(0)}$  is chosen, the first  $F^{(0)}$  is determined. Here we consider that  $F$  satisfies the relation

$$F^{(m)} = F^{(m-1)} - J \cdot (y^{(m)} - y^{(m-1)}) \quad (5.10)$$

where the Jacobian is defined as

$$J_{ij} = -\frac{\partial F_i}{\partial y_j} \quad (5.11)$$

$i, j$  are the grid indices on the  $x$  grid. In general an initial guess of  $J$  is given and the  $m$ th iteration is

$$y^{(m)} = y^{(m-1)} + [J^{(m)}]^{-1} F^{(m)} \quad (5.12)$$

If the generating scheme of  $J$  is known, the new input can be constructed. Then the new output and new order of  $F$  can be obtained. Thus we can do the iteration continually until we can get a converged result in the set accuracy theoretically.

In the usual Broyden method,  $J^{(m)}$  should satisfy the  $F^{(m-1)} - J \cdot (y^{(m)} - y^{(m-1)}) = 0$ , and also should be constrained to the minimization of  $\|J^{(m)} - J^{(m-1)}\|$ . This is reasonable because, when convergence is coming nearer and nearer, the  $J$  should also be nearer and nearer and the difference between two iterations should be minimized. From the latter, the Jacobian matrix can be determined.

$$J^{(m)} = J^{(m-1)} - [\Delta F + J^{(m-1)} \cdot \Delta y^{(m-1)}] J^{(m-1)T} \quad (5.13)$$

where  $\Delta y$  and  $\Delta F$  are normalized differences.

$$\Delta y^{(m)} = (y^{(m)} - y^{(m-1)}) / |y^{(m)} - y^{(m-1)}| \quad (5.14)$$

$$\Delta F^{(m)} = (F^{(m)} - F^{(m-1)}) / |y^{(m)} - y^{(m-1)}| \quad (5.15)$$

Here only the most recent iteration result is used to update this Jacobian matrix.

In D. Vanderbilt and S. G. Louie's paper [86], they proposed to incorporate all previous iterations into each update of the Jacobian matrix with different weights. The  $J$  is determined by the

least square minimization of

$$E = \sum_{l=0}^m \omega_l^2 |J^{(m+1)} \cdot \Delta y^{(l)} + \Delta F^{(l)}|^2 + \omega'^2 |J^{(m+1)} - J^{(0)}|^2 \quad (5.16)$$

With  $\partial E / \partial J_{ij}^{(m+1)} = 0$ , it gives

$$J^{(m+1)} = \gamma^{(m+1)} \cdot (\beta^{(m+1)})^{-1} \quad (5.17)$$

$$\beta^{(m+1)} = \omega'^2 \mathbf{1} + \sum_{l=0}^m \omega_l^2 \Delta y^{(l)} \otimes \Delta y^{(l)T} \quad (5.18)$$

$$\gamma^{(m+1)} = \omega'^2 J^{(0)} - \sum_{l=0}^m \omega_l^2 \Delta F^{(l)} \otimes \Delta y^{(l)T} \quad (5.19)$$

The weights  $\omega'$  and  $\omega_l$  will be input by hand with experience and give the method some flexibility.

This method is called first Broyden method for it directly use the Jacobian matrix and should compute the inverse matrix in the iteration. Especially for Vanderbilt's proposal, it will take more memory and CPU time to store and calculate the inverse matrix. So the second Broyden method, using the inverse Jacobian matrix, can be advantageous. On the other hand, efforts on decreasing the size of the matrix have also been made for improving the efficiency of the method.

In the second Broyden method, with the inclusion of the inverse matrix, now the formulae are

$$y^{(m)} = y^{(m-1)} + [G^{(m)}]F^{(m)} \quad (5.20)$$

where  $G^{(m)} = [J^{(m)}]^{-1}$  and

$$G^{(m)} = G^{(m-1)} + \frac{[(y^{(m)} - y^{(m-1)}) - G^{(m-1)}(F^{(m)} - F^{(m-1)})](F^{(m)} - F^{(m-1)})^T}{(F^{(m)} - F^{(m-1)})^T (F^{(m)} - F^{(m-1)})} \quad (5.21)$$

D. D Johnson [87] also modified the method with the inverse matrix according to Vanderbilt's work.

$$E = \omega_0^2 \|G^{(m+1)} - G^{(0)}\| + \sum_{l=1}^m \omega_l^2 |G^{(m+1)} \cdot \Delta y^{(l)} + \Delta F^{(l)}|^2 \quad (5.22)$$

Using  $\partial E / \partial G_{ij}^{(m+1)} = 0$ , it gives

$$G^{(m+1)} = \gamma^{(m+1)} \cdot (\beta^{(m+1)})^{-1} \quad (5.23)$$

$$\beta^{(m+1)} = \omega'^2 \mathbf{1} + \sum_{l=0}^m \omega_l^2 \Delta F^{(l)} \otimes \Delta F^{(l)T} \quad (5.24)$$

$$\gamma^{(m+1)} = \omega'^2 J^{(0)} - \sum_{l=0}^m \omega_l^2 \Delta y^{(l)} \otimes \Delta F^{(l)T} \quad (5.25)$$

Johnson used a technique to expand the  $(\beta^{(m+1)})^{-1}$  in terms of  $\Delta F$  here.

$$(\beta^{(m+1)})^{-1} = (\omega_0)^{-1} \left( \mathbf{I} - \sum_{k,n=1}^m \omega_n \omega_k \beta_{kn} \Delta F^{(n)} \otimes \Delta F^{(k)T} \right) \quad (5.26)$$

With

$$\beta_{kn} = (\omega_0^2 \mathbf{1})_{kn}^{-1}, a_{ij} = \omega_i \omega_j \Delta F^{(n)} \otimes \Delta F^{(k)T}$$

and finally got

$$G^{(m+1)} = G^{(1)} - \sum_{k,n=1}^m \beta_{kn} (G^{(m)} \Delta F^{(n)} + \Delta y^{(n)}) \Delta F^{(k)T} \quad (5.27)$$

In our code, we have tested both the Broyden methods, and the second Broyden method following [87] is much fast.

### 5.3 Genetic algorithm

The Broyden method is one good method to choose the weight of mixture intelligently. However, it is still not enough because it can only speed up the convergence and has little effect for improving the result. So we have developed the implementation of a genetic algorithm to solve the equations. Our purpose is not only to speed up the program but also to improve the result by using a more intelligent evolution instead of using single iteration. For example, the tail of the conduction band can influence the height of Hubbard band and the convergence of the code, but is difficult to be determined reasonably. We hope to decrease the influence of these manually input numerical influences and, at the same time, remove some defects generated in iterations. Here we will first make an introduction to the method, then show the advantage of the GA method.

#### 5.3.1 Introduction of genetic algorithm

Genetic Algorithm (GA) is an adaptive heuristic search algorithm premised on the evolutionary ideas of natural selection and genomes. It has been widely used in a few rapidly growing areas of artificial intelligence, *e.g.* to get derivative in quantum finance, to solve the Traveling Salesman Problem, and so on.

The initial idea was introduced in the 1960s by I. Rechenberg in his work "Evolution strategies". His idea was then further developed by other researchers. Genetic Algorithms (GAs) were invented by John Holland and developed by him and his students and colleagues. This lead to Holland's book "Adaption in Natural and Artificial Systems" published in 1975.

Just as listed below, the algorithm is started with a set of solutions called population (in our case they are single particle Green's functions). Solutions from one population are taken and used

to form a new population. This is motivated by a hope, that the new population will be better than the old one. Solutions which are selected to form new solutions (offspring) are selected according to their fitness - the more suitable they are the more chances they have to reproduce. Then the procedure is repeated until some condition (for example, number of generations or computation time or fitness of the best solution) is satisfied.

The algorithm can be written down as follows:

1. Randomly generate an initial population  $M(0)$
2. Compute and save the fitness  $u(m)$  for each individual  $m$  in the current population  $M(t)$
3. Define selection probabilities  $p(m)$  for each individual  $m$  in  $M(t)$  so that  $p(m)$  is proportional to  $u(m)$
4. Generate  $M(t+1)$  by probabilistically selecting individuals from  $M(t)$  to produce offspring via genetic operators
5. Repeat from step 2 until satisfactory solution is obtained.

The three most important aspects of using genetic algorithms are:

- (1) definition of the object function (suitable to use GA),
- (2) definition and implementation of the genetic representation (reproduce operators),
- (3) definition and implementation of the fitness function (selection and evaluation operators).

Once these three items have been well defined, the genetic algorithm should work pretty well. Of course, within this framework one can try many different variations to improve the performance.

The advantage of the GA approach is the ease with which it can handle arbitrary kinds of constraints and objectives; all such things can be handled as weighted components of the fitness function, making it easy to adapt the GA scheduler to the particular requirements of a very wide range of possible overall objectives. An effective GA representation and meaningful fitness evaluation are the keys of the success in GA applications. Here the main difficulties are how to select the parents and the rules to generate the offsprings.

### 5.3.2 Implementation

In our implementation, we choose the imaginary part of the Green's function as object function (Self-energy can also be used for object function. But the implementation will be more complex than using Green's function). We borrowed the idea of optimizing a wave function [96, 97] until they obey the Schrödinger equation and carry it over to our optimization problem, *i.e.* finding a Greens function  $G(\omega) = \ll f_\sigma; f_\sigma^\dagger \gg$  that fulfils Eq. (2.97).

The GA algorithm is started with a "population" of initial guesses. The imaginary parts of the

initial population of trial Green's functions are guessed as sums of Gaussians

$$\text{Im} G(\omega) = L \left( e^{-\frac{(\omega-B)^2}{2C^2}} + e^{-\frac{(\omega-B-U)^2}{2C^2}} \right) \quad (5.28)$$

where  $L$  is a normalization factor,  $B, C$  are randomly generated numbers and  $U$  is the Coulomb interaction strength. We use the Kramers-Kronig relation to determine the real part

$$\text{Re} G(\omega) = -\frac{1}{\pi} \int \frac{\text{Im} G(\omega')}{\omega' - \omega} d\omega' \quad (5.29)$$

The population size always depends on the nature of the problem, but typically contains several hundreds or thousands of possible solutions generated randomly and covering the entire range of possible solutions (the search space). However, the solutions may be "seeded" in the areas where optimal solutions are likely to be found. The convergence of the method can be speeded up if the positions of the randomly generated peaks cumulate around the positions of the Hubbard bands known from the atomic limit, which is realized by using nonuniform distribution random generator to let the initial Green's functions locate mostly near the band positions. Besides Gaussians, we have also tested other functional forms of the initial guess, *e.g.*

$$\text{Im} G(\omega) = L \left( \Psi(\omega - B) + \Psi(\omega - B - U) \right) \quad (5.30)$$

where

$$\Psi(x) = \begin{cases} \sqrt{1 - \frac{x^2}{A^2}} & |x| < A \\ 0 & |x| > A \end{cases} \quad (5.31)$$

and it proves that different types of guesses will cause only very little influence in both speed of convergence and final result.

Then we define the fitness function as

$$F[G(\omega)] = \|G(\omega) - \text{rhs}[G(\omega)]\| \quad (5.32)$$

where  $\text{rhs}[G(\omega)]$  represents the right hand sides of Eq. (2.70) or Eq. (2.97) which are functionals of  $G(\omega)$  via the integral terms Eq. (2.72). The norm

$$\|F(\omega)\| = \int d\omega |F(\omega)| \quad (5.33)$$

measures the distance of the trial Green's functions from the self-consistent solutions of Eqs. (2.70) or (2.97). Any trial Green's functions will be evaluated and ordered according to this fitness



function. Then a proportion of the Green's functions are selected to breed a new generation of Green's functions. This procedure is a fitness-based process, where much fitter solutions owning top fitness are more likely to be selected. Moreover, in the GA scheme there are a lot of well developed rating techniques. Some methods rate only a random sample of the population, as this process may be very time-consuming. So further improvement on rating technique in our code can be made in the near future by employing more advanced methods.

In the reproduction procedure, a new "generation" of the population of trial Green's functions is formed by application of the two most usual GA operators, "crossover" and "mutation". Crossover selects genes from parent Green's functions and creates a new offspring. The simplest way to do this is to choose randomly some crossover point and everything before this point copies from a first parent and then everything after a crossover point copies from the second parent. In a mathematical way the GA operators are

$$\begin{aligned}\text{Im } G_1^{\text{offspring}}(\omega) &= L_1 \text{Im} \left\{ G_1^{\text{parent}}(\omega) \Theta(\omega - \omega_0) \right. \\ &\quad \left. + G_2^{\text{parent}}(\omega) \Theta(\omega_0 - \omega) \right\} \\ \text{Im } G_2^{\text{offspring}}(\omega) &= L_2 \text{Im} \left\{ G_1^{\text{parent}}(\omega) \Theta(\omega_0 - \omega) \right. \\ &\quad \left. + G_2^{\text{parent}}(\omega) \Theta(\omega - \omega_0) \right\}\end{aligned}\tag{5.34}$$

where  $\omega_0$  is the randomly chosen crossover position,  $\Theta(\omega)$  is the Heaviside function and  $L_1, L_2$  are normalization factors.

Performed together with crossover, mutation introduces, with a low probability, random small changes in the trial Greens function in order to prevent the population from stabilizing in a local minimum. In our implementation, we have constructed mutation operator as

$$\text{Im } G^{\text{offspring}}(\omega) = L \left( \text{Im } G^{\text{parent}}(\omega) + A e^{-\frac{(\omega-B)^2}{2C^2}} \right)\tag{5.35}$$

where  $A, B, C$  are randomly generated numbers and  $L$  normalizes the function. The crossover and mutation operators can be illustrated as Fig 5.2. The top peak-adding mutation is helpful to approach multi-peak systems, while the bottom negative-peak-adding mutation is considered to be useful to approach the gap shown in real physical systems. For both crossover and mutation, real parts are obtained via the Kramers-Kronig relation.

Now the principles of selection have to be discussed. Some of the best members of a generation are preserved without replacing them by their offspring. Furthermore, the trial Green's functions

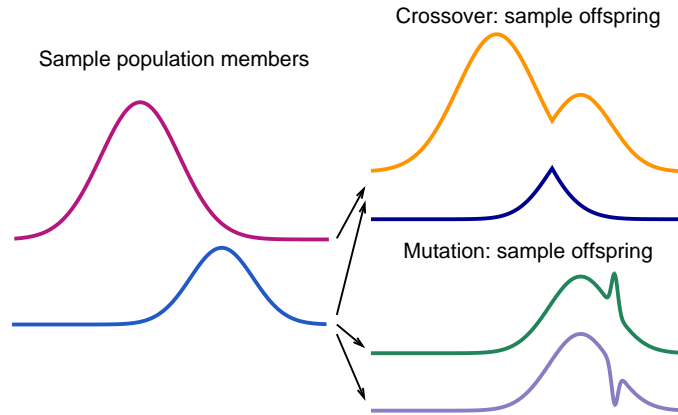


Figure 5.2: Illustration for GA operators

that are actually included into the new generation are obtained by plugging the result of the GA operations into Eqs. (2.70) or (2.97) and calculating one iterative step. While in principle, pure GA operations could be used to find an optimal solution, the strict requirements imposed on a self-consistent solution are more easily met by alternation of GA operations and iterative steps. As the new generation has more than twice as many members as the previous one, many are dropped according to their fitness values. In order to avoid premature convergence of the population to a suboptimal solution, some members with unfavorable fitness values are kept in the population, and some new random trial Green's functions are added to the population. The end of the evolution is determined, as in the iterative solution of the integral equations, by a member of the population reaching the target accuracy. We usually use fitness function values of  $10^{-4}$  as a criterion for terminating the GA procedure. An additional advantage of the GA approach is the ease with which it can handle arbitrary kinds of constraints; they can be included as weighted components of the fitness function.

## 5.4 Results and discussion

Within the GA scheme, the running speed of the code has been improved greatly. In general the solution with the previous iterative method takes at least four times longer than the GA method. Especially when the parameters are near the Mott transition critical point, the iterative solution becomes very slow and inefficient. As we know, for the iterative method with Lorentzian broadening, if the mixing is small enough and the broadening parameter is large enough, one can always get a converged result finally. However, large mixing usually leads far away from a converged

result. In finite  $U$  case, the mixing in the DMFT calculation has to be set to a very small number, nearly of the order of  $10^{-4}$ , which slows down the speed greatly. The GA method has overcome this difficulty. In the generation of offspring, the output Green's function obtained from EOMs can be fully taken into the next evolution. Moreover, occasional crossover and mutation can also greatly urge the Green's function evolving forward using a way different to the iterative method. That's why the GA method can have much faster speed. Another factor that can influence the speed is the grid point number. For the iterative method with linear mixing, usually it needs a very dense mesh because the decrease of mesh points will greatly influence the integrals and the interpolation, while the GA method is not very sensitive to the number of mesh points and needs much less points than the iterative iterative method with linear mixing. In the GA method, the most important factor influencing speed is the population number. So in order to improve the running speed, we should make more efforts to improve the efficiency of the GA selection scheme and decrease the population number as low as possible. In Fig. 5.3 we have compared the results obtained from the pure iterative method with Lorentzian broadening  $\eta = 0.05$  and combined GA method. We can see the GA method has produced much better results. Actually here the convergence accuracy does not have the same meaning. For the GA method, at each step the Green's function is compared with the full Green's function in the last step, while in the iterative method with linear mixing the new Green's function is obtained by mixing the old Green's function with a small part of the newly generated Green's function. Therefore, a GA accuracy of 0.005 may be higher than the accuracy of  $1e^{-5}$  of the iterative method with linear mixing.

Here we give some example speed information of our code. For the single impurity Anderson model,

model	method	mesh	parameters	CPU time
SIAM	GA	1077	population=100, accu=0.005, T=0.01	48.52s
	linear mix	1077	mix=0.5, accu= $10^{-8}$ , $T = 0.01$	2.2s
		1077	mix=0.002, accu= $10^{-8}$ , $T = 0.01$	128.52s

the GA method does not show advantage in speed.

For the Hubbard model,

model	method	mesh	parameters	CPU time
Hubbard	GA	1000	population=100, accu=0.005, T=0.01, U=2.6	244.9s
	linear mix	1150	mix=0.001, dmix = $10^{-5}$ , accu = $10^{-5}$ , $T = 0.01$	1962.0s

the GA method converges much faster than iterative method with linear mixing. In the tables, 'accu' is the difference of the norms between the consecutive Green's functions that we set to terminate the iteration. 'dmix' is the mixing parameter in DMFT iteration.

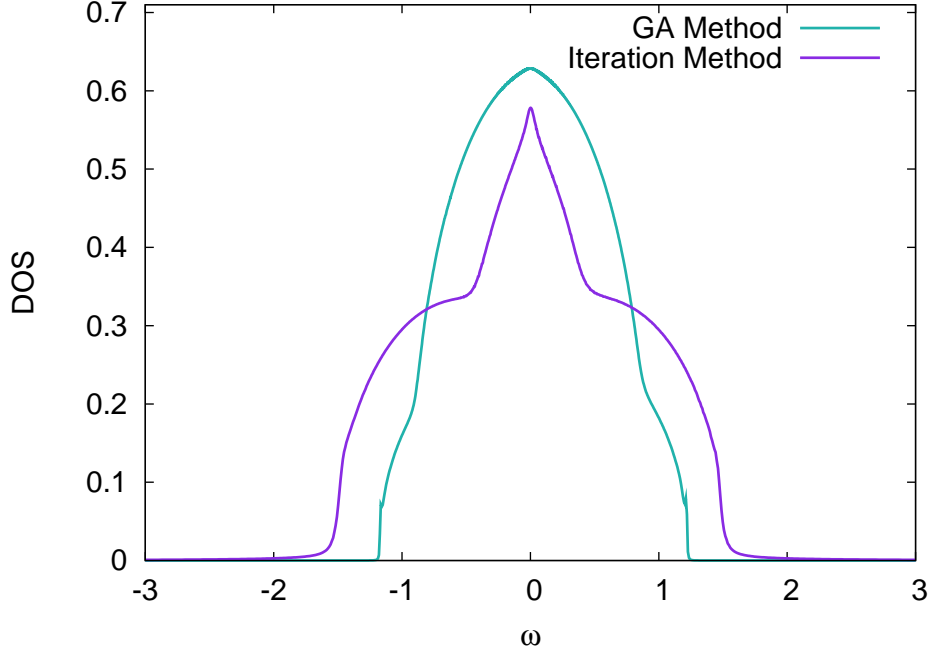


Figure 5.3: Comparison of GA method and conventional iterative method for Bethe lattice ( $U=1$ , GA converged with  $F[G] < 0.005$ , iterative method converged with  $\|G_i - G_{i+1}\| < 10^{-5}$ )

In Fig. 5.4, we show the results obtained from both methods for the same parameter values. In Fig. 5.4, top left, we can see that in the DOS there is a nonzero continuous connection between two Hubbard bands in the result obtained with Lorentzian broadening, which makes it difficult to distinguish the Mott transition clearly when  $U$  approaches the critical value for the transition  $U_c$  because the quasiparticle peak is very small in that case. However, the combined GA and iterative method can give more precise results near the critical point which can be seen from the bottom left DOS figure. For the combined GA method, at  $U = 2.6$  we find an insulating state, while the Lorentzian broadening method still gives a metallic state at the Fermi level. This is due to the fact that the divergent behavior of the imaginary part of the self-energy just above the Mott transition cannot be correctly captured if there exists a finite broadening  $\eta$ . However, in the GA method, the broadening  $\eta$  can be even set to zero, which eliminates the numerical problem induced by  $\eta$ . The right panel of Fig 5.4 shows the comparison of the imaginary part of the self-energy. It is found that the GA method really gives a correct divergent behavior even close to the Mott transition at

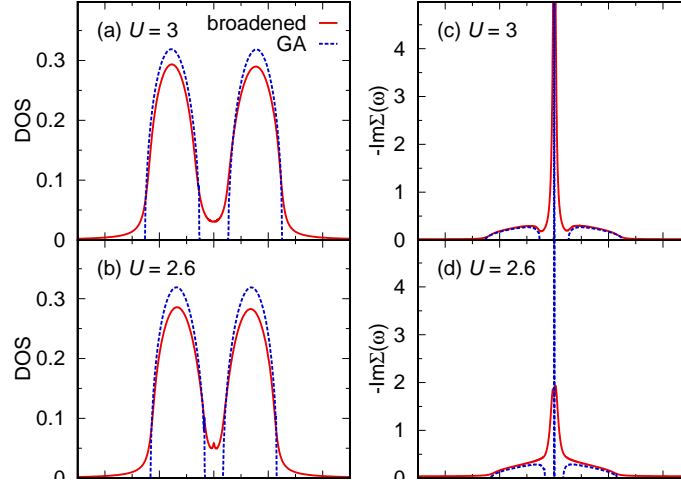


Figure 5.4: Comparison between the GA method and the iterative method with Lorentzian broadening for the particle-hole symmetric Hubbard model on the Bethe lattice: (top) DOS and self-energy for the insulating state with  $U = 3$ . (bottom) DOS and self-energy close to the Mott transition with  $U = 2.2$ .

the Fermi level, while the Lorentzian broadening method does less well.

Moreover, we have used different initial populations: Gaussian and semi-elliptical peaks. We have confirmed that the initial populations with less tail can give less tails in the final Densities of states. However, from the following figure we can see that the difference of initial populations gives little influence in machine accuracy.

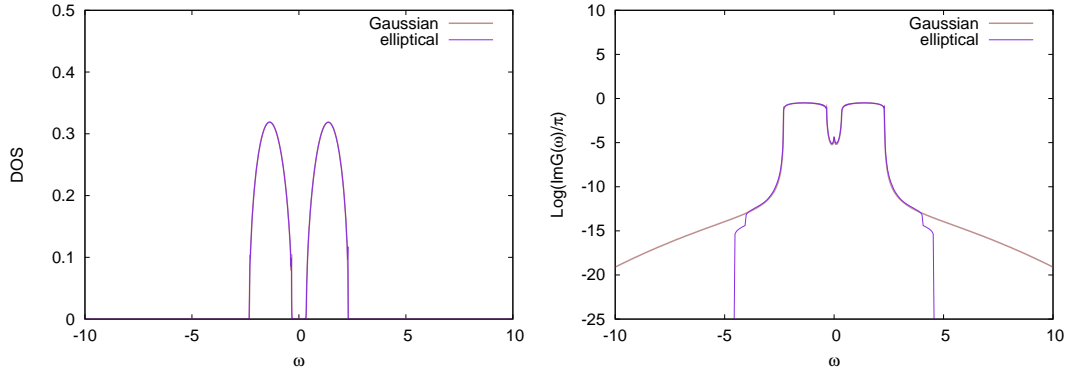


Figure 5.5: comparison of the influence to the tail with different type of initial populations ( $U=2.6$ )

On the other hand, we mention that sometimes the result has a minor difference between different runs. This phenomenon is due to the full randomness of the initial populations. Therefore, this problem can be solved by increasing the size of the population in order to make the search space large enough. However, a larger population size means longer running time. One has to

choose a suitable population size in order to get a sufficient precise result and reducing the running time as much as possible.

With the GA method, we successfully realized our aim to improve both the convergence and running speed. At the same time, the nonphysical peaks at the edge of Hubbard band are removed and the influence of broadening is eliminated. Therefore, we conclude that the GA method is a useful improvement to the previous conventional iterative method.

# Chapter 6 Physical results and Discussion

In this Chapter, we show the results obtained within our numerical method. First, we will present the single impurity Anderson model, on which the calculation of the dynamical mean field theory is effectively based. Then we will show the model calculations for the single band Hubbard model and the periodic Anderson model with spin and orbital degeneracy  $N = 2$ . Next, the large  $N$  cases are investigated for both Hubbard and periodic Anderson models.

We have studied both lattice models in a wide range of control parameters in order to fully test our equation-of-motion method. At the same time, the physical properties, *e.g.* the densities of state, occupation number, quasi-particle weight, and so on, are explored. The Kondo peak and Mott metal-insulator transition are observed at the Fermi level.

In the last part of this Chapter, we will present some recently obtained promising results of the multi-band system, which has been a new highlight in recent model studies of strongly correlated systems.

## 6.1 Single impurity Anderson model

In this Section we will show the results for the single impurity Anderson model. As we have emphasized, the impurity solver is the essence of the DMFT calculation. Whether the quality of the impurity solver is good or not, will greatly influence the applicability of the impurity solver within DMFT. Therefore, as the first step, a reliable impurity solver must work well for the impurity model and reproduce the results obtained with other well-developed numerical methods. Moreover, the speed of the impurity solver is an important factor. The aim of this PhD work is to develop a fast impurity solver for the DMFT calculation based on the EOM method.

In previous Chapters, we have introduced our method where the correlation terms are all obtained self-consistently using spectral theorem. Here, we will show our numerical results in different regimes of parameters, from the infinite  $U$  case to the finite  $U$  case.

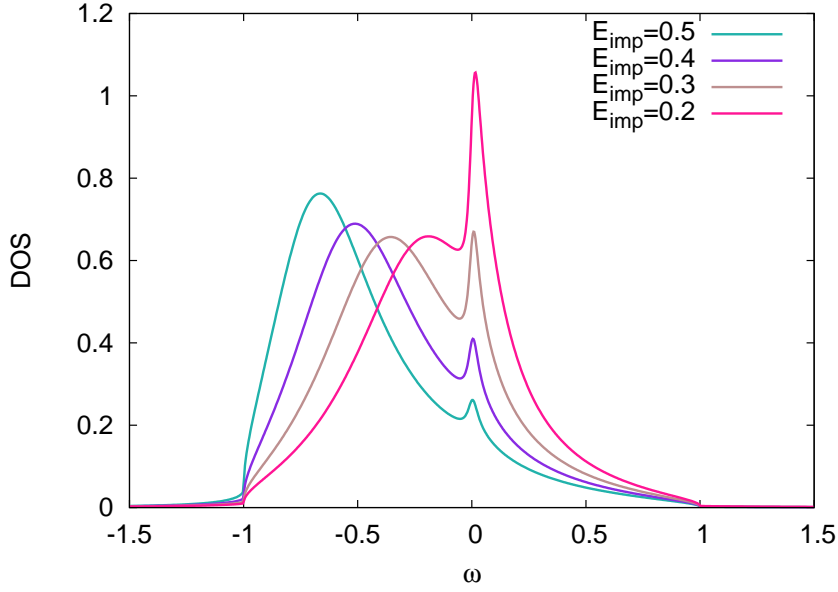


Figure 6.1: Density of states of correlated electrons for the single impurity Anderson model on the Bethe lattice with infinite Coulomb interaction strength  $U$  and temperature  $T = 0.01$ .

In Fig. 6.1, we have calculated the single impurity Anderson model on the Bethe lattice in the limit  $U \rightarrow \infty$ . The following parameters have been considered: The half bandwidth  $D = 2t$  is assumed to be 1, which defines the energy scale. The temperature is  $T = 0.01$ . We can see that, at low temperature, the density of states gives correct behavior in the Kondo limit, *i.e.* with a narrow Kondo peak at the Fermi level. It becomes more and more narrow, and will disappear when the chemical potential  $\mu$  becomes larger. This phenomenon can also be observed in the finite  $U$  cases.

We have also studied the finite  $U$  case. Fig. 6.2 shows the results at half-filling, where particle-hole symmetry is kept. In the figure, we can clearly see this phenomenon that the lower Hubbard band and upper Hubbard band are mirror symmetric. When the Coulomb interaction parameter  $U$  becomes larger, the two Hubbard bands go further away from the Fermi surface symmetrically and the Kondo peak becomes more and more narrow. Finally, the Kondo peak will disappear and the system will go from the metallic state to the insulating state. These results are calculated with the combination of genetic algorithm and iterative method. The bath used here is exactly of semicircle type (no tails, see Sect. 5.1.1).

In Fig. 6.3, we give a benchmark of the DOS of the single impurity Anderson model at half-filling obtained from our method against the results from the numerically exact NRG method from Ref. [98]. The comparison shows a main difference that within our EOM method the Kondo peak



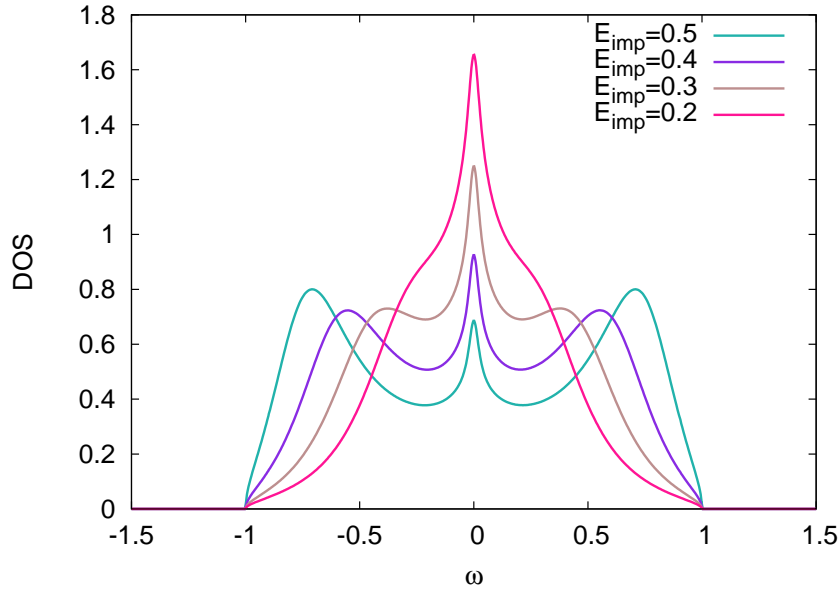


Figure 6.2: DOS of correlated electrons for the half-filled SIAM with finite Coulomb interaction strength  $U$  on the Bethe lattice (with the hybridization  $V = 0.253$  and temperature  $T = 0.01$ ).

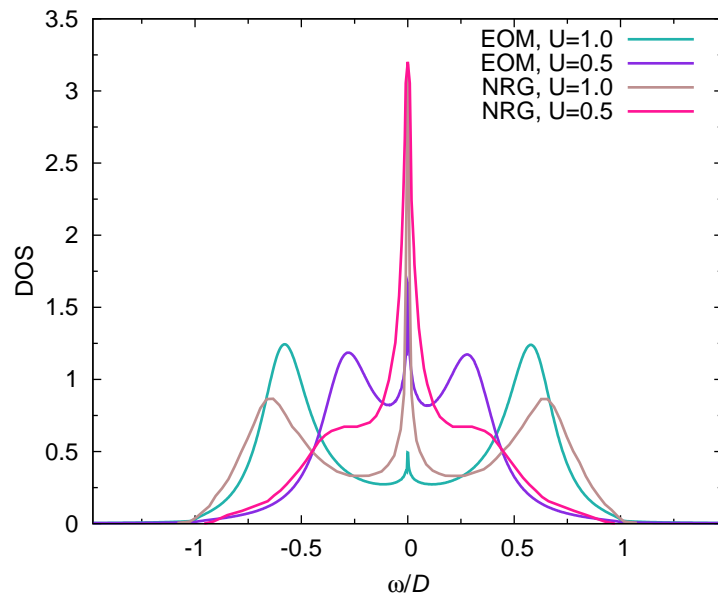


Figure 6.3: DOS of correlated electrons for the single impurity Anderson model on the Bethe lattice at half-filling with two different Coulomb interaction strengths  $U$  and at a temperature  $T = 0.0001$ , compared with the NRG results (taken from [98], with  $\Gamma = \pi V^2 = 0.1$ ).

is not pinned. According to Friedel's sum rule, the Kondo peak at the Fermi level should be fixed (pinned) at one value. One reason for this difference is that our result is calculated at finite temperature (zero temperature is not available for the GA method at present due to a numerical difficulty), while the NRG result is at zero temperature. Moreover, when the Kondo peak is too sharp, it's also difficult to approach in the GA method, because more populations and larger diversity will be needed. Besides the Kondo peak, the lower and upper Hubbard bands are also slightly different in shape and position. However, these differences have no important influence when distinguishing the Mott metal-insulator transition.

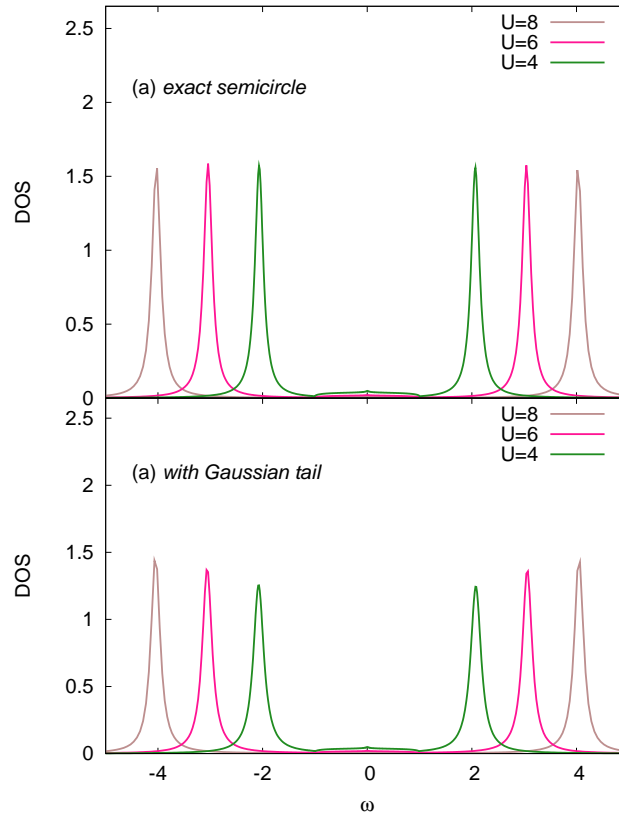


Figure 6.4: Dynamics at large frequency  $\omega$  for the finite  $U$  symmetrical SIAM on the Bethe lattice with broadening  $\eta = 0.1D$  ( $T=0.01$ ): a) the top figure is calculated with exact semicircular bath, b) the bottom figure is calculated with semicircular bath with a Gaussian broadening.

In Fig. 6.4 we show the dynamics in a wide range of frequencies for the half-filled system. For the exact semicircle, the height of the Hubbard band nearly changes only slightly for different  $U$  values. Although we obtain a similar behavior as in the DMRG result [99] when the bath has Gaussian tails, we do not accept "adding a tail" as a reasonable way to solve the equations, because

it has indeed changed the shape of the bath when adding a tail. In the LDA+DMFT calculation, it's also impossible to add a tail to the realistic DOS of electrons obtained from DFT calculations.

In Fig. 6.5 we have studied the SIAM at different temperatures. When the temperature goes to zero, the increasing sharpness of the Kondo peak, and the upper and lower Hubbard bands can be easily detected, indicating that our EOM method can work for any finite temperature.

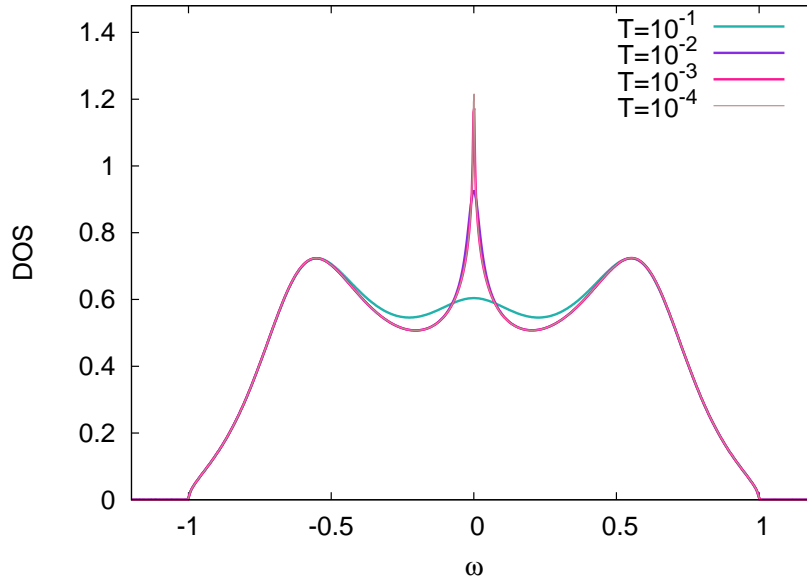


Figure 6.5: DOS of correlated electrons for the SIAM with finite Coulomb interaction strength  $U$ .

## 6.2 Hubbard model

The Hubbard model is the most commonly used and extensively studied lattice model for many-body systems in condensed matter physics. Due to the competition of the Coulomb interaction term and the hopping term, though the model is so simple, it has already given many nontrivial and interesting qualitative descriptions for strongly correlated systems.

In Fig. 6.6, we present the densities of states of correlated electrons for the infinite  $U$  Hubbard model at different impurity positions. When the impurity position approaches the Fermi surface, it gives a much stronger Kondo peak at the Fermi level and a decreased occupation number. From Fig. 6.7, we can clearly see the relation between the density of states and the chemical potential, where the density of states has been plotted as a function of chemical potential  $\mu = -E_{imp}$ . The points with plus signs (red color) are calculated at temperature  $T = 0.03$  and the points with crosses (green color) are for temperature  $T = 0.5$ . When the absolute value of the impurity position is

larger than half the bandwidth, i.e.  $E_{imp} < -D$ , the Kondo peak disappears at the Fermi level.

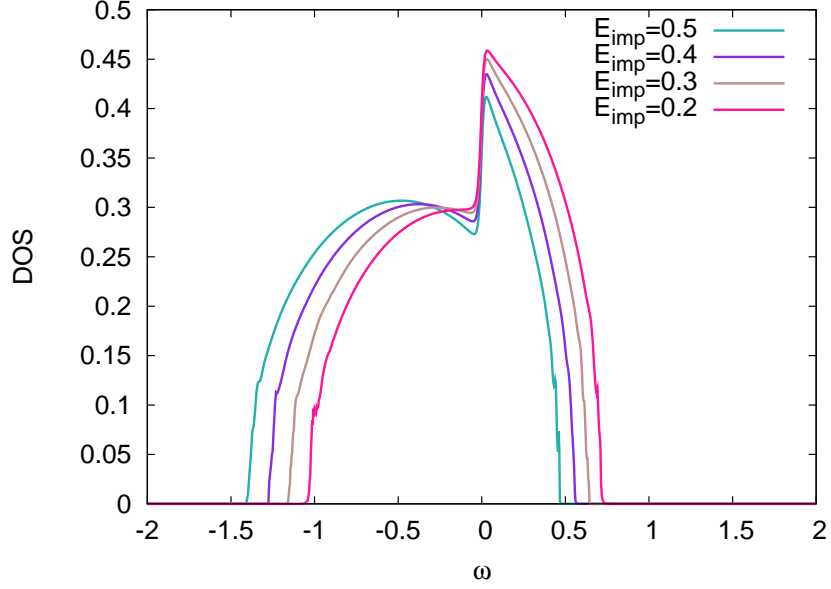


Figure 6.6: Density of states for infinite  $U$  Hubbard model at different impurity positions ( $T = 0.01$ ).

Moreover, we have investigated the band-width controlled Mott metal-insulator transition in the single band Hubbard model. The densities of states at four different values of  $U$  are shown in Fig. 6.8. As expected, the quasi-particle peak as well as the upper and lower Hubbard bands are present in the metallic phase, and transfer of spectral weight from the quasi-particle peak to the Hubbard bands is clearly evident by the reduction of the width of the central peak. In the insulating state, the central peak suddenly vanishes and a gap appears between upper and lower Hubbard bands. Further increasing  $U$  leads to an increasing gap amplitude. The critical value of  $U$  for the Mott transition obtained from our impurity solver is  $U_c \approx 2.5$ . Compared to the critical value from the numerical renormalization group method where  $U_c \approx 2.94$  [46], our result somewhat underestimates the critical value of  $U$  due to the decoupling scheme. We note that in the metallic region, the height of our obtained DOS at the Fermi level is not exactly fixed (no pinning). This is due to the fact that two peaks in the imaginary part of the self-energy are quite close to the Fermi level, resulting in a numerical difficulty in getting a vanishing value of the imaginary part of the self-energy at the Fermi level.

Next, we will study the filling controlled Mott metal-insulator transition in the Hubbard model. In Fig. 6.9, we present the DOS as a function of doping for two different values of  $U$ . It is found that the filling controlled metal-insulator transition occurs at  $U = 3$  while the system remains in

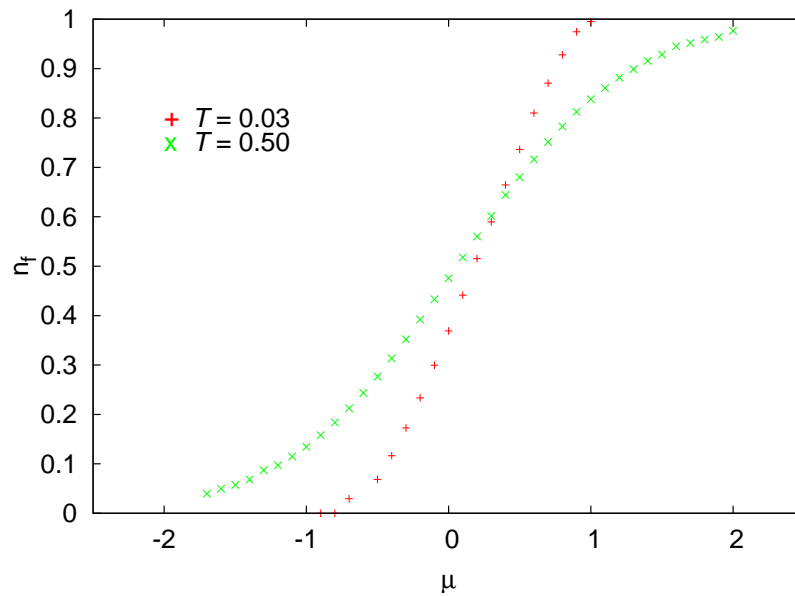


Figure 6.7: Occupation number of correlated electrons as a function of the chemical potential for the infinite  $U$  Hubbard model.

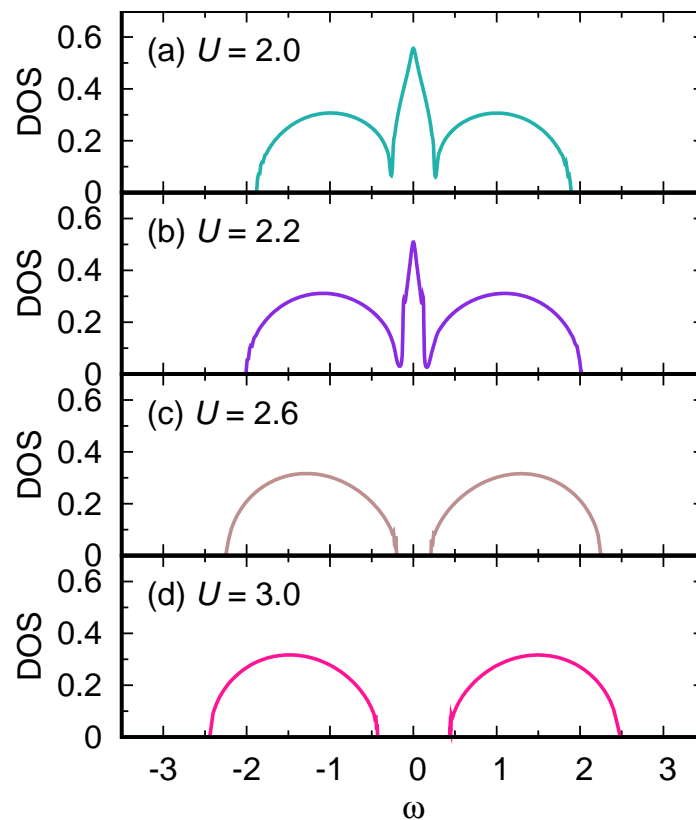


Figure 6.8: DOS calculated with GA method for particle-hole symmetric Hubbard model on the Bethe lattice.

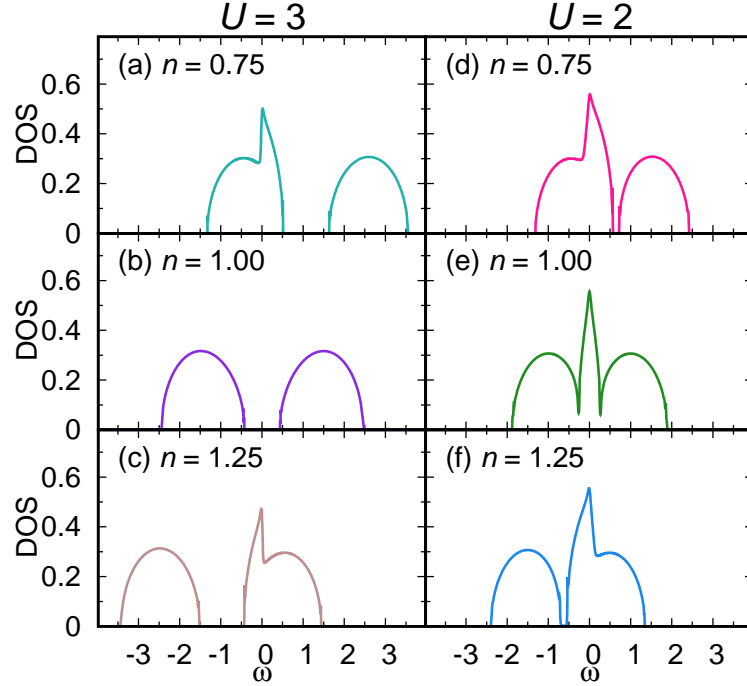


Figure 6.9: DOS for the asymmetrical Hubbard model on the Bethe lattice: filling controlled metal insulator transition.

the metallic state at  $U = 2$ . At  $U = 3$ , we also investigate the effective mass

$$\frac{m^*}{m} = 1 - \left. \frac{\partial \text{Re}\Sigma(\omega)}{\partial \omega} \right|_{\omega \rightarrow 0} \quad (6.1)$$

as a function of doping concentration. It is shown in Fig 6.10 that the effective mass clearly displays a divergent behavior as the doping concentration goes to zero, which seems to obey the Brinkman-Rice picture [101] for the Fermi liquid. In the small doping region, the carriers are easier to be localized. We also studied the metallic states for the Hubbard model, where Fermi liquid behavior should occur. We calculated the self-energies and densities of states for the symmetric Hubbard model on the Bethe lattice in Fig. 6.11. When  $U$  goes towards zero, the imaginary part of the self-energy decreases quickly, which can be seen clearly in the left figure of Fig. 6.11. For  $U = 0.9$ , the self-energy is very small. Hence, when  $U$  continues to approach zero, from the relation between the self-energy and the Green's function,

$$G^{-1}(\omega) = G_0^{-1}(\omega) - \Sigma(\omega) \quad (6.2)$$

one can conclude that the self-energy will give less and less contribution to the Green's function. Moreover, we investigated the low frequency behavior near the Fermi level for the metallic state

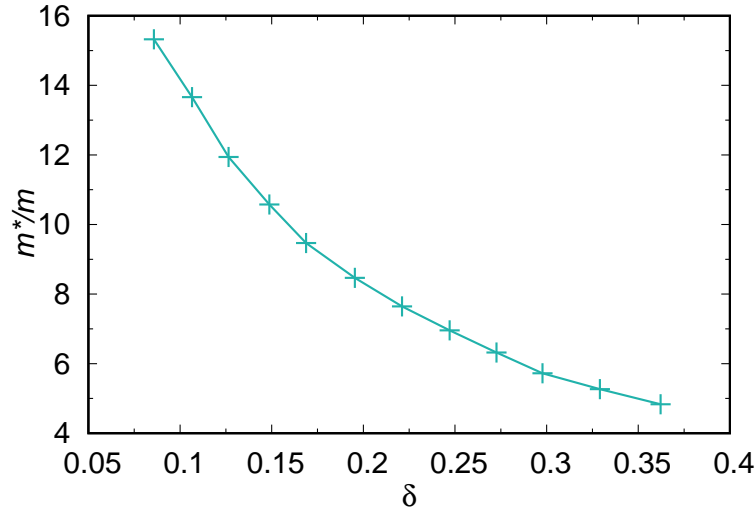


Figure 6.10: Effective mass at different fillings for the Hubbard model on the Bethe lattice.

at different temperatures in more detail, as shown in Fig. 6.12. We obtained that the imaginary part of the self-energy does not exactly follow Fermi liquid behavior under the present decoupling scheme. In the Figure, when the temperature approaches zero, the negative imaginary part of the self-energy decreases accordingly. We would expect that, when the temperature exactly goes to zero, the self-energy at the Fermi level should also be exactly zero, which is one of the phenomena of Fermi liquid behavior. However, the precision of the results at very low temperature is up to now numerically limited due to an instability of the numerical calculation. Therefore, the exact behavior of the imaginary part of the self-energy at the Fermi level at zero temperature is beyond our reach presently in our combined GA scheme. Considering that the equation-of-motion method is not a conserving method, depending on the decoupling scheme, only approximate Fermi liquid behavior can be achieved. Therefore, even though our decoupling scheme qualitatively shows an acceptable behavior, from principal considerations exact Fermi liquid behavior is not to be expected from a decoupling approach.

We have also studied the Hubbard model with different types of bath as shown in Fig. 6.13. The influence of the bath has often been considered to be small since the self-consistent solution will not depend much on the initial guess of the bath. Our result shows that both Bethe lattice and hypercubic lattice produce qualitatively similar results for the Mott transition. However, our results show that different baths yield different critical interaction strengths  $U_c$  at which the Mott transition sets in. For the Bethe lattice, we find  $U_c^{\text{Bethe}} \approx 2.5$ , while for the hypercubic lattice, the result is  $U_c^{\text{hypercubic}} \approx 2.4$ .

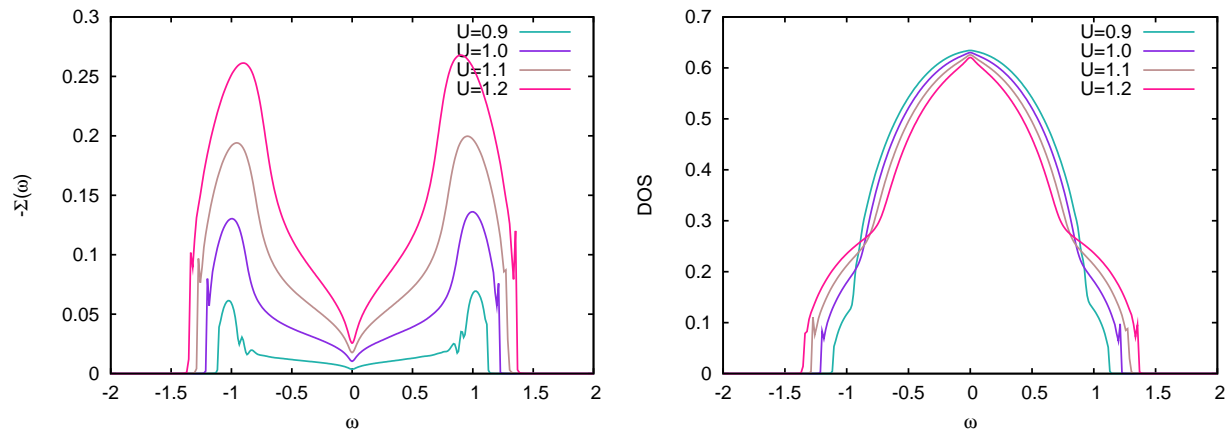


Figure 6.11: Self-energy and densities of states for the metallic state for the particle-hole symmetric Hubbard model on the Bethe lattice. The artifacts in the figure are caused by the numerical methods.

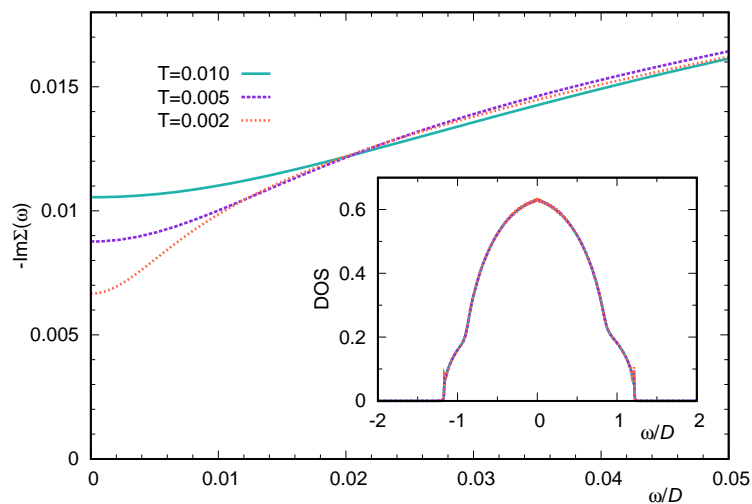


Figure 6.12: Self-energy at low temperature close to the Fermi level for the metallic state ( $U = 1$ ) for the particle-hole symmetric Hubbard model on the Bethe lattice. The inset shows the corresponding DOS.



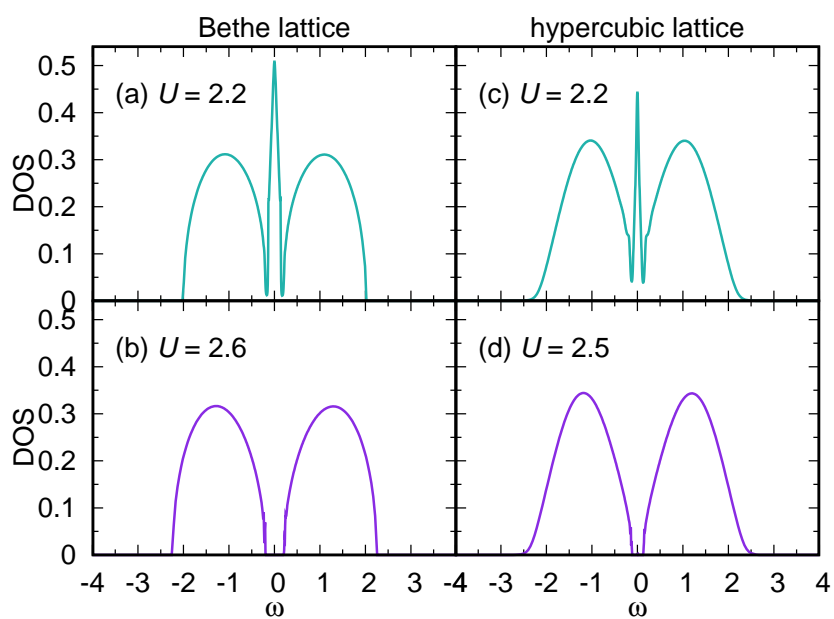


Figure 6.13: Comparison of DOS for the Hubbard model with different kinds of baths: (left) Semicircular bath on the Bethe lattice, (right) Gaussian bath on the hypercubic lattice. The top two figures are for the metallic state, the bottom two figures are for the insulating state just away from the metal-insulator transition point.

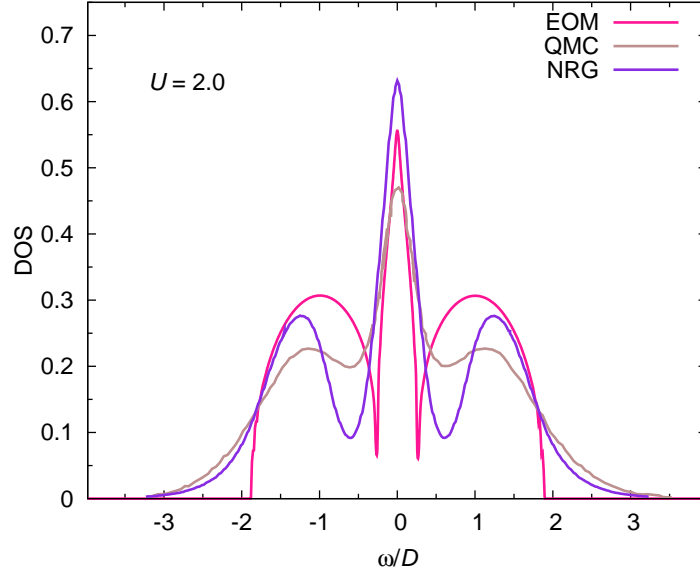


Figure 6.14: The DOS of the single band Hubbard model on the Bethe lattice in half-filled metallic states (the Coulomb interaction strength is  $U = 2$ ), compared with QMC (taken from Ref. [39]) and NRG results (taken from Ref. [100]).

We compare our method to the QMC and NRG methods for the Hubbard model at half-filling. The comparison is shown in Figs. 6.14 and 6.15. In Fig. 6.14, the system shows a metallic state at half-filling for  $U = 2$ . The three methods give very similar spectral functions. Please note that the parameters for each method are not exactly the same: the NRG result is obtained at zero temperature [100], the QMC result is calculated for finite temperature  $T = 0.14$  [39] while our EOM method gives the result at the temperature  $T = 0.01$ . The NRG method gives a pinned Kondo peak. The QMC method gives the result at finite temperature due to the difficulty of the calculation at low temperature. Comparing with these two numerically exact methods, our method yields a very good result. When the temperature approaches zero, the height of the Kondo peak in our EOM method increases, and is expected to approach the pinning point for exactly zero temperature. Moreover, it is clear that our result obtained with EOM and GA methods has removed the tails by setting the broadening  $\eta$  to zero. In Fig. 6.15, all three methods give half-filled insulating states, where the QMC method has shown an interesting feature, the shoulders at the edge of the Hubbard bands. In our EOM method, two very narrow peaks are observed at the edge of the Hubbard bands, which has been confirmed not to be artifacts, but actually exists in the EOM method (possibly generated by the higher order poles of the single particle Green's function).

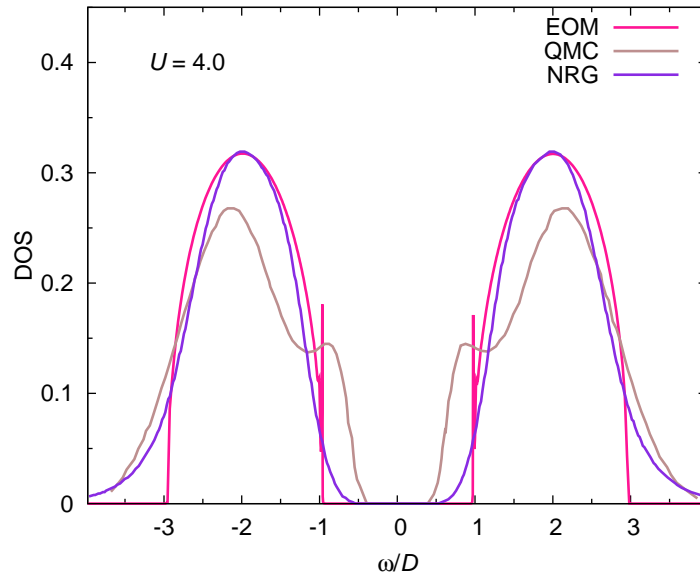


Figure 6.15: The DOS of the single band Hubbard model on the Bethe lattice in half-filled insulating states (the Coulomb interaction strength is  $U = 4$ ), compared with QMC (taken from Ref. [39]) and NRG results (taken from Ref. [100]).

We consider that due to the lack of higher order effects from the higher order terms (which have been truncated by the decoupling scheme), the two peaks are badly resolved.

For the Hubbard model with large degeneracy  $N$ , the result is shown in Fig. 6.16. At low temperature  $T = 0.01$ , the quasiparticle resonance at  $\omega = 0$  is clearly developed. The integrated weight of the Hubbard band up to the chemical potential is roughly proportional to  $1/N$ . At high temperature  $T = 0.1$ , we can see that it just begins to give a quasiparticle resonance at the Fermi level.

For the finite  $U$  Hubbard model with arbitrary degeneracy  $N$ , using the same code, we calculated the density of states  $\rho(\omega)$  of correlated electrons for the half-filling case with degeneracy  $N = 4$  on the Bethe lattice. The results are shown in Fig. 6.17. We can see that we obtain lower and upper Hubbard bands, while the two curves break the particle-hole symmetry, which is a solid rule for the half-filled finite  $U$  Hubbard model due to the  $SU(2)$  symmetry on the charge. However, though the particle-hole symmetry is broken, the result gives correct occupation numbers and band positions. On the other hand, we have also integrated the density of states on the full frequency range, and confirmed that the overall weight fulfills the sum rule. Therefore, we have considered that the result is essentially correct, but only misses a broadening on the upper Hubbard band.

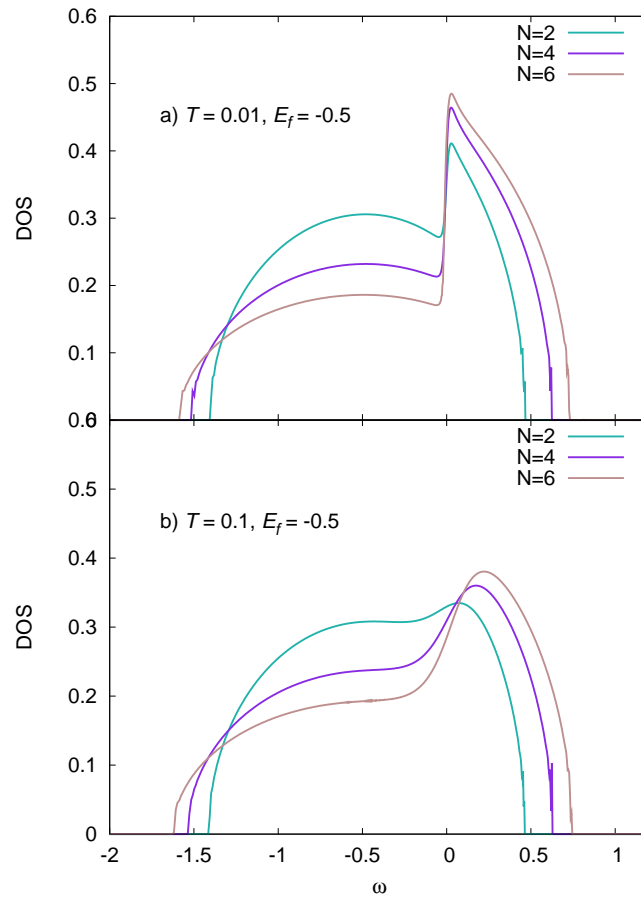


Figure 6.16: Density of states  $\rho(\omega)$  of correlated electrons for the infinite  $U$  Hubbard model at large degeneracy  $N$ .

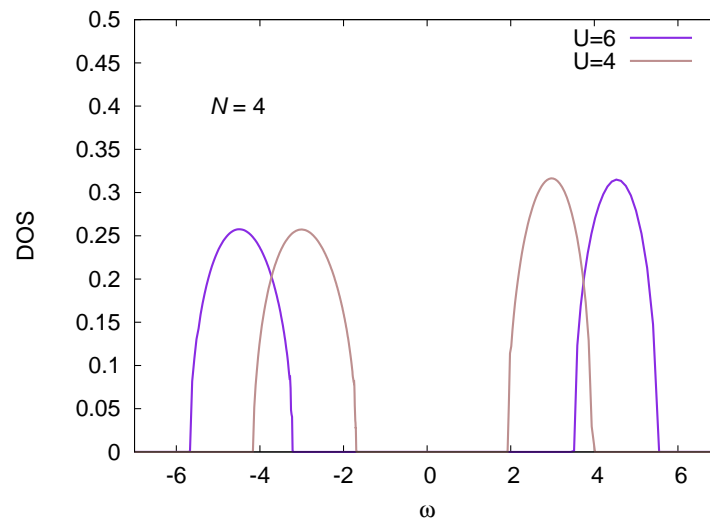


Figure 6.17: Density of states of correlated electrons for the finite  $U$  Hubbard model at half-filling for large degeneracy  $N = 4$  (uncorrect result, see the next for explanation).

In the equation-of-motion method, it can be understood why only the upper Hubbard band loses broadening. In the equation of motion of the single particle Green's function,

$$(\omega - \varepsilon_f - \Delta_1 - A(\Delta_2 \cdot I_1 + I_2))G_f = 1 + A\{\bar{n}_{\sigma'} + I_1\} \quad (6.3)$$

where

$$A = \frac{(N-1)U}{\omega - \varepsilon_f - U - (N-2)U\bar{n}_{\sigma''} - 2\Delta_2 - \tilde{\Delta}_2} \quad (6.4)$$

where we have written  $\Delta$  as  $\Delta_1$  and  $\Delta_2$  according to their origins (still,  $\Delta \equiv \Delta_1 \equiv \Delta_2$  in the calculation). The  $\Delta_1$  is responsible for the major part of the broadening to the lower Hubbard band. This hybridization function is not approximation because it appears in the equation of motion

$$(\omega - \varepsilon_f - \Delta)G_f = 1 + (N-1)UG_{nf} \quad (6.5)$$

and is not coming from the decoupling scheme, while the  $\Delta_2$  and  $\tilde{\Delta}_2$  in the denominator of Eq. (6.4) are responsible for broadening the upper Hubbard band, and they are coming from the details of the decoupling scheme. In that procedure, we have replaced the higher order Green's functions by lower order Green's functions and correlations. Hence, the hybridization function  $\Delta_2$ , though having the same form  $\sum_k \frac{V_k^2}{\omega - \varepsilon_k}$  with  $\Delta_1$  in present decoupling, is actually different from  $\Delta_1$ . The exact form of  $\Delta_2$  (written as  $\Delta_{II}$ ) should be

$$\Delta_{II} = \sum_k \frac{V^2}{\omega - \varepsilon_k - A(\omega, k)}, \quad (6.6)$$

where  $A(\omega, k)$  is an unknown term contributed by the higher order Green's functions. Therefore,  $\Delta_2$  and  $\tilde{\Delta}_2$  act only as the approximations to the exact terms  $\Delta_{II}$  and  $\tilde{\Delta}_{II}$ . Moreover, the prefactors of the  $\Delta_2$  and  $\tilde{\Delta}_2$  are determined by the specific approximations of the decoupling scheme. From the view point of particle-hole symmetry, for the half filled system, the lower Hubbard band will be mirror symmetric to the upper Hubbard band. Therefore, we considered that some broadening of the upper Hubbard band is missing and the asymmetry in Fig. 6.17 is just a systematical error caused by the truncation of the decoupling scheme in the equation-of-motion method.

For  $N = 2$ , the decoupling works well. For larger  $N$ , the particle-hole symmetry is broken. Therefore, we think this missing broadening may be coming from the higher order Green's functions (that do not play a role for  $N = 2$ ). If this is true, the decoupling of the higher order Green's function is not good enough. For the large  $N$  system, the decoupling may have grown worse and

brought us less broadening, effectively destroying the particle-hole symmetry. Of course, another possible reason is that the small terms we have neglected in the  $N = 2$  case, have made more contributions and are not negligible any more, *i.e.* the validity of this decoupling scheme for the Green's functions may differ for different degeneracy  $N$ .

In the consideration of some missing broadening, we have tried to add an *ansatz* to compensate for the missing parts which have been cut and thrown away by the decoupling scheme. In the future, our study of the decoupling schemes may yield insight as to the source of these additional broadenings. Theoretically, this *ansatz* will not change the filling, band position and all other physical observations, but only recover the destroyed particle-hole symmetry for the half-filled system. Numerically, it will depend on how close this *ansatz* is to the deviation of the present kept terms far from the exact self-energy. In principle, this *ansatz* should be a function of  $(\omega, \varepsilon_f, U, N, \Delta, \tilde{\Delta})$ , *i.e.*

$$F(\omega, \varepsilon_f, U, N, \Delta, \tilde{\Delta}) = f(\omega, \varepsilon_f, U, N)\psi(\Delta, \tilde{\Delta}) \quad (6.7)$$

where the first function  $f(\omega, \varepsilon_f, U, N)$  corresponds to the higher order expansion of equations of motion with the increasing power of  $U, N$ . The second function  $\psi(\Delta, \tilde{\Delta})$  corresponds to the presence of  $V^2, V^4, V^6, \dots$ . Therefore, it can be written as a function of  $\Delta, \tilde{\Delta}$ .

This *ansatz* should be determined numerically before we can find the right explanation with analytical methods. We found that the *ansatz* can be taken as

$$F = -C(N - 2)\Delta \quad (6.8)$$

which will be added to the denominator of  $A$  in Eq. (6.4) so that  $A$  turns to be

$$A = \frac{(N - 1)U}{\omega - \varepsilon_f - U - (N - 2)U\bar{n}_{\sigma\sigma} - 2\Delta_2 - \tilde{\Delta}_2 - C(N - 2)\Delta}. \quad (6.9)$$

$C$  is numerically determined as 0.5. Including this *ansatz* into our code, we have found it works uniformly for  $N = (4, 6, 8, \dots)$ . Hence, we updated the results as Fig. 6.18.

In Fig. 6.18, we show the densities of states of correlated electrons for the half-filled Hubbard model on the Bethe lattice in the large  $U$  area. We can see that, with the increase of degeneracy  $N$ , the Hubbard bands move away from the Fermi surface symmetrically. At the same time, the Hubbard bands become lower and wider. This behavior can be well explained physically. For the half-filling case, the total number of electrons will increase with an increase of the degeneracy. Due to the existence of the Coulomb interaction, the total Coulomb interaction will accordingly

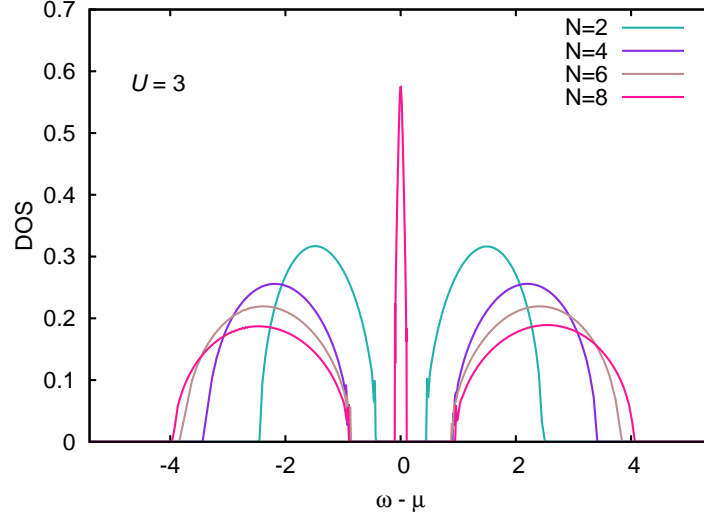


Figure 6.18: Comparison of DOS for Hubbard model at half-filling with different degeneracy  $N$  for large Coulomb interaction strength  $U$  (compared to Fig. 6.19).  $\mu$  is the chemical potential.

increase. Hence, the gap between the two Hubbard bands will become wider, *i.e.* the two Hubbard bands shift further away from the Fermi surface for larger  $N$  systems. However, the critical  $U_c$  also increases with  $N$ . Therefore, at the same  $U$ , the system shows more metallicity for larger  $N$ . The transfer of spectral weight is observed from upper and lower Hubbard bands to the Kondo peak when  $N$  increases. In this sense, we can say, in larger  $N$  systems, the hopping is enhanced for the one particle doped state so that the quasi-particle peak becomes dominant for large degeneracy  $N$  because more weight of the charge excitation peaks is transferred to the quasi-particle peak. This property also appears clearly in the small  $U$  region (with  $U$  still much larger than the kinetic energy), which is shown in Fig. 6.19. Here, the x-axis is  $\omega - \mu$ . For large  $N$  spin-orbit degenerate systems, the existing Coulomb interaction between electrons will increase the repulsive potential of the system along with the increase of  $N$ . Therefore, to approach the half occupied state of all possible orbitals, increasing chemical potentials for increasing  $N$  are required. Hence, the Fermi energy will vary at half-filling for different  $N$  systems.

Besides the symmetrical half-filling cases, we have also studied the asymmetrical Hubbard model with the same  $U$  values and the same impurity position at different degeneracies  $N$ . The results are shown in Fig. 6.20. With increasing  $N$ , the lower Hubbard band behaves like in the infinite  $U$  case. The weight of the lower Hubbard band decreases. At the same time, the band position of the upper Hubbard band moves further away from the Fermi level, and the upper Hubbard band carries more spectral weight than the lower Hubbard band.

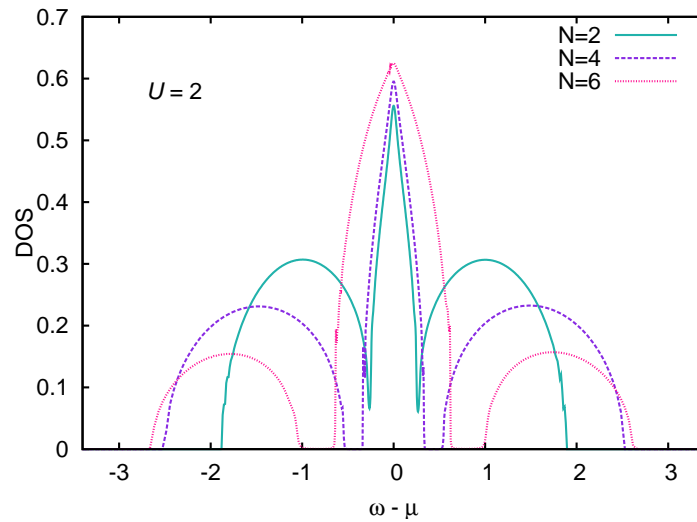


Figure 6.19: Comparison of DOS for Hubbard model at half-filling with different degeneracy  $N$  for small Coulomb interaction strength  $U$  (compared to Fig. 6.18).  $\mu$  is the chemical potential.

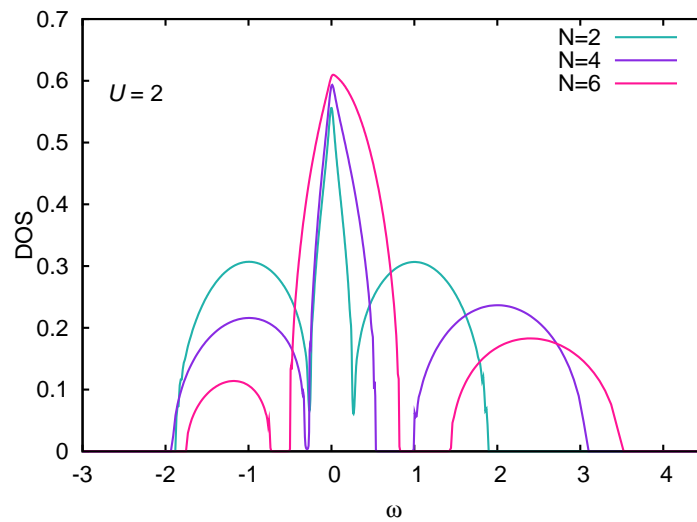


Figure 6.20: Comparison of DOS for asymmetric Hubbard model with different degeneracy  $N$  at fixed impurity position.



### 6.3 Periodic Anderson model

In this Section, we will present the results calculated for the single correlated band periodic Anderson model. The periodic Anderson model has been extensively studied before, *e.g.* [102, 103, 104, 105]. Here, we have studied the paramagnetic phase of the periodic Anderson model within the dynamical mean field theory at low temperature  $T$ . Our numerical results from the equation-of-motion method are consistent with those from other numerical methods such as QMC, confirming the reliability of our method so that it can be used in further research.

In the following, we will call the correlated electrons of the PAM  $f$  electrons even though they could also be from a narrow  $d$  band; conduction electrons (also called uncorrelated electrons) are sometimes called  $c$  electrons. The corresponding band position are called  $E_f$  and  $E_c$ , respectively. When  $U$  goes to infinity, there is only the lower Hubbard band left. In Fig. 6.21, we have plotted the densities of states of correlated electrons and conduction electrons at various impurity band positions. In the left panel, the center of the conduction band is at the Fermi level. In the right panel, the center of the conduction band is at  $E_c = 0.5$ . The hybridization strength we have used in the calculations is  $V = 0.4$ . We can clearly see that the Kondo peak appears at the Fermi level. When the impurity position goes towards the Fermi surface, the Kondo peak becomes larger in both width and height. The weight of the lower Hubbard band up to the Fermi surface is decreasing with the increase of the band energy of correlated electrons. At the same time, in the conduction band a dip appears at the Fermi level, which is connected to the presence of the Kondo peak in the  $f$  DOS. When the Kondo peak in the  $f$  DOS increases, the dip becomes stronger. Moreover, in the conduction band, a satellite appears at the position of the  $f$  band, which is a result of the hybridization term in the Hamiltonian. From the definition of the Green's function and all the Figures of  $f$  DOS shown above, we can see that the  $f$  band is not exactly at  $E_f$ , but is shifted and broadened. When the band position is at  $-\infty$ , there is no interaction between the  $f$  band and the conduction band. If the  $f$  band position moves towards the Fermi level, as soon as the  $f$  band is close enough to the conduction band, hybridization between  $f$  band and conduction band sets in (i.e. the two bands start to overlap), and satellites appear due to the hybridization. When they come closer, these satellites become stronger. On the other hand, when the center of the conduction band  $E_c$  is above the Fermi energy, the weight of the  $f$  band will also shift in the direction towards the  $E_c$  position.

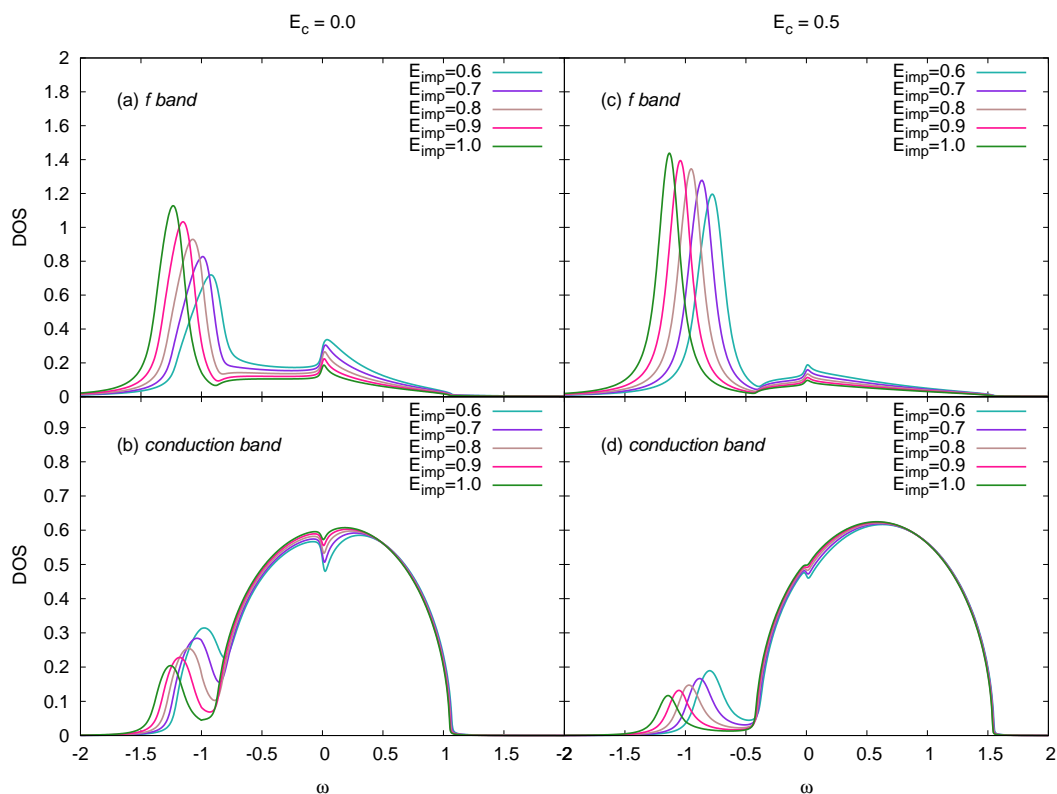


Figure 6.21: Comparison of DOS for the periodic Anderson model in the limit of the Coulomb interaction strength  $U \rightarrow \infty$  for different impurity positions: (left) for the conduction band centered at  $E_c = 0.0$ , (right) for the conduction band centered at  $E_c = 0.5$ . The top two figures are DOS of the  $f$  band, the bottom two figures are DOS of the conduction band (The hybridization strength is  $V = 0.4$ ).

In Fig. 6.22, we present the changes of the densities of states of correlated electrons and conduction electrons according to the changes of the hybridization factor  $V$ . The results are calculated with the parameters  $E_f = -0.6$  and  $U \rightarrow \infty$ . For  $V = 0.1$ , there is almost no Kondo peak at the Fermi level. When the hybridization becomes stronger, the Kondo peak appears at the Fermi level and the  $f$  band shows obvious changes: the  $f$  band position moves further away from the Fermi level; the quasiparticle weight of the Kondo peak is strengthened so that the weight of the  $f$  band up to the Fermi level becomes less. Therefore, we can conclude that the increase of the hybridization  $V$  not only shows up in the increasing amplitude but also leads to the enlargement of the region where hybridization plays a role (we will call this region overlap region). When the hybridization is large, the system has a larger overlap region. Therefore, both the impurity position and the hybridization strength determine the occurrence of the hybridization. The change of the Kondo peak is not linear in the change of the hybridization: when  $V$  changes from 0.4 to 0.6, the Kondo peak is not strengthened, but becomes weaker; at the same time, a feature appears near  $\omega = 0.4$  (it is not the upper Hubbard band because  $U$  is infinity). The origin of this feature is still not clear. One possible reason is that,  $V = 0.6$  is so large that a very strong hybridization between  $f$  band and conduction band occurs, which has caused an unconventional change of the weight of the  $f$  band. From the view point of scattering, a central collision can lead to the back scattering and the momentum and energy of electrons will change greatly, which may relate to this exotic change of the  $f$  DOS. Moreover, the shift of the conduction band shows similar behavior as we have discussed in Fig. 6.21: the hybridization strength between the  $f$  band and the conduction band decreases when the center of the conduction band moves further away from the Fermi level.

In Fig. 6.23, we show the density of states of correlated electrons at finite  $U$  in the half-filled cases ( $U + 2E_f = 0$ ). The lower Hubbard band shows similar behaviors as in the infinite  $U$  case: when the  $f$  band position moves closer to the center of the conduction band (*i.e.*  $U$  approaches zero), the height of the Kondo peak increases and the dip in the conduction band becomes stronger. At the same time, the upper Hubbard band and lower Hubbard band show particle-hole symmetry. When the center of conduction band is not at the Fermi level, the  $f$  band still keeps particle-hole symmetry, but the conduction band gives an asymmetrical density of states.

In Fig. 6.24 we show the density of states for the half-filled case in a wide range of  $U$ . In order to avoid the difficulty that the upper Hubbard bands at high frequency for large  $U$  parameters are too thin to be seen, we have used a broadening of  $\eta = 0.1$  in calculating the results shown in this

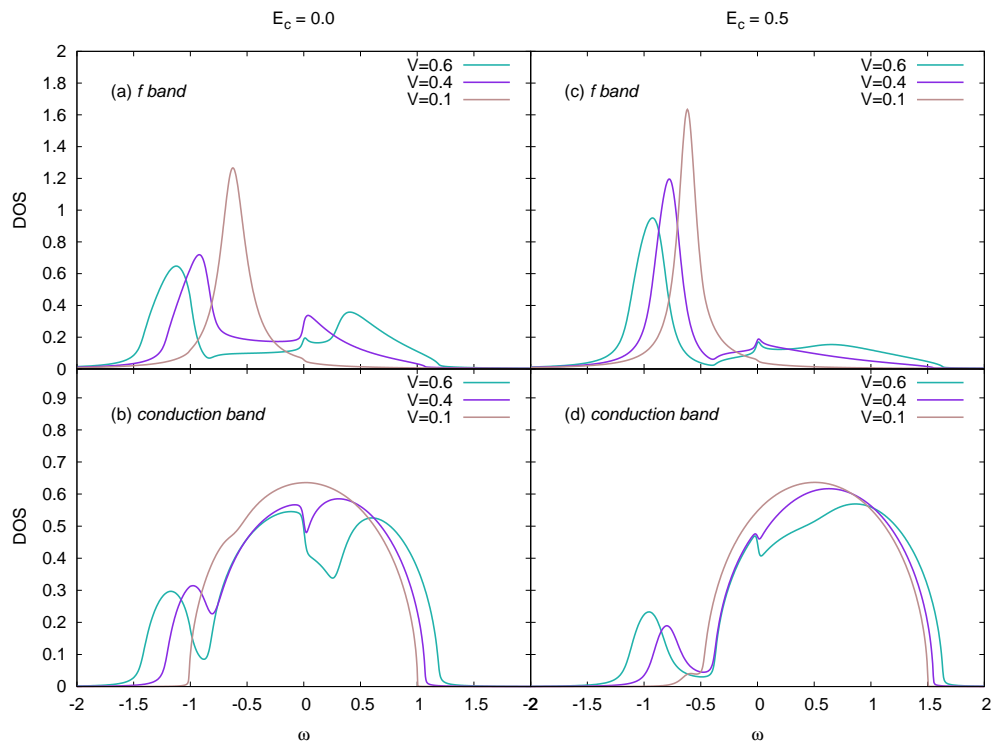


Figure 6.22: Comparison of DOS for the periodic Anderson model in the limit of the Coulomb interaction strength  $U \rightarrow \infty$  for different hybridization parameters  $V$ : (left) for the conduction band centered at  $E_c = 0.0$ , (right) for the conduction band centered at  $E_c = 0.5$ . The top two figures are DOS of the  $f$  band, the bottom two figures are DOS of the conduction band ( $f$  band position  $E_f = -0.6$ ).

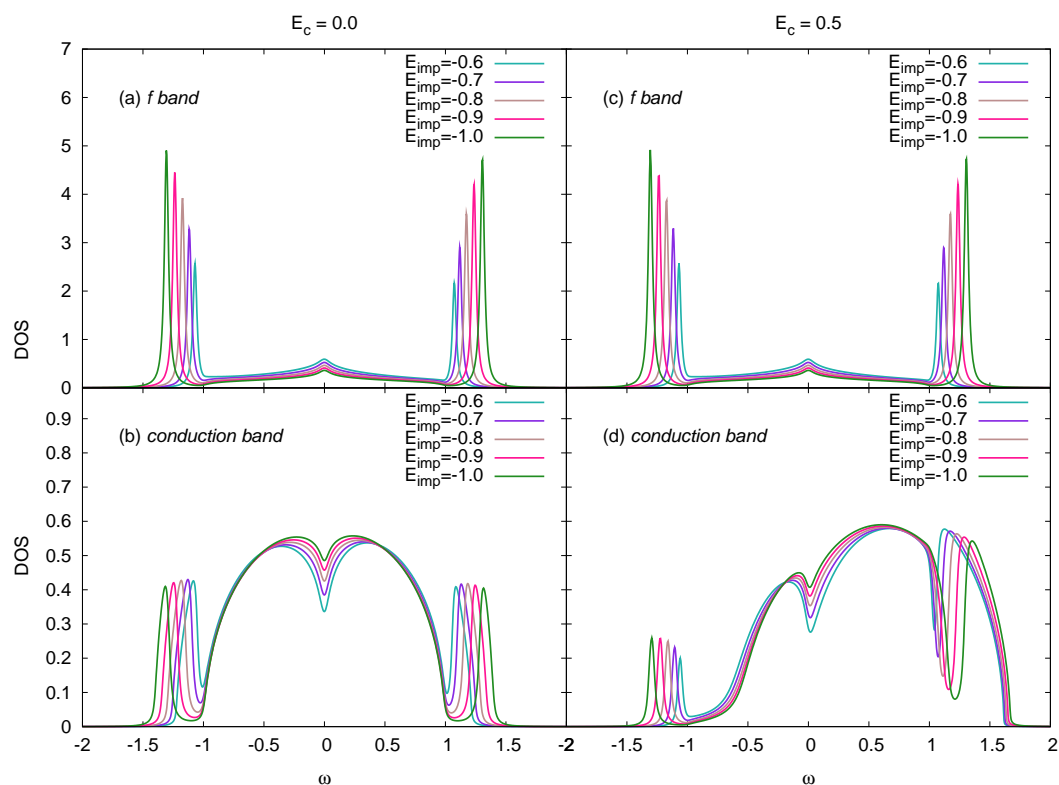


Figure 6.23: Comparison of DOS for the periodic Anderson model for finite Coulomb interaction strength at different impurity positions: (left) for the conduction band centered at  $E_c = 0.0$ , (right) for the conduction band centered at  $E_c = 0.5$ . The top two figures are DOS of the  $f$  band, the bottom two figures are DOS of the conduction band (with the hybridization strength  $V = 0.4$ ).

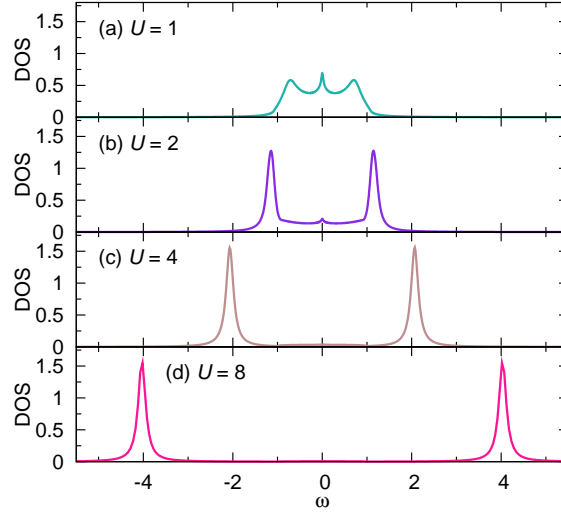


Figure 6.24: Density of states of correlated electrons for the periodic Anderson model for different values of Coulomb interaction strength  $U$ .

figure. For  $U = 1$ , there is an obvious Kondo peak at the Fermi level. Then for  $U = 2$ , the Kondo peak becomes weak. For  $U = 4$ , the Kondo peak completely disappears and the system changes from the metallic state to the insulating state. The Mott metal-insulator transition occurs.

Here, we also studied the periodic Anderson model with large spin and orbital degeneracy  $N$ . The *ansatz* determined for the Hubbard model, see Eq. (6.8), also works well for the periodic Anderson model. In Fig. 6.25, we show the densities of states of correlated electrons and conduction electrons for large spin and orbital degeneracy ( $N = 2, 4, 6$ ). For the half-filled case, the particle-hole symmetry is well preserved. The conduction band also has a symmetrical distribution. For larger  $N$ , it shows clearly much stronger scattering than in the small  $N$  case so that a heavier Kondo peak is observed along with the increase of the value of  $N$ . At the same time, the  $f$  bands and the corresponding satellites in the conduction band are pushed away from the Fermi surface. From the results, we can draw the conclusion that, for larger  $N$ , there will be a larger critical value of  $U$ .

When the center of the conduction band is not at the Fermi level, as shown in Fig. 6.26, though the filling of the  $f$  band stays the same, the particle-hole symmetry is broken. Comparing with Fig. 6.25, for the same  $N$ , the effective hybridization strength becomes weaker due to the increase of the distance between  $f$  band and conduction band.

Fig. 6.27 shows the densities of states for different spin and orbital degeneracy  $N$  for the same band positions. In the figure, the case of  $N = 2$  is at half-filling, while the occupation numbers for

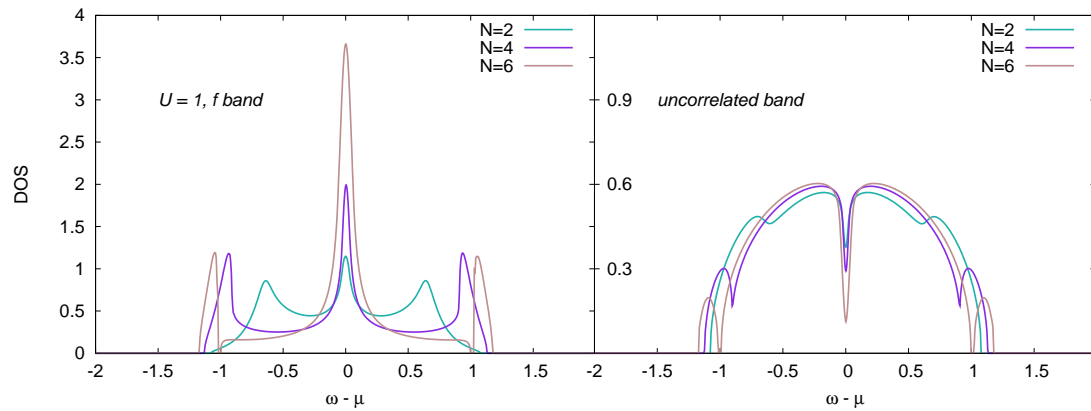


Figure 6.25: DOS for the periodic Anderson model for different degeneracies  $N$  at half-filling (with the conduction band centered at  $E_c = 0.0$ ).

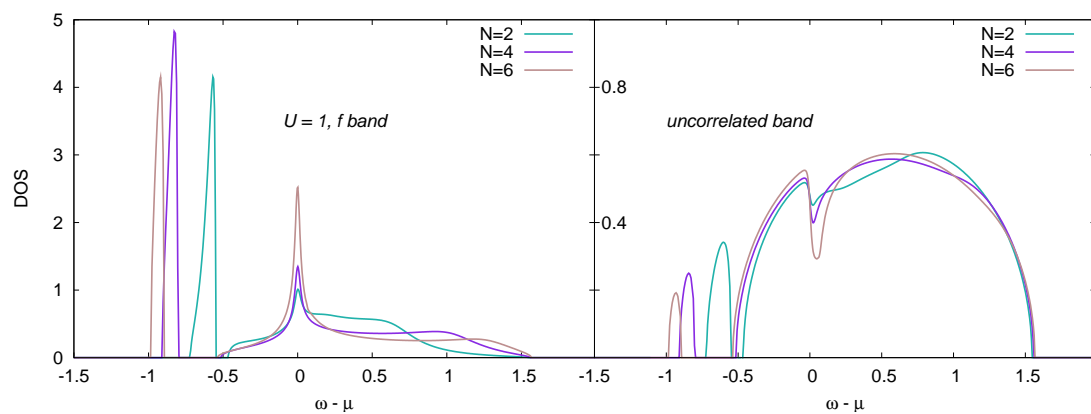


Figure 6.26: DOS for periodic Anderson model for different degeneracies  $N$  at half-filling (with the conduction band centered at  $E_c = 0.5$ ).

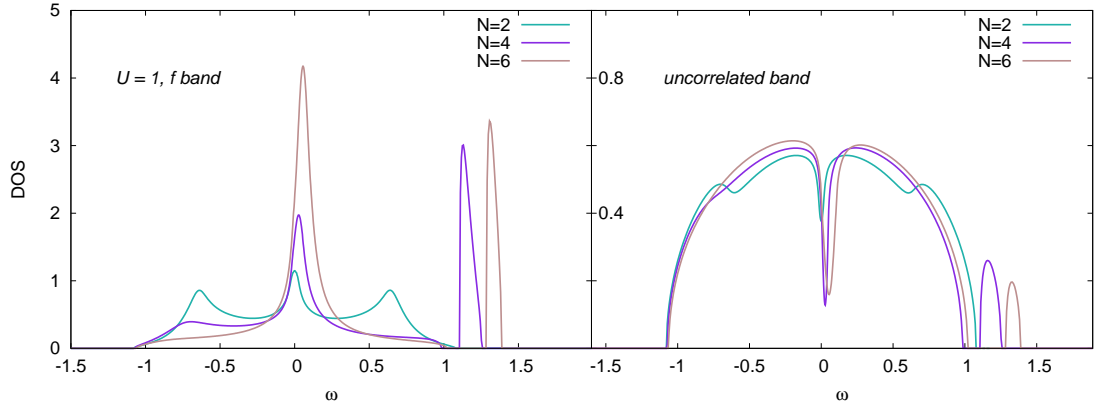


Figure 6.27: DOS for the periodic Anderson model for different degeneracies  $N$  (with band positions at:  $E_f = -0.5, E_c = 0.0$ ).

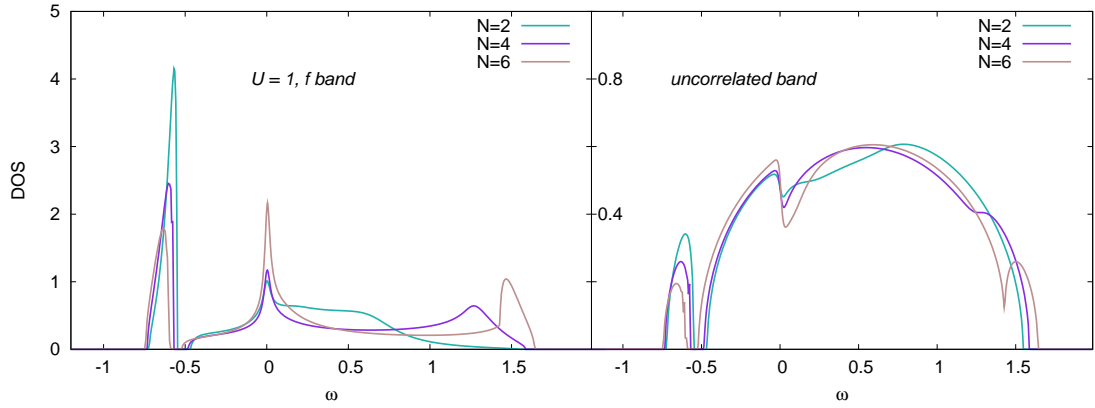


Figure 6.28: DOS for the periodic Anderson model for different degeneracies  $N$  (with band positions at:  $E_f = -0.5, E_c = 0.5$ ).

$N = 4, 6$  are below the half-filled system due to the increase of the effective Coulomb interaction strength when  $N$  increases. Fig. 6.28 correspondingly shows the densities of states of correlated electrons and conduction electrons for large  $N$  systems at the same impurity position, but the center of the conduction band is not at the Fermi level.

## 6.4 Multi-band system

In this section, we will calculate and show the results of those systems that have orbital degrees of freedom, *i.e.* the multi-band Hubbard model. We will mainly study the simplest case, a two-band system, see Chap. 4. We will first present the simple and special cases, then proceed to more general parameters step by step.



### 6.4.1 Two-band Hubbard model

Here, we study the densities of states of the two-band Hubbard model for various Coulomb interaction strengths and hybridization strengths. The dependence of the parameters is shown in Eq. (4.1) and Eq. (4.29). The  $d$  and  $f$  are just symbols labelling the two bands.

$$a) U' = U'' = 0, V_d = 0 \text{ or } V_f = 0 \text{ (not both)}$$

When parameters  $U' = U'' = 0$ , it means that there is no inter-band Coulomb interaction. If in the Hamiltonian the hybridization  $V_f = 0$ , the Hamiltonian returns to the single band Hamiltonian for the " $d$ " band. Hence, the  $d$  band single electron Green's function should also return to the single band result. It's similar for the " $f$ " band when  $V_d = 0$  in the Hamiltonian. In the approximation without inter-band hybridization, we have considered  $\Delta_{df} = 0$ . By setting  $U' = U'' = 0$ , we successfully reproduced the single band result ( $N = 2$ ). This means that our multi-band code can easily return to the single band result by changing only the parameters.

$$b) U = U' = U'' = 0 \text{ (conduction electron limit)}$$

For this set of parameters, the Hamiltonian is

$$\mathcal{H} = \sum_{k\tau\sigma} \varepsilon_k c_{k\tau\sigma}^\dagger + \varepsilon_f \sum_{\tau\sigma} \hat{n}_{\tau\sigma} + \sum_{k\tau\sigma} (V_{k\tau}^* c_{k\tau\sigma}^\dagger f_{\tau\sigma} + V_{k\tau} f_{\tau\sigma}^* c_{k\tau\sigma}) \quad (6.10)$$

i.e. there is no Coulomb interaction between electrons and the two local bands only interact with each other through the bath. For this case, we can get the exact analytical solution that

$$G_d = \frac{1 + \frac{\Delta_{df}}{\omega - \varepsilon_f - \Delta_{ff}}}{\omega - \varepsilon_d - \Delta_{dd} - \frac{\Delta_{df}^2}{\omega - \varepsilon_f - \Delta_{ff}}} \quad (6.11)$$

$$G_f = \frac{1 + \frac{\Delta_{df}}{\omega - \varepsilon_d - \Delta_{dd}}}{\omega - \varepsilon_f - \Delta_{ff} - \frac{\Delta_{df}^2}{\omega - \varepsilon_d - \Delta_{dd}}} \quad (6.12)$$

which will give a two-peak structure if  $\varepsilon_d \neq \varepsilon_f$ , but completely different from the splitting of band in strong correlation systems.

In the approximation without inter-band hybridization, such parameters will give a trivial case

$$G_d = \frac{1}{\omega - \varepsilon_d - \Delta_{dd}}$$

$$G_f = \frac{1}{\omega - \varepsilon_f - \Delta_{ff}}$$

where the two bands are completely independent. For each band, it's just like the mean field

approximation of the single band system, giving only a shift to the peak of the local Green's function  $G_0(\omega)$ .

$$c) U' = U'' \ll U$$

In this case, assuming  $U' = U'' \approx 0$ , the Hamiltonian can be approximately written as

$$\mathcal{H} = \varepsilon_k c_{k\sigma}^\dagger c_{k\sigma} + \sum_{\tau\sigma} \varepsilon_\tau d_{\tau\sigma}^\dagger d_{\tau\sigma} + \frac{1}{2} \sum_{\tau\sigma\sigma'} U_\tau \hat{n}_{\tau\sigma} \hat{n}_{\tau\sigma'} + \sum_{\tau\sigma} (V_{\tau k}^* c_{k\sigma}^\dagger d_{\tau\sigma} + V_{\tau k} d_{\tau\sigma}^\dagger c_{k\sigma}) \quad (6.13)$$

Then the equations of motion will be

$$(\omega - \varepsilon_d) G_d = 1 + U G_{nd} + \sum_k v_{dk} G_c \quad (6.14)$$

$$(\omega - \varepsilon_k) G_c = V_{dk} G_d + V_{fk} G_f \quad (6.15)$$

$$(\omega - \varepsilon_d - U) G_{nd} = \bar{n}_{d\sigma'} + \sum_k (V_{dk} G_{nc} + V_{dk} G_{cdc} - V_{dk}^* G_{cdd}) \quad (6.16)$$

Finally we will obtain the single particle Green's function

$$G_d = \frac{1 + \frac{U}{\omega - \varepsilon_d - U - 2\Delta_{dd} - \bar{\Delta}_{dd} - 2\Delta_{df} - \bar{\Delta}_{df}} (\bar{n}_{d\sigma'} + \sum_k (\frac{V_{dk} \langle d_{\sigma'}^\dagger c_{k\sigma'} \rangle}{\omega - \varepsilon_k} - \frac{V_{dk} \langle d_{\sigma'}^\dagger c_{k\sigma'} \rangle}{\omega + \varepsilon_k - 2\varepsilon_d - U})}{\omega - \varepsilon_d - \Delta_{dd}} \quad (6.17)$$

$$c) U = U' = U''$$

This  $U = U' = U''$  is a slightly unrealistic case. Commonly, due to the Hund's rule coupling  $J$ , there is the relation  $U = U' + 2J$  and  $U'' = U' - J$ . We first study this simplified case because it's easier to compare with the single band system with spin and orbital degeneracy  $N$ . Using the approximation without inter-band hybridization, we got the following results. The first one shows the densities of states of the two bands with identical band energy  $E_d = E_f$ .

From Fig. 6.29, we can see that it is an insulator (half-filling) in the left panel. The right panel is a metallic state and a Kondo peak appears at the Fermi level. For a case with the two local bands at different band energy  $E_d \neq E_f$ , the densities of states of each band are shown in Fig. 6.30. The interesting thing is that one band is in the insulating state, while another one is in the metallic state.

$$e) U > U' = U''$$

In this case, the intraband Coulomb interaction strength  $U$  is different from the inter-band Coulomb interaction strength  $U', U''$ , where the inter-band Coulomb interaction is spin degenerated. This case locates in an intermediate parameter regime from the fully degenerated Coulomb

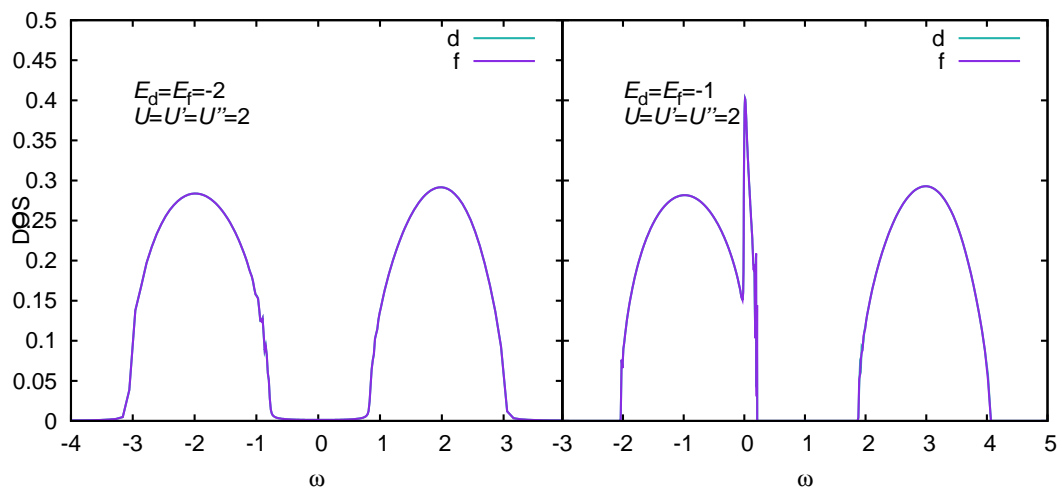


Figure 6.29: Densities of states for a two-band system with uniform Coulomb interaction strength, where the two bands have identical band energy.

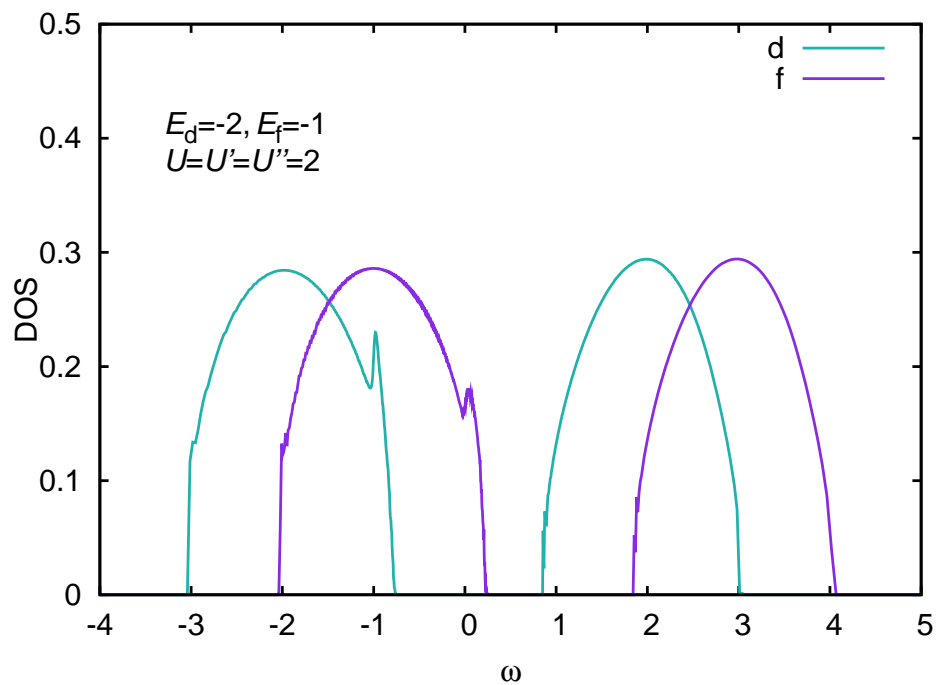


Figure 6.30: Densities of states for a two-band system with uniform Coulomb interaction strength, where the two bands have different band energies.

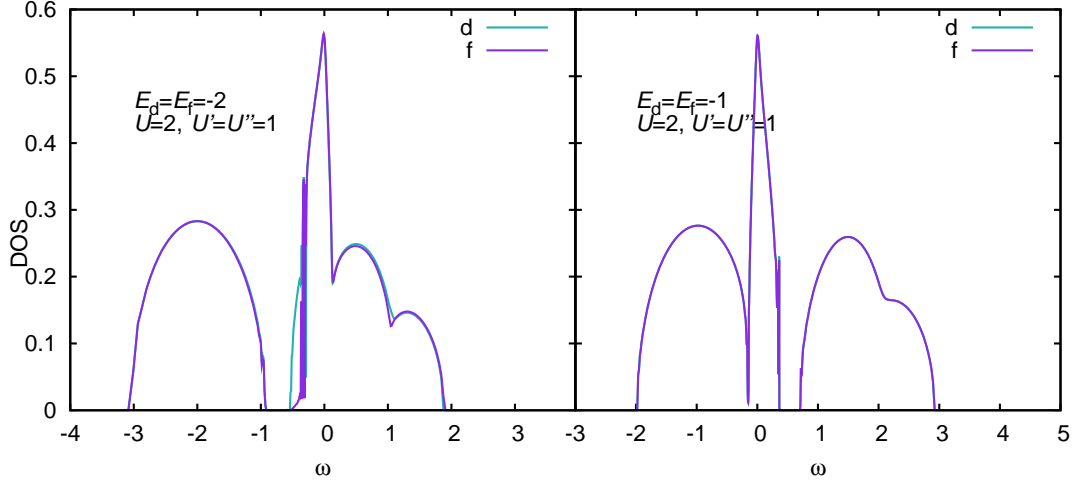


Figure 6.31: Densities of states for a two-band system with degenerate band energies, where the intraband Coulomb interaction strength differs from the inter-band Coulomb interaction strength.

interaction limit to the independent limit of the two bands. We calculate them also separately with degenerate band energies or different band energies. For the former one, the result is shown in Fig. 6.31. We can see that, due to the difference of the  $U$  and  $U', U''$ , the upper Hubbard band shows multi-peak structure. Moreover, when the two bands have different band energies, the densities of states of the two bands show more complicated behavior, shown in Fig. 6.32. Each of the upper Hubbard band has a multi-peak structure. In the Figure, we only present a metallic state. For different sets of  $(U, U', U'')$ , the system can show both insulating states, both metallic states, and one insulating and one metallic state.

In the procedure to calculate the above results, we have forbidden the exchange interaction through the bath between the bands. If this effect is indeed small, these results should be quantitatively good results. However, even for the general case, it shows the occurrence of the Mott metal-insulator transition in the two-band strongly correlated systems, and offers much interesting information for the strongly repulsive behavior. The most important thing is that, the further work taking account of the cross terms can be carried out based on this work.

## 6.5 Summary

With our impurity solver, we have investigated the single impurity Anderson model, Hubbard model, and periodic Anderson model. We made the calculations in a large range of control parameters and get qualitatively exact results. These results show that our impurity solver can be

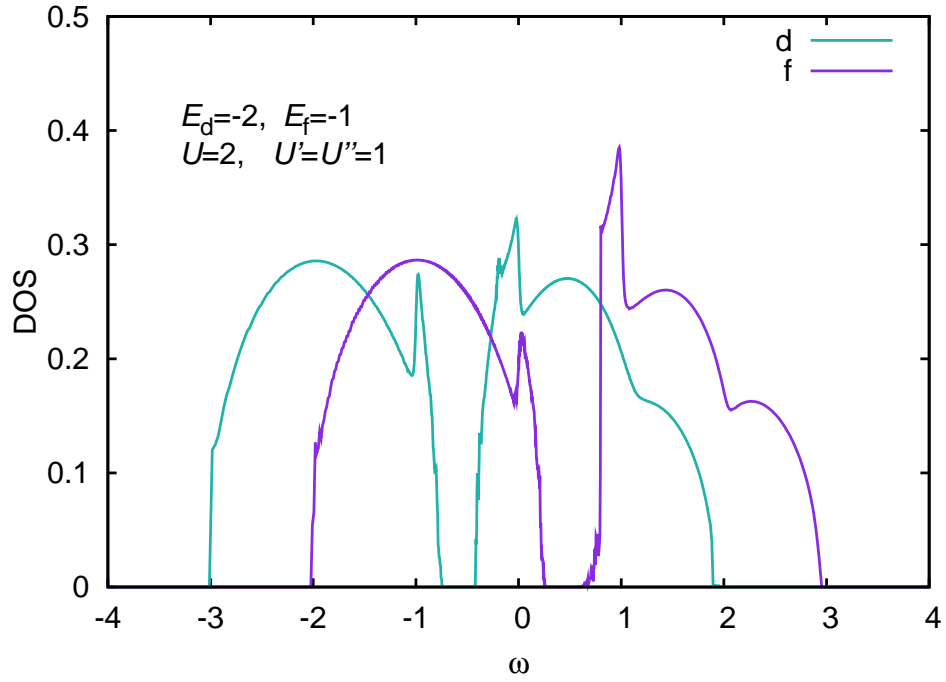


Figure 6.32: Densities of states for a two-band system with uniform Coulomb interaction strength, where the two bands have different band energies.

used to study not only the single band system with arbitrary spin and orbital degeneracy  $N$  but also the multi-band system. Moreover, the impurity solver works well to describe the insulating states and the Mott transition, but weak to describe the Fermi liquid behavior. Part of the results has been published in Phys. Rev. B [106]. Another paper for the two-band impurity solver is in preparation.



# Chapter 7 Conclusions

In the thesis, we have introduced the motivation of our work. The discovery of various exotic properties and interesting phenomena such as heavy Fermionic behaviors, Mott metal-insulator transition, high  $T_c$  superconductivity, shown in studies of transition metal oxides and Lanthanides, pushes forward the study of strongly correlated electron systems. The failure of density functional theory with local density approximation and the success of studies on model Hamiltonians motivate the appearance of the dynamical mean field theory. The LDA+DMFT approach has been proven to be a powerful tool in realistic material simulations. The dynamical mean field theory maps the lattice problem to a single impurity problem with self-consistency conditions. Thus the solving of lattice models is transferred to solving the single impurity Anderson model self-consistently. Due to the fact that all existing numerically exact impurity solvers are computationally expensive and usually limited by the available computer power, a fast and reliable impurity solver is needed, which motivates us to carry out this research.

Through our work, we have developed the equation-of-motion method using a new decoupling scheme for the higher order Green's functions. We have also investigated the convergency problem in solving the integral equations with various numerical techniques. Based on the new decoupling scheme and the new method developed from the iterative method and genetic algorithm, we successfully constructed a fast impurity solver for dynamical mean field theory. This impurity solver works well for the single impurity Anderson model. Moreover, we have also applied this newly developed impurity solver in the study of two important lattice models: the Hubbard model and the periodic Anderson model in the single band case with arbitrary spin and orbital degeneracy  $N$ . We have obtained characteristic and qualitatively exact results for the two lattice models at both infinite and finite Coulomb interaction strength, compared to the results obtained with other impurity solvers. Finally, based on the success of the impurity solver in single band systems, we have developed the impurity solver for multi-band systems and got the first encouraging results.

The impurity solver has contributed to the study of equation-of-motion methods and decoupling scheme. It can work on the real axis. By using the GA method, the convergency problem of purely iterative methods on the real axis for finite Coulomb interaction cases was solved. Moreover, this

has improved the quality of the results and also shows great advantage in the computing speed, compared with the iterative method with linear mixing. We have made comparative runs for various impurity solvers. Even the iterative method with linear mixing is much faster than QMC and ED impurity solvers. So when the impurity solver works on GA mode, it can greatly reduce the CPU time.

Here we list the advantages and disadvantages of our new impurity solver below:

1) The impurity solver shows the Mott metal-insulator transition, and generates comparable results to the QMC method. It obeys the particle-hole symmetry at half-filling and satisfies the sum rule. It can well describe the transfer of spectral weight.

2) The impurity solver works for a large range of control parameters. It can generally work for infinite  $U$  (which is Coulomb interaction strength) and finite  $U$ . It can work for symmetric and nonsymmetric single impurity Anderson model, Hubbard model, and periodic Anderson model. It can work for both single band system with arbitrary spin and orbital degeneracy and multi-band system.

3) The impurity solver can work directly on the real axis (iterative method with linear mixing is for all temperatures, GA method works well above  $T=0.001$  and the GA operators need to be improved below  $T=0.001$ ), which avoids the tail correction of calculation on Matsubara axis and the analytical continuation from the Matsubara axis to real frequency axis, which is needed in the QMC method. Therefore, it does not introduce this numerical error when we making calculations on the real axis.

4) The solution based on GA improves the results by removing the influence of broadening because, in the GA method, the broadening can even be set to zero. Therefore, the GA method gives correct divergent behavior even close to the Mott transition at the Fermi level. Considering 3) and 4), the precision of the impurity solver depends completely on the decoupling.

5) The impurity solver runs very fast and can quickly obtain the results with the implementation of genetic algorithm. The cost of time depends on the chosen population number and the required accuracy of GA method. Normally it costs less than quarter time of the usual Lorentzian broadening and iterative method with linear mixing. Comparing with other computationally expensive methods, *e.g.* QMC, NRG, ED, etc. it saves even much more time.

6) Although the impurity solver gives acceptable behavior for Fermi liquids, it can not give the exact Fermi liquid behavior. This is a general problem for the EOM method because the EOM



method is not a conserving method.

In conclusion, our new method has strongly developed and strengthened the power of equation-of-motion techniques. The impurity solver based on equations of motion and decoupling, and also based on the evolution scheme of genetic algorithm, has been developed as a fast, reliable and applicable method. It can be very useful for LDA+DMFT calculations in the study of strongly correlated systems, especially when the system has large size. We have developed the multi-band solver with the simplest assumptions. In the future, we can explore more precise EOM methods beyond the present level. Further developments of the equation-of-motion techniques in the framework of dynamical mean field theory can be carried out on the basis of this work. Moreover, the application of this impurity solver to LDA+DMFT calculations may widen the applications of dynamical mean field theory and help the study of strongly correlated systems.



# Appendix A An example of FORM code

Here we give an example of the FORM code, see Sec. 2.2.2. This code is first calculating the equations of motion of Green's functions, then employing the decoupling scheme, finally solving the closed set of equations of motion to obtain the single particle Green's function for the Lacroix's decoupling with spin and orbital degeneracy ( $N = 2$ ), *i.e.*

$$G_d = \frac{1 + \frac{U}{\omega - \varepsilon_d - U - 2\Delta - \bar{\Delta}} (\bar{n}_\sigma + I_1)}{\omega - \varepsilon_d - \Delta - \frac{U}{\omega - \varepsilon_d - U - 2\Delta - \bar{\Delta}} (\Delta \cdot I_1 + I_2)} \quad (\text{A.1})$$

with

$$I_1 = \sum_k \left( \frac{V_k \langle d_{\sigma'}^\dagger c_{k\sigma'} \rangle}{\omega - \varepsilon_k} - \frac{V_k \langle d_{\sigma'}^\dagger c_{k\sigma'} \rangle}{\omega + \varepsilon_k - 2\varepsilon_d - U} \right) \quad (\text{A.2})$$

$$I_2 = - \sum_{kk'} \left( \frac{V_k V_{k'} \langle c_{k'\sigma'}^\dagger c_{k\sigma'} \rangle}{\omega - \varepsilon_k} + \frac{V_k V_{k'} \langle c_{k'\sigma'}^\dagger c_{k\sigma'} \rangle}{\omega + \varepsilon_k - 2\varepsilon_d - U} \right) \quad (\text{A.3})$$

In the code, lines 1-58 define the operators, indices, Green's functions, correlations and the Hamiltonian; lines 59-146 calculate the equations of motion using Eq. (2.5); lines 167-179 employ the decoupling scheme; lines 184-249 solve the closed set of equations of motion.

```

1 off stat;
2 Autodeclare indices v;
3 symbols N,V,U,Ed,i,j,m,n,k,kp,kdp,omega;
4 set hh: m,n;
5 set gg: i,j;
6 set ll: i,j,m,n;
7 symbols d,dp,c,cp,t1,t2;
8 set tt: d,dp,c,cp,t1,t2;
9 set tt1: d,dp,c,cp,t1,t2;
10 set tt2: dp,cp,t1,t2;
11 set kk: 0,k,kp,kdp;
12 set kk1: k,kp,kdp;
13 set kk2: k,kp,kdp;
14 function F;
15 cfunction Ek,wmek,wmedmU;

```

```

16 cfunction Gd,Gc,Gnd;
17 cfunction Green1, Green2, Green3,Green4,Green5;
18 cfunction Kdc,Kcc,Nd;
19 cfunction Mfac,InvMfac,TT;
20 cfunction FF(antisymmetric);
21 indices i1,i2,i3,i4,i5,i6,j1,j2,j3,j4,j5,j6,i0,j0;
22 dimension 5;
23 local x1 = F(d,i,0);
24 local x2 = F(c,i,k);
25 local x3 = F(dp,j,0)*F(d,j,0)*F(d,i,0)*deltap_(i,j);
26 local x4 = F(dp,j,0)*F(d,j,0)*F(c,i,k)*deltap_(i,j);
27 local x5 = F(dp,j,0)*F(c,j,k)*F(d,i,0)*deltap_(i,j);
28 local x6 = F(cp,j,k)*F(d,j,0)*F(d,i,0)*deltap_(i,j);
29 local H = (delta_(i,n)+deltap_(i,n))*(Ek(k)*F(cp,n,k)*F(c,n,k)
30   +Ed*F(dp,n,0)*F(d,n,0)
31   +U/2*F(dp,n,0)*F(d,n,0)*F(dp,m,0)*F(d,m,0)*deltap_(m,n)*(delta_(i,m)
32   +deltap_(i,m))+V*F(dp,n,0)*F(c,n,k)+V*F(cp,n,k)*F(d,n,0));
33 local H2= (delta_(i,n)+deltap_(i,n))*(Ek(kp)*F(cp,n,kp)*F(c,n,kp)
34   +Ed*F(dp,n,0)*F(d,n,0)
35   +U/2*F(dp,n,0)*F(d,n,0)*F(dp,m,0)*F(d,m,0)*deltap_(m,n)*(delta_(i,m)
36   +deltap_(i,m))+V*F(dp,n,0)*F(c,n,kp)+V*F(cp,n,kp)*F(d,n,0));
37 local H3= (delta_(j,n)+deltap_(j,n))*(delta_(i,n)
38   +deltap_(i,n))*(Ek(k)*F(cp,n,k)*F(c,n,k)+Ed*F(dp,n,0)*F(d,n,0)
39   +U/2*F(dp,n,0)*F(d,n,0)*F(dp,m,0)*F(d,m,0)*deltap_(m,n)*(delta_(i,m)
40   +deltap_(i,m))*(delta_(j,m)+deltap_(j,m))+V*F(dp,n,0)*F(c,n,k)
41   +V*F(cp,n,k)*F(d,n,0));
42 local H4= (delta_(j,n)+deltap_(j,n))*(delta_(i,n)
43   +deltap_(i,n))*(Ek(kp)*F(cp,n,kp)*F(c,n,kp)+Ed*F(dp,n,0)*F(d,n,0)
44   +U/2*F(dp,n,0)*F(d,n,0)*F(dp,m,0)*F(d,m,0)*deltap_(m,n)*(delta_(i,m)
45   +deltap_(i,m))*(delta_(j,m)+deltap_(j,m))+V*F(dp,n,0)*F(c,n,k)
46   +V*F(cp,n,k)*F(d,n,0));
47 local F1 = x1*H-H*x1;
48 local F2 = x2*H2-H2*x2;
49 local F3 = x3*H3-H3*x3;
50 local F4 = x4*H4-H4*x4;

```

```

51 local F5 = x5*H4-H4*x5;
52 local F6 = x6*H4-H4*x6;
53 local T1=x1*F(dp,i,0)+F(dp,i,0)*x1;
54 local T2=x2*F(dp,i,0)+F(dp,i,0)*x2;
55 local T3=x3*F(dp,i,0)+F(dp,i,0)*x3;
56 local T4=x4*F(dp,i,0)+F(dp,i,0)*x4;
57 local T5=x5*F(dp,i,0)+F(dp,i,0)*x5;
58 local T6=x6*F(dp,i,0)+F(dp,i,0)*x6;

59 repeat;
60 repeat;
61 repeat;
62 repeat;
63 repeat;
64 id F(t1?tt,j?gg,k?kk)*F(t2?tt,m?hh,kp?kk)=(delta_(d,t1)*delta_(dp,t2)
65   +delta_(dp,t1)*delta_(d,t2)+delta_(c,t1)*delta_(cp,t2)
66   +delta_(cp,t1)*delta_(c,t2))*delta_(j,m)*delta_(k,kp)
67   -F(t2,m,kp)*F(t1,j,k);
68 id delta_(k,0)=0;
69 id delta_(kp,0)=0;
70 id delta_(kdp,0)=0;
71 id delta_(d,cp)=0;
72 id delta_(d,dp)=0;
73 id delta_(d,c)=0;
74 id delta_(dp,cp)=0;
75 id delta_(dp,d)=0;
76 id delta_(dp,c)=0;
77 id delta_(c,cp)=0;
78 id delta_(c,dp)=0;
79 id delta_(c,d)=0;
80 id delta_(cp,dp)=0;
81 id delta_(cp,d)=0;
82 id delta_(cp,c)=0;
83 id delta_(m,n)=0;
84 id delta_(i,j)=0;

```

```

85 id F(cp,i,0)=0;
86 id F(c,i,0)=0;
87 id F(d,j?gg,0)*F(d,j?gg,0)=0;
88 id F(dp,j?gg,0)*F(dp,j?gg,0)=0;
89 id F(d,j?gg,0)*F(d,m?hh,0)*delta_(j?gg,m?hh)=0;
90 id F(dp,j?gg,0)*F(dp,m?hh,0)*delta_(j?gg,m?hh)=0;
91 id F(d,m?hh,0)*F(d,j?gg,0)*delta_(j?gg,m?hh)=0;
92 id F(dp,m?hh,0)*F(dp,j?gg,0)*delta_(j?gg,m?hh)=0;
93 id delta_(j?gg,m?hh)*delta_(j?gg,n?hh)*deltap_(m?hh,n?hh)=0;
94 id delta_(j?gg,m?hh)*deltap_(j?gg,m?hh)=0;
95 id delta_(j,m?hh)*delta_(i,m?hh)*deltap_(i,j)=0;

96 *simplification
97 id delta_(j?gg,m?hh)^2=delta_(j,m);
98 id F(t1?tt,m?hh,k?kk)*delta_(j?gg,m?hh)=F(t1,j,k)*delta_(j,m);
99 id F(t1?tt,j?gg,kp)*delta_(k,kp)=F(t1,j,k)*delta_(k,kp);
100 id F(t1?tt,j?gg,kp)*delta_(kp,k)=F(t1,j,k)*delta_(k,kp);
101 id F(t1?tt,j?gg,kdp)*delta_(kp,kdp)=F(t1,j,kp)*delta_(kp,kdp);
102 id F(t1?tt,j?gg,kdp)*delta_(k,kdp)=F(t1,j,k)*delta_(k,kdp);
103 id F(d,i,0)*F(t1?tt,m?ll,k?kk)=delta_(dp,t1)*delta_(i,m)*delta_(k,0)
104                                     -F(t1,m,k)*F(d,i,0);
105 id F(c,i,k?kk)*F(t1?tt2,i,kp?kk)=delta_(t1,cp)*delta_(k,kp)
106                                     -F(t1,i,kp)*F(c,i,k);
107 id F(t1?tt,i,k?kk)*F(t2?tt,j,kp?kk)=-F(t2,j,kp)*F(t1,i,k);

108 id F(d,j,0)*F(c,j,k?kk)=-F(c,j,k)*F(d,j,0);
109 repeat
110 id F(d,j,0)*F(dp,j,0)=1-F(dp,j,0)*F(d,j,0);
111 id F(d,j,0)*F(cp,j,k?kk)=-F(cp,j,k)*F(d,j,0);
112 id F(c,j,k?kk)*F(dp,j,0)=-F(dp,j,0)*F(c,j,k);
113 id F(c,j,k?kk)*F(cp,j,kp?kk)=delta_(k,kp)-F(cp,j,kp)*F(c,j,k);
114 id F(cp,j,k?kk)*F(dp,j,0)=-F(dp,j,0)*F(cp,j,k);
115 id F(cp,j,k)*F(cp,j,kp)=-F(cp,j,kp)*F(cp,j,k);
116 endrepeat;
117 endrepeat;

```

```

118 endrepeat;
119 endrepeat;
120 endrepeat;

121 *remove zero term again
122 id F(d,j?gg,0)*F(d,j?gg,0)=0;
123 id F(dp,j?gg,0)*F(dp,j?gg,0)=0;
124 id F(d,j?gg,0)*F(d,m?hh,0)*delta_(j?gg,m?hh)=0;
125 id F(dp,j?gg,0)*F(dp,m?hh,0)*delta_(j?gg,m?hh)=0;
126 id F(d,m?hh,0)*F(d,j?gg,0)*delta_(j?gg,m?hh)=0;
127 id F(dp,m?hh,0)*F(dp,j?gg,0)*delta_(j?gg,m?hh)=0;

128 id delta_(j?gg,m?hh)*delta_(j?gg,n?hh)*deltap_(m?hh,n?hh)=0;
129 id delta_(j?gg,m?hh)*deltap_(j?gg,m?hh)=0;
130 id delta_(j,m?hh)*delta_(i,m?hh)*deltap_(i,j)=0;

131 id Ek(kp)*delta_(k,kp)=Ek(k)*delta_(k,kp);
132 id Ek(kp)*delta_(kp,k)=Ek(k)*delta_(kp,k);

133 id F(dp,m?hh,0)*F(d,m?hh,0)*F(d,i,0)*delta_(j,m?hh)*deltap_(i,m?hh)
134   =F(dp,j,0)*F(d,j,0)*F(d,i,0);
135 id F(dp,m,0)*F(d,m,0)*F(d,i,0)*deltap_(i,m)=F(dp,j,0)*F(d,j,0)*F(d,i,0);
136 id F(dp,n,0)*F(d,n,0)*F(d,i,0)*deltap_(i,n)=F(dp,j,0)*F(d,j,0)*F(d,i,0);
137 id F(dp,m,0)*F(d,m,0)*deltap_(i,m)*deltap_(j,m)=F(dp,n,0)*F(d,n,0);
138 id F(dp,m,0)*F(d,m,0)*deltap_(j,m)*deltap_(i,m)=F(dp,n,0)*F(d,n,0);
139 id delta_(j?gg,m?hh)=1;
140 id deltap_(j?gg,m?hh)=1;
141 id deltap_(m,n)=1;
142 id deltap_(i,j)=1;
143 id delta_(k,kp)=1;
144 id delta_(kp,kdp)=1;
145 id delta_(k,kdp)=1;
146 .sort

```

```

147 *--for dimension 5--
148 local DETMFAC=e_(1,2,3,4,5)*e_(j1,j2,j3,j4,j5)*Mfac(1,j1)*Mfac(2,j2)
149             *Mfac(3,j3)*Mfac(4,j4)*Mfac(5,j5);
150 local GREEND=e_(1,2,3,4,5)*e_(j1,j2,j3,j4,j5)*Mfac(j2,2)*Mfac(j3,3)
151             *Mfac(j4,4)*Mfac(j5,5)*TT(j1);
152 .sort
153 contract;
154 .sort
155 cfunction oneoverwminusek;
156 local G1=F1*F(dp,i,0);
157 local G2=F3*F(dp,i,0);
158 local G3=F4*F(dp,i,0);
159 local G4=F5*F(dp,i,0);
160 local G5=F6*F(dp,i,0);
161 .sort
162 pushhide;
163 Nhide T1,T2,T3,T4,T5,T6,G1,G2,G3,G4,G5,DETMFAC,GREEND;
164 .sort
165 Cfunction Delta,SDelta;
166 .sort
167 id F(dp,n,0)*F(d,n,0)*F(cp,j,k)*F(d,j,0)*F(d,i,0)=(N-2)*(N-1)*Nd*Green5;
168 id F(dp,n,0)*F(d,n,0)*F(dp,j,0)*F(d,j,0)*F(d,i,0)=(N-2)*(N-1)*Nd*Green2;
169 id F(cp,j,k)*F(d,j,0)*F(d,i,0)*F(dp,i,0)=(N-1)*Green5;
170 id F(dp,j,0)*F(c,j,k)*F(d,i,0)*F(dp,i,0)=(N-1)*Green4;
171 id F(dp,j,0)*F(d,j,0)*F(c,i,k)*F(dp,i,0)=(N-1)*Green3;
172 id F(dp,j,0)*F(d,j,0)*F(d,i,0)*F(dp,i,0)=(N-1)*Green2;
173 id V*F(c,i,k)*F(dp,i,0)=Delta*Green1;
174 id F(d,i,0)*F(dp,i,0)=Green1;
175 id F(dp,j,0)*F(c,j,k)=(N-1)*Kdc;
176 id F(cp,j,k)*F(d,j,0)=(N-1)*Kdc;
177 id F(cp,j,k)*F(c,j,k)=(N-1)*Kcc;
178 id F(dp,j,0)*F(d,j,0)=(N-1)*Nd;
179 id F(dp,n,0)*F(d,n,0)=(N-2)*Nd;
180 id N=2;
181 .sort

```



```
182 pophide;
183 .sort
184 *begin construction of prefactor matrice
185 #do li2=1,5,1
186 #do li1=1,5,1
187 local temp'li1''li2' = G'li1';
188 .sort
189 #enddo

190 pushhide;
191 Nhide
192 #do li1=1,5,1
193 temp'li1''li2',
194 #enddo
195 DETMFAC,GREEND;

196 #do li1=1,5,1
197 if ('li1' == 'li2');
198 id Green'li1' = 1;
199 else;
200 id Green'li1' = 0;
201 endif;
202 #enddo
203 .sort
204 pophide;
205 .sort
206 #enddo
207 .sort
208 #do li3=1,2,1
209 #do li2=1,5,1
210 if ('li3' == 'li2');
211 id Mfac('li3','li2')=temp'li3''li2'-omega;
212 else;
213 id Mfac('li3','li2')=temp'li3''li2';
214 endif;
```

```
215 #enddo
216 #enddo
217 .sort
218 cfunction oneoverwmek,oneoverwmekmuptwoed;
219 #do li3=3,4,1
220 #do li2=1,5,1
221 if ('li3' != 'li2');
222 id Mfac('li3','li2')=temp'li3''li2'*oneoverwmek;
223 else;
224 id Mfac('li3','li2')=-1;
225 endif;
226 .sort;
227 #enddo
228 #enddo
229 #do li2=1,5,1
230 if ('li2' != 5);
231 id Mfac(5,'li2')=temp5'li2'*oneoverwmekmuptwoed;
232 else;
233 id Mfac(5,5)=-1;
234 endif;
235 #enddo
236 .sort
237 unhide;
238 .sort
239 id TT(1)=T1;
240 id TT(2)=T3;
241 id TT(3)=T4*oneoverwmek;
242 id TT(4)=T5*oneoverwmek;
243 id TT(5)=T6*oneoverwmekmuptwoed;
244 id V^2*oneoverwmek=Delta;
245 id V^2*oneoverwmekmuptwoed=SDelta;
246 .sort
247 local Greend=GREEND/DETMFAC;
248 print +s;
249 .end
```

## Appendix B Separating the Green's function into two parts

The single particle Green's function, obtained from solving the equations of motion with Wang's decoupling, is

$$G_f = \frac{1 + \frac{(N-1)U}{\omega - \varepsilon_f - U - (N-2)U\bar{n}_{\sigma'} - 2\Delta - \tilde{\Delta}}(\bar{n}_{\sigma'} + I_1)}{\omega - \varepsilon_f - \Delta - \frac{(N-1)U}{\omega - \varepsilon_f - U - (N-2)U\bar{n}_{\sigma'} - 2\Delta - \tilde{\Delta}}(\Delta \cdot I_1 + I_2)}, \quad (\text{B.1})$$

which can be written in the form

$$G_f = \frac{1 + \frac{U}{\omega - \varepsilon_f - U - (N-2)U\bar{n}_{\sigma'} - 2\Delta - \tilde{\Delta}}A_1}{\omega - \varepsilon_f - \Delta - \frac{U}{\omega - \varepsilon_f - U - (N-2)U\bar{n}_{\sigma'} - 2\Delta - \tilde{\Delta}}A_2}. \quad (\text{B.2})$$

by introducing some new symbols  $A_1, A_2$ .

Now we want to separate it into two terms similar to the form in the Hubbard-I approximation

$$G_f = \frac{1 - \bar{n}_{\sigma'}}{\omega - \varepsilon_f - \Delta} + \frac{\bar{n}_{\sigma'}}{\omega - \varepsilon_f - \Delta - U} \quad (\text{B.3})$$

where one term corresponds to the lower Hubbard band and another one relates to the upper Hubbard band. In this separated form, it will be much easier to analyze the properties of the Green's function, especially at half-filling.

Eq. (B.2) can be written as

$$G_f = \frac{1}{\omega - \varepsilon_f - \Delta - BA_2} + \frac{UA_1}{(\omega - \varepsilon_f - U - 2\Delta - \tilde{\Delta})(\omega - \varepsilon_f - \Delta - BA_2)}, \quad (\text{B.4})$$

where

$$B = \frac{U}{\omega - \varepsilon_f - U - (N-2)U\bar{n}_{\sigma'} - 2\Delta - \tilde{\Delta}}. \quad (\text{B.5})$$

Comparing Eq. (B.3) with Eq. (B.4), we find that, if we have successfully separated the single particle Green's function into two terms, in which one term has the denominator

$$\omega - \varepsilon_f - \Delta - BA_2,$$

the first term in Eq. (B.4) will not change. The second term will be split as two terms with same numerator but opposite sign, *i.e.*

$$\begin{aligned} G_{f2} &= \frac{UA_1}{(\omega - \varepsilon_f - U - (N-2)U\bar{n}_{\sigma'} - 2\Delta - \tilde{\Delta})(\omega - \varepsilon_f - \Delta - BA_2)} \\ &= \frac{-X}{\omega - \varepsilon_f - \Delta - BA_2} + \frac{X}{Y}. \end{aligned} \quad (\text{B.6})$$

We also mention that

$$(\omega - \varepsilon_f - \Delta)A_1 - (\omega - \varepsilon_f - \Delta - U)A_1 = UA_1. \quad (\text{B.7})$$

Thus we can make a guess that

$$X = A_1 + \alpha \quad (\text{B.8})$$

$$Y = \omega - \varepsilon_f - \Delta - U + \beta \quad (\text{B.9})$$

Moreover, Eq. (B.4) can also be written as

$$G_f = \frac{1}{\omega - \varepsilon_f - \Delta - BA_2} + \frac{BA_1}{\omega - \varepsilon_f - \Delta - BA_2}. \quad (\text{B.10})$$

Then, we obtain

$$\frac{BA_1 + A_1 + \alpha}{\omega - \varepsilon_f - \Delta - BA_2} = \frac{A_1 + \alpha}{\omega - \varepsilon_f - \Delta - U + \beta} \quad (\text{B.11})$$

and

$$\left\{ B(\omega - \varepsilon_f - \Delta - U + \beta) - U - \beta - BA_2 \right\} A_1 + (U + \beta + BA_2)\alpha = 0. \quad (\text{B.12})$$

If the symbols meet the requirements:

$$\begin{cases} \alpha = 0 \\ B(\omega - \varepsilon_f - \Delta - U + \beta) - U - \beta - BA_2 \equiv 0 \end{cases}, \quad (\text{B.13})$$

Eq. (B.12) will always be satisfied. Hence, one possible solution is

$$\beta = \frac{B(\omega - \varepsilon_f - \Delta - U - A_2) - U}{B + 1} \quad (\text{B.14})$$

and the single particle Green's turns to be

$$G_f = \frac{1 - A_1}{\omega - \varepsilon_f - \Delta - \frac{UA_2}{\omega - \varepsilon_f - U - (N-2)U\bar{n}_{\sigma'} - 2\Delta - \tilde{\Delta}}} + \frac{A_1}{\omega - \varepsilon_f - \Delta - U + \frac{B(\omega - \varepsilon_f - \Delta - U - A_2) - U}{B + 1}}. \quad (\text{B.15})$$

If  $B$  is small, we have approximately

$$\beta \approx \{B(\Delta + \tilde{\Delta}) - BA_2\}(1 - B), \quad (\text{B.16})$$

which can be further approximated as

$$\beta \approx \{B(\Delta + \tilde{\Delta}) - BA_2\} \quad (\text{B.17})$$

Thus, in the approximation above, the single particle Green's function can be written as the following separated form

$$G_f = \frac{1 - A_1}{\omega - \varepsilon_f - \Delta - \frac{UA_2}{\omega - \varepsilon_f - U - (N-2)U\bar{n}_{\sigma'} - 2\Delta - \tilde{\Delta}}} + \frac{A_1}{\omega - \varepsilon_f - \Delta - \frac{UA_2 - U(\Delta + \tilde{\Delta})}{\omega - \varepsilon_f - U - (N-2)U\bar{n}_{\sigma'} - 2\Delta - \tilde{\Delta}}}. \quad (\text{B.18})$$



# Appendix C Calculation of two-particle correlations

The two-particle correlation  $\langle \hat{n}_{\sigma'} \hat{n}_{\sigma} \rangle$  is related to the two-particle Green's function  $G_{nd}$ . We notice,  $G_{nd}$  is connected to the single particle Green's function  $G_d$  by the equation of motion

$$(\omega - \varepsilon_d - \Delta)G_d = 1 + (N - 1)UG_{nd}. \quad (\text{C.1})$$

The single-particle Green's function  $G_d$  is obtained after each iteration. Assuming  $G_d$  is approaching the converged result, we can get the nearly exact  $G_{nd}$  from Eq. (C.1). Thus the two-particle correlation  $\langle \hat{n}_{\sigma'} \hat{n}_{\sigma} \rangle$  can be calculated by the spectral theorem, *i.e.*

$$\begin{aligned} \langle \hat{n}_{\sigma'} \hat{n}_{\sigma} \rangle &= -\frac{1}{\pi} \int d\omega' f(\omega') \text{Im} G_{nd} \\ &= -\frac{1}{\pi} \int d\omega' f(\omega') \text{Im} \left[ \frac{(\omega - \varepsilon_d - \Delta)G_d - 1}{(N - 1)U} \right] \\ &= -\frac{1}{\pi} \int d\omega' f(\omega') \text{Im} \left[ \frac{(\omega - \varepsilon_d - \Delta)G_d}{(N - 1)U} \right] \end{aligned} \quad (\text{C.2})$$

The corresponding connected correlation is given as

$$\begin{aligned} \langle \hat{n}_{\sigma'} \hat{n}_{\sigma} \rangle_c &= -\frac{1}{\pi} \int d\omega' f(\omega') \text{Im} G_{nd}^c \\ &= -\frac{1}{\pi} \int d\omega' f(\omega') \text{Im} [G_{nd} - \bar{n}_{\sigma'} G_d] \\ &= -\frac{1}{\pi} \int d\omega' f(\omega') \text{Im} \left[ \frac{(\omega - \varepsilon_d - \Delta)G_d - 1}{(N - 1)U} - \bar{n}_{\sigma'} G_d \right] \\ &= -\frac{1}{\pi} \int d\omega' f(\omega') \text{Im} \left[ \frac{(\omega - \varepsilon_d - \Delta)G_d}{(N - 1)U} - \bar{n}_{\sigma'} G_d \right] \end{aligned} \quad (\text{C.3})$$

Another two-particle correlation  $\langle c_{k\sigma'}^\dagger d_{\sigma'} \hat{n}_{\sigma} \rangle$ , which appears in the higher order approximations, corresponds to the Green's function  $G_{cdd}$  through

$$\langle c_{k\sigma'}^\dagger d_{\sigma'} \hat{n}_{\sigma} \rangle = -\frac{1}{\pi} \int d\omega' f(\omega') \text{Im} G_{cdd}. \quad (\text{C.4})$$

However, we notice, in the equations of motion, all such correlations appear together with  $V_k$  in  $k$ -summation terms. For convenience, we will calculate  $V_k \langle c_{k\sigma'}^\dagger d_{\sigma'} \hat{n}_{\sigma} \rangle$  instead of calculating

$\langle c_{k\sigma}^\dagger d_{\sigma'} \hat{n}_\sigma \rangle$ . Thus, in the Hubbard model, we do not need to calculate the  $V_k$  in each iteration. The densities of states of conduction electrons also do not appear in the calculations, as discussed in the calculation of  $\Delta$  and the integrals in Chap.2.

Because all the Green's functions involving  $c$  operators appear in the summation over  $k$  in the equations of motion, it's difficult to get the exact analytical expression of  $k$  dependent Green's functions. Hence, such Green's functions should be calculated with their own equation of motion along with the decoupling of higher order terms. Due to the different decoupling schemes, we can get different forms of Green's functions. Here we just discuss the methods. Which method is more reasonable will be tested and determined from physical considerations and numerical calculations.

For example, a) if the three-particle Green's function  $\ll \hat{n}_\zeta c_{k\sigma'}^\dagger d_{\sigma'} d_\sigma; d_\sigma^\dagger \gg$  is decoupled as

$$\ll \hat{n}_\zeta c_{k\sigma'}^\dagger d_{\sigma'} d_\sigma; d_\sigma^\dagger \gg \approx \bar{n}_\zeta \ll c_{k\sigma'}^\dagger d_{\sigma'} d_\sigma; d_\sigma^\dagger \gg \quad (\text{C.5})$$

and

$$G_{cc'd} \approx \langle c_{k'\sigma'}^\dagger c_{k\sigma'} \rangle G_d, \quad G_{cdc'} \approx \langle c_{k\sigma'}^\dagger d_{\sigma'} \rangle G_c = \langle c_{k\sigma'}^\dagger d_{\sigma'} \rangle \frac{V_{k'} G_d}{\omega - \varepsilon_{k'}}, \quad (\text{C.6})$$

The equation of motion of  $G_{cdd}$  now turns out to be

$$\begin{aligned} & (\omega + \varepsilon_k - 2\varepsilon_d - U - 2(N-2)U\bar{n}_\zeta) G_{cdd} \\ &= \langle c_{k\sigma'}^\dagger d_{\sigma'} \rangle - V_k G_{nd} + \sum_{k'} V_{k'} \langle c_{k'\sigma'}^\dagger c_{k\sigma'} \rangle G_d + \sum_{k'} V_{k'} \langle c_{k\sigma'}^\dagger d_{\sigma'} \rangle \frac{V_{k'} G_d}{\omega - \varepsilon_{k'}} \end{aligned} \quad (\text{C.7})$$

The combined correlation  $V_k \langle c_{k\sigma'}^\dagger d_{\sigma'} \hat{n}_\sigma \rangle$  is here given as

$$\begin{aligned} V_k \langle c_{k\sigma'}^\dagger d_{\sigma'} \hat{n}_\sigma \rangle &= -\frac{1}{\pi} \int d\omega' \text{Im} V_k G_{cdd} \\ &= -\frac{1}{\pi} \int d\omega' \text{Im} \left[ \frac{V_k \langle c_{k\sigma'}^\dagger d_{\sigma'} \rangle}{\omega + \varepsilon_k - 2\varepsilon_d - U - 2(N-2)U\bar{n}_\zeta} \right. \\ &\quad \left. + \frac{-V_k^2 G_{nd} + V_k \sum_{k'} V_{k'} \langle c_{k'\sigma'}^\dagger c_{k\sigma'} \rangle G_d + V_k \langle c_{k\sigma'}^\dagger d_{\sigma'} \rangle \Delta G_d}{\omega + \varepsilon_k - 2\varepsilon_d - U - 2(N-2)U\bar{n}_\zeta} \right] \\ &= -\frac{1}{\pi} \int d\omega' \text{Im} \left[ \frac{V_k \langle c_{k\sigma'}^\dagger d_{\sigma'} \rangle}{\omega + \varepsilon_k - 2\varepsilon_d - U - 2(N-2)U\bar{n}_\zeta} \right. \\ &\quad \left. - \frac{V_k^2 \frac{(\omega - \varepsilon_d - \Delta) G_d - 1}{(N-1)U}}{\omega + \varepsilon_k - 2\varepsilon_d - U - 2(N-2)U\bar{n}_\zeta} \right. \\ &\quad \left. + \frac{V_k \sum_{k'} V_{k'} \langle c_{k'\sigma'}^\dagger c_{k\sigma'} \rangle G_d + V_k \langle c_{k\sigma'}^\dagger d_{\sigma'} \rangle \Delta G_d}{\omega + \varepsilon_k - 2\varepsilon_d - U - 2(N-2)U\bar{n}_\zeta} \right] \end{aligned} \quad (\text{C.8})$$



and the corresponding connected correlation is

$$\begin{aligned}
V_k \langle c_{k\sigma'}^\dagger d_{\sigma'} \hat{n}_\sigma \rangle_c &= -\frac{1}{\pi} \int d\omega' \text{Im} V_k G_{cdd}^c \\
&= -\frac{1}{\pi} \int d\omega' \text{Im} V_k [G_{cdd} - \langle c_{k\sigma'}^\dagger d_{\sigma'} \rangle G_d] \\
&= -\frac{1}{\pi} \int d\omega' \text{Im} \left[ \frac{V_k \langle c_{k\sigma'}^\dagger d_{\sigma'} \rangle}{\omega + \varepsilon_k - 2\varepsilon_d - U - 2(N-2)U\bar{n}_\zeta} \right. \\
&\quad \left. - \frac{V_k^2 \frac{(\omega - \varepsilon_d - \Delta)G_{d-1}}{(N-1)U}}{\omega + \varepsilon_k - 2\varepsilon_d - U - 2(N-2)U\bar{n}_\zeta} \right. \\
&\quad \left. + \frac{V_k \sum_{k'} V_{k'} \langle c_{k'\sigma'}^\dagger c_{k\sigma'} \rangle G_d + V_k \langle c_{k\sigma'}^\dagger d_{\sigma'} \rangle \Delta G_d - V_k \langle c_{k\sigma'}^\dagger d_{\sigma'} \rangle G_d}{\omega + \varepsilon_k - 2\varepsilon_d - U - 2(N-2)U\bar{n}_\zeta} \right] \quad (\text{C.9})
\end{aligned}$$

b) If the three-particle Green's function is decoupled as

$$\ll \hat{n}_\zeta c_{k\sigma'}^\dagger d_{\sigma'} d_\sigma; d_\sigma^\dagger \gg \approx \langle \hat{n}_\zeta c_{k\sigma'}^\dagger d_{\sigma'} \rangle \ll d_\sigma; d_\sigma^\dagger \gg, \quad (\text{C.10})$$

the equation of motion of  $G_{cdd}$  reads

$$\begin{aligned}
&(\omega + \varepsilon_k - 2\varepsilon_d - U)G_{cdd} \\
&= \langle c_{k\sigma'}^\dagger d_{\sigma'} \rangle - 2(N-2)U \langle \hat{n}_\zeta \ll c_{k\sigma'}^\dagger d_{\sigma'} - V_k G_{nd} + \sum_{k'} V_{k'} \langle c_{k'\sigma'}^\dagger c_{k\sigma'} \rangle G_d + \sum_{k'} V_{k'} \langle c_{k\sigma'}^\dagger d_{\sigma'} \rangle \frac{V_{k'} G_d}{\omega - \varepsilon_{k'}} \gg \rangle. \quad (\text{C.11})
\end{aligned}$$

Then, the correlation is given as

$$\begin{aligned}
V_k \langle c_{k\sigma'}^\dagger d_{\sigma'} \hat{n}_\sigma \rangle &= -\frac{1}{\pi} \int d\omega' \text{Im} V_k G_{cdd} \\
&= -\frac{1}{\pi} \int d\omega' \text{Im} \left[ \frac{V_k \langle c_{k\sigma'}^\dagger d_{\sigma'} \rangle}{\omega + \varepsilon_k - 2\varepsilon_d - U} + \frac{V_k 2(N-2)U \langle \hat{n}_\zeta c_{k\sigma'}^\dagger d_{\sigma'} \rangle G_d}{\omega + \varepsilon_k - 2\varepsilon_d - U} \right. \\
&\quad \left. + \frac{-V_k^2 \frac{(\omega - \varepsilon_d - \Delta)G_{d-1}}{(N-1)U} + V_k \sum_{k'} V_{k'} \langle c_{k'\sigma'}^\dagger c_{k\sigma'} \rangle G_d + V_k \langle c_{k\sigma'}^\dagger d_{\sigma'} \rangle \Delta G_d}{\omega + \varepsilon_k - 2\varepsilon_d - U} \right] \quad (\text{C.12})
\end{aligned}$$

Moving the term involving  $\langle c_{k\sigma'}^\dagger d_{\sigma'} \hat{n}_\sigma \rangle$  on the right hand side (rhs) of Eq. (C.12) to the left hand side (lhs), we obtain

$$V_k \langle c_{k\sigma'}^\dagger d_{\sigma'} \hat{n}_\sigma \rangle = A/B \quad (\text{C.13})$$

$$\begin{aligned}
A &= -\frac{1}{\pi} \int d\omega' \text{Im} \left[ \frac{V_k \langle c_{k\sigma'}^\dagger d_{\sigma'} \rangle}{\omega + \varepsilon_k - 2\varepsilon_d - U} + \frac{-V_k^2 \frac{(\omega - \varepsilon_d - \Delta)G_{d-1}}{(N-1)U} + V_k \sum_{k'} V_{k'} \langle c_{k'\sigma'}^\dagger c_{k\sigma'} \rangle G_d + V_k \langle c_{k\sigma'}^\dagger d_{\sigma'} \rangle \Delta G_d}{\omega + \varepsilon_k - 2\varepsilon_d - U} \right] \\
B &= 1 + \frac{2(N-2)U}{\pi} \int d\omega' f(\omega') \text{Im} \frac{G_d}{\omega + \varepsilon_k - 2\varepsilon_d - U} \quad (\text{C.14})
\end{aligned}$$

The corresponding connected correlation is

$$V_k \langle c_{k\sigma'}^\dagger d_{\sigma'} \hat{n}_\sigma \rangle_c = A_1/B_1 \quad (\text{C.15})$$

$$\begin{aligned} A_1 &= -\frac{1}{\pi} \int d\omega' \text{Im} \left[ \frac{V_k \langle c_{k\sigma'}^\dagger d_{\sigma'} \rangle - V_k^2 \frac{(\omega - \varepsilon_d - \Delta) G_{d-1}}{(N-1)U} + V_k \sum_{k'} V_{k'} \langle c_{k'\sigma'}^\dagger c_{k\sigma'} \rangle G_d + V_k \langle c_{k\sigma'}^\dagger d_{\sigma'} \rangle \Delta G_d}{\omega + \varepsilon_k - 2\varepsilon_d - U} \right. \\ &\quad \left. - V_k \langle c_{k\sigma'}^\dagger d_{\sigma'} \rangle G_d \right] \\ B_1 &= 1 + \frac{2(N-2)U}{\pi} \int d\omega' f(\omega') \text{Im} \frac{G_d}{\omega + \varepsilon_k - 2\varepsilon_d - U} \end{aligned} \quad (\text{C.16})$$

c) Similarly, if the three-particle Green's function is decoupled as

$$\ll \hat{n}_\zeta c_{k\sigma'}^\dagger d_{\sigma'} d_\sigma; d_\sigma^\dagger \gg \approx \bar{n}_\zeta \ll c_{k\sigma'}^\dagger d_{\sigma'} d_\sigma; d_\sigma^\dagger \gg + \langle \hat{n}_\zeta c_{k\sigma'}^\dagger d_{\sigma'} \rangle \ll d_\sigma; d_\sigma^\dagger \gg, \quad (\text{C.17})$$

the corresponding correlation and connected correlation are given by

$$V_k \langle c_{k\sigma'}^\dagger d_{\sigma'} \hat{n}_\sigma \rangle = A/B \quad (\text{C.18})$$

$$V_k \langle c_{k\sigma'}^\dagger d_{\sigma'} \hat{n}_\sigma \rangle_c = A_1/B \quad (\text{C.19})$$

$$\begin{aligned} A &= -\frac{1}{\pi} \int d\omega' \text{Im} \left[ \frac{V_k \langle c_{k\sigma'}^\dagger d_{\sigma'} \rangle}{\omega + \varepsilon_k - 2\varepsilon_d - U - 2(N-2)U\bar{n}_\zeta} \right. \\ &\quad \left. + \frac{-V_k^2 \frac{(\omega - \varepsilon_d - \Delta) G_{d-1}}{(N-1)U} + V_k \sum_{k'} V_{k'} \langle c_{k'\sigma'}^\dagger c_{k\sigma'} \rangle G_d + V_k \langle c_{k\sigma'}^\dagger d_{\sigma'} \rangle \Delta G_d}{\omega + \varepsilon_k - 2\varepsilon_d - U - 2(N-2)U\bar{n}_\zeta} \right] \\ B &= 1 + \frac{2(N-2)U}{\pi} \int d\omega' f(\omega') \text{Im} \frac{G_d}{\omega + \varepsilon_k - 2\varepsilon_d - U - 2(N-2)U\bar{n}_\zeta} \end{aligned} \quad (\text{C.20})$$

$$\begin{aligned} A_1 &= -\frac{1}{\pi} \int d\omega' \text{Im} \left[ \frac{V_k \langle c_{k\sigma'}^\dagger d_{\sigma'} \rangle}{\omega + \varepsilon_k - 2\varepsilon_d - U - 2(N-2)U\bar{n}_\zeta} \right. \\ &\quad \left. + \frac{-V_k^2 \frac{(\omega - \varepsilon_d - \Delta) G_{d-1}}{(N-1)U} + V_k \sum_{k'} V_{k'} \langle c_{k'\sigma'}^\dagger c_{k\sigma'} \rangle G_d + V_k \langle c_{k\sigma'}^\dagger d_{\sigma'} \rangle \Delta G_d}{\omega + \varepsilon_k - 2\varepsilon_d - U - 2(N-2)U\bar{n}_\zeta} - V_k \langle c_{k\sigma'}^\dagger d_{\sigma'} \rangle G_d \right] \end{aligned} \quad (\text{C.21})$$

# Bibliography

- [1] G. Stewart, *Heavy-fermion Systems*, Rev. Mod. Phys. **56**, 755 (1984).
- [2] A. Amato, *Heavy-Fermion Systems Studied by  $\mu$ SR Technique*, Rev. Mod. Phys. **69**, 1119 (1997).
- [3] N. F. Mott, *Metal-Insulator Transitions* second edition (Taylor & Francis, London, 1990).
- [4] P. Hohenberg and W. Kohn, *Inhomogeneous Electron Gas*, Phys. Rev. **136**, B864 (1964).
- [5] W. Kohn and L. J. Sham, *Self-Consistent Equations Including Exchange and Correlation Effects*, Phys. Rev. **140**, A1133 (1965).
- [6] R. G. Parr, W. Yang, *Density-Functional Theory of Atoms and Molecules* (Oxford University Press, New York, 1989).
- [7] R. Dreizler, E. Gross, *Density Functional Theory* (Plenum Press, New York, 1995).
- [8] A. Georges, G. Kotliar, W. Krauth, M. J. Rozenberg, *Dynamical mean-field theory of strongly correlated fermion systems and the limit of infinite dimensions*, Rev. Mod. Phys. **68**, 13 (1996).
- [9] W. Metzner, D. Vollhardt, *Correlated Lattice Fermions in  $d = \infty$  Dimensions*, Phys. Rev. Lett. **62**, 324 (1989).
- [10] A. Georges, G. Kotliar, *Hubbard model in infinite dimensions*, Phys. Rev. B **45**, 6479 (1992).
- [11] P. W. Anderson, *Localized Magnetic States in Metals*, Phys. Rev. **124**, 41 (1961).
- [12] J. Hubbard, *Electron Correlations in Narrow Energy Bands*, Proc. Roy. Soc. London Ser. A **276**, 238 (1963).
- [13] N. F. Mott, R. Peierls, *Discussion of the paper by de Boer and Verwey*, Proc. Phys. Soc. **49**, 72 (1937); N. F. Mott, *The Basis of the Electron Theory of Metals, with Special Reference to the Transition Metals*, Proc. Phys. Soc. A **62**, 416 (1949).

- [14] N. F. Mott, *On the transition to metallic conduction in semiconductors*, Can. J. Phys. **34**, 1356 (1956); *The transition to the metallic state*, Philos. Mag. **6**, 287 (1961).
- [15] F. Gebhard, *The Mott metal-insulator transition* (Springer, 1997).
- [16] M. Imada, A. Fujimori, Y. Tokura, *Metal-insulator transitions*, Rev. Mod. Phys. **70**, 1039 (1998).
- [17] E. H. Lieb, F. Y. Wu, *Absence of Mott Transition in an Exact Solution of the Short-Range, One-Band Model in One Dimension*, Phys. Rev. Lett. **20**, 1445 (1968).
- [18] B. Sutherland, *An Introduction to the Bethe Ansatz in Exactly Solvable Problems in Condensed Matter and Relativistic Field Theory*, ed. S. B. Shastri, S. S. Jha, V. Singh (Springer-Verlag 1985).
- [19] J. Hubbard, *Electron Correlations in Narrow Energy Bands. II. The Degenerate Band Case*, Proc. Roy. Soc. A **277**, 237 (1964).
- [20] J. Hubbard, *Electron Correlations in Narrow Energy Bands. III. An Improved Solution*, Proc. Roy. Soc. A **281**, 401 (1964).
- [21] E. Müller-Hartmann, *Correlated fermions on a lattice in high dimensions*, Z. Phys. B **74**, 507 (1989); *The Hubbard model at high dimensions: some exact results and weak coupling theory*, *ibid.* **76** 211 (1989).
- [22] U. Brandt, C. Mielsch, *Thermodynamics and correlation functions of the Falicov-Kimball model in large dimensions*, Z. Phys. B **75**, 365 (1989); *Thermodynamics of the Falicov-Kimball model in large dimensions II*, *ibid.* **79**, 295 (1990); *Free energy of the Falicov-Kimball model in large dimensions*, *ibid.* **82**, 37 (1991).
- [23] P. G. J. van Dongen, D. Vollhardt, *Exact mean-field Hamiltonian for fermionic lattice models in high dimensions*, Phys. Rev. Lett. **65**, 1663 (1990).
- [24] M. H. Hettler, A. N. Tahvildar-Zadeh, M. Jarrell, T. Pruschke, and H. R. Krishnamurthy, *Nonlocal dynamical correlations of strongly interacting electron systems*, Phys. Rev. B **58**, 7475 (1998).

- [25] G. Kotliar, S. Y. Savrasov, G. Palsson, and G. Biroli, *Cellular Dynamical Mean Field Approach to Strongly Correlated Systems*, Phys. Rev. Lett. **87**, 186401 (2001).
- [26] M. Fleck, A. I. Liechtenstein, A. M. Oleś, L. Hedin, V. I. Anisimov, *Dynamical Mean-Field Theory for Doped Antiferromagnets*, Phys. Rev. Lett. **80**, 2393 (1998).
- [27] G. Kotliar, S. Y. Savrasov, K. Haule, V. S. Oudovenko, O. Parcollet, and C. A. Marianetti, *Electronic structure calculations with dynamical mean-field theory*, Rev. Mod. Phys. **78**, 865 (2006).
- [28] V. I. Anisimov, J. Zaanen, O. K. Anderson, *Band theory and Mott insulators: Hubbard  $U$  instead of Stoner  $I$* , Phys. Rev. B **44**, 943, (1991); V. I. Anisimov, F. Aryasetiawan, and A. I. Lichtenstein, *First-principles calculations of the electronic structure and spectra of strongly correlated systems: the LDA+  $U$  method*, J. Phys.: Condens. Matter **9**, 767 (1997).
- [29] X. Y. Zhang, M. J. Rozenberg, G. Kotliar, *Mott transition in the  $d = \infty$  Hubbard model at zero temperature*, Phys. Rev. Lett. **70**, 1666 (1993).
- [30] H. Kajueter, G. Kotliar, *New Iterative Perturbation Scheme for Lattice Models with Arbitrary Filling*, Phys. Rev. Lett. **77**, 131 (1996).
- [31] T. Fujiwara, S. Yamamoto, Y. Ishii, *Generalization of the Iterative Perturbation Theory and Metal-Insulator Transition in Multi-Orbital Hubbard Bands*, J. Phys. Soc. Jpn. **72**, 777 (2003).
- [32] H. Keiter, J. C. Kimball, *Diagrammatic Approach to the Anderson Model for Dilute Alloys*, J. Appl. Phys. **42**, 1460 (1971).
- [33] N. Grewe, H. Keiter, *Diagrammatic approach to the intermediate-valence compounds*, Phys. Rev. B **24**, 4420 (1981).
- [34] Y. Kuramoto, *Self-consistent perturbation theory for dynamics of valence fluctuations*, Z. Phys. B **53**, 37 (1983).
- [35] K. Haule, S. Kirchner, J. Kroha, and P. Wölfle, *Anderson impurity model at finite Coulomb interaction  $U$ : Generalized noncrossing approximation*, Phys. Rev. B **64**, 155111 (2001).
- [36] L. Chioncel, L. Vitos, I. A. Abrikosov, J. Kollár, M. I. Katsnelson, and A. I. Lichtenstein, *Ab initio electronic structure calculations of correlated systems: An EMTO-DMFT approach*, Phys. Rev. B **67**, 235106 (2003).

- [37] V. Drchal, V. Janis, J. Kudrnovsky, V. S. Oudovenko, X. Dai, K. Haule and G. Kotliar, *Dynamical correlations in multiorbital Hubbard models: fluctuation exchange approximations*, J. Phys.: Condens. Matter **17**, 61 (2005).
- [38] J. E. Hirsch, R. M. Fye, *Monte Carlo Method for Magnetic Impurities in Metals*, Phys. Rev. Lett. **56**, 2521 (1986).
- [39] M. Jarrell, *Hubbard model in infinite dimensions: A quantum Monte Carlo study*, Phys. Rev. Lett. **69**, 168 (1992).
- [40] M. J. Rozenberg, X. Y. Zhang, and G. Kotliar, *Mott-Hubbard transition in infinite dimensions*, Phys. Rev. Lett. **69**, 1236 (1992).
- [41] P. Werner, A. Comanac, L. de' Medici, M. Troyer, A. J. Millis, *Continuous-Time Solver for Quantum Impurity Models*, Phys. Rev. Lett. **97**, 076405 (2006).
- [42] A. N. Rubtsov, V. V. Savkin, A. I. Lichtenstein, *Continuous-time quantum Monte Carlo method for fermions*, Phys. Rev. B **72**, 035122 (2005).
- [43] M. Caffarel, W. Krauth, *Exact diagonalization approach to correlated fermions in infinite dimensions: Mott transition and superconductivity*, Phys. Rev. Lett. **72**, 1545 (1994).
- [44] Q. Si, M. J. Rozenberg, G. Kotliar, A. E. Ruckenstein, *Correlation induced insulator to metal transitions*, Phys. Rev. Lett. **72**, 2761 (1994).
- [45] R. Bulla, A. C. Hewson, and Th. Pruschke, *Numerical renormalization group calculations for the self-energy of the impurity Anderson model*, J. Phys.: Condens. Matter **10**, 8365 (1998).
- [46] R. Bulla, *Zero Temperature Metal-Insulator Transition in the Infinite-Dimensional Hubbard Model*, Phys. Rev. Lett. **83**, 136 (1999).
- [47] D. J. Garcia, K. Hallberg, M. J. Rozenberg, *Dynamical Mean Field Theory with the Density Matrix Renormalization Group*, Phys. Rev. Lett. **93**, 246403 (2004).
- [48] M. Karski, C. Raas, G. S. Uhrig, *Single-particle dynamics in the vicinity of the Mott-Hubbard metal-to-insulator transition*, Phys. Rev. B **77**, 075116 (2008).
- [49] H. O. Jeschke, G. Kotliar, *Decoupling method for dynamical mean-field theory calculations*, Phys. Rev. B **71**, 085103 (2005).

- [50] J.-X. Zhu, R. C. Albers, J. M. Wills, *Equation-of-Motion Approach to Dynamical Mean Field Theory*, Mod. Phys. Lett. B **20**, 1629 (2006).
- [51] Y. Qi, J. X. Zhu, C. S. Ting, *Validity of the equation-of-motion approach to the Kondo problem in the large- $N$  limit*, Phys. Rev. B **79**, 205110 (2009).
- [52] K. Held and D. Vollhardt, *Article Microscopic conditions favoring itinerant ferromagnetism: Hund's rule coupling and orbital degeneracy*, Eur. Phys. J. B **5**, 473 (1998).
- [53] A. C. Hewson, *The Kondo problem to Heavy Fermions* (Cambridge, 1993)
- [54] R. O. Jones, O. Gunnarsson, *The density functional formalism, its applications and prospects*, Rev. Mod. Phys. **61**, 689 (1989).
- [55] W. J. de Haas, J. H. de Boer, G. J. van den Berg, *The electrical resistance of gold, copper and lead at low temperatures*, Physica **1**, 1115 (1934).
- [56] J. Kondo, *Resistance Minimum in Dilute Magnetic Alloys*, Prog. Theor. Phys. **32**, 37 (1964).
- [57] J. Friedel, *On Some Electrical and Magnetic Properties of Metallic Solid Solutions*, Can. J. Phys. **34**, 1190 (1956).
- [58] M. C. Gutzwiller, *Effect of Correlation on the Ferromagnetism of Transition Metals*, Phys. Rev. Lett. **10**, 159 (1963).
- [59] J. Kanamori, *Electron Correlation and Ferromagnetism of Transition Metals*, Prog. Theor. Phys. **30**, 275 (1963).
- [60] Y. A. Uzyumov, *Hubbard model and strong correlations*, Phys.-Usp. **38**, 385 (1995).
- [61] H. Tasaki, *The Hubbard model - an introduction and selected rigorous results*, J. Phys.: Condens. Matter **10**, 4353 (1998).
- [62] F. H. L. Essler, H. Frahm, F. Göhmann, A. Klümper, V. E. Korepin, *The One Dimensional Hubbard model* (Cambridge, 2005).
- [63] P. W. Anderson, *The Resonating Valence Bond State in  $La_2CuO_4$  and Superconductivity*, Science **235**, 1196 (1987)

- [64] F. C. Zhang, T. M. Rice, *Effective Hamiltonian for the superconducting Cu oxides*, Phys. Rev. B **37**, 3759 (1988).
- [65] T. Arai, M. H. Cohen, M. P. Tosi, *Functional-derivative study of the Hubbard model. I. Perturbation method and first-order approximation*, Phys. Rev. B **15**, 1817 (1977).
- [66] V. M. Zharkov, *Perturbation theory and the exchange interaction in the one-dimensional Hubbard model*, Theoret. and Math. Phys. **46**, 88 (1981).
- [67] T. Koma, *An Extension of the Thermal Bethe Ansatz - One-Dimensional Hubbard model*, Prog. Theor. Phys. **83**, 655 (1990).
- [68] M. C. Gutzwiller, *Correlation of Electrons in a Narrow s Band*, Phys. Rev. **137**, A1726 (1965).
- [69] C. Noce, *The periodic Anderson model: Symmetry-based results and some exact solutions*, Phys. Rep. **431**, 173 (2006).
- [70] C. Lacroix, *Density of states for the Anderson model*, J. Phys. F: Metal Phys. **11**, 2389 (1981).
- [71] C. Lacroix, *Density of states for the asymmetric Anderson model*, J. Appl. Phys. **53**, 2131 (1981).
- [72] G. Czycholl, *Equation-of-motion treatment of the N-fold-degenerate Anderson model in the large-N limit*, Phys. Rev. B **31**, 2867 (1984).
- [73] J. Petru, *Self-consistent treatment of the Anderson model*, Z. Phys. B **91**, 351 (1993).
- [74] K. Kang and B. I. Min, *Equation-of-motion treatment of the impurity Anderson model with a finite on-site Coulomb repulsion*, Phys. Rev. B **52**, 10689 (1995).
- [75] D. N. Zubarev, *Double-time Green Functions in Statistical Physics*, Sov. Phys. Usp. **3**, 320 (1960).
- [76] J. A. M. Vermaseren, *Symbolic Manipulation with FORM*, Tutorial and reference manual, CAN, Amsterdam (1991).
- [77] S.-J. Wang, W. Kassing, *Explicit treatment of N-body correlations within a density-matrix formalism*, Annals of Physics **159**, 328 (1985).



- [78] H. G. Luo, J. J. Ying, S.-J. Wang, *Equation of motion approach to the solution of the Anderson model*, Phys. Rev. B **59**, 9710 (1999).
- [79] G. D. Mahan, *Many Particle Physics* (Springer, 2007).
- [80] P. Coleman, *Introduction To Many Body Physics* (Rutgers University, 2004).
- [81] P. A. Martin and F. Rothen, *Many Body Problems and Quantum Field Theory - An Introduction* (Springer, 2002).
- [82] H. Bruus and K. Flensberg, *Many-Body Quantum Theory in Condensed Matter Physics: An Introduction* (Oxford University Press, 2004).
- [83] H. J. Vidberg and J. W. Serene, *Solving the Eliashberg equations by means of N-point Padé Approximations*, J. Low Temp. Phys. **29**, 179 (1977).
- [84] K. S. D. Beach, R. J. Gooding and F. Marsiglio, *Reliable Padé analytical continuation method based on a high-accuracy symbolic computation algorithm*, Phys. Rev. B **61**, 5147 (2000).
- [85] G. P. Srivastava, *Broyden's method for self-consistent-field convergence acceleration*, J. Phys. A: Math. Gen. **17**, 317 (1984).
- [86] D. Vanderbilt, S. G. Louie, *Total energies of diamond (111) surface reconstructions by a linear combination of atomic orbitals method*, Phys. Rev. B **30**, 6118 (1984).
- [87] D. D. Johnson, *Modified Broyden's method for accelerating convergence in self-consistent calculations*, Phys. Rev. B **38**, 12807 (1988).
- [88] V. Eyert, *A Comparative Study on Methods for Convergence Acceleration of Iterative Vector Sequences*, J. Comput. Phys. **124**, 271 (1996).
- [89] O. Gunnarsson, E. Koch, R. M. Martin, *Mott transition in degenerate Hubbard models: Application to doped fullerenes*, Phys. Rev. B **54**, R11026 (1996).
- [90] G. Kotliar, H. Kajueter, *Effects of orbital degeneracy on the Mott transition in infinite dimensions*, Phys. Rev. B **54**, R14221 (1996); *Band Degeneracy and Mott Transition: Dynamical Mean Field Study*, Int. J. Mod. Phys. B **11**, 729 (1997).

- [91] M. J. Rozenberg, *Integer-filling metal-insulator transitions in the degenerate Hubbard model*, Phys. Rev. B **55**, 4855 (1997).
- [92] J. E. Han, M. Jarrell, D. L. Cox, *Multiorbital Hubbard model in infinite dimensions: Quantum Monte Carlo calculation*, Phys. Rev. B **58**, 4199 (1998).
- [93] A. Koga, T. Ohashi, Y. Imai, S. Suga, N. Kawakami, *Effects of Degenerate Orbitals on the Hubbard Model*, J. Phys. Soc. Jpn. **72**, 1306 (2003).
- [94] A. Liebsch, *Absence of orbital-dependent Mott transition in  $Ca_{2-x}Sr_xRuO_4$* , Europhys. Lett. **63**, 97 (2003); *Mott Transitions in Multiorbital Systems*, Phys. Rev. Lett. **91**, 226401 (2003); *Single Mott transition in the multiorbital Hubbard model*, Phys. Rev. B **70**, 165103 (2004).
- [95] C. A. Perroni, H. Ishida, A. Liebsch, *Exact diagonalization dynamical mean-field theory for multiband materials: Effect of Coulomb correlations on the Fermi surface of  $Na_{0.3}CoO_2$* , Phys. Rev. B **75**, 045125 (2007).
- [96] I. Grigorenko, M. E. Garcia, *An evolutionary algorithm to calculate the ground state of a quantum system*, Physica A **284**, 131 (2000).
- [97] I. Grigorenko, M. E. Garcia, *Ground-state wave functions of two-particle systems determined using quantum genetic algorithms*, Physica A **291**, 439 (2001).
- [98] R. Zitko, T. Pruschke, *Energy resolution and discretization artifacts in the numerical renormalization group*, Phys. Rev. B **79**, 085106 (2009).
- [99] C. Raas, G. Uhrig, F. B. Anders, *High-energy dynamics of the single-impurity Anderson model*, Phys. Rev. B **69**, 041102 (2004).
- [100] R. Bulla, *Dynamical mean-field theory: from quantum impurity physics to lattice problems*, Phil. Mag. **86**, 1877 (2006).
- [101] W. F. Brinkman, T. M. Rice, *Application of Gutzwiller's Variational Method to the Metal-Insulator Transition*, Phys. Rev. B **2**, 4302 (1970).
- [102] C. Grenzebach, T. Pruschke, F. B. Anders, G. Czycholl, *Transport properties of heavy-fermion systems*, Phys. Rev. B **74**, 195119 (2006).

- [103] G. Sordi, A. Amaricci, and M. J. Rozenberg, *Metal-Insulator Transitions in the Periodic Anderson Model*, Phys. Rev. Lett. **99**, 196403 (2007).
- [104] U. Yu, K. Byczuk, and D. Vollhardt, *Ferromagnetism and Kondo Insulator Behavior in the Disordered Periodic Anderson Model*, Phys. Rev. Lett. **100**, 246401 (2008).
- [105] A. Amaricci, G. Sordi, and M. J. Rozenberg, *Non-Fermi-Liquid Behavior in the Periodic Anderson Model*, Phys. Rev. Lett. **101**, 146403 (2008).
- [106] Q. Feng, Y-Z. Zhang, H. O. Jeschke, *Fast impurity solver based on equations of motion and decoupling*, Phys. Rev. B **79**, 235112 (2009).
- [107] Y. F. Yang, *Dynamical Mean-Field Theory for Manganites*, Ph.D. dissertation (2007).
- [108] C. Raas, *Dynamic Density-Matrix Renormalization for the Symmetric Single Impurity Anderson model*, Ph.D. dissertation (2005).
- [109] N. Blümer, *Mott-Hubbard Metal-Insulator Transition and Optical Conductivity in High Dimensions*, Ph.D. dissertation (Shaker Verlag, 2003).
- [110] C. Gros, *Equation-of-motion approach to the Hubbard model in infinite dimensions*, Phys. Rev. B **50**, 7295 (1994).

## Acknowledgments

First I would like to thank Dr. Harald O. Jeschke to host my Ph.D study in his Emmy Noether junior research group at the institute of theoretical physics, Goethe-University Frankfurt. I wish to thank him for introducing me into this challenging area and for all the help from him during the work. I would like to thank Prof. Maria-Roser Valentí for supporting the working place and computers. I also want to thank Dr. Yuzhong Zhang for very helpful discussions, and thank Dr. Zhe Xu, Dr. Yuzhong Zhang, Dr. Qingfeng Li, Dr. Nan Su, Dr. Dongfeng Gao, Dr. Yuanyuan Zhao in first read and comments on this thesis, and thank Dr. Ingo Opahle and Dr. Marc-Thilo Figge in help of revising the german abstract.

By the way, I would like to thank our secretaries Mrs. Vogel and Mrs. M. Kolokotsa for their help in dealing with matters, and all other people in the condensed matter group for their supports. I would also like to give special thanks to all my Chinese friends in the department of physics and the Frankfurt institute for advanced studies for their friendly helps.

Finally, I would like give my best thanks to my parents for their ever encouragements during these years, especially when my work is in difficulties.

## Zusammenfassung

Die Dynamische Molekularfeldtheorie (DMFT) ist für stark korrelierte Systeme weit verbreitet. In dieser Arbeit wurde das Einzel-Störstellen-Anderson-Modell untersucht und eine neue und schnelle Lösungsmethode für das effektive Einzel-Störstellenmodell im Rahmen der Dynamischen Molekularfeldtheorie entwickelt. Auf dieser Basis wurde das Hubbard-Modell und das periodische Anderson-Modell in verschiedenen Fällen untersucht. Die Arbeit ist motiviert durch die breite Anwendbarkeit der Dynamischen Molekularfeldtheorie bei der Untersuchung von stark korrelierten Systemen. Die am häufigsten verwendeten Methoden wie Quanten-Monte-Carlo (QMC) oder exakte Diagonalisierung sind rechenzeitintensiv und ihre Verwendung wird durch die verfügbare Rechenleistung begrenzt. Daher ist eine schnelle und zuverlässige Lösungsmethode für das effektive Störstellenproblem nicht nur wünschenswert sondern auch notwendig.

Diese neue Methode für das effektive Störstellenproblem wurde auf Basis der Bewegungsgleichungsmethode (Entkopplung von Greenfunktionen) entwickelt. Wir gehen von den Hamiltonian für das Einzel-Störstellen-Anderson-Modell

$$\mathcal{H} = \sum_{k\sigma} \varepsilon_k c_{k\sigma}^\dagger c_{k\sigma} + \sum_{\sigma} \varepsilon_f f_{\sigma}^\dagger f_{\sigma} + \frac{U}{2} \sum_{\sigma \neq \sigma'} \hat{n}_{\sigma} \hat{n}_{\sigma'} + \sum_{k\sigma} (V_{k\sigma}^* c_{k\sigma}^\dagger f_{\sigma} + V_{k\sigma} f_{\sigma}^\dagger c_{k\sigma}) \quad (\text{C.22})$$

aus. Zunächst wurden die Bewegungsgleichung für die retardierten Greenfunktionen hergeleitet mit der Formel

$$\omega \ll A; B \gg = \langle [A, B]_+ \rangle + \ll [A, \mathcal{H}]; B \gg . \quad (\text{C.23})$$

$\ll A; B \gg$  stellt die Greenfunktionen dar. Die Bewegungsgleichungen sind

$$(\omega - \varepsilon_k - \Delta)G_f = 1 + (N - 1)G_{nf} \quad (\text{C.24})$$

$$(\omega - \varepsilon_f - U)G_{nf} = \bar{n}_{\sigma'} + (N - 2)UG_{nnf} + V \sum_k (G_{nc} + G_{fcf} - G_{cff}) \quad (\text{C.25})$$

$$V \sum_k G_{nc} = \sum_k \frac{V^2}{\omega - \varepsilon_k} G_{nf} + \sum_{kk'} \frac{V^2}{\omega - \varepsilon_k} (G_{fc'c} - G_{c'fc}) \quad (\text{C.26})$$

$$V \sum_k G_{fcf} = \sum_k \frac{V \langle f_{\sigma'}^\dagger c_{k\sigma'} \rangle}{\omega - \varepsilon_k} + \sum_k \frac{V^2}{\omega - \varepsilon_k} G_{nf} - \sum_{kk'} \frac{V^2}{\omega - \varepsilon_k} G_{c'cf} + \sum_{kk'} \frac{V^2}{\omega - \varepsilon_{k'}} G_{fc'c} \quad (\text{C.27})$$

$$V \sum_k G_{cff} = \sum_k \frac{V \langle f_{\sigma'}^\dagger c_{k\sigma'} \rangle + V(N - 2)UG_{ncff} - V^2 G_{nf}}{\omega + \varepsilon_k - 2\varepsilon_f - U} + \sum_{kk'} \frac{V^2}{\omega + \varepsilon_{k'} - 2\varepsilon_f - U} (G_{c'fc} + G_{c'fc}) \quad (\text{C.28})$$

Mit einer Entkopplungsmethode wurde ein geschlossenes System von Gleichungen erzielt. Durch selbstkonsistente Lösung dieses Gleichungssystems erhält man die Einteilchen-Greenfunktion des

Einzel-Störstellen-Anderson-Modells, zum Beispiel

$$\ll f_\sigma; f_\sigma^\dagger \gg = \frac{1 + A \cdot \left\{ \bar{n}_{\sigma'} + \sum_k \left( \frac{V_{k\sigma'} \langle f_{\sigma'}^\dagger c_{k\sigma'} \rangle}{\omega - \varepsilon_k} - \frac{V_{k\sigma'}^* \langle c_{k\sigma'}^\dagger f_{\sigma'} \rangle}{\omega + \varepsilon_k - 2\varepsilon_f - U - 2(N-2)U\bar{n}_\zeta} \right) \right\}}{\omega - \varepsilon_f - \Delta - A \cdot B} \quad (\text{C.29})$$

mit

$$A = \frac{(N-1)U}{\omega - \varepsilon_f - U - (N-2)U\bar{n}_\zeta - 2\Delta - \bar{\Delta}} \quad (\text{C.30})$$

$$B = \left[ (N-2)U \langle \hat{n}_\zeta \hat{n}_{\sigma'} \rangle_c + \sum_{k,k'} \left( - \frac{V_{k\sigma'} V_{k'\sigma'}^* \langle c_{k'\sigma'}^\dagger c_{k\sigma'} \rangle}{\omega - \varepsilon_k} + \frac{V_{k\sigma'} V_{k'\sigma} V_{k'\sigma}^*}{(\omega - \varepsilon_k)(\omega - \varepsilon_{k'})} \langle f_{\sigma'}^\dagger c_{k\sigma'} \rangle \right) \right. \\ \left. - \sum_k \frac{2(N-2)U \langle \hat{n}_\zeta c_{k\sigma'}^\dagger f_{\sigma'} \rangle_c}{\omega + \varepsilon_k - 2\varepsilon_f - U - 2(N-2)U\bar{n}_{\sigma''}} - \sum_k \frac{V_{k\sigma'}^* \sum_{k'} \left( \frac{V_{k'\sigma} V_{k'\sigma}^* \langle c_{k\sigma'}^\dagger f_{\sigma'} \rangle + V_{k'\sigma'} \langle c_{k\sigma'}^\dagger c_{k'\sigma'} \rangle \right)}{\omega + \varepsilon_k - 2\varepsilon_f - U - 2(N-2)U\bar{n}_{\sigma''}} \right] \quad (\text{C.31})$$

mit der Entkopplungsmethode von Wang. Anschließend wurde das Einzel-Störstellen-Anderson-Modell zusammen mit zusätzlichen Selbstkonsistenzbedingungen im Rahmen der DMFT gelöst. In dieser Arbeit wurden zwei Entkopplungsmethoden untersucht und verglichen. Darüber hinaus wurden auch mögliche Näherungen höherer Ordnungen abgeleitet, die in Zukunft geprüft werden.

Neben der analytischen Arbeit wurde die Methode auch numerisch implementiert und geprüft. Die Integralgleichungen wurden zunächst mit iterativen Methoden unter Zuhilfenahme von linearer Mischung und Broyden-Mischung gelöst. Allerdings eignen sich diese zwei Methoden nicht für die selbstkonsistente Lösung der DMFT-Gleichungen, da es schwierig ist, zu konvergierten Ergebnissen zu gelangen. Darüber hinaus ist der Rechenzeitaufwand dieser beiden Methoden unbefriedigend. Insbesondere die iterative Lösung mit linearer Mischung benötigt durch das erforderliche kleine Mischungsverhältnis sehr viel Rechenzeit. Deshalb wurde eine neue Methode entwickelt, die in einer Kombination aus einem genetischen Algorithmus und iterativer Methode besteht.

Im GA Algorithmus sind die Imaginärteile der ersten Greenfunktionen als Summen von Gauss-Funktionen

$$\text{Im } G(\omega) = L \left( e^{-\frac{(\omega-B)^2}{2C^2}} + e^{-\frac{(\omega-B-U)^2}{2C^2}} \right), \quad (\text{C.32})$$

wobei  $L$  ein Normierungsfaktor, und  $B, C$  zufällige Zahlen sind. Wir bestimmen die Realteile mittels der Kramers-Kronig Relation

$$\text{Re } G(\omega) = -\frac{1}{\pi} \int \frac{\text{Im } G(\omega')}{\omega' - \omega} d\omega' \quad (\text{C.33})$$

Als nächstes definieren wir die Fitness-Funktion

$$F[G(\omega)] = \|G(\omega) - \text{rhs}[G(\omega)]\| \quad (\text{C.34})$$

mit der Norm

$$\|F(\omega)\| = \int d\omega |F(\omega)|, \quad (\text{C.35})$$

die die Entfernung der Greenfunktionen von der selbstkonsistenten Lösung mißt.

Die Gruppe der Greenfunktionen wird mit der Fitness-Funktion bewertet und gewichtet. Als nächstes wird eine neue Gruppe von Greenfunktionen aus den ausgewählten Greenfunktionen erzeugt. Dieses Verfahren ist ein Fitness-Prozess.

Die neue Gruppe der Greenfunktionen wird durch den GA Operator produziert. Crossover und Mutation sind dabei zwei wichtige Operatoren. Der Crossover-Operator macht die neue Generation von Greenfunktionen. In dieser Arbeit wird der Crossover-Operator durch

$$\begin{aligned} \text{Im } G_1^{\text{offspring}}(\omega) &= L_1 \text{Im} \left\{ G_1^{\text{parent}}(\omega) \Theta(\omega - \omega_0) \right. \\ &\quad \left. + G_2^{\text{parent}}(\omega) \Theta(\omega_0 - \omega) \right\} \\ \text{Im } G_2^{\text{offspring}}(\omega) &= L_2 \text{Im} \left\{ G_1^{\text{parent}}(\omega) \Theta(\omega_0 - \omega) \right. \\ &\quad \left. + G_2^{\text{parent}}(\omega) \Theta(\omega - \omega_0) \right\} \end{aligned} \quad (\text{C.36})$$

konstruiert, wobei  $\omega_0$  eine zufällig gewählte Crossover-Position,  $\Theta(\omega)$  die Heavisidesche Stufenfunktion und  $L_1, L_2$  Normierungsfaktoren sind.

Der Mutations-Operator bewirkt eine geringfügige Änderung in den Greenfunktionen. Wir konstruieren den Mutation-Operator wie folgt:

$$\text{Im } G^{\text{offspring}}(\omega) = L \left( \text{Im } G^{\text{parent}}(\omega) + A e^{-\frac{(\omega-B)^2}{2C^2}} \right) \quad (\text{C.37})$$

wobei  $A, B, C$  zufällige Zahlen und  $L$  ein Normierungsfaktor sind. Die Wirkung der Crossover- und Mutations- Operatoren wird in Abb. C.1 veranschaulicht. Diese neue Methode löst erfolgreich die Konvergenzprobleme, sodass das konvergierte Resultat rasch erreicht werden kann. Für das Hubbard Modell:

Modell	Methode	Maschenöffnung	Parameter	CPU Zeit
Hubbard	GA	1000	population=100, accu=0.005, T=0.01, U=2.6	244.9s
	lineare Mix	1150	mix=0.001, dmix = $10^{-5}$ , accu = $10^{-5}$ , T = 0.01	1962.0s

Zusätzlich erhöht die neue Technik die Genauigkeit der numerischen Ergebnisse, weil sie ohne Verbreiterung auskommt, siehe Abb. C.2.

Mit dieser neuen Herangehensweise an das Einzel-Störstellenproblem haben wir das Einzel-Störstellen-Anderson-Modell, das Einband-Hubbard-Modell, das periodische Anderson-Modell mit

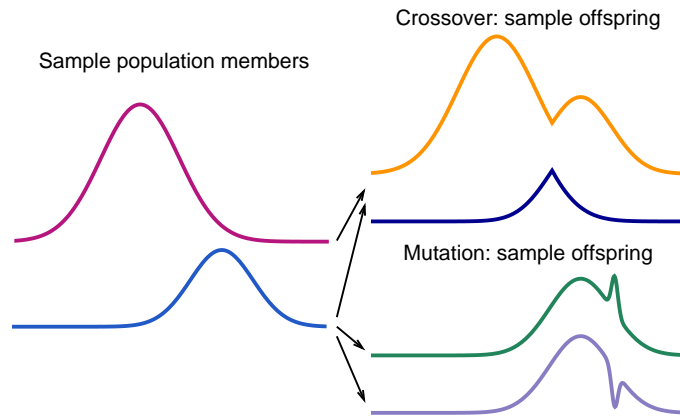


Abbildung C.1: Veranschaulichung für die GA Operatoren.

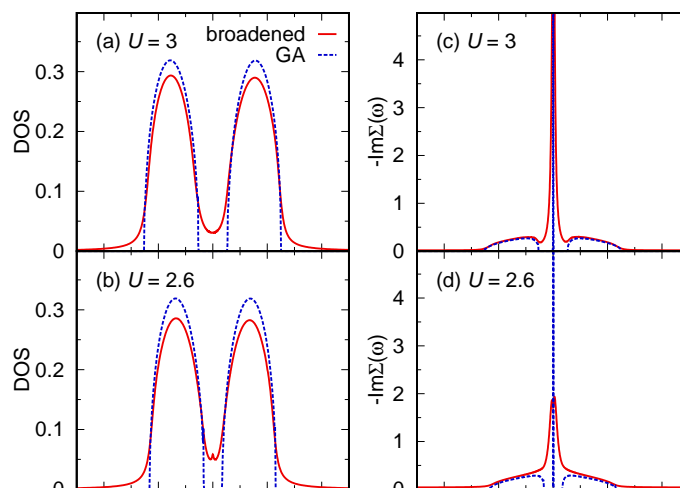


Abbildung C.2: Vergleich zwischen dem GA-Methode und die iterative Methode mit Lorentzian Erweiterung für die Teilchen-Loch-symmetrische Hubbard Model auf dem Bethe-Gitter: (top) DOS und die Selbstversorgungen-Energie für die Isolier-Staat mit  $U = 3$ . (bottom) DOS und die Selbstversorgungen-Energie nahe an der Mott-Übergang mit  $U = 2.2$ .



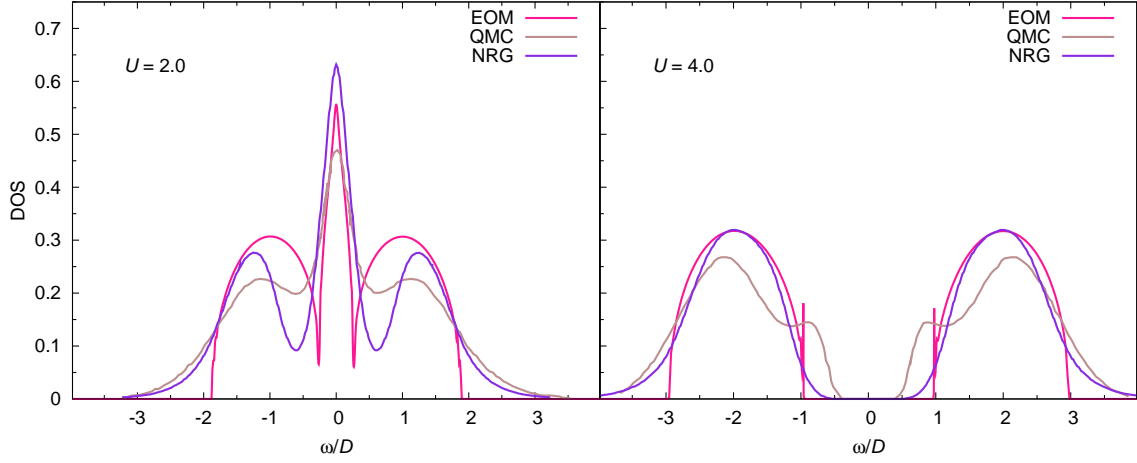


Abbildung C.3: Die Zustandsdichte der einzigen Band Hubbard-Modell auf der Bethe Gitter in der Hälfte gefüllten Staaten (das Coulomb Interaktion Stärke ist  $U = 2$ ), vergleich mit QMC (getroffen aus Ref. [39]) und NRG Ergebnisse (getroffen aus Ref. [100]).

beliebiger Spin- und Bahndrehimpuls-Entartung  $N$  auf der reellen Frequenzachse studiert. Für das Einzel-Störstellen-Anderson-Modell wurden die Spektralfunktionen für endlich und unendlich starke Coulomb-Wechselwirkung berechnet. Sie wurden auch in Abhängigkeit von Parametern wie der Störstellenenergie und der Hybridisierungsstärke untersucht. Beim Hubbard-Modell haben wir für die Spin- und Bahndrehimpuls-Entartung  $N = 2$  den Bandbreiten-kontrollierten und den Füllungs-kontrollierten Mott-Metall-Isolator-Übergang untersucht. Die kritische Wechselwirkungsstärke  $U_c$  sowie die Spektralfunktionen sind vergleichbar mit Ergebnissen von QMC oder numerischer Renormierungsgruppe in Abb. C.3. Wir haben auch das Quasiteilchengewicht und die Selbstenergie für metallische Zustände untersucht. Dabei findet man näherungsweise Fermiflüssigkeitsverhalten. Schließlich haben wir die Zustandsdichten für das Hubbard-Modell mit beliebiger Spin- und Bahndrehimpuls-Entartung  $N$  in Fig. C.4 berechnet. Die Formel ist jetzt für die verschiedenen Entartung  $N$

$$A = \frac{(N-1)U}{\omega - \varepsilon_f - U - (N-2)U\bar{n}_{\sigma''} - 2\Delta_2 - \tilde{\Delta}_2 - 0.5(N-2)\Delta}. \quad (\text{C.38})$$

Das periodische Anderson-Modell als weiteres wichtiges Gittermodell wurde ebenfalls für verschiedene Kombinationen von Parametern wie Coulomb-Wechselwirkungsstärke, Störstellenenergie, Leitungsbandposition, Hybridisierungsstärke und Spin- und Bahndrehimpuls-Entartung gelöst. Zusammenfassend lässt sich sagen, dass die Methode für das Hubbard-Modell und das periodische

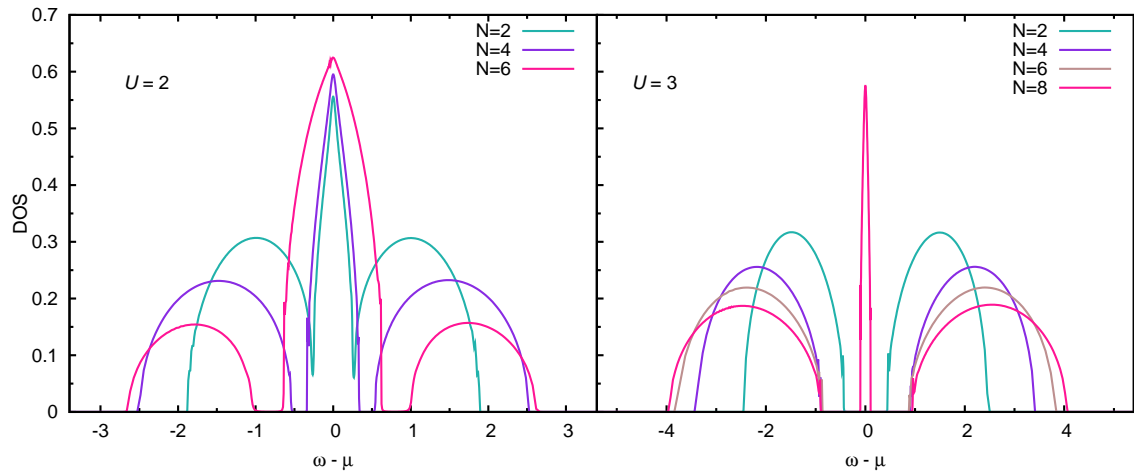


Abbildung C.4: Vergleich der Zustandsdichte für das halb gefüllte Hubbard Modell mit verschiedener Entartung  $N$ .  $\mu$  ist das chemische Potential.

Anderson-Modell in einem großen Parameterbereich funktioniert und gute Resultate liefert. Daher könnte diese Methode für das effektive Störstellenproblem für LDA+DMFT-Rechnungen nützlich werden.

Schließlich wurde auch eine vorbereitende Studie des Mehrband-Modells, aufbauend auf dem Erfolg beim Einband-Modell, unternommen. Zunächst wurde das Zweiband-System in einer einfachen Näherung unter Vernachlässigung der Wechselwirkung der zwei Bänder über das Bad untersucht. Das ergibt vielversprechende numerische Ergebnisse für das Zweiband-Hubbard-Modell. Außerdem haben wir analytisch die Gleichungen für die Behandlung der Wechselwirkung zwischen den Bändern in Molekularfeldnäherung und in Hubbard-I-Näherung abgeleitet. In Molekularfeldnäherung haben wir vom Zweiband-System auf ein beliebiges  $M = N/2$ -Band-System verallgemeinert. Auf der Basis dieser Arbeit lassen sich bessere Lösungen für Mehrband-Modelle implementieren.

# Curriculum Vitae

## **Qingguo Feng**

Birth: Jan 17, 1976, in Shandong, China

Nationality: Chinese

## **Education**

Ph.D, Theoretical Physics, Goethe-University Frankfurt, Frankfurt/M, Germany, Aug 2004 -

Thesis: *Study of single impurity Anderson model and dynamical mean field theory based on equation-of-motion method*

Advisor: Dr. H. O. Jeschke

M.Sc, Theoretical Physics, Institute of high energy physics, Chinese Academy of Sciences, Beijing, China, Sep 1998 - Mar 2002.

M.Sc thesis: *Relativistic Quark model and meson cloud effect*

Advisor: Prof. Yubing Dong

B.Sc, Lanzhou University, Lanzhou, China, Sep 1994 - July 1998.

Tutor: Dr. W. B. Jia

B.Sc thesis: *Study on fission of 8.25 Mev/u O+Au experiment*

Advisor: Prof. H. Y. Wu, Dr. L. M. Duan, Dr. Q. B. Gou

## **Other experience**

Research asistant, Institute of modern physics, Chinese Academy of Sciences, Lanzhou, China  
work for B.Sc thesis in Prof. H. Y. Wu's research group, Jan. 1998 - July. 1998.

## **Language skill**

Mandarin (native), English (fluent), German (Basic)

## **computer skill**

OS: Linux, Windows; Programming: C++, FORTRAN, Mathematica

## **Research interests**

Strongly correlated electron and spin system

Mott-Hubbard transition and Dynamical Mean Field Theory (DMFT)

Realistic material *ab initio* simulation and LDA+DMFT approach

Computational physics and method developments

Cross research of condensed matter and nuclear physics

## **Selected Publications**

Qingguo Feng, Y.-Z. Zhang, H. O. Jeschke, Phys. Rev. B **79**, 235112 (2009).

Qingguo Feng, Y. B. Dong, Chin. Phys. C (HEP & NP) **26**, 21 (2002).